Electron beam lithography of molecular glass resist films prepared by physical vapor deposition

Dissertation

zur Erlangung des akademischen Grades

Doktor der Naturwissenschaften (Dr. rer. nat.)

im Fach Chemie der Fakultät für Biologie, Chemie und Geowissenschaften

der Universität Bayreuth

vorgelegt von

Tristan Kolb

geboren in Coburg

Bayreuth, 2014

Die vorliegende Arbeit wurde in der Zeit von Juni 2008 bis Dezember 2013 am Lehrstuhl für Makromolekulare Chemie I der Universität Bayreuth unter der Betreuung von Prof. Dr. Hans-Werner Schmidt angefertigt.

Vollständiger Abdruck der von der Fakultät für Biologie, Chemie und Geowissenschaften der Universität Bayreuth genehmigten Dissertation zur Erlangung des akademischen Grades eines Doktors der Naturwissenschaften (Dr. rer. nat.)

Dissertation eingereicht am: 24.01.2014

Zulassung durch die Promotionskommission: 29.01.2014

Wissenschaftliches Kolloquium: 14.05.2014

Amtierender Dekan:
Prof. Dr. Rhett Kempe

Prüfungsausschuss:
Prof. Dr. Hans-Werner Schmidt   (Erstgutachter)
Prof. Dr. Stephan Förster   (Zweitgutachter)
Prof. Dr. Carlo Unverzagt   (Vorsitz)
Prof. Dr. Andreas Fery

Table of contents

Abbrevations

193i	193 nm immersion lithography
ABR	acid-base-resist
BBE	beam blanker electronics
CAR	chemically amplified resist
EBL	electron beam lithography
EUV	extreme ultraviolet
HPLC	high performance liquid chromatography
IC	integrated circuit
ITRS	International Technology Roadmap for Semiconductors
l/s	line to space proportion
LER	line edge roughness
PAB	post application bake
PAG	photoacid generator
PEB	post exposure bake
PVD	physical vapor deposition
QC	quartz crystal
QCM	quartz crystal microbalance
SEM	scanning electron microscope
SPL	single pixel line
T_g	glass transition temperature
UV	ultraviolet

1. Introduction

1.1. Lithographic patterning process applied in the fabrication of integrated circuits

Jack Kilby was awarded with the Nobel Prize in Physics 2000 for his invention of the integrated transistor design - called integrated circuits (ICs) - back in 1958.[1] It differed from the formerly utilized separated components of resistors, capacitors, transistors and diodes in the approach of integrating all of them into one single device. The integration allowed superior features, which were fundamental for the age of information society. Important developments for the information society were already expected by Gordon Moore in 1965.[2] He mentioned home computers, personal portable communications equipment, and possible applications in telephone communication, which all came true, as we know in our days. He developed this vision of the future when investigating the increase in components' numbers in one single IC since their invention. He realized that the relative manufacturing cost of a single component in ICs has an optimum relating to the number of components in the IC (**Figure 1.1 left**), which decreases along with the technology improvements year after year. By comparing these optimum component numbers, he identified an annual doubling (**Figure 1.1 right**). Based on this result he predicted that the trend would continue, which became known as "Moore's Law".
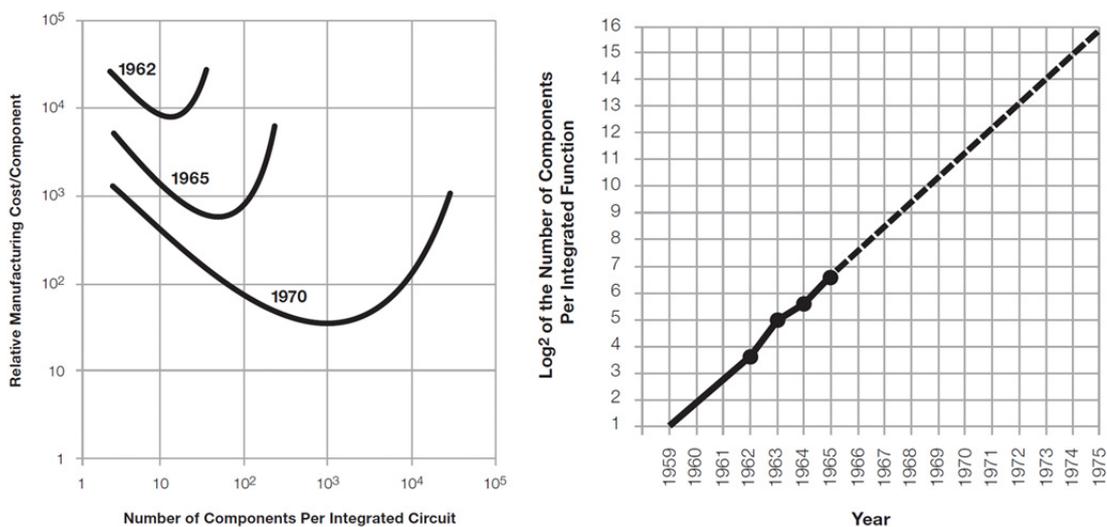
Figure 1.1: **Left**: The relative manufacturing costs of a component in single ICs depends on the components' quantity in an IC and decreases due to technology improvements year after year. The graph shows a cost minimum for a certain number of components in every year.
Right: The number of components per IC for this cost minimum is predicted to double every year.[2]

As history shows, his prediction was correct. The number of components - later specified to the number of transistors - doubled every 18 months. This progress was only possible due to a reduction in transistors' size, which demanded an ongoing steady improvement in lithographic techniques. Such photolithographic techniques are already in use since the production of the first IC on monolithic silicon back in 1959.[3] Thus only one year after the invention of the IC, the interconnected development between lithography and the IC fabrication began. Therefore, the lithographic techniques had to continuously advance in order to fulfill the demands for smaller feature sizes in improved IC architectures. As a result, today production of 22 nm microprocessors is feasible, a technology which is being utilized i.e. by the Intel Corporation for its most current processor architecture "Haswell" - introduced in 2013 - as well as for its predecessor "Ivy Bridge" - introduced in 2011.[4] Such complex processors with more than a billion transistors are manufactured in about 800 processing steps, which comprises multiple lithography and etch processes for pattern transfer.[5] A general overview of one pattern transfer process is shown in **Figure 1.2**. All single steps together result in a total cycle time from starting bare silicon wafer to the final and packaged product of up to 60 days.[6]

A lithographic process starts with the preparation of the substrate by removing contaminations and the deposition of a uniform film of functional material (**Figure 1.2 A**), which will be patterned during the following steps.[6] The utilized materials range from insulators (e.g. silicon dioxide, silicon nitride) to conductors (e.g. aluminum, copper), which are applied for example by oxide growth - oxidation of the silicon substrate -, chemical vapor deposition, physical vapor deposition, atomic layer deposition or sputtering. Afterwards absorbed water is removed by a dehydration bake usually followed by the application of an adhesion promoter. The most common one is hexamethyl disilazane, which replaces silanol groups by trimethylsilyl groups to enhance the adhesion of the photoresist.

Afterwards the photoresist film is usually applied by spin coating (**Figure 1.2 B**). Therefore the photoresist, dissolved in a solvent, is applied to the substrate forming the resist film in the subsequent spin process. The resultant film thickness depends on the viscosity of the solution, the concentration of the resist, the final spin speed and the applied acceleration speed. Typically, the spin coated films contain between 20 wt% and 40 wt% solvent. This is being reduced by a subsequent annealing process, called post-apply bake (PAB), to a residual solvent level between 3 wt% and 10 wt%.
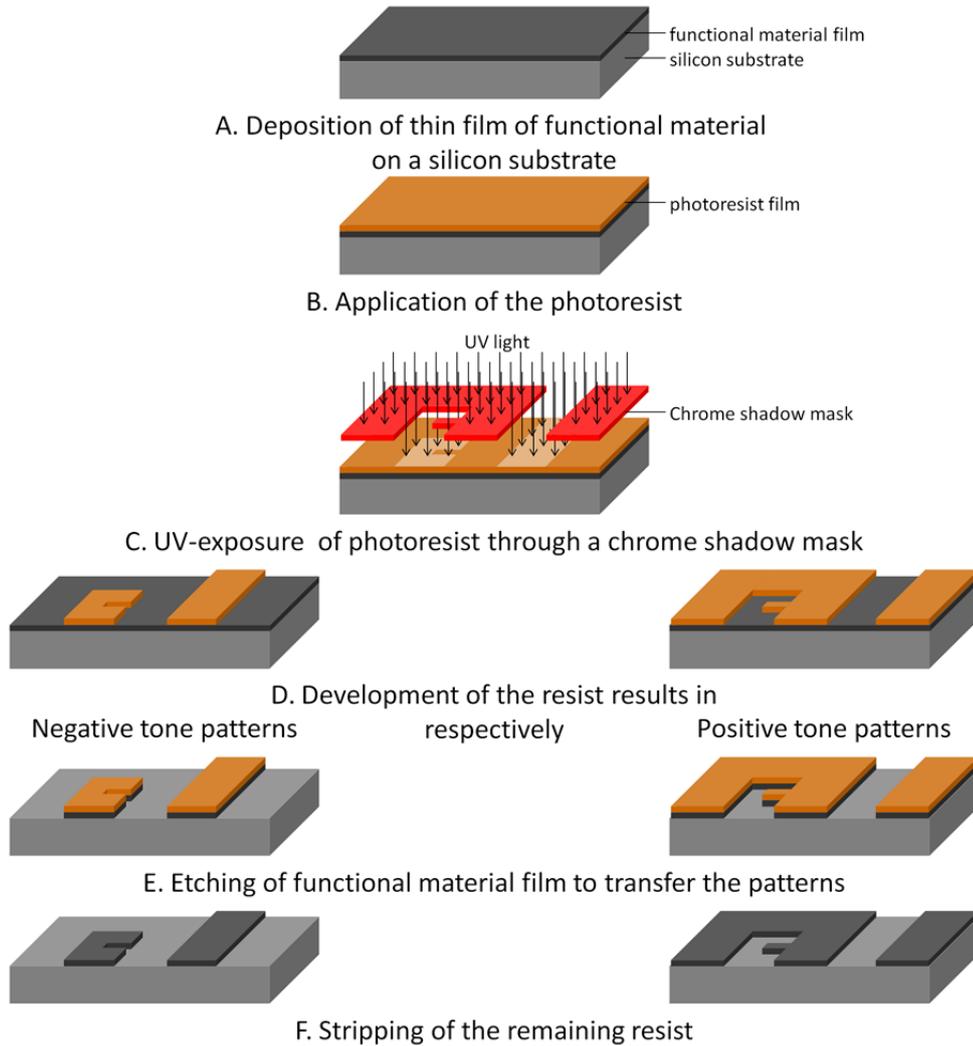
Figure 1.2:   General overview of the photo lithography pattern transfer process.

The next step in the lithographic process is the exposure step, during which the mask design of a shadow mask is transferred onto the resist film (**Figure 1.2 C**). This exposure activates the photoactive compound in the resist film. Besides ultraviolet (UV) exposure also other methods like exposure by electron beam[7] respectively ion beam[8] are currently under investigation. The photoactive compound converts itself due to this activation. Depending on the resist material class, it may or may not operate as catalytic reactant to change the photoresist solubility in the exposed areas or it just becomes soluble itself. For such catalytic processes an annealing step, called post exposure bake (PEB), is applied subsequently.

The yielded solubility change is being utilized in the development step to reveal the transferred mask design (**Figure 1.2 D**). In positive tone resists, the exposed areas are being removed during this development process, while in negative tone resists the unexposed resist

material is soluble in the developer. As developer usually an aqueous tetramethyl ammonium hydroxide solution (TMAH) is applied with a concentration of 0.26 N. However, in some cases also alternative developers like supercritical CO_2[9], organic solvents[10] or methyl siloxanes[11] are used.

Afterwards usually the resist patterns are hardened to withstand the harsh conditions of the subsequent etching process. Therefore a postbake is applied, in which the resist material cross-links thermally. Additionally this process reduces remaining solvents and water resulting in an improved resist adhesion. Beside the postbake also high intensity UV exposure and electron beam bombardments are used sometimes for resist hardening.

The next step is the etch pattern transfer, which is performed usually after an inspection step, called "after develop inspect".[6] If in the inspection step defects are detected, the resist film is stripped off and the lithographic step is restarted. This allows the cost-beneficial rework of the wafer instead of scrapping, which is necessary, if defects are identified after the pattern transfer in the final inspection. The pattern transfer is commonly performed by etching (**Figure 1.2 E**). Thereby the resist protects the functional material from the etchant while it is removed in the unprotected areas. In wet etching the etchant is usually an acid solution, while in the more common dry etching, usually a plasma process is utilized with the support of a reactive gas to enhance the etching selectivity.[6] Alternatively to an etching process, a selective deposition of materials (e.g. by electroplating) in the unprotected areas as well as ion implanting (doping) may be performed.

Finally the remaining photoresist is removed by wet or dry stripping techniques (**Figure 1.2 F**). In the case of wet stripping, organic or inorganic solvents are used, while in the more common dry stripping, oxygen plasma is applied, which removes the mainly organic photoresist materials but leaves the inorganic wafer surface untouched.

This whole lithographic process is repeated several times until the whole microprocessor is created. The fabrication of defect free microprocessors however requires optimized processing conditions in each step. Thus the processing variables, like annealing temperature, annealing time, exposure dose and material composition, to name but a few, must be adjusted absolutely precisely. However, the optimization of these conditions is complicated by the fact that these variables interact with each other. This means that a non-optimized applied variable one can impact the adjustments of other ones under this condition and normally generates a bad performance. Thus in order to identify the overall best conditions a huge number of single experiments is necessary. A more elegant way is the application of combinatorial

approaches.[12] By arranging several processing variable variations in one single experiment in orthogonal fashion, a combinatorial library can be realized. The combinatorial library then allows the identification of trends between the applied variables and their optimization in dependence of each other.

1.2. Exposure techniques for lithographic patterning

The most crucial process in the lithographic pattern transfer is the exposure. This process has to be improved constantly to achieve the size reduction demanded by the semiconductor industry. The industrial mass production is currently based on optical lithography, which utilizes light to transfer the design of a shadow mask into the photoresist film. The easiest way for this transfer is contact or proximity lithography, during which the mask is placed directly on top respectively with a small gap above the photoresist coated substrate.[13] Due to their high defect density respectively poor resolution capability, both techniques were replaced by projection lithography in the mid-1970. For this technique, light is collected from the source and focused on the shadow mask by a condenser lens. Afterwards the light is focused by a second lens to transfer the mask design into the photosensitive material. The maximal theoretical resolution of such exposure systems can be calculated by the Rayleigh criteria:[14]

$$\text{Resolution} = k_1 \lambda / \text{NA} \tag{1.1}$$

As the equation describes, the resolution depends on the wavelength λ of the applied light, the numerical aperture NA of the lens system and a process-dependent proportional constant k_1. The improvement up to the currently utilized 22 nm technology was only possible with the optimization and improvement of all three parameters. The k_1 constant has no real optical definition, but summarizes the resolution capability of the lithographic process.[14] It is impacted by imperfections in the imaging system (stray light, vibration, lens aberrations), diffraction effects and imperfections of the exposure at the photoresist material (reflections from the substrate, standing waves).[15] Besides the reduction of these effects, the factor can be improved by the application of a phase shift mask, off-axis illumination and optical proximity correction. With these improvements the k_1 value of commercially available imaging systems could be reduced from 0.8 in 1983 to 0.31 in 2005 and has even been approaching the theoretical limit of 0.25 for single exposure processes during the last

years.[16],[17] In recent years, highly sophisticated double respectively multi-patterning techniques like "higher order pitch division" or "self aligned double patterning" were developed and applied.[18],[19] These techniques allow the beating of the theoretical limit of 0.25, but suffer from the disadvantage that more process steps are needed, which increases the overall costs of the pattern transfer process distinctly.

The numerical aperture of a lens system is defined by the following equation:[6]

$$NA = n \sin \theta_{max} \tag{1.2}$$

Thus the numerical aperture depends on the maximal half-angle θ_{max} of diffracted light, which enters the lens system and on the refraction index n of the surrounding medium. An optimization of the lens architecture allows an increase of θ_{max}, which is realized by an increase of the lens's acceptance angle. By such optimizations NA values of 0.85 and higher were achieved.[20] With the change to water based immersion lithography ($n = 1.44$ for a light wavelength of 193 nm), lens systems featuring a NA of 1.35 are realized in the currently utilized standard tools for ArF immersion lithography.[21] For further improvements, scanning interference evanescent wave lithography is being investigated, which should allow tools with a NA of even 1.85.[22]

The last, but similar important parameter for resolution enhancement is the wavelength λ of the applied light.[23] The applied wavelength was adjusted each time the industry reached the resolution limit of the specific wavelength by optimizing k_1 and NA. So first the g-line emission band (436 nm) of the mercury discharge lamp was applied, which was substituted by the i-line emission (365 nm) of the same lamp type. The next generation lithography tools utilized Krypton-Fluoride (KrF, 248 nm) excimer lasers, which were followed by the currently still used Argon-Fluoride (ArF, 193 nm) excimer lasers. These wavelength changes had an enormous impact on lithographic processing. New generation exposure sources always required a sufficient intensity to maintain a similar throughput as with the previous technology. Additionally new photoresist materials had to be invented and adapted to the new exposure wavelength. Furthermore the processing tools and the manufacturing process had to be adapted to the new wavelength. This adaption to a new wavelength was not always successful. For example, it had been planned to substitute the ArF technology for the 65 nm node in 2005 with the F_2 excimer laser technology (157 nm). However, the high price and the low supply of the utilized lens material calcium fluoride as well as immature photoresists and pellicles in 2003 led to the Intel®'s decision to drop this technology and to instead extend the

193 nm technology further.[24] By applying the already mentioned immersion lithography for high NA and double exposure techniques for low k_1 these extensions allowed the realization of the current 22 nm processor technology.[4]

For future resolution enhancements, the International Technology Roadmap for Semiconductors (ITRS) names the following lithography techniques in its 2012 update: 193 nm immersion lithography (193i) with multi-patterning, nanoimprint lithography, direct self-assembly in combination with a lithography process, extreme ultraviolet (EUV) lithography, and maskless lithography (ML2).[25]

The application of 193i with multi-patterning techniques would be an extension of the currently utilized immersion technology with double-patterning. However, multi-patterning requires more process steps, which distinctly increases the costs of the fabrication process. But as long as alternative next generation techniques are not available for mass manufacturing, the focus seems to remain on this option.[26]

The nanoimprint lithography utilizes a patterned stamp, which is pressed into a resist layer to create a replication.[27],[28] During this imprinting process, usually a UV exposure is applied to crosslink the resist material and thus stabilize the patterns prior to the removing of the stamp. This direct pattern transfer method allows a high throughput, but due to the direct replication it requires masters with feature sizes identical to the upcoming nodes. The biggest issue is the sticking of cured resist at the mold, which results in defects in the achieved patterns.

The directed self-assembly technique utilizes a block copolymer, which forms domains of the different polymer blocks substructures in between of alignment features due to phase separation.[29],[30],[31] Usually the different polymer materials in the blocks differ in their physical properties, which allow a selective removal of one of the materials e.g. by plasma treatment. This bottom-up approach is assumed to significantly reduce costs, but additional work is needed to make it applicable for mass-production.

In contrary to the hitherto described next generation lithography technologies, EUV lithography continues to follow the concept of resolution enhancement of optical lithography by decreasing the applied wavelength to 13.5 nm.[32] However, the absorption of these high energy photons does not directly activate the resist material like in UV resists, but instead photo electrons are released.[33] These photo electrons ionize the resist material further. Beside the formed photo electrons itself, the thereby formed secondary electrons are responsible for the activation of the resist material. An important issue with this exposure technique is the

fact, that EUV light is absorbed by all kind of materials. Thus the exposure is taking place in vacuum and the optical components - shadow mask and lenses - have to be replaced by a reflective mask and mirrors.[32] Despite of the necessary tool and process changes it is the preferred technique of the semiconductor industry.[25],[34] But by now, the realized power of the light source still is far behind the proposed values, so that actual beta tools show a too low processing throughput. Additionally, the supply of resists, which allow the fabrication of the desired small feature sizes, is still an issue.[35] In 2012 an implication strategy was announced.[36] The implication is expected to take place for equal or lower costs compared to 193i multi-patterning, which is assumed to happen for the 14 nm node.

Additionally, ML2 techniques are competing for application in next generation lithography. Such maskless techniques differ from the hitherto mentioned techniques due to direct exposure or pattern creation without the utilization of masks or masters. This term covers direct laser writing, scanning probe lithography, ion beam lithography and electron beam lithography. The direct laser writing utilizes focused laser beams, whose focal spot scans the resist layer to apply the exposure process. Following the application of two photon absorption and inhibiting strategy features with 9 nm resolution - far below the diffraction limit - were reported recently.[37] In scanning probe lithography a heated scanning probe tip or an E-field supported tip is used to locally remove the resist material by applying a heat impulse. Thus the features are directly generated without a development step. By this technique objects, as e.g. a micrometer sized 3D replica of the Matterhorn, as well as sub-10 nm features are realizable.[38],[39] In ion beam lithography accelerated ions as gallium, protons or helium are utilized to directly remove resist material (focus ion beam technique) or produce an exposure contrast similar to optical lithography, which is utilized in the subsequent development.[40] For a recent study, a helium ion beam was utilized to pattern graphene with feature sizes as low as 10 nm.[8],[41]

However, all three techniques are far from application for high volume fabrication in contrary to the electron beam technique, which competes with EUV as direct successor of 193i multi-patterning.[7] This direct write technique utilizes an electron beam, which is moved electronically controlled over the substrate to expose the resist film pixel by pixel. The activation of the resist material is thereby originating - similar to the EUV exposure - from impacting (primary) electrons as well as from secondary electrons formed due to the ionization of the resist material by primary electrons.[42] The utilized pixel by pixel exposure thereby lacks throughput. But with the utilization of a digital pattern layout, this technique has

become the established one for the fabrication of high value low volume products like master devices of next generation microelectronic layouts or masks for the alternative lithography techniques.[43] Recently the throughput issue was addressed by several companies (e.g. MAPPER Lithography B.V., IMS Nanofabrication AG, KLA-Tencor).[44],[45],[46],[47] In order to make them competitive to optical lithography techniques, they are developing tools operating with multiple electron beams - even up to over a million - in parallel.

In summary, none of the next generation exposure technique by now shows all capabilities to completely replace 193i multi-patterning. Further developments and achievements in the years still to come will have to show which one of them is going to win the race.

1.3. Photoresist materials

The semiconductor industry shows increasing demands on tailored photoresist materials to maintain the successful manufacturing of new products. The main driving force behind this demand is the desire for cost reduction, which is mostly realized by miniaturization. Therefore applied photoresist materials must be developed to realize the continuously decreasing feature sizes utilizing the applied lithographic technique. However, in the beginning of the fabrication of semiconductor devices, the feature size was not the most important parameter. Instead more important was the property to withstand the etchant hydrofluoric acid for the pattern transfer. At first, Poly(vinylcinnamate) (**Figure 1.3A**) was taken into consideration, which demonstrated good etch resistance and a switchable solubility due to photoinduced dimerization.[48] However, the issue of non-sufficient adhesion to oxidized wafers could not be solved with this material. Consequently, a promising resist material has not only to be appropriate for the realization of the desired feature sizes, but must be compatible to all applied processing steps.

Instead of Poly(vinylcinnamate), a resist consisting of a bis-azide (2,6-bis (4-azidobenzal)-4-methylcyclohexanone) and cyclized poly(cis-isoprene) rubber (**Figure 1.3B**) was invented from Kodak®. This negative tone resist became the work horse of the semiconductor industry until its resolution limit of about 2 µm was reached in 1972. It was followed by a resist consisting of novolac - a phenol-formaldehyde resin - and diazonaphthoquinone (DNQ) sulfonate esters (**Figure 1.3C**).[49] This positive tone resist shows less swelling behavior during the development, which allowed the realization of features even below 300 nm.
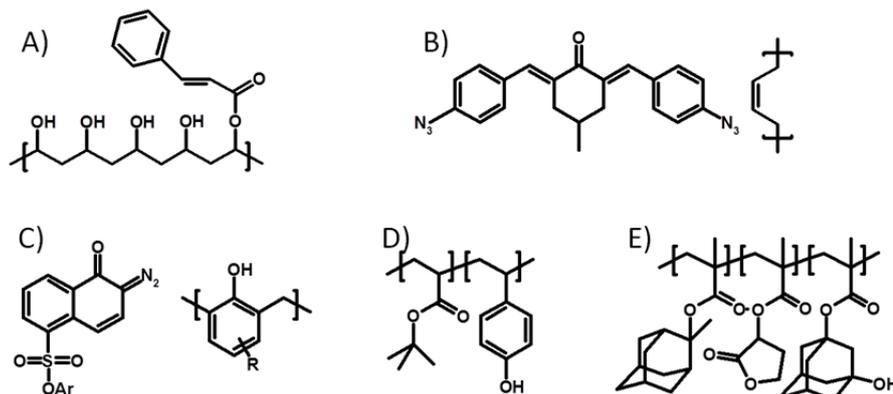
Figure 1.3:   Chemical structures of polymers utilized as tailored resist materials:
A: Poly(vinylcinnamate) based resist.[48]
B: Kodak thin film resist (KTFR), consisting of bis-azide (2,6-bis (4-azidobenzal)-4-methylcyclohexanone) and cyclized poly(cis-isoprene) rubber.[48]
C: Resist based on novolac (phenol-formaldehyde resin) and diazonaphtho-quinone (DNQ) sulfonate esters.[49]
D: Chemically amplified ESCAP resist based on a random copolymer of 4-hydroxystyrene with t-butyl acrylate and an additional PAG compound (not shown).[50]
E: Chemically amplified resist based on a alicyclic methacrylate polymer and an additionally PAG compound (not shown).[51]

For further feature size reduction, a change of the UV exposure wavelength to deep UV region (~250 nm) was necessary.[52] However, the light sources for this wavelength - 254 nm emission band of Xe-Hg lamps as well as the 248 nm emission from Krypton Fluoride (KrF) excimer lasers - were less intense compared to the prior utilized i-line emission (365 nm) of Xe-Hg lamps. Thus for maintaining the wafer throughput in semiconductor production, the resist sensitivity had to be increased dramatically. This issue was solved by applying the 1982 proposed concept of chemical amplification.[53],[54] It is based on the formation of an active species by exposure. This active species catalyzes in the following processing the chemical reactions, which are responsible for the solubility change of the resist material between the exposed and unexposed areas. By utilizing this chemical amplification concept, the deep UV technology was reported from IBM in 1990 covering the first implementation of 1000 nm feature size and got extended by the semiconductor industry to the 130 nm node.[55],[52] The most prominent resist for this deep UV processing was the ESCAP resist (environmentally stable chemical amplification positive resist) which is based on random copolymer of 4-hydroxystyrene with tert-butyl acrylate (**Figure 1.3D**) mixed with a photoacid generator (PAG).[50]

The next step of resolution improvement required the change of the exposure wavelength to 193 nm (Argon Fluoride (ArF) excimer laser). Unfortunately, the benzene building block in the ESCAP resists featured a high absorption at this wavelength, so that a change of the resist material was also necessary. Polymethacrylates feature a low absorption at this wavelength and thus became the material of choice. However, it was necessary to incorporate bi- and tri-alicyclic (e.g. adamatane, norborane) in the polymer to receive resist materials, which feature similar etch resistance as the ESCAP resist utilized so far (**Figure 1.3E**).[56],[51] Together with the introduced immersion technology and double patterning approaches, such 193 nm resists allow the realization of the 22 nm node at industry scale in our days.

For the time being, it is not certain yet, which resist materials will be utilized to realize the future smaller nodes. Therefore, research is focused in improving the currently utilized resist material as well as in switching the material class.

First works are done to exchange the linear polymer architecture by star-shaped ones, which feature a higher sensitivity and solubility contrast.[57] A change of the resist material itself is assumed to be necessary for the upcoming EUV exposure technique in order to ensure a high enough absorption and thus a sufficient resist sensitivity. The incorporation of hafnium atoms into the resist material has already shown some promising results.[58]

Furthermore, the industry is on the way to reaching the diffusion length of the acid in chemically amplified resists (CARs) with resolutions below 20 nm and is thus approaching the resolution limit of this resist class. To overcome this issue, polymer bond PAGs are being discussed to exchange the currently applied resist-PAG blends, whereby the acid diffusion length shall be reduced.[59] Such materials already allow the realization of resolutions below 20 nm.[60] However, the ITRS Report 2011 mentions that it is still unclear, if such diffusion reduction methods will be sufficient to realize the future nodes.[61] Consequently, even abandoning CAR systems is being discussed.

Besides resolution reduction also the roughness of the realized features is an issue. It must be reduced to allow a successful patterning at these sophisticated resolutions. A possible solution was mentioned by Mike Mayberry, director of components research and vice president of technology and manufacturing of Intel Corporation, at Techcon 2010.[62] He mentioned that molecular glass resists featuring smaller molecular weight compared to the conventional polymer materials should reduce the grain size and thus hopefully the feature roughness, too. Such molecular glass materials are, according to Shirota, who once introduced this term, "low molecular-weight organic compounds that readily form stable amorphous glasses above room

temperature".[63] The first utilization of molecular glasses in the lithographic area was investigated by Shirota and his coworkers. In this early work from 1996, he investigated a non chemically amplified resist based on branched phenylbenzene and triphenyleneamine structures for electron beam lithography and successfully realized 70 nm features.[64] The transfer of this material class to chemically amplified resists enabled sensitivities within the same range as with polymeric materials. This was shown for a tert-butoxy carbonyl (t-BOC) protected 1,3,5-trihydroxyphenyl benzene, which allowed the realization of isolated line features of 25 nm, electron beam exposed to a dose of 66 µC/cm².[65] For a half protected hexa(hydroxyphenylbenzene) material (**Figure 1.4 A**) the successful patterning of sub 30 nm dense features by EUV lithography has been reported.[66] By utilizing an adamantyl based protection group (**Figure 1.4 B**) such phenolic molecular glasses were even capable to realize 25 nm line space features.[67]
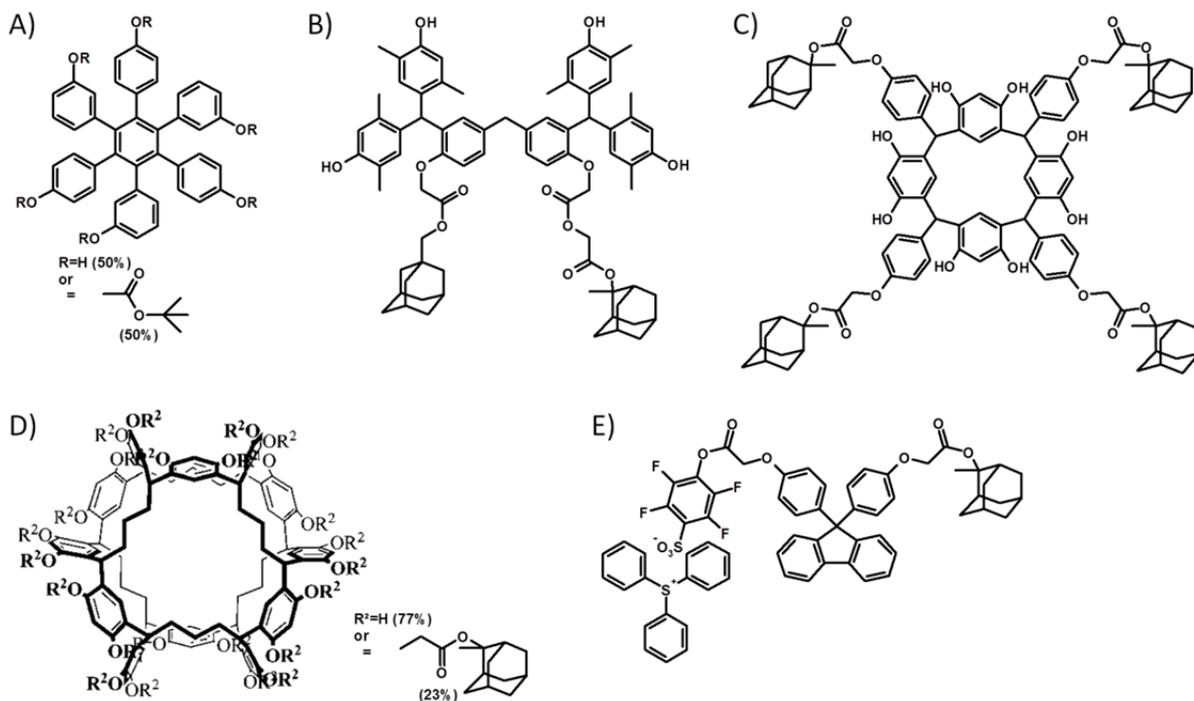
Figure 1.4: Investigated molecular glass resists for electron beam respectively EUV lithography:
A) partly t-Boc protected branched molecular glass resist investigated by EUV lithography;
B) adamantyl protected branched molecular glass resist investigated by electron beam lithography;
C) adamantyl protected Phenylcalix[4]resorcinarene investigated by electron beam and EUV lithography;
D) partly adamantyl protected noria derivative investigated by EUV lithography;[68]
E) single component molecular glass electron beam resist material featuring a bounded PAG and an adamantyl protection group.

Beside these branched molecular glass architectures also ring shaped ones have been intensively investigated as chemically amplified resist materials. Calix[4]resorcinarene was the first core material from this class to be investigated serving as a negative tone chemically amplified resist for 365 nm lithography.[69],[70] Recently negative[71] as well as positive[72] tone resists with this core architecture were investigated by electron beam respectively EUV lithography. The realization of 40 nm line space features could be shown for positive tone Calix[4]resorcinarene resists with adamantyl based protection groups (**Figure 1.4 C**). By introduction of hexafluoro alcohol groups in the calix[4]resorcinarene core, the solubility of this resist class was improved.[73] The obtained resist showed good contrast and sensitivity in electron beam as well as in EUV lithography.

Beside these ring shaped materials also double ring shaped ones, called noria, were investigated as a core material for negative[74] and positive tone resists[68],[75]. The best results could be achieved in positive tone with partly protection by an adamantyl group (**Figure 1.4 D**), which allowed the realization of 26 nm line features after EUV exposure.

All of these mentioned chemically amplified molecular glass resists are being utilized in a mixture with a PAG component as photosensitive material. Beside these and analogous to the polymer resists, PAG-bound molecular glass materials were investigated, to reduce acid diffusion and to ensure a homogeneous PAG distribution in the resist.[76] The latest work on this topic utilized a fluorene core with bonded acid-labile methyl-adamantyl protecting group and triphenylsulfonium PAG with the anion bounded to the molecular glass (**Figure 1.4 E**).[77] This resist allowed the realization of 50 nm line space features with a good sensitivity to electron beam lithography.

An overview of additionally investigated molecular glass resists and their development has been provided in published reviews.[78],[79] They highlight the overall potential of this resist class, but also mention the need for additional research efforts, in order to close up to and maybe surpass the highly optimized polymeric resists in performance.

1.4. Thin film preparation techniques and their impact on the film's physical properties

For the fabrication of microprocessors the preparation of uniform amorphous thin films is of crucial importance, too. Beside their usage for lithographic purpose they also play an important role in current and emerging research fields, such as display technologies,[80] solar cells,[81] SAMFETs,[82] and data storage[83]. Thereby the different applications require tailored film preparation techniques. These techniques can be classified as solvent based processes, whereby the film forming materials are applied from solution and solvent-free processes, whereby the materials are deposited out of a gas phase.

The most prominent solvent based thin film preparation techniques are doctor blading and spin coating.[84] In the first mentioned technique a blade is placed at a fixed distance from the substrate, and in its front, the coating solution is applied. The film is then prepared by moving the blade over the substrate with a constant velocity and by subsequently drying of the obtained film in order to evaporate the solvent. The achieved film thickness depends on the gap distance, the concentration of the coating solution and the velocity of the blade movement.

For spin coating on the other hand, the solution is applied on a stationary substrate mounted on a rotatable chuck, which afterwards is accelerated to the defined rotational speed. [85] Alternatively the solution is applied onto an already rotating substrate. In both cases the material is spread and excess material gets removed, followed by solvent evaporation. After a time period of several seconds up to a few minutes, the solid material is typically obtained as a uniform, smooth film on the substrate. Advantages of spin coating are high reproducibility and uniform film formation on planar substrates up to diameters of more than 30 cm.[86] Thereby film thicknesses from several nanometers up to even millimeters are feasible in dependence of the solvent, the concentration and viscosity of the applied solution, the acceleration speed and the final number of revolutions per minute used in the spin coating process.[87] Typically, applied material classes range from inorganic materials to organic polymeric or low molecular weight materials.[88],[89],[90]

In contrary to these solvent based techniques, solvent-free film preparation deals with material deposition on the substrate out of the gas phase. In principle, there are two different kinds of solvent-free film preparation. These are chemical vapor deposition (CVD) and physical vapor

deposition (PVD). Both processes are usually vacuum processes, and have in common that the utilized materials must be transferred in the gas phase.

For CVD the deposited materials are precursor materials.[91] These precursors react in vicinity to the substrate in an activated environment (heat, light, plasma) and form the material film on the substrate. In contrary to CVD, in PVD no chemical reaction takes place. Instead, the unmodified material is transferred to the gas phase by evaporation or sublimation followed by the molecule by molecule deposition on the substrate.[92] The material evaporation can be performed by different techniques ranging from thermal heating or energetic particle bombardment by electrons, atoms, ions, molecules, or photons. The different evaporation techniques allow the realization of controllable evaporation rates, which gives the precise control over the film thickness even in the nanometer range (monitored by quartz crystal microbalances). The combination of several material sources - each monitored by a quartz crystal microbalance - allows the preparation of multi-component films by coevaporation, whereby the material composition is controlled by the individual evaporation rates of the components (**Figure 1.5**).[93]
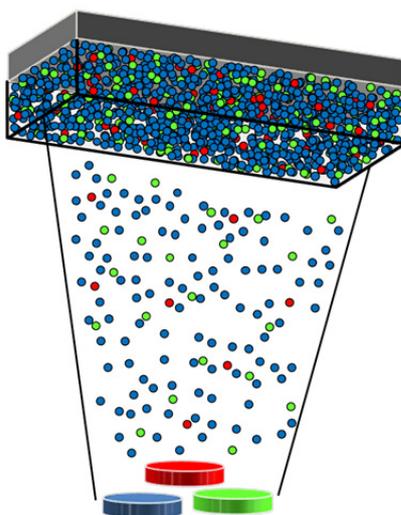
Figure 1.5: Schematic illustration of the preparation of a multi-component film by physical vapor deposition (PVD): The different materials are coevaporated by heating under high vacuum. The precisely controllable evaporation rate of each material is monitored by quartz crystal microbalances. By controlling the temperature of each material source, the respective evaporation rates can be adjusted to prepare a film with defined composition.

In combination with shadow mask techniques, it is possible to design straightforward combinatorial libraries featuring e.g. different compositions and different film thickness.[94] The PVD technique is most commonly applied for inorganic materials, but is also utilized for

the preparation of films consisting of low molecular weight organic compounds.[95] The achieved films are pinhole-free and free from other impurities such as dust or solvent residues which may influence film formation and physical properties[6]. This technique favors the formation of amorphous films, which are indispensable for the application in photolithography. Additionally, the obtained amorphous films show exceptional thermodynamic and kinetic stability by proper adjustment of the evaporation conditions, as well as a higher density [96] and modulus[97] compared to glassy material films obtained by cooling the liquid phase. However, a serious disadvantage of this technique is the requirement on applied materials to be evaporable or sublimable without thermal decomposition during the PVD process. Consequently, polymeric materials are usually not applicable.

However, in the semiconductor industry the resist market is currently dominated by polymeric resist materials. For processing these materials usually the spin coating technique is used. Beside these polymeric materials, during the last decade also molecular glass resists have been under investigation. They feature a well-defined low molecular weight and those of them with a high thermal stability are applicable to the film preparation by PVD.[78]

The previously presented dry and wet film preparation techniques differ completely in the film forming mechanism. While in the wet techniques the whole film is forming over the complete thickness during solvent evaporation, in dry techniques it is growing up continuously by a molecule by molecule deposition. These different physical processes crucially impact the physical properties of the achieved films. Additionally it is known that solvent residues may remain in the films produced by wet techniques even after the applied annealing process. [6] These differences have been investigated in several research fields in the last decade.

Fluorescent pigment films, applicable in ultraviolet charged couple devices, show differences upon annealing in the crystalline behavior.[98] While thin films below 12 nm prepared by PVD are amorphous, spin-coated films are crystalline for all film thicknesses. Chalcogenide glasses show different refraction indices and optical bandgaps in the bulk state as well as in films prepared by spin coating or PVD, once tested with material evaporation by thermal heating and once tested with material evaporation by pulsed laser ablation.[99] As a result of this investigation, even films prepared by the related PVD techniques which differed in the evaporation method have been found to form different microstructures which influence the film physical properties. Furthermore, the investigation of Zirconium dioxide films,

applicable as high refractive index material for optical coatings, has been demonstrating differences between PVD and the spin coating of a sol-gel precursor.[100] These films differ in the absorption, the porosity ratio and the laser-induced damage threshold. For organic field-effect transistors, the change of the film preparation technique from dry processes to wet processes has been investigated to enable low cost fabrication.[101] Wang et al. identified an appropriate precursor for realizing similar films by spin coating as well as by PVD. However, the spin coated sample showed decreased carrier mobility by one order of magnitude.

In addition, for two or more component systems the miscibility and blending of these different components have to be considered. In such systems the occurrence of segregation[102] or phase separation[103] might interfere with homogeneous material distribution. But the material distribution in the achieved film is not only affected by the miscibility of the materials but also by the preparation technique. This effect plays an important role for example during the processing of organic light emitting devices, whereby quenching of the phosphorescence emitter has to be avoided by ensuring a sufficiently high dispersion.[104] The usually utilized preparation technique PVD[105] allows the desired statistically controlled homogeneous material distribution by the molecule by molecule deposition. In addition, this technique allows the fabrication of the established multilayer device architecture of OLEDs.

In summary, every film preparation technique has its advantages and disadvantages and thus the most suitable technique with respect to the required properties of the technical application has to be carefully identified.

1.5. Physical vapor deposition in lithography

In the field of lithography, the PVD technique has been occasionally utilized as film preparation method for organic resist materials since the early 1980s with the intention to realize an all-dry resist processing.[106] The term all-dry implies a resist processing concept, whereby both solution based film preparation and wet development are replaced by dry processing steps. The film preparation is therefore performed by a PVD process and the development is performed in a thermal vacuum development utilizing differences in the evaporation temperature of exposed and unexposed material. During this development process, the sample is annealed under vacuum, thus the material with the lower evaporation temperature is removed.
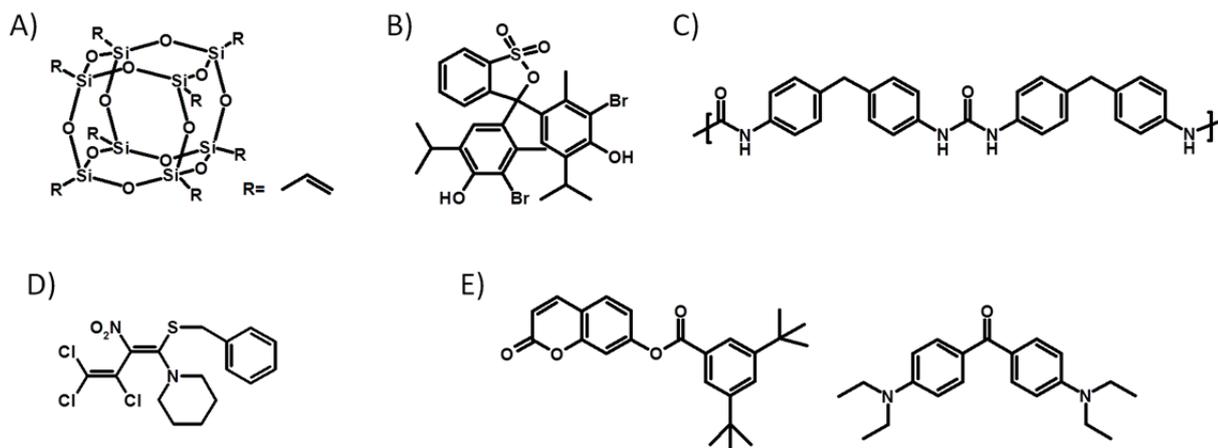
Figure 1.6:   Molecular glass resist materials utilized for film preparation by PVD:
A: Octavinylsilsesquioxane
B: Bromthymol blue
C: Polyurea formed by the reaction of 4,4'-diaminodiphenylmethane and 4,4'-diphenylmethanediisocyanate
D: 1-Benzylthio-1-Piperidino-2-nitro-3,4,4-Trichloro-1,3-butadien
E: 3,5-Di-tert-butylbenzoiccoumarinester (left) and sensitizer Michler's ethyl ketone (right)

The concept of all-dry resist processing was first realized in 1983 with an Octavinylsilsesquioxane resist (**Figure 1.6A**) by Korchkov et al., who successfully realized 200 nm features by electron beam exposure.[106] Continuous work with this all-dry resist even allowed the realization of 50 nm half-pitch-features.[107] In 1985 an all-dry resist for ion beam lithography on the basis of pyrene was patented.[108] The application of the all-dry concept for UV exposure was reported first in 1994, when bromthymol blue (**Figure 1.6B**) was investigated.[109] However, no patterns were shown as well as no information were given about the realized resolution. Sato et al. utilized a quite different resist system in 1995. They evaporated the monomers 4,4'-diaminodiphenylmethane and 4,4'-diphenylmethanediisocyanate, which form polyurea oligomers during deposition on the substrate surface (**Figure 1.6C**).[110] During UV exposure, the polymerization degree is increased locally, causing the delayed evaporation in the exposed areas during the vacuum development process. This approach allowed the realization of 5 μm features. In 1996 an all-dry resist based on 1-Benzylthio-1-Piperidino-2-nitro-3,4,4-Trichloro-1,3-butadien (**Figure 1.6D**) was patented, which was capable of realizing 1 μm features for UV exposure.[111] A carbazol derivatives based UV resist system was presented by Azarko et al. in 1999.[112] However no information was given about the realized resolution. In recent years, Dikusar et al. and Bei et al. have reported about the synthesis of several Schiff bases[113],[114],

azomethine[115] as well as maleopimaric and citraconopimaric esters[116] and the screening of these compounds for their applicability as all-dry photo resist material. They report about resolution capabilities of up to 1 μm for the partly very low sensitive resist materials, but did not show any image of the achieved patterns. Pfeiffer et al. have reported about an all-dry resist based on the dimerization of coumarin derivatives (**Figure 1.6E**).[117] By the coevaporation with the sensitizer Michler's ethyl ketone, the sensitivity of this resist system could be successfully improved. Beside this all-dry approach Pfeiffer et al. also investigated the reduced concept of just dry film preparation for chemically amplified resist materials. The negative tone resist materials consisted of a triphenolic compound, a crosslinker and a non-ionic photoacid generator, which was optimized by combinatorial approaches for 365 nm UV exposure.[93] By exchanging the triphenolic compound with tetraphenolic compounds even a water developable resist system could be realized, which allowed the realization of 400 nm features.[118]

In addition, all-dry resists for laser abrasion lithography have been reported.[119],[120],[121] In laser abrasion lithography, the exposure is performed under vacuum, which allows the direct evaporation and thus the removing of locally heated up resist material. The investigated materials are usually dye molecules, which are processible to resist films by PVD methods. In the subsequent exposure process under vacuum, they are heated up locally by the laser light adsorption resulting in the successive evaporation of the material. By utilizing di-substituted perylene diimides, resolutions of up to 400 nm were realized with this technique.[120]

In summary there have been first investigations on physical vapor deposition in the research field of lithography which introduce applicable novel resist material classes and alternative promising resist processing options. The rising requirements for aimed highly-sophisticated line features of below 10 nm resolution might maybe induce a need for such alternative film preparation techniques in the near future and thus they should be investigated in parallel to the standard solvent based thin film preparation techniques.

2.   Aim and Motivation

The semiconductor industry is seeking for its way to realize higher performance in micro processors. This target is tackled by fulfilling Moore's Law[2], which postulates a cost-efficient doubling of the transistor count every two years. Therefore the size of a transistor has to decrease progressively and along with that the capability of the utilized lithography techniques has to increase. This progress requires the scrutinizing and consequent optimization of both the lithographic processing and exposure techniques as well as the development of new resist materials which are patternable in the currently highly sophisticated resolution regime.

The aims of this thesis are the investigation of physical vapor deposited electron beam resists. The following four main subjects are covered in this thesis:

1) *Characterization of the utilized electron beam lithography facility and the establishment of processing procedures.*

2) *Investigation of physical vapor deposition as alternative film preparation technique in lithography.*

3) *Synthesis and characterization of positive tone chemically amplified resist materials utilizable for PVD.*

4) *Investigation of a novel physical vapor depositable resist material concept based on exposure induced salt formation.*

The first chapter deals with the *characterization of the utilized electron beam lithography facility and the establishment of processing procedures.*
In this chapter the following objectives are addressed:

a) *Characterization* of the electron beam lithography tool Leo1530 (equipped with Raith Elphy Plus) and the *determination of tool properties* important for the utilization as electron beam lithography tool.

b) Investigation of the *tool settings' impact* on the tool properties and the achieved pattern quality.

c) Establishment of a *processing routine* for the realization of a reproducible patterning process.

d) Adjustment and continual improvement of the *write field design* to create a tool box for resist characterization and optimization.

The second chapter deals with the *investigation of physical vapor deposition as alternative film preparation technique in lithography*. Here the advantage of the homogeneous material distribution in coevaporated resist films due to its molecule by molecule deposition is used to investigate the mixing behavior in multi-component chemically amplified resist films. Based on published Monte Carlo simulations, the impact of photo acid generator aggregate formation is identified by analyzing achievable resist characteristics. Consequently, the identification of variations of resist properties due to the PVD processing technique in contrast to the state of the art spin coating is the main topic of this chapter.

The chapter covers the following aspects:

a) *Adapting* of a literature known negative tone molecular glass resist for the application as a vapor depositable resist formulation.

b) *Systematical investigation* of *resist characteristics* of standard solvent processed as well as of PVD processed resist films and the identification of differences originating from the different processing.

c) *Combinatorial optimization* of the resist processing for *PVD processed* resist films.

The third chapter covers the s*ynthesis and characterization of positive tone chemically amplified resist materials utilizable for PVD*. Such materials have not yet been described in literature. Thus in this chapter for the first time different material classes shall be investigated with respect to their PVD processability in order to identify promising ones.

The main objectives of this chapter cover:

a) *Identification* of *suitable functional groups* for PVD processible positive tone chemical amplified resists.

b) Investigation of the *PVD processability of carbonate ester protected* molecular glasses in cooperation with the workgroup of Prof. Ober from Cornell University.

c) *Synthesis and thermal characterization of ester protected* molecular glass materials and estimation of their potential as PVD processible chemically amplified resists.

The fourth chapter of this thesis addresses the *investigation of a novel physical vapor depositable resist material concept based on exposure induced salt formation* as a novel high resolution resist for sub 20 nm features. Such resolutions are indicated by the International Technology Roadmap for Semiconductors (ITRS) to be difficult to realize with the existing resist concepts because of the diffusion issue within the currently utilized chemically

amplified resists. The novel resist type is based on the salt formation between a base molecule and an acid released during the exposure process. To establish this novel resist concept, the principle patternability as well as the potential of this resist concept is investigated.

The main objectives of this chapter cover:

a) Testing of the *proof of principle* for this novel resist material concept by investigation of the *dissolution behaviors* of exposed and unexposed resist materials to identify dissolution contrasts between these two states and promising developers.

b) *Combinatorial screening* on *different base molecules* in a mixture with an electron beam sensitive photo acid generator for their pattern performance. The aim is both to identify trends on the resist characteristics in dependence of the utilized base and to find a promising candidate for the estimation of the potential of this novel resist material concept.

c) *Combinatorial optimization* of the *most promising* resist candidate with respect to processing and the goal of realizing high resolution features.

3. Characterization of the pattern capability of the utilized electron beam lithography facilities and the underlying processes of an electron beam exposure

3.1. Introduction

Electron beam lithography (EBL), developed in the late 1960s, is an important patterning technique besides the optical lithography.[122] EBL uses a focused electron beam for the exposure process, whose intensity profile follows a Gaussian distribution. While for optical lithography the patterns are realized by exposure of a shadow mask in one step, the patterns are realized pixel by pixel with the Gaussian beam for EBL. That is why optical lithography is most suitable for the mass production of repeating motives as for microprocessor fabrication by the semiconductor industry. However the ongoing trend towards a further miniaturization of microprocessors demands adjustments especially in the processing step exposure: the targeted change to the wavelength of 13.5 nm (extreme ultra violet; EUV) as well as additional processing efforts, for instance double exposure, become necessary. EBL in contrary – being a direct write technique and offering an high realizable maximal resolution – is established for series with low quantities and thus is the method of choice for high resolution mask fabrication used in optical lithography. The main disadvantage of this direct write technique is the high time consumption due to the "pixel by pixel" exposure. But since the 1970s developments have been performed to increase the throughput of EBL for industrial small series applications.[123] One of the first measures taken in order to achieve that goal was to switch from exposure by a Gaussian beam to exposure by shaped beams – rectangles or triangles, which expose thousands of pixels parallel – and later to projection techniques allowing the exposure of millions of pixels at once. However for academic research a high throughput isn't crucial, so mainly EBL tools with Gaussian beams are used for the investigation of new resists and processing improvements. EBL tools using the Gaussian beam technique can be categorized into two classes: The first class comprises dedicated tools built exclusively for EBL, which are also applied in industry for mask and prototype fabrication. The second class comprises standard scanning electron microscopes (SEMs) combined with a pattern generator. Thus the latter tools can be utilized as normal SEM, but also have the ability to perform EBL.

3.2.   Characterization of the utilized equipment for electron beam lithography

3.2.1.   Characterization of the Zeiss Leo 1530 equipped with Raith Elphy Plus and establishment of a procedure for electron beam lithography

3.2.1.1. Instrument setup

The EBL facility at the Bayreuth Institute of Macromolecular Research (BIMF) consists of a Zeiss Leo 1530 SEM equipped with a Raith Elphy Plus control unit (**Figure 3.1**).

Figure 3.1:   Image of the EBL facility in the Bayreuth Institute of Macromolecular Research: This tool consists of a Zeiss LEO 1530 equipped with a Raith Elphy Plus control unit.

Based on this tool design the fundamental principle of an EBL tool should be discussed. The SEM is equipped with a thermal field effect cathode, the Gemini® column, a mechanical stage, an inlense detector (secondary electrons) and several additional detectors (Everhard Thornley detector for secondary electrons, energy-dispersive X-ray detector, back scattered electron detector, cathodoluminescence detector) not important for the utilization as an EBL device. **Figure 3.2** shows a schematic sketch of the electron beam path in the Gemini column and the relevant devices and manipulation mechanism of this SEM.
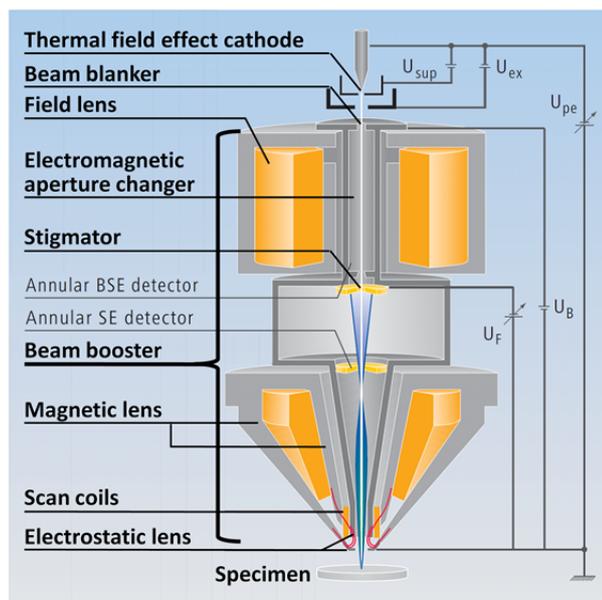
Figure 3.2: Schematic sketch of the principle design of the Gemini column in the LEO 1530. The original figure, published by Zeiss[124], was modified to highlight the parts mentioned hereinafter and to additionally feature the positions of the cathode, the beam blanker and the stigmator.

The thermal field effect cathode (zirconium oxide coated tungsten needle) is the electron source of choice for a Gaussian beam device for EBL guaranteeing stable and constant electron output over longer periods.[122] This feature is very important for an EBL device to enable long exposure processes up to several hours or even days. The source offers acceleration potentials, called extra high tension (EHT), from 300 V to 30 kV tantamount to electron energies from 300 eV to 30 keV. After the beam generation and formation, in this Zeiss SEM the so called beam booster - an additional acceleration potential U_B of 8 kV - is applied near the beam blanker position to make the beam less susceptible to ambient magnetic or electrical interfering fields while passing the optics. However, due to radiation protection the beam booster is only activated for acceleration potentials up to 20 kV. Afterwards, the accelerated electron beam passes next an electromagnetic aperture changer, which offers the option of changing the beam current by partially blanking the beam. Therefore, the aperture changer is equipped with six circular apertures featuring diameters of 7.5 μm, 10 μm, 20 μm, 30 μm, 60 μm, and 120 μm. After passing the aperture, the beam is manipulated by a combination of magnetic and electrostatic lenses utilized for focusing the beam exactly on the sample surface. This ensures an infinitesimal beam diameter, which is mandatory for gathering high resolution images in the SEM mode as well as for the realization of high resolution patterns by EBL. The electrostatic lenses are thereby charged with an 8 kV

potential, decelerating the electrons to the initially adjusted EHT and terminating the beam boosting effect. However, the manipulation of an electron beam by electrical and magnetic field lenses leads to astigmatism due to lens aberrations. This means that the circular beam profile becomes elliptic, resulting in blurry images and reduced patterning resolution. To overcome this issue, a stigmator – consisting of magnetic coils – is installed in the column. By applying magnetic fields during astigmatism correction, the beam profile is modified to become ideally circular and as small as possible on the sample surface.

The deflection of the beam on the substrate is performed by magnetic scan coils. The highest possible deflection determines the field of view, which is defined by the chosen magnification. So a lower magnification results in a bigger field of view, but also in a decreased spatial resolution. Additionally, the substrate itself can be moved by the mechanical stage, where the substrate holder is mounted to. For EBL applications, the substrate holder has to feature a uniform flat metal surface to prevent local charging on the substrate. Two substrate holders in different sizes are available with this feature. In the small one (**Figure 3.3 left**), originally bought together with the EBL equipment from Raith, the useable metal surface for holding substrates has a size of 2.5 cm x 3.5 cm. In addition, this holder offers a built-in Faraday cup for the measurement of the beam current and also a tilting mechanism to compensate for a stage that is not installed in ideal perpendicularity to the column. The big one, designed during this thesis (**Figure 3.3 right**), holds even a complete silicon wafer with a diameter of 10 cm, but the restricted stage drive limits the patterning area to a central zone of 6 cm x 6 cm in size. The construction was performed by the engineering workshop of the University of Bayreuth. Besides a uniform flat metal surface covering the whole diameter, it features a tilting mechanism to adjust the surface to the column and a fixation mechanism for the standard 10 cm diameter wafer in order to allow a precise wafer repositioning.
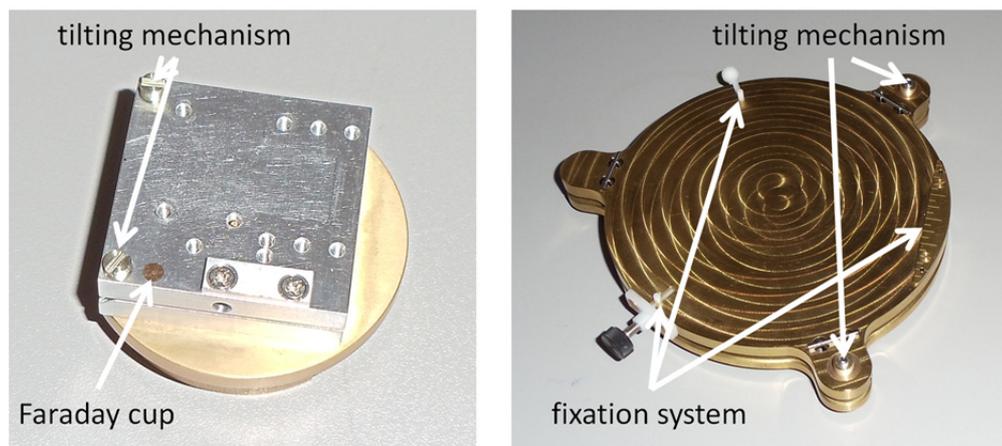
Figure 3.3: **left**: Photograph of the original substrate holder from Raith: Besides a Faraday cup for beam current measurements, it features a tilting mechanism and a flat metal surface. It tolerates a maximum substrate size of 2.5 cm x 3.5 cm. **right**: Image of the self-designed substrate holder: It features a flat metal surface adjustable by a tilting mechanism. It tolerates a substrate size of 10 cm in diameter. Its fixation system allows an exact repositioning and with that an easy rediscovery of the exposure position after the development process. Due to the limited stage drive, the patterning can only be performed in the center area (6 cm x 6 cm) of the substrate.

Because of the interaction of the beam with the sample and substrate, electrons are emitted and detected afterwards. As the inlense detector - located in the Gemini column - features the highest possible spatial resolution for top-view images of all installed detectors, it is the detector of choice for gathering images in SEM mode and performing the beam adjustments for an EBL process in this thesis. However, this detector only works with an activated beam booster. That is why it can only be used for acceleration voltages up to 20 kV. As the realization of high resolution features by EBL requires a proper beam adjustment, the highest possible acceleration voltage for an EBL process is 20 kV for this setup.

Connected to the Zeiss LEO 1530 are the beam blanker electronics (BBE) and the EBL control unit from Raith. The latter processes the mask design and takes control over beam and beam blanker during an EBL process. For the beam blanker, acquired in June 2009, two plates were installed in the Gemini column ahead of the aperture changer. While both plates are charged in the on-state with the potential of the beam booster of 8 kV, in the off-state one of the plates is charged with an additional voltage of 250 V. This results in a deflection of the beam from the aperture and thus the beam is blanked within about 25 ns.[125] This allows the avoidance of unintended exposure during an EBL process.

3.2.1.2. Characterization of the electron beam lithography (EBL) device

For an EBL process, the overall process time for the pure exposure depends on the beam current, the required dose for the utilized resist and the pattern design. Beam current and diameter both are important process variables and viable performance indicators for EBL devices. The LEO1530 allows its adjustment by the aperture changer with different aperture diameters, which will be evaluated later below. For this measurement, the beam is deflected into the Faraday cup of the substrate holder. Then the current is being measured by a picoamperemeter (Keithley 486 Picoammeter) interposed between the ground port and a grounded part of the SEM. The measured beam currents for the standard utilized EHT of 20 kV for the different apertures are listed in **Table 3.1**. However, the beam current depends on the age of the cathode, the vacuum, and the extractor voltage to name but a few. That is why the listed values may just serve as an indicator for the proportions between the different apertures.

Table 3.1: Overview of the available aperture diameters with the corresponding beam current and beam diameter for an EHT of 20 kV.

aperture diameter [μm]	beam current [a] @20 kV [nA]	beam diameter [b] @20 kV [nm]
7.5	0.007	3.7 ± 0.5
10	0.023	2.8 ± 0.5
20	0.091	2.1 ± 0.2
30	0.161	2.1 ± 0.3
60	0.904	5.0 ± 1.9
120	3.652	18.5 ± 6.9

[a] Beam currents depend on e.g. cathode's age, vacuum, and extractor voltage to name but a few. The here presented values just have exemplary character for the proportion between the different apertures.
[b] The noted values for the beam diameter are the mean out of three measurements with their standard deviation.

With the adjustment of the aperture the beam current can be varied by a factor of 530 from 0.007 nA for the 7.5 μm aperture up to 3.652 nA for the 120 μm aperture. So the utilization of an increased aperture diameter can dramatically decrease the overall processing time of an exposure process.

However, the chosen aperture also affects the beam diameter of the resultant beam. This is also a very important device specific variable for the EBL process, as it has to be sufficiently small to realize high resolution features. The determination of the electron beam diameter is performed following the standard procedure of Raith[1], which is based on the NIST procedure E986-04. It is performed with a standard sample featuring Sn-spheres on carbon. On this standard several small Sn-spheres with about 300 nm diameter and ideally no adjacent spheres are selected for the measurement. The selected spheres for the measurement performed during the making of this study are highlighted in the overview SEM image shown in **Figure 3.4 left**. For the measurement itself a line scan is performed on the edge of the Sn-spheres in highest possible magnification. The beam diameter is calculated from the resultant detector signal along the line scan (**Figure 3.4 right**). Therefore the top and bottom level of the detector signal before respectively after the edge of the sphere is determined. The beam diameter is equivalent to the gap between the 80% and 20% detector signal at the edge of the sphere.
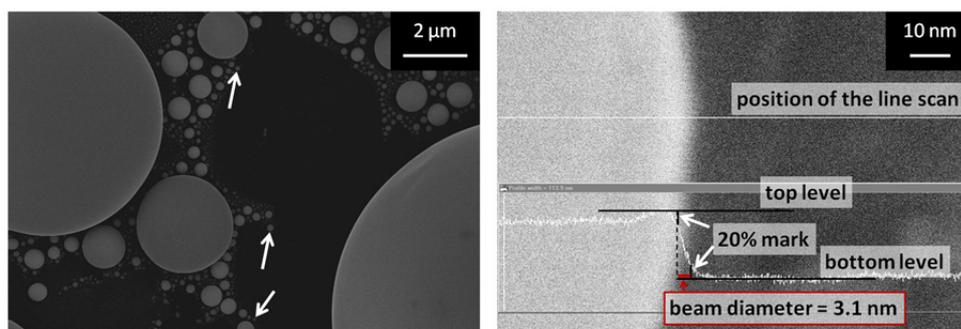
Figure 3.4:   **Left**: Overview SEM image of Sn-spheres on carbon used for the determination of the beam diameter for each aperture. The measurement was performed on the highlighted spheres (white arrows).
Right: Image of a line scan for the determination of the beam diameter: An image is observed at the edge of a Sn-sphere at highest magnification (background image) to control no adjacent small spheres are present at the position of the subsequent line scan. Then the line scan, showing the detector signal along the scanned line, is performed over the edge of the sphere (inset). This is evaluated by identifying the top and bottom level of the detector signal at the edge. The top level represents the detector signal on the edge of the Sn-sphere, while the bottom level stands for the detector signal of the carbon underground. The steep increase in between represents the movement of the beam above this edge and thus a continuous changing contribution of the carbon underground and the Sn-sphere. The beam diameter is defined as the gap between the 20% and the 80% level of the intensity drop exemplarily shown for the in the 7.5 μm aperture resulting in a beam diameter of 3.1 nm. In **Table 3.1** the averages of respectively three measurements beside their standard deviation are presented for each aperture.

---

[1] Oral information of Raith support.

With beam diameters down to 2.1 nm, this EBL tool offers a sufficiently high resolution for investigations of high resolution resists. There is a slight increase in the beam diameter for the 7.5 µm and 10 µm, due to the fact that the beam path of the SEM is optimized for the 30 µm aperture. There is also a significant beam diameter increase for the bigger apertures of 60 µm and 120 µm, disqualifying them for high resolution applications. But due to their high beam current, they dramatically decrease the exposure time for patterning of macroscopic objects, which does not require a high resolution.

3.2.1.3. Procedure of an electron beam lithography process

In the following the procedure is explained for carrying out an EBL process using the Zeiss Leo 1530 equipped with the Raith Elphy Plus patterning generator. At the beginning the actual beam current for the desired aperture is measured. This measured beam current as well as the desired exposure dose D are entered into the exposure parameter calculation of the Raith Elphy Plus software for calculating the step size S and the dwell time t_{dwell} for the planned exposure modes. Such exposure modes can be single dots, single pixel lines (SPLs), and areas. The exposure of single dots is tantamount to separately exposed pixels. For the exposure SPLs –one pixel wide lines – the parameter step size describes the gap between an exposed pixel from a prior exposed one, finally forming a line of pixels. Area exposures are realized by the apposition of several SPLs exposed next to each other always with a gap of one step size in between them. The dwell time describes the time the beam is located on the resist film actually exposing one pixel. These two variables – step size and dwell time – and the beam current define the exposure dose for the selected exposure mode according to the following equations:

dots:

$$dot\ dose\ D_d = (beam\ current\ I * dwell\ time\ t_{dwell}) \qquad (3.1)$$

single pixel lines:

$$line\ dose\ D_l = (beam\ current\ I * dwell\ time\ t_{dwell})\ /\ (step\ size\ S) \qquad (3.2)$$

area elements:

$$area\ dose\ D_a = (beam\ current\ I * dwell\ time\ t_{dwell})\ /\ (step\ size\ S)^2 \qquad (3.3)$$

As the equations show, it is possible to realize a certain desired exposure dose for a dot exposure with different beam currents, realized by different apertures, by a properly chosen dwell time. In a similar fashion the exposure dose for SPLs and areas correlates with the

parameter triple of beam current, dwell time, and step size. However, the minimum adjustable dwell time is limited to 167 ns by the 6 MHz writing speed of the pattern generator in the Elphy Plus control unit. As a consequence, the step size variable has to be used in order to adapt for the reduced process time following an increased beam current. However, an oversized step size would result in a bead chain of the written pixels for SPLs respectively a very rough edge of an area element. For this reason the adjustment of the writing parameter is always a trade-off between shorter process time and the realization of a high pattern quality. The step size's minimum value is determined by the 16-bit deflection system in the Raith Elphy Plus control unit and the size of the design, which should be exposed in one process. Such designs are called write fields and are prepared with the *GDSII Editor* module of the Elphy Plus software. A write field with an edge length of 100 μm for example features a minimum spatial addressability of 1.6 nm. In principle, the write field could be increased to allow bigger designs for exposure. But then the step size would be limited by the addressability, which could ultimately lead to the formation of a bead chain. Additionally, lens aberrations would lead to deviations from the planned design in the corners of big write fields. As a consequence, no bigger write fields than ones with 400 μm edge length were exposed with this tool. To expose bigger areas, usually several write fields are exposed next to each other, which is called stitching. However, the mechanical stage of this tool only allows coarse accuracy (deviation up to 50 μm) in positioning and even shows a drift after long range movements. This fact inhibits the application of stitching or pattern overlay (exposure of two designs exactly on top of each other) with this tool.

After the exposure parameters are adjusted, the exposure positions on the sample have to be set. For this purpose, the Elphy Plus software uses a distinct internal UV coordinate system to define the exposure positions on the substrate (adjust UV window). For the definition of this Cartesian coordinate system usually two easily recognizable positions of the substrate (e.g. edges) are used. This way, it can be realigned after the development process to allow an easy localization of the written patterns. Afterwards, a pattern design is entered into a position list and the respective UV coordinates for the desired position on the substrate are set. In case of multiple exposures of the same design on the sample, multiple entries are prepared the same way or by a matrix copy of the first entry. After all entries in the position list are set, it is absolutely necessary to ensure, that the beam is focused for every desired exposure position on the substrate. Otherwise the exposed pattern would be affected and no optimum result could be obtained. Therefore focus, astigmatism, and aperture alignment have to be

performed. For a process with only one exposure this alignment is made next to the position of the exposure, but with a gap big enough not to affect the final writing position. Therefore a contamination point is created, which is used for this alignment.

However, for an exposure process with multiple pattern design entries, an alignment for every position is time consuming. To overcome this issue from the inevitable substrate tilting, a global adjustment procedure is necessary. Astigmatism and aperture alignment are nearly unaffected from substrate tilting, thus they are only adjusted once prior to the entire exposure process. The distance to the column (and thus the focus of the beam) on the contrary is directly affected by substrate tilting; the focus correction is performed by the adjustment of the working distance. For the global adjustment the Elphy Plus controlling software provides the definition of a focus surface by adjusting the focus in three positions on the substrate. These three positions are chosen in vicinity to the edges of the substrate, so that each exposure position is ideally located within the focus surface. Based on this focus surface, the software automatically corrects the focus during the exposure to enable large area patterning without intermediate focus adjustment. The rest of the exposure process is fully automated.

3.2.2. Jeol JBX-9300FS 100 kV electron beam lithography system

Unlike the Zeiss LEO1530 (equipped with Raith Elphy Plus control unit as described above), the Jeol JBX-9300FS[126] (**Figure 3.5**) is a dedicated EBL tool, designed only for the lithographic patterning process. This EBL tool is located in the Cornell NanoScale Science and Technology Facility (CNF), Cornell University, Ithaca, USA. It was used in this thesis for selected experiments due to its higher acceleration voltage of 100 kV. This tool utilizes a thermal field emission electron source resulting in beam currents between 50 pA and 50 nA. The minimum beam spot size of 4 nm allows the reproducibly realization of sub-twenty-nanometer features. With its 20-bit deflection system a 1 nm address grid is realizable in 500 μm write fields. Due to an accurate positioning of a laser interferometer stage, stitching of write fields and multilayer exposures with an accuracy of less than 20 nm are also possible. Substrate wafers with a diameter of up to 30 cm are applicable, which can be patterned in the central area with a diameter of 22.5 cm.

Figure 3.5: Image of Jeol JBX-9300FS[2]: This dedicated EBL tool is located in the clean room of the Cornell NanoScale Science and Technology Facility (CNF).

3.3. Investigation of equipment's influences on the patterning process

For the investigation of new resist materials by EBL patterning, it is necessary to recognize, analyze, and resolve the origin of negatively affected patterns. On the one hand, the unknown processing conditions of the new resist system itself influence the obtained pattern quality. But on the other hand, the utilized equipment and adjustments in the patterning process can also show an influence.

3.3.1. Influences of parameters utilized for beam adjustment

As already mentioned in the previous chapter, a proper adjustment of the optics in the SEM tool by focus, stigmator and aperture alignment for an EBL process is mandatory. In the following the impact of incorrect adjusted parameters shall be investigated. Poly(methy methacrylate) (PMMA) - an established electron beam resist - was used for these patterning investigations, which were performed with the Zeiss LEO 1530 equipped with the Raith Elphy Plus control unit. The patterning of PMMA, a positive tone resist, is based on the scission of the polymer backbone into fragments by interacting with electrons, resulting in a better solubility in the standard developer. Exposed by very higher doses, this resist can also behave as negative tone resist, as formed radicals lead to crosslinking and thus increasing

---

[2] The image was taken by Marie Krysak (Cornell University).

41

insolubility in the developer solution. In this negative tone exposure dose regime, the material surrounding the exposed areas has become soluble and is removed during development due to the background exposure from backscattered electrons.

A silicon wafer coated with a 55 nm thick film of PMMA prepared by spin coating followed by a post application bake (PAB) at 170 °C for 15 min served as sample. In the following, several patterns were exposed with precisely adjusted parameters of focus, stigmator and aperture alignment as well as defined changes in one of these parameters in similar experiments, which shows the impact of an incorrect adjustment. The exposure was carried out with an acceleration of 20 kV and an aperture diameter of 10 µm resulting in a beam current of 0.031 nA. The pattern consisted of dot arrays with dot doses between 0.12 fC and 491.52 fC as well as line arrays of 25 nm and 50 nm line width with area doses between 40.0 µC/cm² and 206.4 µC/cm², defining an exposure dose gradient for dot and area exposures. The dose gradient was applied to consider necessary adjustments to the exposure dose when changing the adjustment parameters. After the exposure, the development was performed in a mixture of methyl isobutyl ketone and isopropyl alcohol (1:3) for 120 s, followed by a short immersion into pure isopropyl alcohol to stop the development. In **Figure 3.6** a schematic sketch of the pattern layout is presented. Additionally, SEM images of the realized features with the different layouts and the applied exposure doses are shown.

Due to precisely adjusted parameters, lines with a width of 64 nm for the 50 nm features l/s 1/1 (**B**; exposure dose of 57.6 µC/cm²) and respectively 43 nm for the 25 nm features l/s 1/2 (**D**; 82.9 µC/cm²) were received. The difference in the respective exposure dose can be explained by the different pattern layout. In the 50 nm pattern with l/s 1/1, half of the area is exposed, while in the 25 nm pattern with l/s 1/2, it is only one third. This causes a difference in the amount of backscattered electrons formed in the respective area and thus in the background dose which is present for the respective layout. Looking back at the realized features, the trend of getting thicker feature sizes than the actually exposed feature size in the layout is obvious, which could be caused by too high exposure doses. The slightly reduced exposure doses of 48.0 µC/cm² for the 50 nm features (**A**) and of 69.1 µC/cm² for the 25 nm features (**C**) lead to line widths narrower by 4 nm, which however have not been completely developed. Thus a too high exposure dose cannot be responsible for this trend. Instead, the exposure process itself must be responsible for the feature widening.
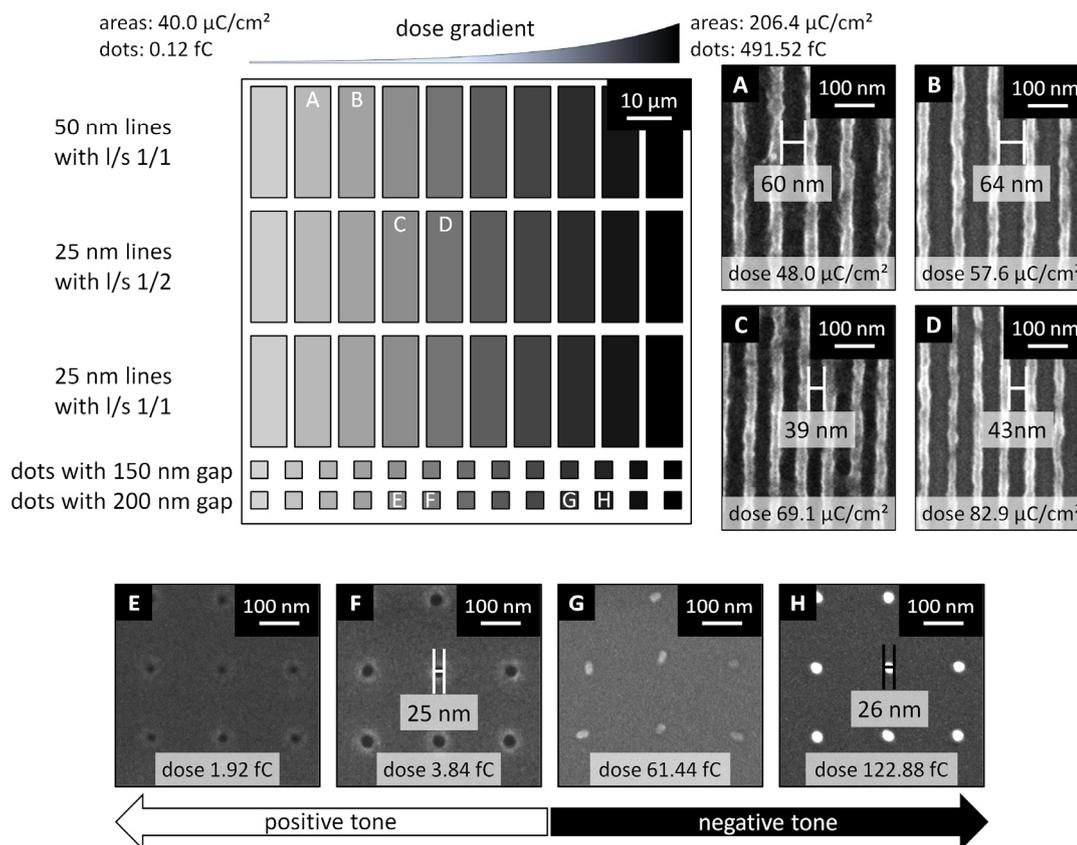
Figure 3.6: Schematic sketch of the pattern design for the investigation of PMMA with precisely adjusted focus parameter and SEM images of the realized patterns: The pattern design consists of an exponential dose gradient from the left to the right for elements out of lines and dots: It ranges for lines from 40.0 µC/cm² to 206.4 µC/cm², while for dots the range was between 0.12 fC and 491.52 fC. Dots were exposed with a gap of 150 nm and 200 nm, while lines were exposed with a width of 50 nm (line to space proportion (l/s) of 1 to 1) and 25 nm (l/s 1/1 and 1/2). Beside the features with optimal dose, also the slightly underexposed features are presented. The exposed 50 nm wide lines (l/s 1/1) for an exposure dose of 48 µC/cm² resulted in not fully developed and thus slightly underexposed lines (**A**) with a width of 60 nm, while for 57.6 µC/cm² optimally exposed features (**B**) with a slightly bigger width of 64 nm were realized. The 25 nm wide lines (l/s 1/2) gave underexposed features (**C**) at 69.1 µC/cm² with a width of 39 nm and optimal exposed ones (**D**) at 82.9 µC/cm² with a width of 43 nm. The 25 nm lines with l/s 1/1 could not be resolved and thus show a limit of this EBL equipment. In contrary to the line features, the much steeper dose gradient for the dot features allowed the realization of positive tone dots for low exposure doses as well as negative tone ones for high exposure doses. As the pattern with a gap of 150 nm and 200 nm show similar behavior, only the latter will be evaluated here. Slightly underexposed positive tone dots (**E**) were realized for an exposure dose of 1.92 fC, while 3.84 fC resulted in well exposed ones with 25 nm diameter (**F**). The much higher exposure dose of 61.44 fC (**G**) shows the transition of this resist to negative tone as collapsed negative type dots were realized. Well exposed negative type dots were realized for the next higher exposure dose of 122.88 fC (**H**) with a diameter of 26 nm.

The area exposure is performed, as already mentioned, dot by dot in several lines with the adjusted step size in between until the programmed feature with i.e. 50 nm is completely filled. However, the beam has no infinitesimal diameter, so the resultant line width is enlarged for the first and last line respectively by a half beam diameter. The effective beam diameter for the exposure not only depends on the beam diameter of the EBL device (evaluated for the LEO1530 in chapter 3.2.1.2), but also on the interaction of the electrons in the resist. There the forward scattering, which will be discussed in detail in chapter 3.3.3, widens the beam in dependence of the acceleration voltage, so the effective beam diameter is bigger compared to the measured beam diameter values (presented in **Table 3.1**). This process occurs independently from the feature size, so smaller elements are affected relatively stronger. The exposed 25 nm features show a widening of 18 nm while the exposed 50 nm features show nearly the same widening of 14 nm. The with 25 nm lines and l/s 1/1, also exposed features, could not be resolved at all, obviously due to the widening from the effective beam and the, already discussed, relatively high amount of backscattered electrons in the l/s 1/1 design.

It's not feasible to estimate the effective beam diameter and thus the resolution limit of the EBL device from this area exposure due to the fact that the local exposure dose is the sum of the locally exposed dot dose and the dose fractions of the widened beam of the neighboring exposed dots. Instead, such estimation is possible from dot exposures, where only one spot is exposed. Therefore, in this study, dots with different doses were exposed with a gap of 150 nm and 200 nm. As the patterns with a gap of 150 nm and 200 nm show similar behavior, only the latter ones will be evaluated here.

In this experiment dots were realized in positive tone PMMA with a minimal feature size of 25 nm in diameter for a dose of 3.84 fC (**F**) and in negative tone PMMA 26 nm diameter for a dose of 122.88 fC (**H**) respectively. For the positive tone PMMA, the lower exposure dose of 1.92 fC (**E**) leads to not fully developed dots. For the negative tone PMMA, the next lower exposure dose of 61.44 fC (**G**) was the lowest dose showing negative tone features. However, these had an oval shape obviously due to collapsing. Consequently, the realized dot diameter of around 25 nm in positive as well as in negative tone PMMA represents the minimal realizable resolution and thus gives an estimation of the effective beam diameter for a 55 nm thick PMMA resist at an acceleration voltage of 20 kV and the utilized 10 μm aperture for the Zeiss Leo1530.

Based on the determination of the maximum pattern ability with precisely adjusted exposure parameters, the influence of the single parameters can be discussed. This discussion focuses

on the positive tone PMMA patterning of dot features with 200 nm gap with defined changes in the parameters focus, stigmator alignment and aperture alignment, as the resultant features allow the direct evaluation of changes in the beam shape. In **Figure 3.7** SEM images of the highest resolution dot features using both precisely adjusted (**A**) and redefined (**B-F**) parameters are presented. All of these features have been realized for a similar exposure dose of 3.84 fC.
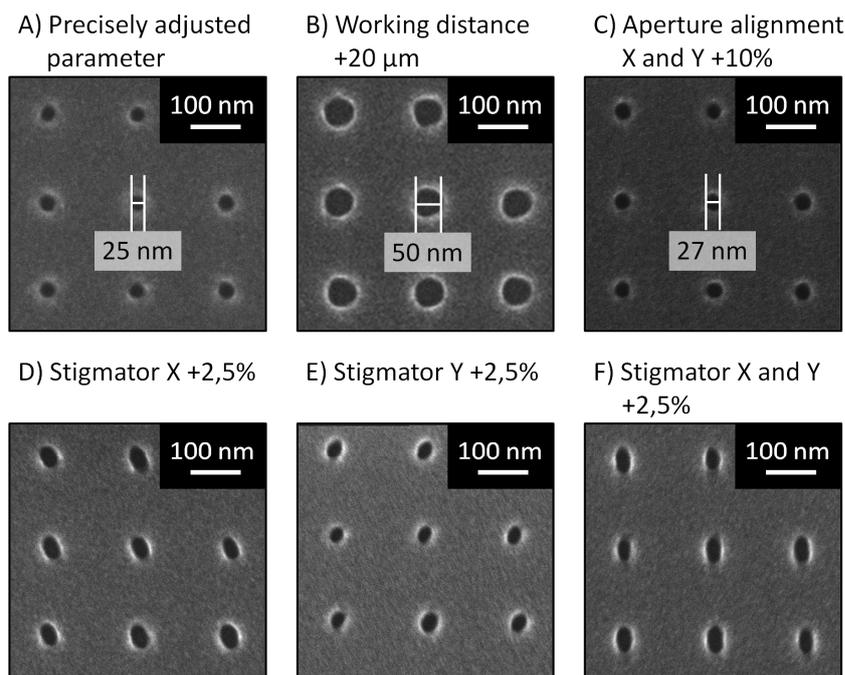
Figure 3.7: SEM images of dot features resultant from precisely adjusted parameters (**A**) and from defined changes in the processing parameters (**B-F**): For comparability, all images were observed at a similar exposure dose of 3.84 fC. The change in the working distance (**B**) dramatically influences the effective beam diameter resulting in an increased dot diameter. The change in aperture alignment (**C**) in contrary has only minor influences on the resultant dot features. The stigmator alignment - as already mentioned - is responsible for the compensation of astigmatism appearing to an electron beam when passing electrostatic or magnetic lenses. Such compensation is performed in X and / or Y direction for the correction of astigmatism (**D-F**) occurring in different spatial directions.

The varied parameters influence the beam both in diameter and in shape. The major effect on diameter enlargement turns out to be the working distance responsible for focus adjustment. A change of only 20 μm in working distance doubles the beam diameter from 25 nm (**A**) to 50 nm (**B**). So it is necessary to precisely perform the three point alignment using the Raith software to reduce deviations in working distance and to thus minimize the beam diameter.

After adjusting the three point alignment in a square of 6 cm edge length, the remaining deviation in working distance is ideally around 4 μm.

The change of the aperture alignment (**C**) resulted in a minor increase of the beam diameter from 25 nm to 27 nm. This beam diameter increase is negligible small, although the aperture alignment change was enormous, meaning that this parameter has no huge impact on patterning performance. The stigmator alignment – manipulation of the beam with magnetic fields in the column – is responsible for the compensation of the beam's astigmatism. This stigmator alignment was varied, first using only the X axis (**D**), then using just the Y axis (**E**) and finally varying in both directions (**F**), each time at a degree of 2.5 %. Depending on the set stigmator alignment variation in X and/or Y, the circular beam shape is elongated, while in the direction perpendicular to it, the width stays close to the width in the beginning and results in an ellipse. Thus this factor has a big impact on the beam shape and with that on the created patterns. However, a precise adjustment of focus and stigmator requires also the correctly setting of the aperture alignment. In conclusion, all parameters should be set in the alignment procedure properly to allow high resolution patterning, so that new resist systems can be studied under consistent conditions within the patterning process.

3.3.2. Impact of the mechanical stage in LEO 1530 on the patterning process

With its coarse accuracy in positioning and its irregular occurring stage drift, the mechanical stage inhibits the application of stitching and the pattern overlay technique. The former separates the overall pattern design in several smaller write fields, which are exposed consecutively in direct vicinity. This allows a more precise positioning of the beam and thus a higher patterning quality. In the latter technique, the exposure is performed twice with respectively half of the exposure dose, which shows advantages in the suppression of exposure defects. As both techniques are not applicable due to the mechanical stage, write fields are designed in this work to feature the whole design, which will be exposed in one patterning process. If the experimental layout requires the application of several write fields in vicinity to each other to ensure a similar processing, they are still placed with enough space in between to prevent overlap due to possible stage drift. Even so, the stage drift can interfere with the exposure process of a single write field, as it is shown in **Figure 3.8**.
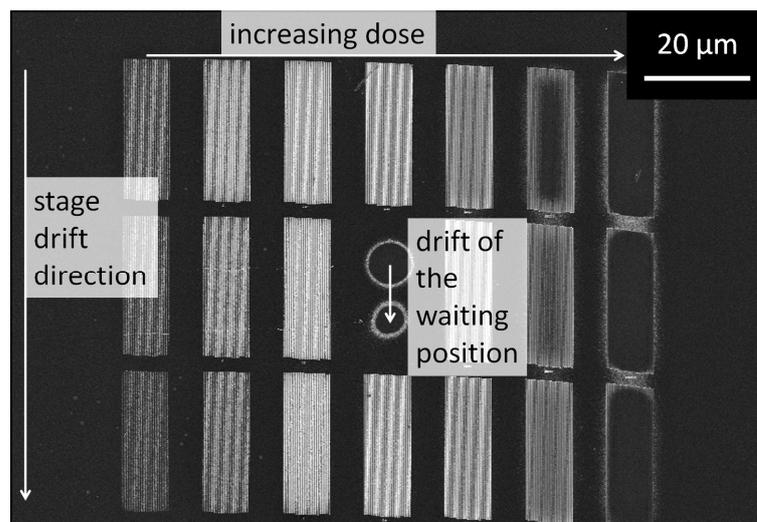
Figure 3.8: SEM image of a patterned negative tone resist showing the impact of an occurred stage drift during the exposure process: The exposed pattern features a dose gradient associated with increasing dwell times from left to the right from block to block (each block consists of 44 100 nm lines with 100 nm space in between). Additionally, free space is provided for the waiting position of the electron beam in the middle of the write field as the exposure was performed without beam blanker. During the exposure of this write field, the stage and thus the substrate was drifting, obviously noticeable for the waiting position at the beginning (top position) and after the exposure is completed (bottom position). The drift can also be seen by the downwards shifted blocks and even within the blocks of the higher doses.

After moving to the targeted position for the exposure of a write field, the stage still moves at a speed of several nanometers per second (**Figure 3.8**). Due to this stage drift, the exposed lines as well as the waiting position shifted during the exposure of the whole write field (overall exposure time of shown write field: 103 s). To avoid this issue, a waiting time between the movement step and the exposure start was implemented. But the stage drift can continue even for minutes, thus a sufficiently long waiting time dramatically increases the overall processing time. Another approach with less impact on the overall exposure time is to divide the movement process into two parts: The first, main part of the movement runs to a position, which is 0.1 mm in U and V coordinates apart from the targeted exposure position. With the second part of the movement, the final position is approached. Due to this second short range movement, the stage drift can be dramatically reduced. Thanks to this technique, in the experiments performed afterwards, no such issues occurred.

3.3.3. Influence of the acceleration voltage on the patterning process

The acceleration voltage determines the energy of the electrons, so-called primary electrons, in the electron beam. The energy of these electrons decreases by elastic and inelastic scattering processes while traveling through the resist film and the substrate, thereby forming low energy electrons, the so-called secondary electrons. These secondary electrons have energies between 2 eV and 50 eV.[122] This energy level is in the range of the energy in molecular bonds of organic material. That is why secondary electrons are responsible for the bulk of the exposure process. These perform the bulk of actual resist exposure process. They scatter by a few nanometers and in this way also affect areas up to 10 nm apart from the effective beam diameter, which limits the theoretical maximum resolution of EBL. Such secondary electrons are formed from primary electrons even if they are scattered, so their way through the resist and substrate is of interest for understanding the exposure process and the effects occurring from a changed acceleration voltage. The physical processes of electron scattering are well understood and so the pathway of electrons crossing solid materials can be simulated by Monte Carlo methods. Such a simulation has been performed during this study for 10 kV as well as for 20 kV acceleration voltage with the Casino software. For both theoretical experiments, a PMMA film of 100 nm thickness on a silicon substrate and a beam radius of 2 nm were assumed (additional simulation parameters are described in the experimental part; chapter 9.1.5). The results of the simulated pathways of 1000 electrons for the respective acceleration voltage are shown in **Figure 3.9**.

The pathway of an electron through solid material is characterized by small angle as well as large angle scattering. The electrons are slightly deflected by small angle scattering, while they maintain their preferential direction. This so called forward scattering is the reason for the widening of the effective beam diameter becoming particularly obvious at the bottom of the resist layer. This can be seen in the inset in **Figure 3.9A** showing an enlarged cross section of the impact region for utilizing an electron beam with 10 kV acceleration voltage. The diameter of the beam at the bottom of the 100 nm PMMA film is dramatically increased compared to the original beam, which makes this phenomenon an issue for higher film thicknesses. The deflection of the electrons thereby depends on the kinetic energy, thus forward scattering can be reduced with higher acceleration voltages. This is shown in the simulation for an acceleration voltage of 20 kV (**Figure 3.9B)**, where the beam diameter is roughly halved compared to the forward scattered beam of the simulated 10kV acceleration voltage.
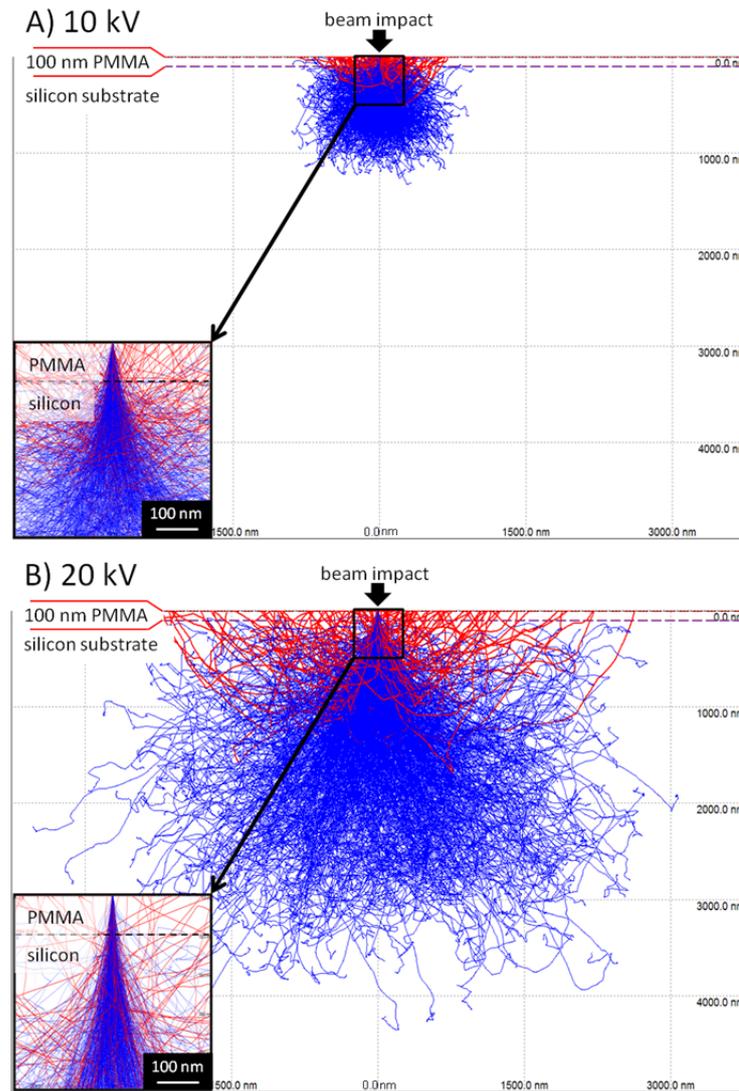
Figure 3.9:   Images of the primary electron pathways simulated by the Casino software: The simulation was performed assuming a PMMA film of 100 nm thickness on a silicon substrate, a beam radius of 2 nm, a total number of 1000 electrons and an acceleration voltage of 10 kV for image **A** respectively 20 kV for image **B**. The pathways of backscattered electrons leaving the sample are colored in red, while the pathways of the scattered electrons lost in the sample are colored in blue. **A**: With an acceleration voltage of 10 kV, the electrons penetrate the substrate up to a depth of around 1.2 µm and within a radius up to 0.9 µm away from the impact position. In the inset, the impact region is enlarged featuring a huge amount of strongly scattered electrons beside a huge amount of backscattered electrons. The numerical evaluation of the redmarked backscattered electrons leaving the sample shows a total of 138 electrons. **B**: For the acceleration voltage of 20 kV, the maximal penetration depth is around 4 µm and the electrons even reach positions within a radius of 3 µm away from the impact position. As the inset displays, the electrons now tend to keep their straight direction into the sample and the amount of backscattered electrons in proximity to the impact position is dramatically decreased. This is a consequence of a nearly similar amount (124) of backscattered electrons leaving the sample and the increased affected area.

In contrast to small angle scattering, electrons are even scattered backwards by large angle scattering and are so-called backscattered electrons (colored in red in **Figure 3.9**). Due to this behavior, these electrons can cross the resist layer for a second time and may expose the resist at these exit positions. That's why the surrounding area of the exposed feature exhibits a background dose. This additional dose differs: In the middle of comparatively larger exposed features, the dose is evenly distributed compared to e.g. corners of exposed features. This fact results in differently exposed areas of resist material due to a varying local dose. Thus elements of a feature placed inside an area with a high background dose might be overexposed, while other elements of this feature with a low local background dose might be underexposed, although the entire feature is exposed with the set dose. This is known as the proximity effect. To prevent this effect, usually proximity calculations are performed simulating the effect of electron scattering. This allows the adjustment of the exposure dose for a respective element considering the level of the local background dose. However, such calculations are specific for the used resist layer as each resist system contributes differently to electron scattering. The most important parameters of such a calculation are substrate material, resist material composition, resist layer thickness, acceleration voltage of the beam and the pattern design itself. Instead of proximity calculations, in this work an alternative way was followed to realize features unaffected from the proximity issue. For this purpose the write field design was improved (see chapter 3.4) to contain elements which are large enough to feature a uniform background dose in their central part.

It is also possible to reduce the background dose itself by increasing the penetration depth of the electron beam into the substrate. Thus less of the backscattered electrons cross the resist layer in direct vicinity to the beam impact position again. This can be realized by increasing the higher acceleration voltage or even by changing the substrate to materials with lower atomic numbers. The effect of a higher acceleration voltage can be seen in the insets in **Figure 3.9**. They show that the amount of backscattered electrons is decreased dramatically in vicinity to the beam impact position. This is a consequence from a slight decrease in the number of backscattered electrons leaving the sample (138 for 10 kV; 124 for 20 kV) and the dramatically increased affected area (roughly 0.9 μm distance from the beam impact position for 10 kV, respectively 3 μm for 20 kV). What this means for the actual patterning is that the area in vicinity to an exposed element is affected from a higher background dose when patterned with a lower acceleration voltage compared to the experiment with a higher one. Such a higher background dose can result in the formation of residues in vicinity to exposed

elements. This effect can be seen in **Figure 3.10**, where SEM images of features patterned with 20 kV (Leo1530 with Raith Elphy Plus) respectively 100 kV (Jeol JBX-9300FS) are shown.

The patterned negative tone resist system - investigated in detail in chapter 4 - forms residues due to the background dose in between the features. With 20 kV a huge amount of residues is formed, while with 100 kV significantly fewer residues are formed. Consequently, a higher acceleration dose significantly reduces the background dose due to backscattering.
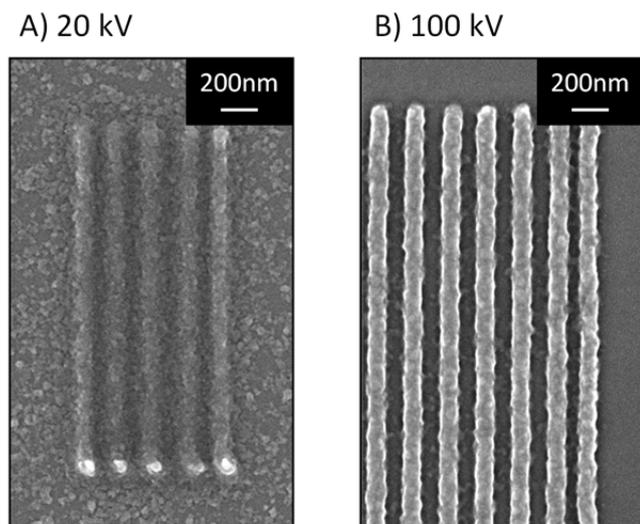
Figure 3.10: SEM images of features realized for patterning with 20 kV (Leo1530 with Raith Elphy Plus) respectively 100 kV (Jeol JBX-9300FS): Due to backscattering, the negative tone resist - investigated in detail in chapter 4 - forms different amounts of residues in dependence to the background dose. The features realized for 20 kV (**A**) show a huge amount of residues in vicinity to the lines due to backscattering. For 100 kV in contrary, the residue formation was strongly reduced due to the applied higher acceleration voltage. However, even for the higher acceleration voltage some residues are formed.

3.3.4.   Advantages and disadvantages of the usage of an electrostatic beam blanker

As already mentioned, the electrostatic beam blanker prevents exposure defects by blanking the electron beam between the exposures of elements. In **Figure 3.11**, SEM images of the occurring exposure defects in absence of an electrostatic beam blanker are shown: electron beam movement path between different write fields (left), the beam's waiting position in a write field (left) and the settling dot at a pattern element in the beginning of the exposure (right).
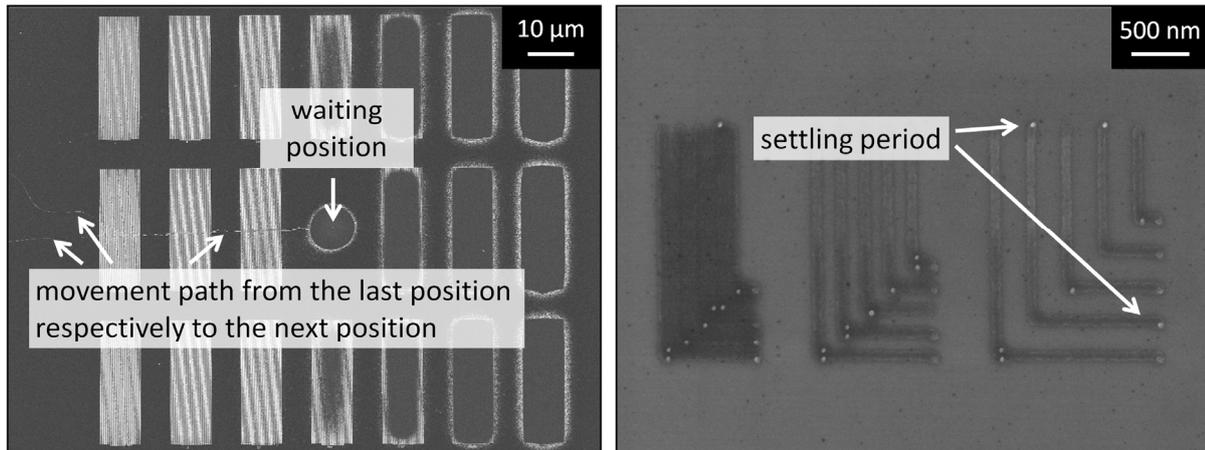
Figure 3.11: SEM images of exposure defects occurring for exposures without an electrostatic beam blanker: **Left**: In the middle of the image the electron beam's waiting position is shown, where it is placed before and after the exposure process of the write field, as well as the traces of the moving stage between different exposure positions. **Right**: Spots with increased exposure dose are formed at the beginning of each rectangular pattern element due to the settling period.

A major issue is the so-called waiting position of the electron beam between the exposures of pattern elements. At this defined position in the write field the beam is positioned always when no exposure of pattern elements takes place. This comprises the movement between different exposure positions, the times between the movement and the start of the exposure as well as the time between the exposure of the last element in a write field design and the subsequent movement to the next position. However, during the movement between different exposure positions the substrate is moved, thus the trace of the movement is exposed. This can be seen in **Figure 3.11 left**. During the waiting times before and after the movement process in contrary, the write field is stationary on the substrate and thus the beam is indeed positioned on a single position (waiting position) on the substrate. As the electron beam dwells relatively long on this position, it – and due to the backscattering also its adjacent area – is totally overexposed (**Figure 3.11 left**). While for exposures with beam blanker the beam is blanked during this periods, this waiting position has to be considered when conducting an electron beam exposure without a beam blanker. Consequently, the write field has to be designed without features close to this position.

The pattern formation is also affected as it is interfered by the settling time while exposing without beam blanker. Time for settling is necessary to ensure that the beam has reached the desired position of the respective element in the write field instead of being somewhere else

due to a delay between the computer signal and the reaction of the scan coils for the beam deflection. Usually this time period is automatically set to 50 ms per moved millimeter. Due to this settling time, a spot of increased intensity is received at the beginning of an element while exposing without beam blanker (as shown in **Figure 3.11 right**). These spots can be avoided by reducing the settling time to zero, but in this case, a curved start of the structure element can occur due to a not settled beam.

Besides these above described effects during an exposure process without a beam blanker, the installed beam blanker from Raith has one main disadvantage: If the beam blanker electronics (BBE) is switched on, the beam is affected by a 50 Hz fluctuation, which consequently influences the SEM performance (as shown in **Figure 3.12**). This frequency was determined out of the gathered image by the Raith support.

A) Beam blanker off
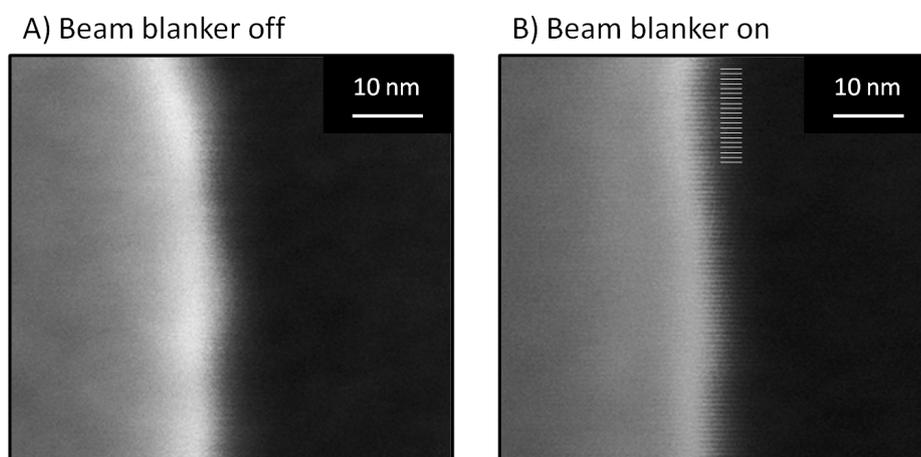
B) Beam blanker on

Figure 3.12: Sections of taken SEM images (500000 x magnification) clarify the consequence of the beam blanker electronic (BBE) switched on: **A**: SEM image with BBE switched off shows a smooth edge of a pattern of an organic resist material (bright; dark is the substrate). **B**: SEM image with BBE switched on shows a fluctuating beam resulting in a sinus curve on the edge. The maximums of the sinus curve are highlighted in the upper part.

A prior smooth edge (**Figure 3.12 left**) in the gathered highly magnified image of a pattern shows reduced image sharpness due to sinus profile at the edge with BBE switched on (**Figure 3.12 right**). These irregularities result from small beam deflection originated from the 50 Hz fluctuation of the BBE and slightly shifts the beam positions during the image is taken line by line. The investigation of the origin of the 50 Hz fluctuation led to a second source of disturbance: The fluorescent lamp of the room the SEM is operating in results in a similar fluctuation. These fluctuations also affect the beam during the EBL exposure process and thus the received patterns can exhibit periodic defects shown in **Figure 3.13**.
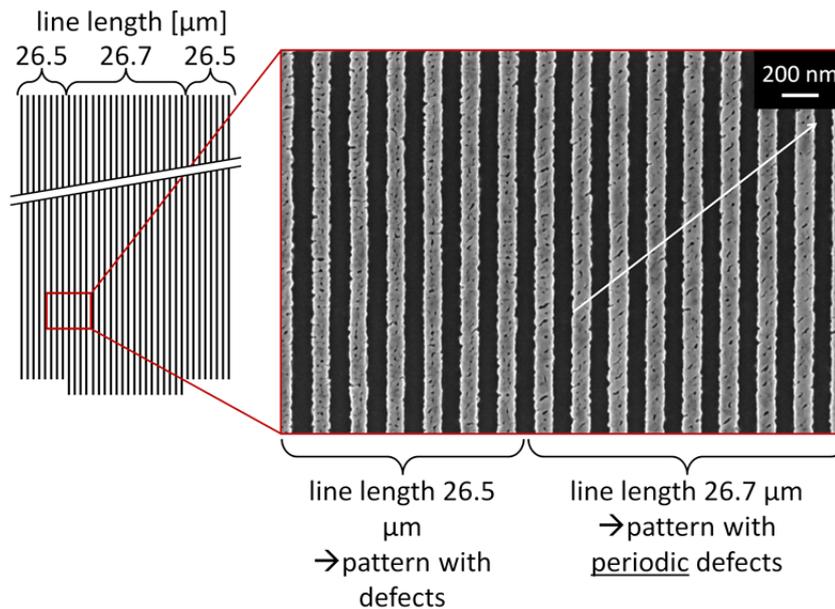
Figure 3.13:   **Left**: Schematic sketch of the line length variation in motive utilized for the exposure with BBE switched on of a not chemically amplified resist. **Right**: SEM image of the 100 nm wide features (l/s 1/1) realized at the transition between the different line lengths: For the longer line length of 26.7 μm, the 50 Hz fluctuation fits the exposure time of each single pixel line in the area element, so that neighboring pixels show a similar dose variation. This results in the formation of periodic defects, which are oriented towards the marked direction. For the shorter line length of 26.5 μm, no cooperative effect occurs, thus features were formed with spot-like defects.

The experiment performed with BBE switched on clearly shows a dependence of periodic defects formation on the line length. While the features with 26.7 μm line length show periodic defects, spot-like defects are formed for the line length of 26.5 μm. Thereby, the line length determines the time needed for the exposure of each single pixel line a 100 nm wide feature is comprised of. Beside the line length, this time also depends on the dwell time of each pixel and the step size. In **Figure 3.14**, the effects of beam deflections on single pixel lines (SPLs) are schematically sketched beside their impact on the exposure of area elements with different line lengths.
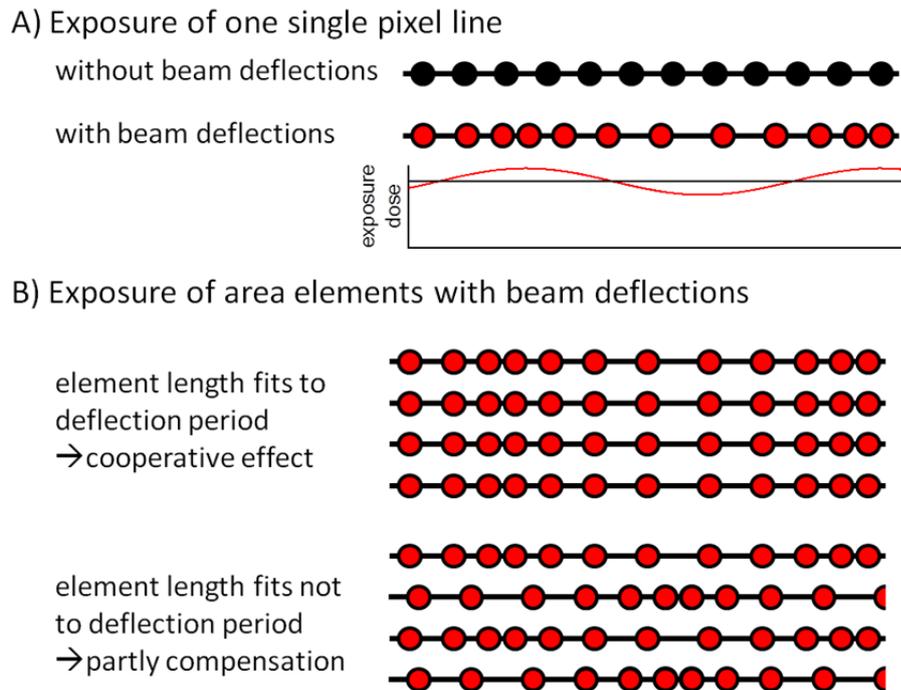
Figure 3.14: **A)** Schematic sketch of beam deflections on the exposure of a single pixel line (SPL): For simplicity, the beam deflection occurs along the SPL. Without beam deflections, the dot-like exposure is performed with the gap of the step size. The beam deflections in contrary lead to a periodic change in the exposure position along the SPL. This results in a periodic change of the exposure dose in contrary to the linear dose profile for the absence of beam deflections. **B)** Schematic sketch of the beam deflections effect on the exposure of area elements: The exposure of area elements is performed by the successive exposure of SPLs beside each other. In the first case, the element length fits the deflection period, which results in a cooperative effect. The consequence is a periodic change of the area elements exposure dose along the element. In the second case, where the element length is not fitting, the fluctuation in the exposure dose of a single SPL is partly compensated by the neighboring SPL, Thus the exposure dose is distributed more homogeneously.

Due to the beam deflections the dots for the SPL exposure are slightly repositioned. This results in a periodic changing exposure dose along the SPL in contrary to the homogeneous behavior without beam deflections (**A**). This periodic changing exposure dose has impact on the exposure of area elements, because therefore successive SPLs are exposed beside each other (**B**). In the first case the exposure time for one SPL fits to the deflection frequency, so that in neighboring SPLs the areas with high respectively low exposure dose are adjoined. This cooperative effect results in a macroscopic dose fluctuation along the area element, which is responsible for the formed periodic defects for 26.7 µm length and the 50 Hz fluctuations of the BBE. In the second case the exposure time of one SPL does not fit to the

fluctuation frequency, so that the low exposure dose of one SPL are adjoined with areas of high exposure dose from the neighboring SPL. This results in partly compensation of the dose fluctuation. This represents the case of the 26.5 μm length. However, the occurring spot-like defects for this length indicate that still areas can occur, where a slightly decreased exposure dose is present.

As already mentioned, the exposure time for a SPL depends on the step size and the dwell time. These two parameters together with the beam current define the exposure dose and thus the appearance of such periodic defects is also dose depended. The standard pattern designs usually contain a dose gradient, realized by increasing the dwell time for different elements. Consequently several realized doses can show periodic defects, while other doses do not.

The approach of exchanging the BBE has not solved the issue of the 50 Hz fluctuations. Indeed, the manufacturer afterwards confirmed that this issue is a known phenomenon. However, for resists usually used by the industry, no such issues are known. Indeed, this issue occurred only during the investigation of the non chemically amplified resists based on salt formation, which features a very sharp development contrast (chapter 6). Similar to the chemically amplified resist investigated in chapter 4, the patterned non chemically amplified resist PMMA with its weak development contrast showed no such defects. For the chemically amplified resist type, local dose fluctuations are additionally compensated by the acid diffusion. Thus for these resist types, the beam blanker only shows the mentioned advantages.

3.4.   Overview of write field design's progress

A write field design has to include proper features to evaluate properties and potentials of new resist systems. These designs were constantly adjusted and improved during this thesis to offer a proper tool for the characterization and optimization of investigated resist systems.

The write field design (**Figure 3.15**) formerly used for the realization of high resolution patterns had been created by Wolfgang-Andreas Bauer. This design was the first one to be utilized for the optimization of new resist systems and provided a basis for improved concepts.
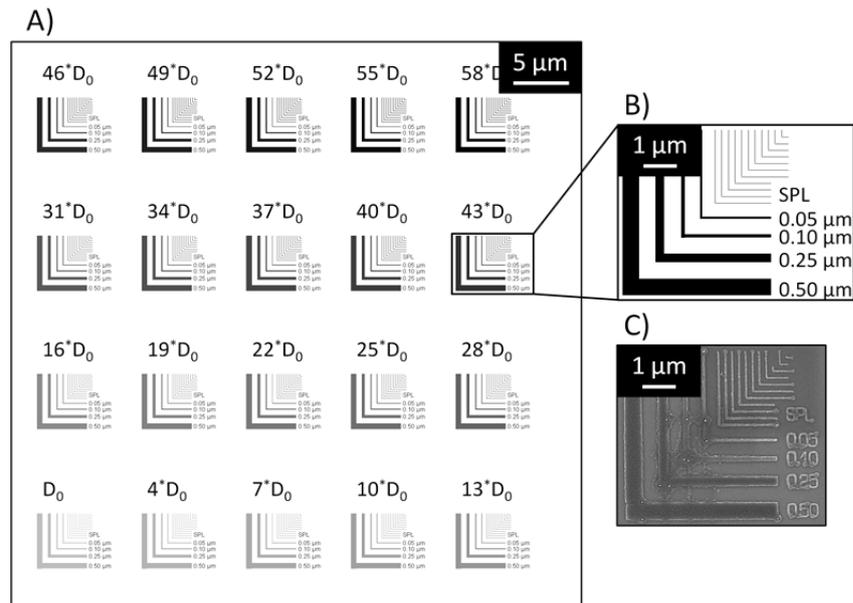
Figure 3.15: Schematic sketch of the write field design created by Wolfgang-Andreas Bauer: The write field design features a linear internal exposure dose gradient ranging from the start dose D_0 in the bottom left to 58^*D_0 in the top right (**A**). This dose gradient is adapted to a basic motive enlarged in the right (**B**). It features L-shaped single pixel lines (SPL) and area elements with widths of 0.05 μm, 0.10 μm, 0.25 μm, and 0.50 μm. **C** shows a SEM image of features realized by Wolfgang-Andreas Bauer that were exposed to this write field design.[127]

This first write field with an edge length of 51.2 μm was designed for the combinatorial optimization of new resist systems and consists of 20 patterns. Each pattern consists of eleven L-shaped single pixel lines with a gap of 200 nm and area elements of 0.05 μm, 0.10 μm, 0.25 μm, and 0.50 μm widths with a gap of 500 nm, respectively. The patterns differ in the applied exposure dose for single pixel lines as well as for area elements. The dose variation was performed in a linear fashion, thus defining an exposure dose gradient from the start dose D_0 in the bottom left to 58^*D_0 in the top right.

The improvements for the 2nd generation write field design were orientated towards the standard processes for the evaluation of resist performance. In such standard processes, the realization of features with defined dimensions is investigated, which is important for the industrial application in e.g. the production of transistors with partly complicated structures. For this purpose the single pixel lines and the single area elements in the basic motive were exchanged by multiple L-shaped 100 nm wide area elements (**Figure 3.16**).
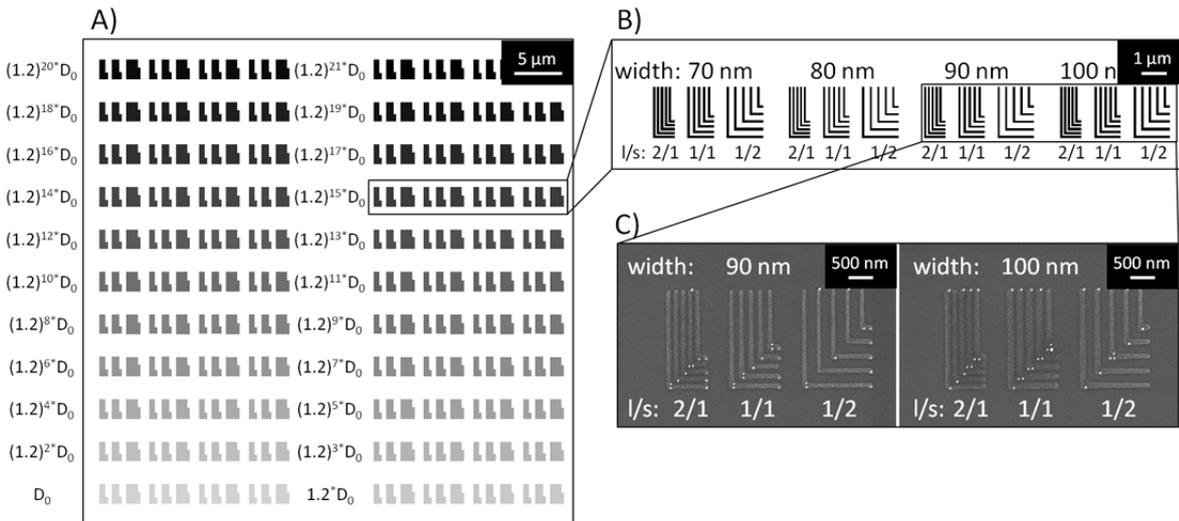
Figure 3.16: Schematic sketch of the 2nd generation write field design: It features in a 51.2 µm x 51.2 µm sized write field an exponential exposure dose gradient, which is performed on 22 feature arrays, each of them assigned with a multiple of the starting dose D_0 (**A**). One array (**B**) contains four similar sets of elements differing in the written element width (70 nm, 80 nm, 90 nm, and 100 nm) while the space in between is enlarged by the difference of the element width to 100 nm to allow the regarding of by standard to thick written lines. Each set of different written element width consists of respectively five L shaped areas for line to space proportions (l/s) of 2/1, 1/1 and 1/2 based on the desired 100 nm feature width. In **C**, two SEM images of features with element width of 90 nm and 100 nm are present, both of them realized for the same exposure dose. They clearly show the effect of the smaller written size especially for the l/s 1/1. For the 100 nm width, the resist material in the space is not completely removed, while for 90 nm the lines are distinct.

These multiple L shaped area elements allow an investigation of defined features in vicinity to similar elements with a defined gap realized by the l/s 2/1, 1/1 and 1/2. These elements together with similar motives for the observation of overexposed features form the basic array (**B**) for the exposure dose gradient. These motives feature reduced area width of 90 nm, 80 nm and 70 nm, while the respective space was increased by the width difference. The effect of such a smaller width can be observed in the SEM images (**C**), showing patterns for 100 nm and 90 nm: The l/s 1/1 features with a width of 100 nm are still connected by resist residues, whereas they are separated for a width of 90 nm. The basic array is applied in a matrix-like shape in the write field and the allocated exposure doses differ for each case to feature an exposure dose gradient (**A**). The linear dose gradient in the original design got replaced by an exponential dose gradient (increase factor of 1.2 giving an overall dose range from 1x up to

46x the base dose D_0) to overcome different growth rates for lower and higher doses and thus to ensure a more homogeneous dose variation.

In experiments using this write field design, issues occurred with the L-shaped area elements - as already described in chapter 3.3.4 - resulting in dots with higher exposure dose in the corner (as can be seen in the SEM images in **Figure 3.16**). Such dots originate from the settling period during an exposure step without utilizing a beam blanker. The L-shaped elements are separated into two rectangles for the exposure process and thus these dots occur at the beginning of each elongated area in the pattern.

Because of the negative effect of these dots to the subsequent evaluation of the patterned elements, the L-shape pattern had to be simplified to an I-shape pattern in the 3rd generation write field design, featuring parallel lines of equal length (**Figure 3.17**).
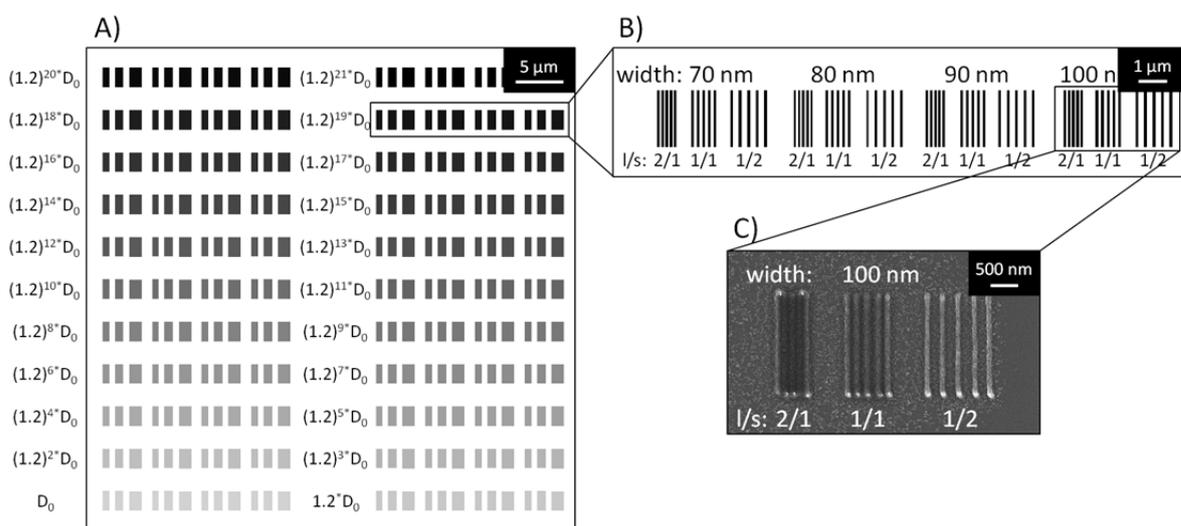
Figure 3.17: Schematic sketch of the 3rd generation write field featuring an edge length of 51.2 µm and an exponential exposure dose gradient from D_0 to $1.2^{21}*D_0$ ($\triangleq 46*D_0$). The exposure dose gradient is performed using 22 feature arrays, each assigned with a multiple of a set starting dose D_0 (**A**). One array contains four similar sets of elements differing in the written element width (70 nm, 80 nm, 90 nm, and 100 nm) while the space in between is enlarged by the difference of the element width to 100 nm in order to allow the observation of by standard to thick written lines. Each set of different written element width consists of respectively five I shaped areas showing l/s of 2/1, 1/1 and 1/2 based on the desired 100 nm feature width (**B**). The SEM image in **C** shows patterns realized with an element width of 100 nm. The visible residues around the features are caused by the utilized resist, which is quite sensitive to backscattered electrons.

These 2 µm long I-shaped patterns were applied in arrays (**B**) with different area widths (100 nm, 90 nm, 80 nm, and 70 nm), different line to space proportions (2/1, 1/1, and 1/2),

and an exponential exposure dose gradient (increase factor of 1.2 of the starting dose D_0; overall dose range from 1x up to 46x) (**A**). Observed features are exemplarily shown (**C**) for a resist which is very sensitive to backscattered electrons, and thus forms clearly visible residues around the features.

In literature the evaluation of resist performance is usually performed with designs featuring a set of multiple long lines. These are necessary for the evaluation of the line edge roughness (LER), which is an important performance characteristic of a resist system. The LER describes the deviation of the realized edge from the ideal linear shape. For its correct calculation it is necessary to realize a set of long line-shaped elements, which allow a statistical evaluation of this deviation out of top-down SEM images of the developed features. In this context a 4th generation write field design (see **Figure 3.18**) was adapted to comprise a set of 30 lines with a width of 100 nm and a l/s of 1/1, and a length of 26.5 µm as basic array. 24 of such arrays were applied matrix-like in a write field with a dose increase factor of 1.2 featuring an exposure dose gradient from 1x to 66x of the starting dose D_0. The size of the write field was increased from 51.2 µm to 100 µm in order to feature enough space for the 24 arrays. However, it goes along with the reduction of the spatial resolution of the beam from 0.8 nm to 1.6 nm, which is still more than sufficient for 100 nm features.
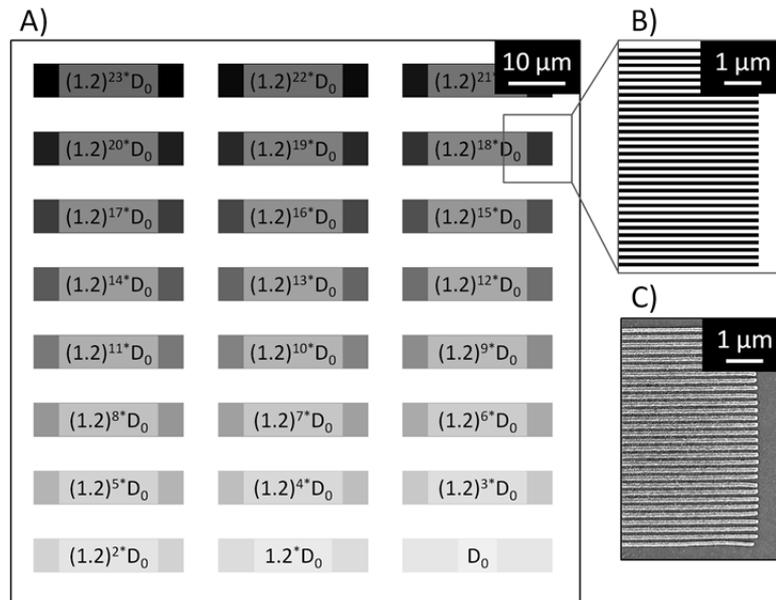
Figure 3.18: Schematic sketch of the 4th generation write field design: the write field design features 24 basic arrays, each a set of 30 lines (**B**) with a width of 100 nm, l/s of 1/1, and a length of 26.5 µm. These 24 arrays were applied matrix-like in a write field of 100µm edge length with a dose increase factor of 1.2 featuring an exposure dose gradient from 1x to 66x of the starting dose D_0 (**A**). The SEM image shows an end of one basic array (**C**).

The patterning with this design resulted for resists, which are even sensitive to minor dose variations, in a non-uniform line width in the line array due to the different amount of backscattered electrons. In the middle of the line array, more backscattered electrons are present than in the edges of the array. This fact results in a dose gradient from the middle to the edges which negatively affects the overall quality of all lines. This can be observed in the SEM image (**C**), where at the edge of the element the line width is reduced and the line ending even is bent. More obvious is the change in the amount of residues formed due to backscattering in the shown resist: In the middle of the basic motive the gap is fully filled by residues, while at the edge nearly no residues are present. The changing background dose affected even the central region of the line array, thus inhibiting a proper LER evaluation. For solving this issue in a final improvement step, the maximal backscattering range of 3 µm in radius around the beam impact position for the utilized acceleration voltage of 20 kV was considered (already discussed in chapter 3.3.3). As a consequence, in the 5th write field design (**Figure 3.19**) the number of lines in the basic array was increased from 30 to 44. This allows the realization of enough line space pairs with uniform dose contribution from the electron beam and the backscattering in the middle of the array for LER evaluation.
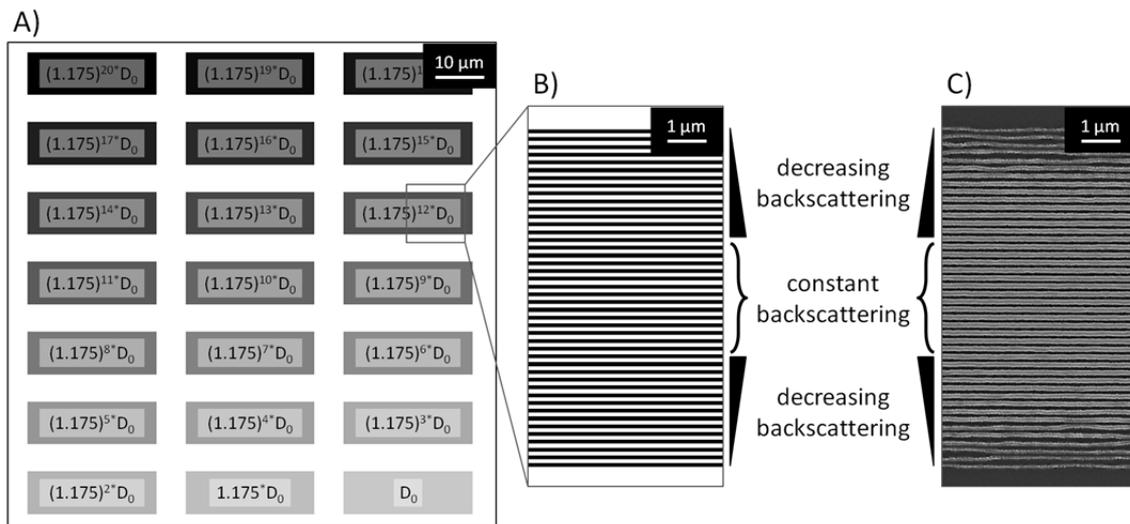
Figure 3.19: Schematic sketch of the 5th generation write field design: It features a write field with an edge length of 100 µm, an exponential dose gradient of 21 different doses and an exponential factor of 1.175 resulting in a gradient going up to 25x of the starting dose D_0(**A**). The dose gradient is performed in 21 arrays, each of them containing 44 lines with 100 nm width (l/s of 1/1) and a line length of 26.7 µm (**B**). With these 44 lines, the line array is wide enough to feature a uniform backscattering dose at 20 kV acceleration voltage in the middle of the array. In the SEM image (**C**) uniform exposure conditions can be seen in the middle of the array, while at the edges decreasing backscattering leads to irregularities.

The SEM image in **Figure 3.19** C shows one line array of the 5th generation write field. While the additional dose of backscattered electrons is increasing from the edge to the middle (from line 1 to 15), the middle-lines (from 16 to 29) have a constant contribution of backscattered electrons and thus a uniform additional dose. With this uniform dose to these lines in the middle of the array, they feature a constant line width, which is necessary for an LER evaluation (described in the experimental part; chapter 9.1.8). However, due to the increased size of the line array, the amount of line arrays for the dose gradient had to be reduced from 24 to 21 to fit into the write field of an edge length of 100µm. Thus the exposure dose gradient ranges with the dose scaling factor of 1.175 from the starting dose D_0 to $25*D_0$, which is sufficient to evaluate the region of interest in combinatorial approaches for new resist system. If the investigated resist system requires a different exposure dose range, the dose scaling factor can easily be adjusted in the pattern design editor.

Based on the region of interest, which can be efficiently identified utilizing the 5th generation write field design, the investigation of the resolution limits of a new resist system is the next step. Thus a mask design was developed, which includes a resolution study. A schematic sketch of the developed resolution investigation write field design is shown in **Figure 3.20 B**. The combinatorial resolution investigation consists of line arrays with different line width ranging from 6 nm up to 126 nm (l/s 1/2) (**B**). A similar design was also prepared with l/s 1/1 features, which is not shown here, because it is identical to the one discussed here apart from the different line spacing. Similar to the 5th generation design, the line arrays for each line width consisted of enough line to space pairs to provide a center area with uniform backscattering contributions and thus uniform dose for the resolution study (**C**). In **Figure 3.20A,** it is shown how a dose gradient can be performed with this design. Therefore several of such write fields are exposed with the internal resolution gradient next to each other while assigning an increasing exposure dose (D_1 - D_x). In comparison to the dose gradient realized with the 5th generation write field design, where it is realized within a quite small 100 µm write field, this dose gradient is spread out over the substrate. This has to be considered, when this design is applied in combinatorial libraries.
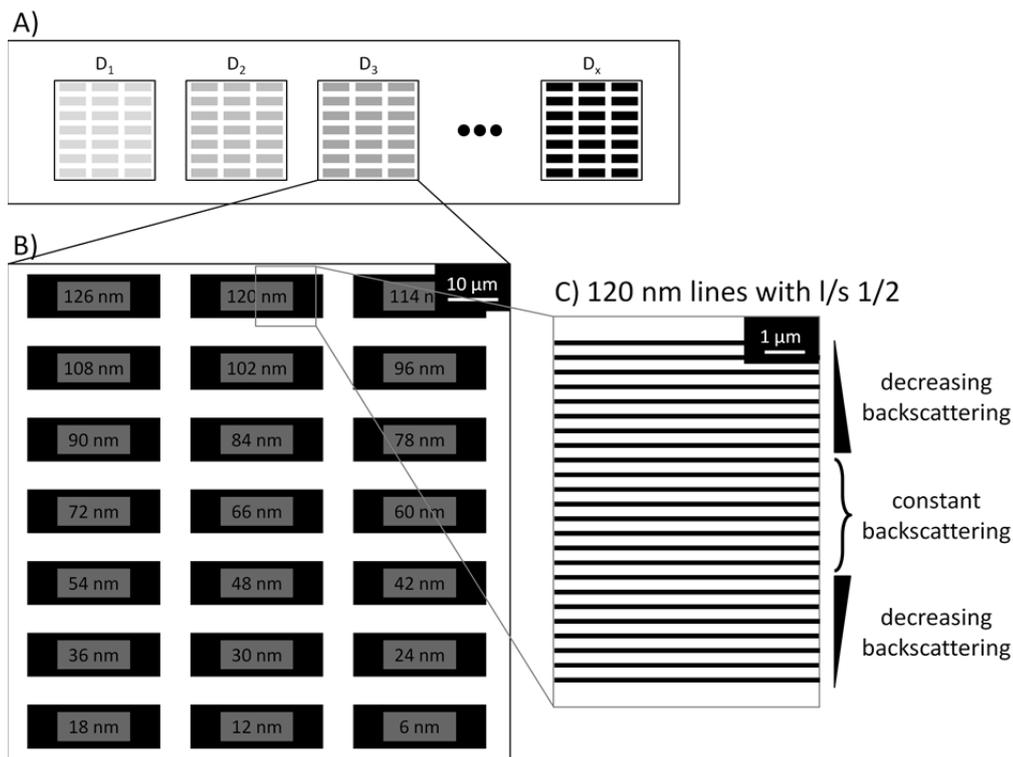
Figure 3.20: Schematic sketch of the write field design for the resolution studies: It features a write field with an edge length of 100 µm. Each write field consists of area elements with a length of 26.5 µm and a width gradient from 6 nm up to 126 nm with l/s 1/2 (**B**). With these different area element widths, the maximum realizable resolution for an investigated resist system is evaluable. Each of these line arrays features similar to the 5th generation write field design (**Figure 3.19**) enough line to space pairs to ensure that a sufficiently large area with uniform backscattering contribution is present in the middle of the array for the exposure with a 20 kV acceleration voltage (**C**). This write field design is usually utilized in a combinatorial experiment where minor dose adjustments are necessary. Thus a dose gradient is performed by exposing several write fields beside each other (**A**). Each write field is assigned therefore to a specific base dose D_1 to D_x, featuring the exposure dose gradient.

The designs presented so far allow the evaluation of the resolution limits and the LER of an investigated resist. Beside these two material parameters, the sensitivity is an additional performance parameter of a resist system. This term describes the necessary exposure dose for the realization of positive tone respectively negative tone features. For an industrial application of new resists, the sensitivity should be as high as possible, to ensure a fast exposure process time and thus allow a cost efficient patterning process. The sensitivity is evaluated by measuring a contrast curve (described in the experimental part; chapter 9.1.6). It describes the dose dependence of the measured obtained feature height. For this measurement it is necessary to realize large enough features, which are easily recognizable on the substrate

and are suitable for the measurement of feature heights obtained after development. The write field design therefore features three squares with 20 µm times 100 µm edge length (**Figure 3.21 B**).
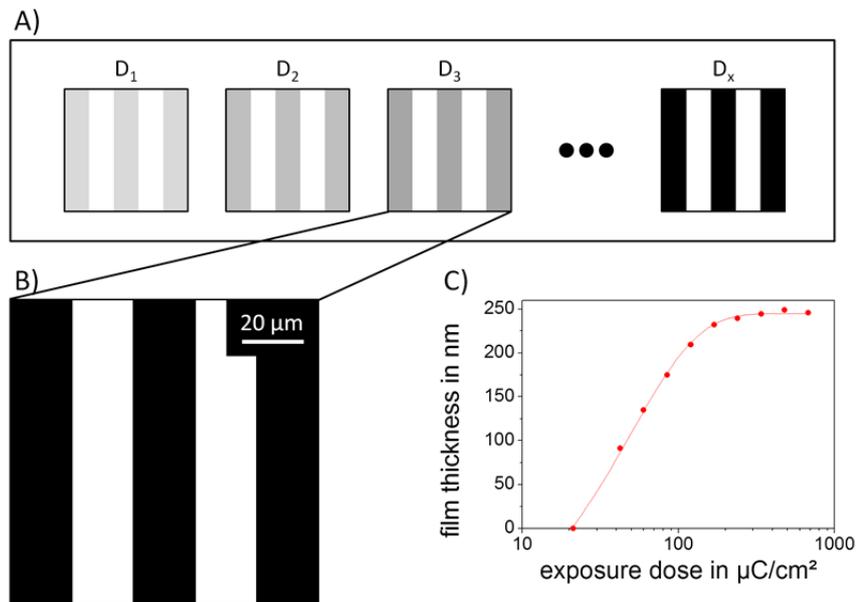
Figure 3.21: Schematic sketch of the write field design for the measurement of a contrast curve to evaluate the resist sensitivity: The design features in a 100 µm times 100 µm sized write field three squares with 20 µm times 100 µm edge length (**A**). Such write fields are exposed multiple times on the substrate beside each other with the adjusted exposure dose (D_1 -D_x) to feature an exposure dose gradient (**B**). By measuring the obtained feature heights after the development process, the contrast curve of the resist is received (exemplarily shown for a negative tone resist in **C**).

Such write fields are exposed beside each other with the respective adjusted exposure dose D_1 - D_x to realize an exposure dose gradient (**A**). After the development, the obtained feature heights are measured and plotted against the exposure dose in a contrast curve. An exemplarily plotted contrast curve is shown in **Figure 3.21 C** for a negative tone resist. According to Mack et al.[128], significant values in terms of sensitivity can be calculated out of these contrast curves, allowing an evaluation of different resists' sensitivity. A detailed calculation and evaluation is performed in chapter 4.4 for a negative tone resist.

In summary, the optimized 5th generation write field design together with the designs for resolution study and sensitivity measurement offer tailored and suitable tools to efficiently investigate and optimize new resist systems.

4. Improving resist sensitivity: a comparison of physical vapor deposition and spin coating as film application method[3]

4.1. Introduction

In lithography the standard film preparation technique is spin coating, which allows the reproducible realization of smooth and uniform films, which are essential for the preparation of high performance features. However, such solvent based processes are known to show tendencies for segregation[102] and phase separation[129] in multi component films in some cases. State of the art photo resist systems are polymeric chemically amplified photoresists (CARs). Such systems consist of at least a photo acid generator (PAG) and an acid sensitive matrix material, so consequently such phenomena could also occur. Indeed, an irregular distribution of the PAG in the matrix material is assumed to contribute to the issue of line edge roughness (LER).[130] Due to this relevance, the material distribution in small domains was studied by NMR techniques for similar systems.[131],[132] However, this method could not prove molecular blending at small dimensions for materials of good miscibility, but systems of poor miscibility showed phase separation. This investigation was conducted only for bulk samples, whose properties might differ from thin films necessary for application in lithography. Furthermore a theoretical study of the PAG distribution was conducted by two-dimensional Monte Carlo simulations.[133] This study demonstrated that the PAG aggregate size affects the acid diffusion length and thus the resist performance characterized by resolution, line edge roughness and sensitivity. The result concerning LER was also confirmed in three-dimensional simulations.[134] Consequently, distinctions in blending caused by different film preparation techniques should affect the overall performance of the resist, e.g. sensitivity, pattern quality to name a few.

In this chapter a comparison of two different film preparation techniques is conducted. Therefore resist films prepared by the standard film preparation technique spin coating are compared to those prepared by physical vapor deposition (PVD). The two techniques feature a completely different film forming as one is solution-based and the other is based on a solvent-free molecule by molecule deposition. Such change in the preparation technique

---

[3] Parts of this chapter are already published: T. Kolb, C. Neuber, M. Krysak, C. K. Ober, H.-W. Schmidt, Multicomponent physical vapor deposited films with homogeneous molecular material distribution featuring improved resist sensitivity, *Adv. Funct. Mater.* **2012**, *22*, 3865–3873.

should show an influence in resist performance and thus is investigated in this chapter for the application in lithography.

However, the physical vapor deposition process requires a resist consisting of materials which are evaporable without decomposition.[78] This was realized by utilizing a chemically amplified molecular glass resist plus a nonionic PAG instead of the standard polymer resists and ionic PAGs.

Considering these requirements, a literature known molecular glass negative electron beam resist[135] - consisting of a phenolic compound, a crosslinking agent and PAG - is selected for the study of performance distinctions originating from the applied film preparation technique. However, it was necessary to exchange the ionic PAG utilized in literature by a nonionic one. The films prepared with this resist are investigated concerning the dissolution behavior, the sensitivity and the overall performance in lithographic patterning. It is assumed that due to molecular deposition in PVD the three components are well distributed without aggregate formation. In contrary, the spin coating sample might feature PAG aggregates, which should affect the lithographic performance (**Figure 4.1**).
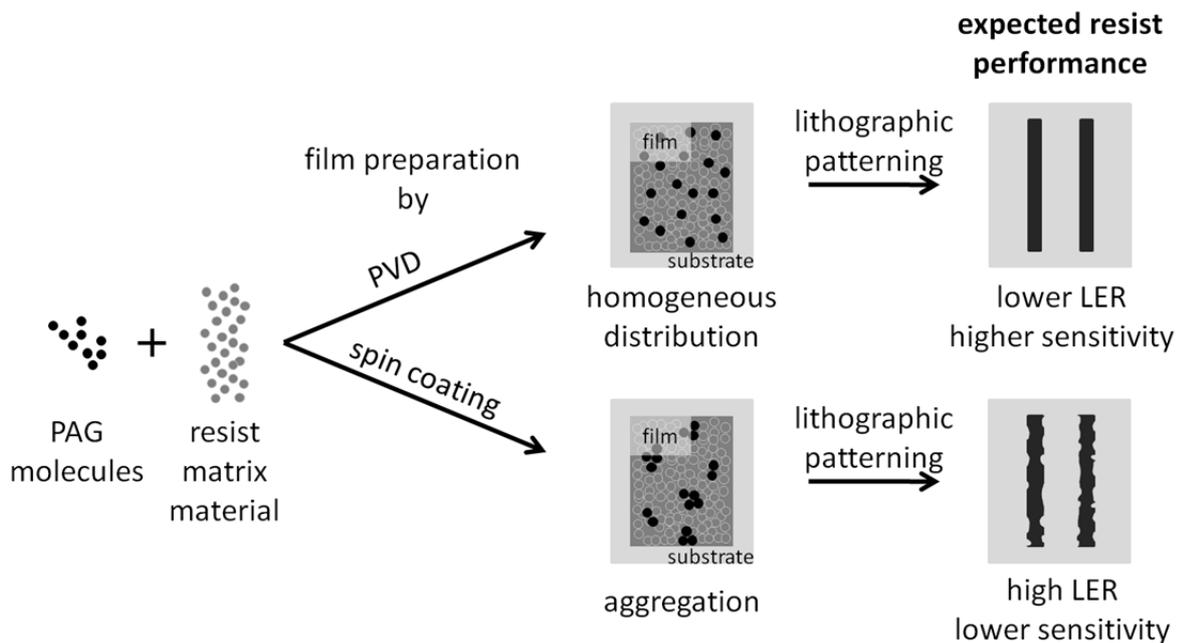
Figure 4.1:   Schematic illustration of the expected resist performance originating from the film application technique by the different photoacid generator distribution in a chemically amplified photoresist.

4.2. Solvent-based resist composition optimization for the applied non-ionic photoacid generator

The selected negative tone molecular glass photoresist consisted of the phenolic matrix 4,4'-[[4-[1-(4-Hydroxyphenyl)-1-methylethyl]phenyl]methylene]bisphenol (here called trisphenol), the crosslinking agent Tetrakis-(methoxylmethyl)glycoluril (here called crosslinker) and the nonionic PAG 1,2,3-Tris(methylsulfonyloxy)benzene (here called PAG1), as substitution for the ionic PAG (**Figure 4.2**). The PAG1 was chosen because of its literature known electron beam sensitivity.[136]
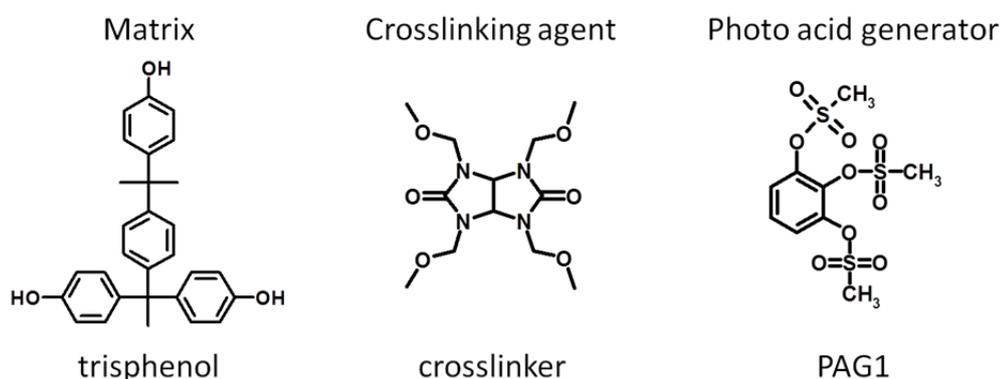
Figure 4.2: Structure formula of the investigated molecular glass photoresist system: It consists of the phenolic matrix 4,4'-[[4-[1-(4-Hydroxyphenyl)-1-methylethyl]phenyl]methylene]bisphenol, here called trisphenol, the crosslinking agent Tetrakis-(methoxylmethyl)glycoluril, here called crosslinker, and the nonionic PAG 1,2,3-Tris(methylsulfonyloxy)benzene, here called PAG1.

Due to the changed PAG, the resist system is altered and thus the composition of this resist system has to be optimized in the first place. As a changed composition influences the relevant parameters - exposure dose and post exposure bake (PEB) temperature - a combinatorial approach was utilized to adjust the resist composition. Therefore a ternary combinatorial library was designed. For the solution-based combinatorial experiment a film with an internal composition gradient was prepared on a HMDS primed Si-wafer. The composition gradient of trisphenol and the crosslinker with a constant PAG1 content was realized with the syringe pump approach recently published.[12] Therefore two solutions out of PGMEA were prepared with 2.5 wt% organic materials content. Solution 1 consisted of 5.0 wt% PAG1 and 95.0 wt% trisphenol, while solution 2 consisted of 5.0 wt% PAG1 and 95.0 wt% crosslinker. Out of these solutions, the composition gradient was realized by co-injection with the syringe pump system (Cetoni) into a custom made active mixing chamber

stirred with 80 rpm. During extrusion of the resultant gradient mixture on the silicon wafer with a constant velocity of 10 mm/s, the flow rates of the two solutions were continuously changed by ensuring a constant overall flow rate of 30 µl/s. Afterwards the resultant gradient mixture extrudate with the internal composition variation was doctor bladed in orthogonal direction to the application direction followed by the fixation step post apply bake (PAB) for 30 s at 115 °C. The evaluation of the so realized film was performed by cutting a stripe of the wafer into defined pieces and analyzing the respective film composition of each piece by HPLC measurements (described in the experimental part; chapter 9.1.2). The composition gradient film featured a decreasing trisphenol content from 91 wt% to 42 wt% and an increasing crosslinker content from 4 wt% to 53 wt%, while the PAG content stayed constant at around 5 wt%. The subsequent electron beam exposure process (20 kV acceleration voltage) was performed with write fields applied matrix-like on the substrate. The matrix consisted of 20 columns along the composition gradient (1-20) times five rows (A-E). The utilized 1st generation write field design (see chapter 3.4) includes an exposure dose gradient ranging from 9 µC/cm² up to 414 µC/cm² on a basic motive of multiple L-shaped areas with 100 nm line width. After the exposure a PEB temperature gradient ranging from 64 °C to 102 °C (A-E) was applied for 30 s orthogonal to the composition gradient. Finally the development was performed for 30 s in 0.02 N tetramethylammonium hydroxide (TMAH) solution simultaneously using ultrasound. This combinatorial library was evaluated by scanning electron microscopy (SEM) of the non-sputtered patterns. In **Figure 4.3**, schematically the ternary library as well as the optimized sector is shown.

The optimized features were found in the sector C5 representing a composition of 79 wt% trisphenol, 16 wt% crosslinker and 5 wt% PAG1, a PEB temperature of 83 °C and an exposure dose of 67 µC/cm². However the features show defects as the lines are broken and some residues are present between the lines. These may originate from the coarse PEB temperature gradient with only five investigated temperatures within the investigated temperature range of 64 °C to 102 °C meaning the investigation of 9.5 K temperature steps. Another reason may be the not adjusted development conditions. Thus the optimization of these two processing parameters is focused in more detail in subsequent patterning experiments. Thereby the optimized resist composition identified in this combinatorial investigation was used as a fixed value.
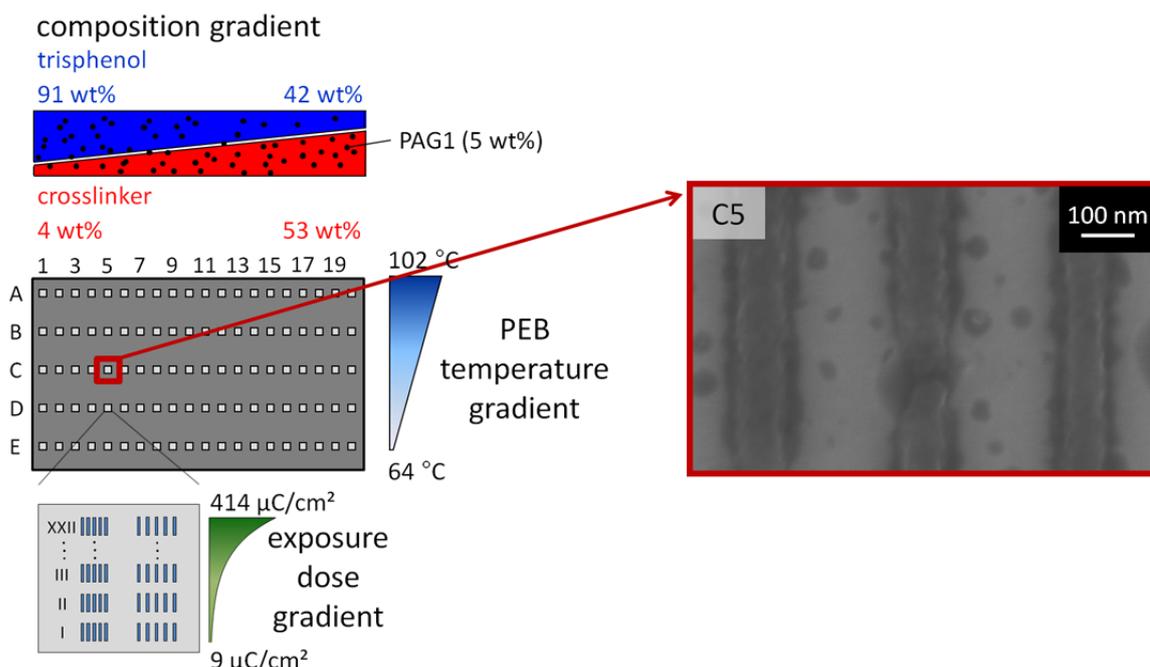
Figure 4.3: **Left**: Schematic sketch of the three dimensional combinatorial library of the optimization of the resist composition: For this experiment a composition gradient (1-20) was applied on a Si-wafer, featuring a decreasing trisphenol content (91 wt% → 42 wt%) and an increasing crosslinker content (4 wt% → 53 wt%) by maintaining a constant PAG1 content of around 5 wt%. After the PAB at 115 °C for 30 s, the subsequent electron beam exposure was conducted in 100 write-fields (20 x 5 matrix). In each write field an internal exposure dose gradient was realized featuring a dose range from 9 μC/cm² to 414 μC/cm². Orthogonally to the composition gradient, the PEB temperature gradient (A-E) ranging from 64 °C to 102 °C was applied for 30 s for each investigated film composition. Finally the development was performed for 30 s in 0.02 N TMAH solution simultaneously with ultrasound.
Right: The evaluation of the combinatorial library was performed by gathering SEM images of each sector. The optimized features were realized in sector C5 for a composition of 79 wt% trisphenol, 16 wt% crosslinker and 5 wt% PAG1, a PEB temperature of 83 °C and an exposure dose of 67 μC/cm^2.

4.3. Investigation of the dissolution behavior of spin coated and by physical vapor deposition prepared films

The knowledge about the dissolution behavior of a photoresist system is crucial for selecting appropriate development conditions. Therefore the dissolution contrast between exposed and unexposed areas of the resist film defines the patternability itself and thus the resist performance. In this context the applied film application techniques and the resulting intrinsic film properties such as density, smoothness, and uniformity of material blending should affect

the dissolution behavior. The dissolution investigations (described in the experimental part; chapter 9.1.3) deal with unexposed (non crosslinked) and flood exposed plus afterwards annealed (fully crosslinked) resist films on a quartz crystal microbalance (QCM) representing material conditions before as well as after the lithographic process. The measurement principle is based on monitoring the damp of the quartz crystals' (QCs') oscillation frequencies resulting from deposited or dissolved material on/of the QCs' surface.[137] For this investigation films were applied onto QCs by PVD as well as by spin coating (composition: 76 wt% trisphenol, 19 wt% crosslinker and 5 wt% PAG1). All spin coated samples were annealed for PAB. Afterwards flood exposure was performed on two different prepared films with a dose of 246 mJ/cm² (240 nm - 290 nm). This high dose guaranteed a high photo activation ratio of the PAG resulting in a high crosslinking density during the PEB process step at the elevated temperature of 95 °C. In this way QCs with crosslinked and with unexposed native photoresist films prepared by the investigated solvent-free and a solvent-based techniques were available for the dissolution investigations. These QCs were fixed into the QC-holder and the monitoring of the oscillation frequency was started. The prepared QC-holders were dipped into a stirred beaker containing deionized water. During monitoring the developer strength was increased in several steps by adding defined amounts of a concentrated TMAH solution, so the dissolution behavior was studied over a broad concentration range.
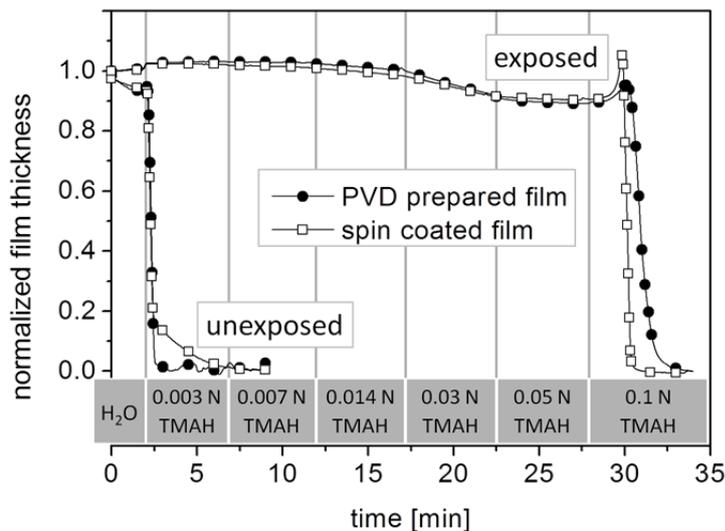
Figure 4.4: Dissolution behavior investigations of spin coated and PVD prepared films by quartz crystal microbalance measurements: Unexposed and exposed films (UV exposure: 240 nm - 290 nm, 246 mJ/cm², PEB 30 s at 95 °C) were dipped into stirred, deionized water. Then in several steps the concentration of the developer strength was increased by adding defined amounts of concentrated TMAH solution (1.104 N).

In **Figure 4.4** the graphs of the dissolution behavior investigations of spin coated and PVD prepared films are shown both in the unexposed and exposed state. The unexposed material shows a nearly identical behavior for the spin-coated as well as for the PVD prepared film. Thus no different dissolution behavior originated from the film preparation technique was measured by the QCM measurement. The measured dissolution behaviors show a slight decrease in film thickness in pure water explainable by the modest solubility of the unexposed resist. After the addition of a defined amount of concentrated TMAH solution (resulting in a 0.003 N solution) the unexposed resist material dissolves immediately. The films flood exposed and afterwards annealed in comparison showed a dissolution contrast. However, again a nearly identical dissolution behavior was measured irrespective of the applied film preparation technique. The QCM measured film thickness is nearly constant up to a 0.007 N TMAH concentration, decreases slightly between the TMAH concentrations of 0.014 N to 0.05 N, and drops remarkably at the TMAH concentration of 0.1 N after a short swelling period. In conclusion this measurement demonstrates the stripping off behavior of the exposed negative tone resist film at a 0.1 N TMAH concentration. For this reason the development step for the following experiments were performed with stirred 0.05 N TMAH. This means the development is performed at the highest acceptable contrast between unexposed and exposed resist material. By this investigation it was also shown that irrespective of the applied film preparation technique the photoresist films have the same measured dissolution characteristics. Consequently there are no measureable dissolution differences or the QCM measurement is unable to detect existing slight differences. However, this experiment demonstrates that the QCM technique, in combination with the stepwise increase of the developer strength, is a powerful tool for measuring crucial dissolution characteristics of film materials.

4.4. Investigation of resist's sensitivity of spin coated and by physical vapor deposition prepared films

In the following section the lithographic sensitivity of films prepared by both spin coating and PVD were investigated. For this purpose the standard technique of measuring a lithographic contrast curve[66] was performed by utilizing an electron beam exposure (described in the experimental part; chapter 9.1.6). Therefore the two different prepared films (composition: 79 wt% trisphenol, 16 wt% crosslinker and 5 wt% PAG1) were exposed by electron beam

with a pattern of multiple squares (20 μm x 100 μm) of defined increasing doses. After the PEB (80 °C for 30 s) and development step (20 s; 0.05 N TMAH solution) the resulting pattern height of the corresponding doses was measured by a stylus profiler. In **Figure 4.5** the contrast curves, hence the dose dependence of the measured pattern heights in nm, for the spin coated and PVD prepared films are shown.
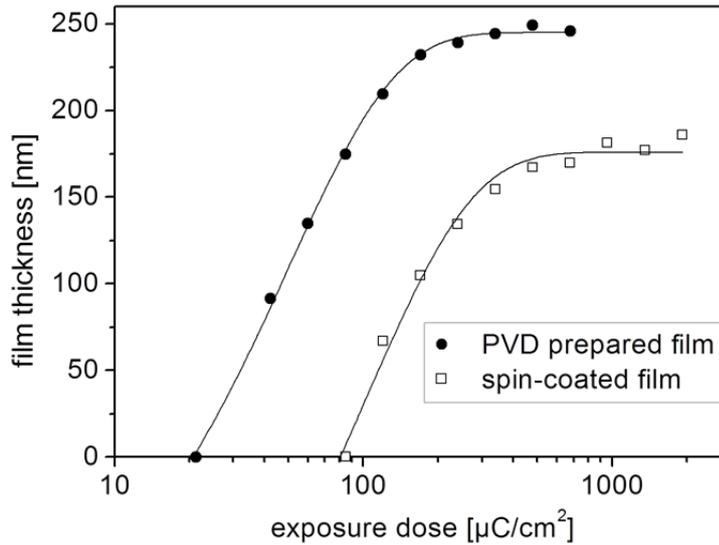
Figure 4.5:   Contrast curves of resist films prepared by spin coating (open squares) and PVD (circles) with the applied fit (equation 4.1): The PVD prepared film shows a contrast curve shifted towards lower exposure doses , which shows a significantly higher sensitivity. The slope of the contrast curve is quite similar, thus the contrast of the resist is almost the same for both film preparation methods.

The graphs show that the resist contrast - defined by the slope of the contrast curve - of both films are almost the same. This is expected due to the fact that this value is dependent on the material's composition which is the same for both prepared films. However a clear distinction in sensitivity is observed whereas all lithographic processing steps and conditions were applied alike. The already mentioned theoretical simulation[133] investigating the impact of PAG aggregates on resist performance showed lower resist sensitivity for assumed PAG aggregates in comparison to a homogeneously distributed one. Consequently this experiment indicates that the two investigated film preparation techniques, spin coating and PVD, have different blending capabilities. The PVD technique provides obvious advantages due to its single molecule by molecule deposition of a well distributed mixture of the three components through the complete resist film. In contrast, the solvent based spin coating process produces resist films of lower sensitivity. This fact can be explained by possible aggregate formation of

the different components (trisphenol, crosslinker and PAG1). Such aggregates of the PAG compound were responsible for a lower resist sensitivity in simulation[133].

Mack et al.[128] introduced a way to calculate significant values (listed in **Table 4.1**) in terms of sensitivity based on the experimental data of the measured film thickness T_r and the corresponding applied exposure dose E by fitting the contrast curve with equation 4.1.

$$T_r = T_0 - \Delta T_{max} e^{-E/E_n} \tag{4.1}$$

Herein T_0 describes the native resist film thickness, ΔT_{max} the theoretical value of the maximal crosslinkable resist thickness, and E_n the sensitivity term for negative type resists. By applying these fitting parameters to equation 4.2, which also was introduced by Mack et al. in the same paper, the gel dose E_0 can be calculated. This value characterizes the theoretical dose, where first material remains after development in the exposed areas.

$$E_0 = -E \ln\left(\frac{T_0}{\Delta T_{max}}\right) \tag{4.2}$$

Table 4.1: Significant values in terms of sensitivity calculated from the fitted contrast curves (**Figure 4.1**) and out of these calculated gel dose E_0 for a quantitative sensitivity investigation of films prepared by spin coating respectively PVD.

	T_0 [a] [nm]	ΔT_{max} [b] [nm]	E_n [c] [$\mu C/cm^2$]	E_0 [$\mu C/cm^2$]
Spin coating	175.9	386.1	102.6	80.6
PVD	244.9	347.0	51.3	17.9

[a] Native resist film thickness. [b] Maximal crosslinkable resist thickness. [c] Sensitivity term for negative resists.

The values calculated with these equations 4.1 and 4.2 show a four time increase in sensitivity quantified by the gel dose E_0 and a two time increase in the sensitivity term E_n for the investigated PVD prepared resist films in comparison to spin coated samples. In conclusion lithographic contrast curves of an identical resist system are highly sensitive to the applied film application technique and this indicates a different blending of the photo acid generator within the resist material.

4.5. **Investigation of resist's performance of spin coated and by physical vapor deposition prepared films**

In addition to dissolution behavior and sensitivity, the resist performance in general and its dependence on the film preparation technique was investigated. Therefore the applied processing variables of the delicate lithographic process to the spin-coated and PVD prepared films were optimized individually. This issue was addressed by the systematic variation of the important processing variables of exposure dose, PEB temperature and development conditions. Due to the fact that all of these variables depend on each other, this variation was realized in one experiment by gradients in a ternary combinatorial library. The combinatorial libraries based on spin-coated and PVD prepared films allowed a fast and efficient observation of the overall performance. The resist composition (79 wt% trisphenol, 16 wt% crosslinker, 5 wt% PAG1) for these investigations was thereby selected on the basis of the solvent based composition optimization (chapter 4.2). The arrangement of the investigated variable gradients in the combinatorial libraries is shown schematically in **Figure 4.6**.
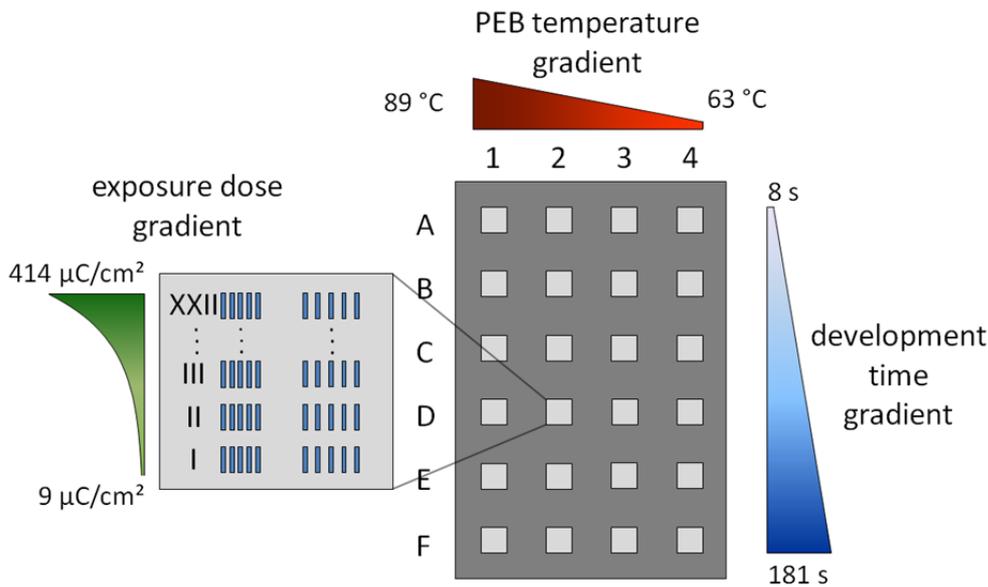
Figure 4.6: Schematic illustration of the investigated combinatorial library for the optimization of exposure dose, PEB temperature and development time in one experiment. The ternary combinatorial library consists of an exposure dose gradient in each sector ranging from 9 µC/cm² to 414 µC/cm² (I-XXII), a horizontal PEB temperature gradient ranging from 89 °C to 63 °C (1-4), and a vertically development time gradient from 8 s to 181 s (A-F).

For the electron beam exposure the defined sectors were arranged matrix-like by 4 columns (1-4) and 6 rows (A-F) on the substrate. Every sector consisted of 22 motives (I-XXII) each assigned with a different exposure dose resulting in the exposure dose gradient (9 µC/cm² to 414 µC/cm²). The motive consisted of 100 nm features (1/1 and 1/2 line to space proportion (l/s)). For the film prepared by spin coating the 1st generation write field design (see chapter 3.4), which features L-shaped patterns, was utilized. Due to the lack of additional scientific information on the L-shaped pattern, the pattern was simplified to I-shaped ones in the utilized 2nd generation write field design for the following lithographic investigation on the film prepared by physical vapor deposition. The exposed substrate was then annealed for 30 s with the horizontal PEB temperature gradient (89 °C to 63 °C). For the development step a time gradient between 8 s and 181 s in stirred 0.05N TMAH solution was arranged orthogonally to the applied temperature gradient. All three gradients were similarly applied to the spin-coated and the PVD prepared films, thus comparable combinatorial libraries were prepared. **Figure 4.7A** shows the SEM image of combinatorial optimized 100 nm L-shaped line pattern of the film prepared by spin coating. In **Figure 4.7B** the optimized I-shaped pattern for the PVD prepared sample is shown.

A) Pattern of spin coated film   B) Pattern of PVD prepared film
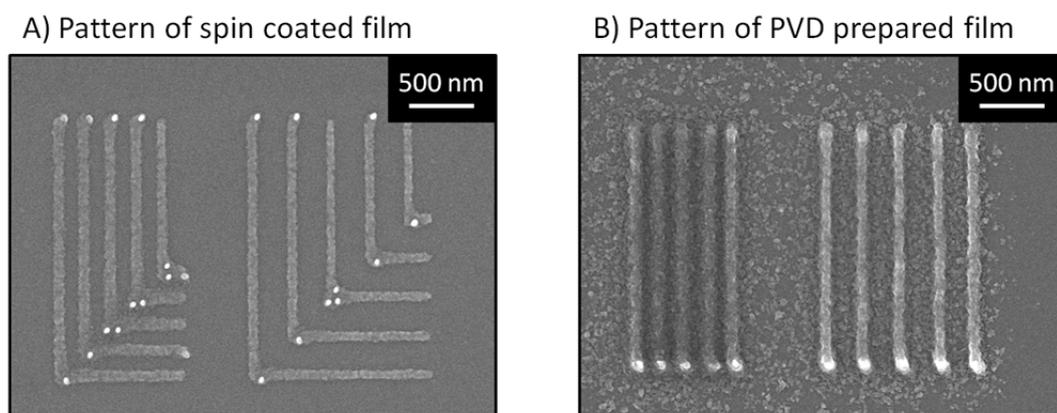
Figure 4.7: The SEM images of patterns show the optimized sectors of the combinatorial library based on spin coated (**A**) and PVD prepared (**B**) films:
A) The best feature quality for the spin coated film was found in sector B2 with exposure dose of 96 µC/cm², PEB of 80 °C, and development time of 43 s. The features are well developed and show clear lines.
B) The best feature quality for the PVD prepared film was found in sector D2 with exposure dose of 58 µC/cm², PEB of 80 °C, and development time of 113 s. The pattern shows residual material around the distinct lines. These residues are caused by backscattered electrons due to the increased sensitivity of PVD prepared films.

The best pattern of the spin-coated film (**A**) was observed at an exposure dose of 96 µC/cm² (dose XIV) in sector B2 corresponding to a PEB at 80 °C and development time of 43 s in stirred 0.05 N TMAH solution. The pattern is obviously well developed and shows clear lines. For the PVD prepared film the best pattern (**B**) was observed at the lower dose of 58 µC/cm² (dose XI) in sector D2 corresponding to a PEB at 80 °C and development of 113 s in stirred 0.05 N TMAH solution. In contrast to the spin-coated film, the pattern of the PVD prepared film shows significant amounts of residual material around but mainly between the distinct lines even at the obviously lower exposure dose and the drastic elongation of the development time period. The observation, that these residues are only observable in the vicinity of pattern and that they cannot be removed even under enhanced developing conditions, indicates the presence of crosslinked photoresist materials as a result of backscattered electrons passing the resist. This fact is also confirmed by the lower calculated gel dose E_0 of 17.9 µC/cm² (**Table 4.1**) for the PVD prepared film. In conclusion these observations and the applied lower electron beam dose demonstrate a crucially increased sensitivity of the same resist system utilizing PVD as film preparation technique. However, the higher sensitivity makes the resist more susceptible to the formation of residues due to backscattering.

4.6. Investigation of targeted photoacid generator aggregate formation

In the previous chapter an increased sensitivity was found for utilizing PVD instead of spin coating as film preparation technique. However, this sensitivity increase can originate from both the assumed more homogeneous PAG distribution and missing solvent residues from the solvent-based film preparation method. To exclude the latter, experiments were performed ensuring PAG aggregate formation on the one hand as well as a homogeneous PAG distribution on the other hand utilizing the same preparation technique. An excellent technique for this approach is physical vapor deposition, whereby different components are individually evaporated. For regular film preparation these different components are coevaporated, but for the investigation of a directed PAG aggregate formation, films with layers consisting of one to two components were realized. By this method a film was prepared with alternating single component PAG-only layers and two component layers out of trisphenol and crosslinker. So in comparison to the film with homogeneous distribution prepared in the previous chapter, the layered PVD prepared film includes PAG aggregates within the PAG-only layers. By evaporation of such layers alternately and with proper layer

thickness a film with a similar overall composition as the film with homogeneous PAG distribution could be achieved. Therefore the evaporation process was controlled on the basis of the respective evaporation rates for alternating PAG layers (0.5 nm thickness) and trisphenol/crosslinker layers (9.5 nm thickness). The final film consisted of ten of these layer stacks giving in total a film thickness of approximately 100 nm. However, due to this sequences the question of a possible adhesion issue of a PAG-only layer respectively trisphenol/crosslinker layer on the silicon substrate came up. Therefore two films were prepared, one with a PAG-only bottom layer and one with a trisphenol/crosslinker bottom layer. This was done in one experiment by evaporating an additional PAG-only layer on half of the substrate. On top of this substrate the ten layer stacks were evaporated simultaneously, to ensure a similarly composed resist film in these ten layer stacks. The composition of these layer stacks was evaluated by the resultant film without PAG-only bottom layer. This film had an overall resist composition of 73 wt% trisphenol, 20 wt% crosslinker, 7 wt% PAG1 which is quite similar to the film with homogeneous PAG distribution from the previous chapter (79 wt% trisphenol, 16 wt% crosslinker, 5 wt% PAG1). A schematic sketch of the two different layered films beside the homogeneous material distributed film is shown in the upper part of **Figure 4.8**.

The patterning of both layered films was oriented towards the optimal processing for the film with homogeneous PAG distribution from the previous chapter. Both films were exposed with the same write field design featuring I-shaped 100 nm features (l/s 2/1, 1/1 and 1/2) and an internal exponential exposure dose gradient (9 μC/cm² to 414 μC/cm² in 22 steps) (2nd generation write field design; see chapter 3.4). Afterwards the PEB was performed at 80 °C for 30 s. However the subsequent development process was weakened to consider the already mentioned possible adhesion issues. So both films were developed for 20 s in an unstirred 0.05 N TMAH solution. The resultant features were investigated by SEM without sputtering, whereby organic material appears dark due to charging. Consequently, occurring residues are more obvious on the grey silicon surface. This can be seen in the bottom part of **Figure 4.8**, where SEM images of the optimized realized features for each of the layered films (**A, B**) are shown. Additionally the SEM image of the optimized features for the homogeneous PAG distributed film (Pt-sputtered) from the previous chapter is shown for comparison reasons (**C**).
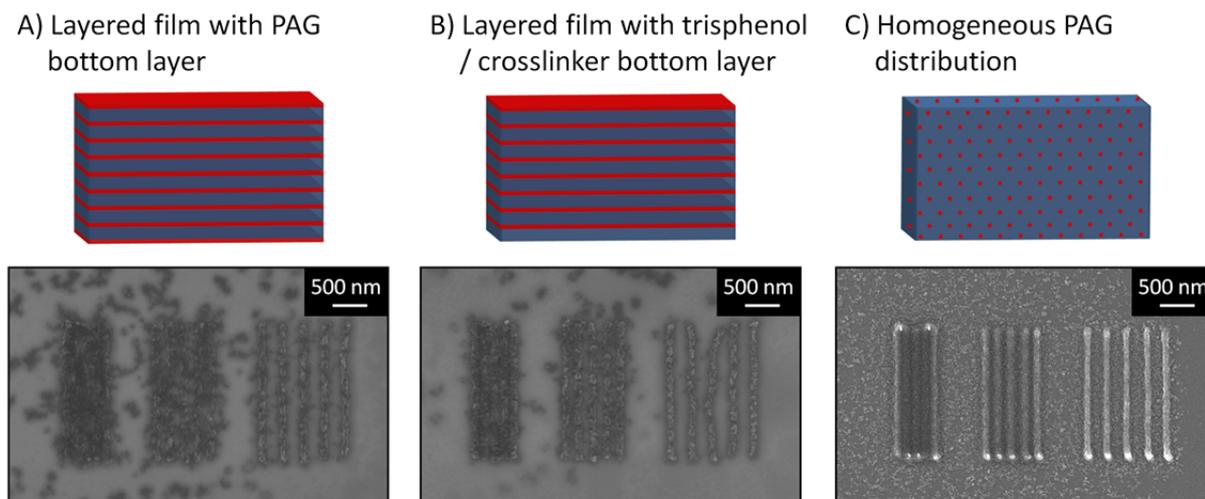
Figure 4.8: Schematic illustration of the different realized film architectures and SEM images of received patterns of these films:
A) Pattern for the layered film with PAG bottom layer were received with an exposure dose of 96 µC/cm², a PEB temperature of 80 °C and a development for 20 s in unstirred 0.05 N TMAH. The SEM image of the non-sputtered features shows very rough lines, which are surrounded by some residues originated from backscattered electrons.
B) Pattern for the layered film with trisphenol/crosslinker bottom layer were observed for similar processing conditions (exposure dose of 96 µC/cm², PEB temperature of 80 °C and development for 20 s in unstirred 0.05 N TMAH). The SEM image of the non-sputtered features shows similar rough lines. However, the reduced amount of residues and bending of the features in the right part of the image suggest weaker adhesion to the silicon substrate and perhaps also some suppression of residue formation due to backscattering.
C) The optimized pattern for the homogeneous PAG distribution was observed, as already mentioned in the previous chapter, at an exposure dose of 58 µC/cm², a PEB of 80 °C and a development time of 113 s in stirred 0.05 N TMAH. The SEM image of the Pt-sputtered sample shows smooth lines with a high amount of surrounding residues due to backscattering.

The SEM images show very rough lines for both layered films (**A**, **B**) in contrast to the smooth lines for the film with homogeneous PAG distribution (**C**). The rough lines obviously originated from the successfully realized PAG aggregates in the layered films. This result is consistent to the already mentioned Monte Carlo simulation,[133] which predicts that PAG aggregates lead to increased line edge roughness beside a decreased sensitivity. The decreased sensitivity is also shown in this experiment as the layered films - despite its higher PAG content - needed a noticeably higher exposure dose (90 µC/cm² at 7 wt% PAG) than the film with homogeneously distributed PAG (58 µC/cm² at 5 wt% PAG) by utilizing a similar PEB temperature and even weaker development conditions. The application of a similarly harsh

development procedure would have led to an even higher required exposure dose and might even have completely inhibited pattern formation due to stripping. Consequently, this experiment supports the assumption made in the previous chapters. The higher sensitivity from PVD prepared films prepared by coevaporation in comparison to spin-coated ones is caused by a more homogeneously distributed PAG. However, an additional effect from film processing residues cannot be excluded by this experiment, which might also be responsible for the sensitivity difference identified in the previous chapter.

When comparing both layered films to each other, they show, besides similar rough features, differences in the amount of residues and the bending of the developed features. The film with the trisphenol/crosslinker bottom layer (**B**) shows less residues and also features a slight bending of the central line of the feature with l/s 1 to 2 (right side of the image). This can originate from a weaker adhesion of the features to the substrate. The adhesion results from the hydrophobic interaction between the HMDS primed silicon surface and the crosslinked material. This prevents the intrusion of the water based developer into the contact area and thus the stripping off of the features. However, both different layered films were prepared on the same wafer in one process, so the surface of the wafer itself is similar. Consequently, the missing PAG at the bottom is the reason for the lower adhesion. In this case the acid has to diffuse through the whole bottommost trisphenol/crosslinker layer to reach the wafer surface in order to catalyze the crosslinking reaction of trisphenol and crosslinker there. Thus it is conceivable that the crosslinking ratio on the wafer surface is lower compared to the layered film with PAG bottom-only layer, where the acid is released on both sides of this bottommost trisphenol/crosslinker layer. Due to this lower crosslinking ratio, locally more polar non-crosslinked resist material is present which shows a decreased adhesion. This can also be the reason for the decreased amount of residues due to backscattering found with the layered film with a trisphenol/crosslinker bottom layer. In general, the layered films show a decreased number of large-sized residues compared to the coevaporated ones, which again confirms the PAG aggregation and the resulting decreased sensitivity. Additionally it is conceivable that the thin PAG free layer at the bottom acts like a spacer layer between the silicon substrate, the main origin of backscattered electrons, and the PAG molecules in the resist. This would lead to a decreased amount of backscattered electrons reaching the PAG and thus of the formed residues. If the latter assumption is correct, the addition of a spacer material between the silicon substrate and the resist material should reduce the amount of residues from backscattered electrons.

4.7. Investigation of bottom layers for the reduction of backscattering residues in sensitive by physical vapor deposition prepared resist films

The experiments in the previous chapter indicated decreased residue formation by applying a resist film with a PAG-free bottom layer in comparison to a PAG-only bottom layer. This may result from a decreased adhesion but also from the role of the trisphenol/crosslinker as a spacer layer between the substrate and the PAG. The latter may result in a reduced amount of backscattered electrons. These electrons, which are mainly formed in the silicon substrate, would then activate less PAG molecules and thus minimize the amount of formed residues. In the experiment of the previous chapter the PAG-free layer was only 10 nm thick. Although the contribution of residue reduction for such a thin film is supposed to be only minor, a bigger PAG-free bottom layer might have the potential to improve the resist quality. The feature of residue reduction of an additional PAG-free bottom layer is investigated in this work.

An important feature of bottom layer materials is the atomic composition, as the amount of backscattered electrons increases with increased electron density and thus with higher atomic numbers. To investigate the effect on the residue reduction of a bottom layer with smaller atomic number compared to the normal silicon substrate, a film consisting of Poly-(2-vinyl-pyridine) (P2VP) was investigated. To prove the concept, a bottom layer with a larger atomic number consisting of platinum was also investigated, which was supposed to result in an increased residue formation. The bottom layer out of P2VP (MW 300,000-400,000) was prepared by spin coating of a 10 wt% solution in PGMEA (PAB 2 min @ 130°C), resulting in a 600 nm thick film, while the 5 nm platinum bottom layer was prepared by sputtering. Resist films on both bottom layers and on one blank HMDS primed silicon wafer were prepared by spin coating of a 2.5 wt% PGMEA solution consisting of trisphenol (79 wt%), crosslinker (16 wt%) and PAG1 (5 wt%). The spin coating process was thereby instantly started after the application of the resist solution to prevent swelling of the polymeric bottom layer material. After PAB at 110 °C for 60 s each film was exposed with the 2nd generation write field design (see chapter 3.4) featuring I-shaped 100 nm features (l/s 2/1, 1/1 and 1/2) and an internal exponential exposure dose gradient (15 µC/cm² to 690 µC/cm² in 22 steps). After the PEB at 90 °C for 30 s the films were developed in unstirred 0.05 N TMAH solution for 20 s. The evaluation was performed by observing SEM images of features (l/s 1/1 and 1/2) and a subsequent comparison of the amount of formed residues (**Figure 4.9**). The l/s 1/2 features

were exposed to the fitting exposure dose and no residues could be observed. But for the slightly overexposed l/s 1/1 features even the simpler solvent based film processing lead to residue formation, allowing the discussion of the effect of bottom layers. The residues are formed from the higher background dose which is present due to the increased feature density in comparison to the l/s 1/2.
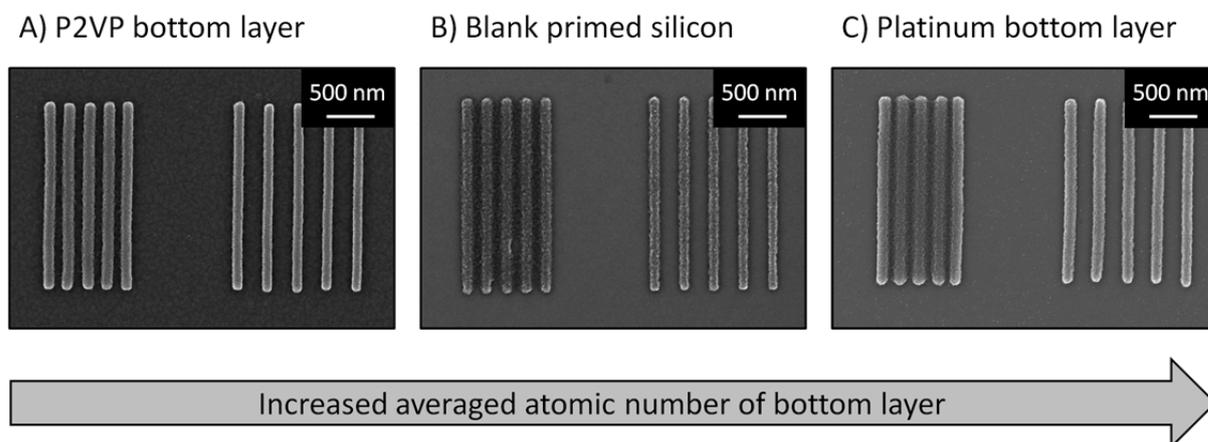
Figure 4.9: SEM images of the realized features (l/s 1/1 and 1/2) on different pretreated substrates: silicon wafer with P2VP bottom layer, blank primed silicon wafer and silicon wafer with platinum bottom layer. All shown features were realized under similar processing conditions (spin-coated resist, composition: 79 wt% trisphenol 16 wt% crosslinker and 5 wt% PAG1), PAB of 60 s at 110 °C, exposure dose of 231 µC/cm², PEB of 30 s at 90 °C, development of 20 s in unstirred 0.05 N TMAH. The l/s 1/2 features are exposed on all bottom layers with the fitting exposure dose, which results in residue free features. The feature quality for the P2VP bottom is increased compared to the other investigated surfaces, which is indicated by the smoother features. The l/s 1/1 features are slightly overexposed, recognizable by the slightly too thick lines and the small amount of residues formed between them. For the different bottom layers the amount of residues is increasing beginning from P2VP (**A**) over blank silicon (**B**) to platinum (**C**), following the trend of the respective atomic number.

The images of the l/s 1/1 features realized for an exposure dose of 231 µC/cm² show residues originating from backscattering in between the lines for all different surfaces. However, their amount depends on the atomic number of the applied bottom layer materials, giving the best performance for P2VP (**A**; averaged atomic number: 3.7), a medium performance for blank silicon (**B**; 14) without a bottom layer and the weakest performance for platinum (**C**; 78). Thus the polymeric material P2VP utilized as bottom layer successfully decreases the amount of backscattered electrons reaching the resist. Additionally the shown images of the l/s 1/2

features indicate smoother lines for the P2VP bottom layer compared to the blank silicon, so the application of a polymeric bottom layer might increase overall the resist performance.

The effect of a polymeric bottom layer with respect to backscattered electrons was also investigated by simulating the electron scattering with the Casino software (as already utilized in chapter 3.3.3). For this simulation an acceleration voltage of 20 kV, a beam radius of 2 nm and a resist layer of 100 nm thickness (PMMA; standard electron beam resist) were utilized. The PMMA resist layer was placed directly on top of the silicon substrate in the first simulation representing the experiment on the HMDS primed silicon (**Figure 4.10A**). For the second simulation a 600 nm thick layer out of P2VP was placed between the resist layer and the silicon substrate as a bottom layer (**Figure 4.10B**). Figures **A** and **B** show the resultant images of the simulated pathways of 1000 electrons for both film architectures.
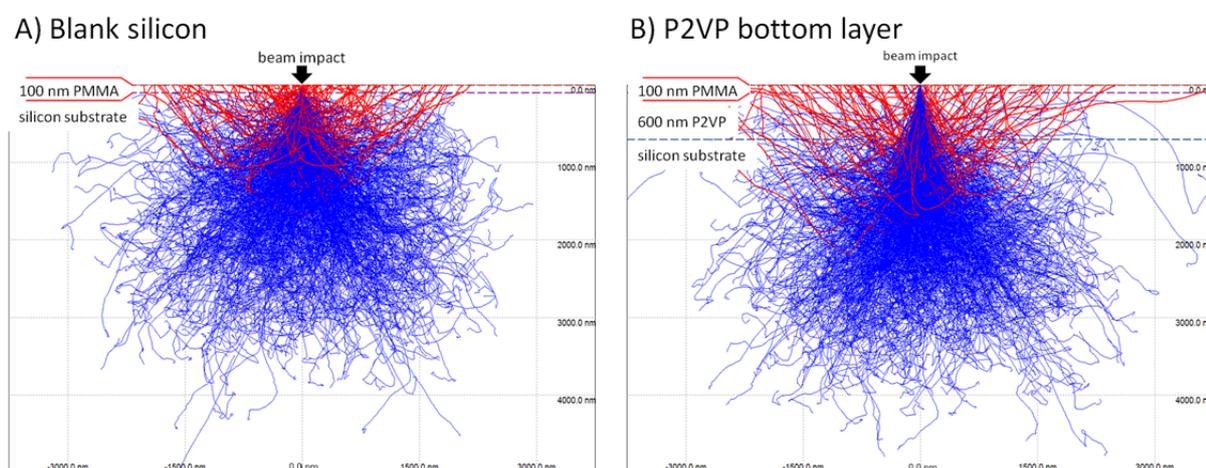
Figure 4.10: Images of electron pathways through organic layers and silicon simulated by the Casino software. The simulation was performed with a beam radius of 2 nm, a total number of electrons of 1000 and an acceleration voltage of 20 kV. All backscattered electrons leaving the film are colored in red, while the rest of the electrons are colored in blue.
A) The blank silicon sample consisted of a 100 nm thick PMMA resist film on top of a silicon substrate.
B) The P2VP bottom layer sample consisted of a 100 nm PMMA resist film on top of an additional applied 600 nm thick P2VP film on a silicon substrate. The simulated electron pathways for the two architectures show that the electrons in b) keep their preferential direction longer, which is apparent from the deeper ranging dark blue area. Additionally, quite an amount of electrons enter the P2VP layer, but do not cross it towards the resist, thus do not contribute to the formation of residues. This leads to a reduced amount of backscattered electrons with the additional P2VP layer. This visible effect is supported by a numerical evaluation of the red marked backscattering electrons leaving the sample giving 132 backscattered electrons for the blank silicon that are concentrated around the impact point, while with the P2VP 25% less and more widely spread electrons (99) are counted.

The simulation shows the dramatic effect of an additional P2VP layer on the electron scattering. With this polymeric bottom layer the electrons keep their orientation much longer, thus most of the electrons penetrate deeper. This is a result from the different atomic numbers in the electron-passed layers as a higher atomic number results in increased scattering of electrons. Thus a smaller fraction of electrons is scattered when passing the same depth in P2VP compared to silicon. Additionally the P2VP acts as a spacer layer between the silicon substrate and the resist layer. This additional layer extends the path the backscattered electrons have to pass from their origin (mainly in the silicon substrate). Thus due this longer path of the backscattered electrons, but also due to absorption respectively further scattering, the amount of backscattered electrons reaching the resist layer is significantly reduced. Such absorbed electrons appear in **Figure 4.10** as blue pathways ending in the P2VP layer. A numerical evaluation of the backscattered electrons leaving the resist gives 132 electrons concentrated around the impact point for the blank silicon sample, while for the P2VP layer 25 % fewer and more widely spread electrons (99) are counted. Consequently such a polymeric bottom layer can obviously decrease the amount of backscattered electrons and thus help to reduce the residues originating from backscattering for PVD prepared resist films in particular.

4.8.   Sensitivity investigations of alternative photoacid generators

Beside the positive effect of a bottom layer in reducing backscattered electrons it is also known that an increased acceleration voltage of an electron beam tool reduces the local dose originating from backscattered electrons due to an increased penetration depth.[138] So for successful residue reduction a combination of the bottom layer approach with an increased acceleration voltage of 100 kV is most beneficial. Such investigations were performed using the 100 kV dedicated electron beam tool (Joel JBX-9300FS) in Cornell NanoScale Science and Technology Facility. Therefore the optimized composition of the trisphenol/crosslinker resist should be investigated. Indeed the utilized PAG is crucial for sensitivity and overall resist performance. To optimize this resist with respect to the PAG, sensitivity screenings with different non-ionic PAGs (shown in **Figure 4.11**) were performed to identify the most sensitive non-ionic electron beam PAG. For this purpose resist films with selected PAGs and the resist materials trisphenol and crosslinker were prepared with quite similar resist

compositions by PVD[4]. Afterwards a dose gradient ranging from 10 µC/cm² to 450 µC/cm² featuring macroscopic squares was exposed on each resist film. After the subsequent PEB at 90 °C for 30 s the development was performed for 20 s in unstirred 0.05 N TMAH solution. The resulting pattern height of the different squares was measured by a stylus profiler in dependence on the applied exposure dose.
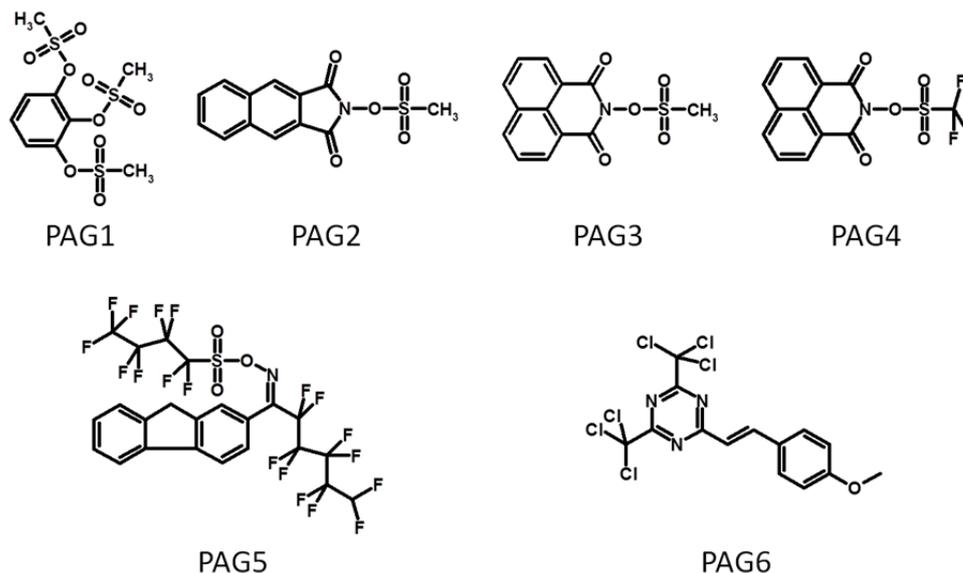
Figure 4.11: Overview of PAGs investigated in the sensitivity screening:
1,2,3-Tris (methylsulfonyloxy)benzene (PAG1); Methanesulfonic acid 1,3-dihydro-1,3-dioxo-2*H*-benz[*f*]isoindol-2-yl ester (PAG2); Methanesulfonic acid 1,3-dioxo-1*H*-benz[*de*]isoquinolin-2(3*H*)-yl ester (PAG3); Trifluoromethanesulfonic acid 1,3-dioxo-1*H*-benz[*de*]isoquinolin-2(3*H*)-yl ester (PAG4); 1-(9*H*-fluoren-2-yl)-2,2,3,3,4,4,5,5,6,6-decafluoro-1-Hexanone *O*-[(1,1,2,2,3,3,4,4,4-nonafluorobutyl)sulfonyl]oxime (PAG5); 2-[2-(4-methoxyphenyl)ethenyl]-4,6-bis(trichloromethyl)-1,3,5-Triazine (PAG6)

From the investigated PAGs only for PAG1, PAG2, PAG3 and PAG4 the entire initial film height was received at the highest applied dose. PAG5 and PAG6 in contrary had only 25% of the initially film height even for the highest dose. Thus the latter mentioned two PAGs show less or nearly no electron beam sensitivity. For the attractive four electron beam sensitive PAGs, the contrast curves with normalized film thickness are shown in **Figure 4.12**.

---

[4] By HPLC determined resist compositions: PAG1: 21 wt% crosslinker, 5 wt% PAG1, 74 wt% trisphenol

PAG2: 15 wt% crosslinker, 3 wt% PAG2, 82 wt% trisphenol

PAG3: 19 wt% crosslinker, 8 wt% PAG3, 73 wt% trisphenol

PAG4: 17 wt% crosslinker, 8 wt% PAG4, 75 wt% trisphenol

PAG5: 17 wt% crosslinker, 11 wt% PAG5, 72 wt% trisphenol

PAG6: 20 wt% crosslinker, 5 wt% PAG6, 74 wt% trisphenol
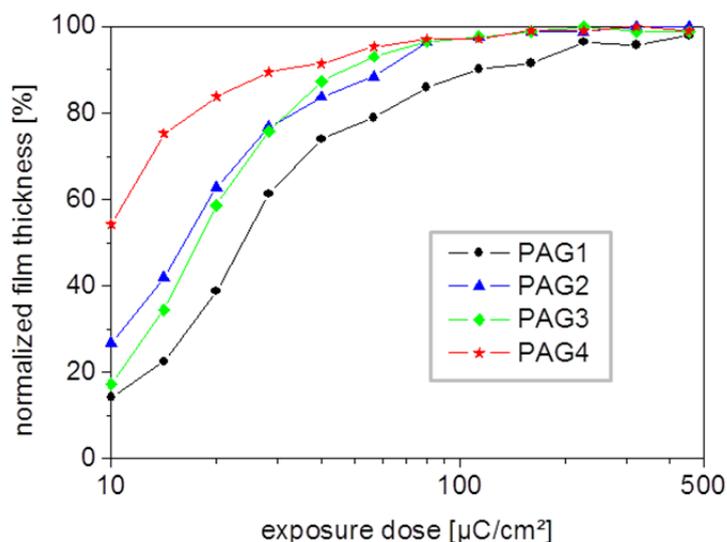
Figure 4.12: Contrast curves of negative tone resist films with selected attractive electron beam sensitive PAGs prepared by physical vapor deposition: The connected lines are added as guide for the eyes. PAG1 shows the lowest sensitivity, which is obvious by the right shifted curve (black circles). Out of the investigated four PAGs, PAG4 shows the highest sensitivity (red stars).

The sensitivity screening with these four PAGs shows that all PAGs with a cyclic imide group are more electron beam sensitive compared to the benzene based PAG1. Out of the three cyclic imide based PAGs, PAG4 is the most promising due to the highest measured sensitivity. This is explainable due to the more acidic and thus more reactive trifluoromethanesulfonic acid released in comparison to the methanesulfonic acid for PAG1, PAG2 and PAG3. The most sensitive non-ionic electron beam PAG identified in this comparison - PAG4 - consequently is the best choice for the investigated trisphenol crosslinker resist system and thus PAG4 will be applied for the investigation of the resist system with the dedicated 100 kV electron beam tool.

4.9. Investigation of resist performance for patterning with a dedicated 100 kV electron beam lithography tool

An increased acceleration voltage for the electron beam patterning process can reduce the local dose originating from backscattered electrons due to an increased penetration depth.[138] Thus the PVD prepared resist with the most sensitive electron beam photoacid generator PAG4 identified in the previous chapter was investigated at the 100 kV dedicated electron beam tool JOEL JBX-9300FS. Therefore a resist film was prepared on a HMDS primed wafer

with a composition of 75.9 wt% trisphenol, 22.8 wt% crosslinker and 1.3 wt% PAG4 by PVD. For this investigation a combinatorial library was designed allowing the optimization of exposure dose, PEB temperature and development time in one experiment shown in **Figure 4.13**. For this library several sectors were arranged in a grid of 25 columns (PEB temperature) and 3 rows (development time) where each sector consists of 24 dose arrays. Each dose array, consisting of a feature size gradient from 12 nm to 144 nm (l/s 1/1), was exposed with a dose range from 24 μC/cm² to 215 μC/cm² defining the exposure dose gradient.

After exposure, the exposed substrate was annealed for 30 s by a PEB temperature gradient ranging from 77 °C to 105 °C. For development in unstirred 0.05 N TMAH solution a time step gradient of 10 s, 20 s and 30 s was applied perpendicularly to the PEB temperature gradient.
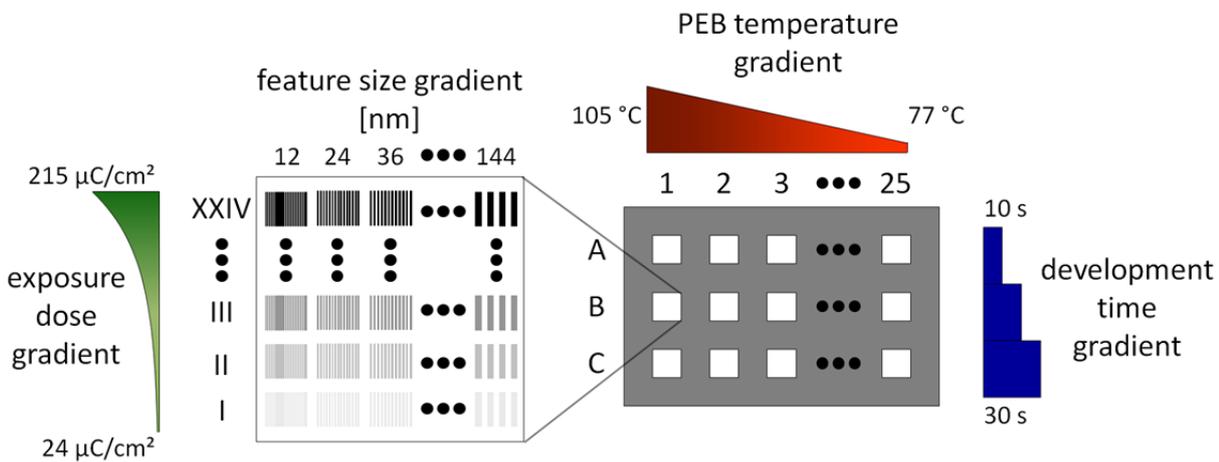
Figure 4.13: Schematic illustration of the investigated combinatorial library for the optimization of exposure dose, PEB temperature and development time in one experiment. The combinatorial library consists of an exposure dose gradient ranging from 24 μC/cm² to 215 μC/cm² (100 kV) applied in each sector, a PEB temperature gradient ranging from 77 °C to 105 °C (30 s) and a development time gradient featuring 10 s, 20 s and 30 s (0.05 N TMAH) . Additionally each exposure dose contained a feature size gradient for l/s 1/1 features, ranging from 12 nm to 144 nm.

The optimized patterns of this experiment concerning residue formation and blur were found in sector A20. An SEM image of a selected realized 96 nm pattern is shown in **Figure 4.14**. The image shows compact lines with some remaining residues. However in comparison to the 100 nm features achieved with the 20 kV electron beam tool (chapter 4.5), a crucial reduction of residue formation is observable just as a result of the exchange of PAG and the utilization of a higher acceleration voltage.
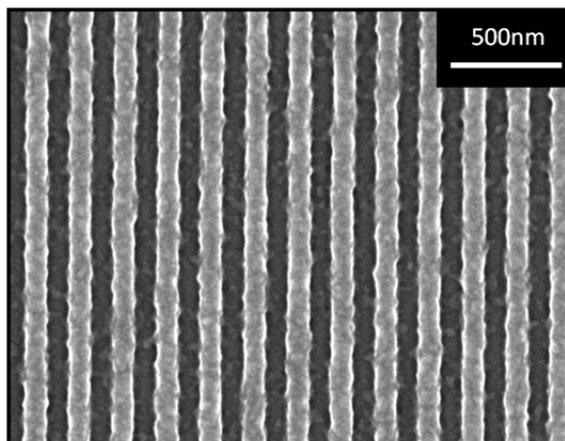
Figure 4.14: SEM image of line pattern observed in the optimized sector A20 of the combinatorial library of PVD prepared resist (composition: 75.9 wt% trisphenol, 22.8 wt% crosslinker and 1.3 wt% PAG4) patterned with a 100 kV electron beam tool: 96 nm lines were observed at a PEB of 99 °C, a development time of 10 s and an exposure dose of 75 µC/cm² at 100 kV. The features show compact lines with fewer residues in between.

In addition, to overcome the issue of residue formation due to backscattering, the bottom layer approach identified in chapter 4.7 was used: A 100 nm film of P2VP was applied by spin coating on the silicon wafer, followed by the PVD process giving a resist film with 78.4 wt% trisphenol, 19.3 wt% crosslinker and 2.3 wt% PAG4. This received sample was investigated afterwards by applying a similar combinatorial library (**Figure 4.13**) for the optimization of exposure dose, PEB temperature and development conditions. Once again, several sectors were arranged in a grid of 25 columns and 3 rows, where each sector consisted of 24 dose arrays. Each dose array, comprising a feature size gradient from 12 nm to 144 nm (l/s 1/1), was exposed with a dose range from 24 µC/cm² to 215 µC/cm² defining the exposure dose gradient. Afterwards the exposed substrate was annealed for 30 s by a PEB temperature gradient ranging from 77 °C to 105 °C. For development in unstirred 0.05 N TMAH a time step gradient of 10 s, 20 s and 30 s perpendicular to the PEB temperature gradient was applied. The overall best pattern of the combinatorial library concerning residue formation and blur is shown in **Figure 4.15**.
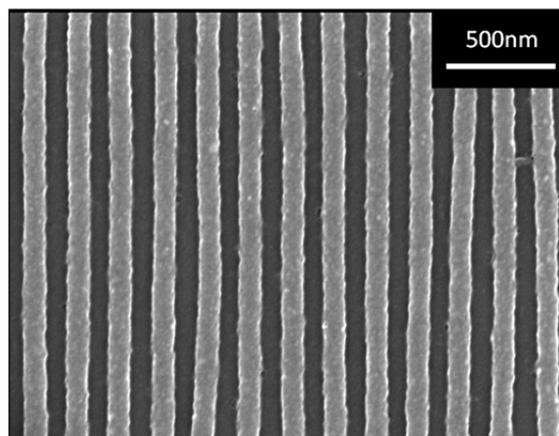
Figure 4.15: SEM images of the line pattern observed at the optimized sector B25 of the combinatorial library of PVD prepared resist (composition: 78.4 wt% trisphenol, 19.3 wt% crosslinker and 2.3 wt% PAG4) with an additionally applied bottom layer: 96 nm lines were observed at a PEB of 105 °C, a development time of 20 s and an exposure dose of 26.4 µC/cm². No residues are observable.

The 96 nm lines were achieved at a PEB temperature of 105 °C, a development time of 20 s and an exposure dose of only 26.4 µC/cm². The observed clear lines at the quite low needed exposure dose demonstrate that the introduction of the bottom layer P2VP has no impact on the high sensitivity of this optimized PVD resist. But the additional bottom layer successfully suppresses the residue formation due to backscattered electrons. Unfortunately, the lines are not perfectly parallel, a sign for weak anchoring of the exposed resist to the bottom layer interface.

In conclusion this work demonstrates that the application of the solvent-free film coating technique PVD is not only an alternative high quality film preparation technique but rather improves the resist performance by homogeneous material blending. Additionally it was shown, that the impact of backscattered electrons can be reduced by introducing an organic bottom buffer layer between a high sensitive resist material and the silicon substrate.

5. Synthesis of novel positive tone chemically amplified molecular glass resist materials applicable by physical vapor deposition

5.1. Introduction

In chapter 1.5 literature known resist materials applicable by physical vapor deposition (PVD) have been summarized. It is conspicuous that so far, only a few examples of chemically amplified resists (CARs) have been investigated by PVD and the results published. In the negative tone regime resists are known, which consist of a phenolic compound, a crosslinker and a non-ionic photoacid generator.[93],[118] After exposure this resist type undergoes a thermally activated and acid-catalyzed crosslinking reaction defining the development contrast to the unexposed material. The resist system obviously benefits from the application of the solvent-free film preparation method PVD, since it is known that solvent residues manipulate physical properties of the film and thereby the performance of the resist.[6] It has also been shown in chapter 4 that in multi-component systems film preparation by PVD allows a more homogeneous material distribution within the film. This makes itself felt - especially due to the more homogeneously distributed PAG - through increased resist sensitivity.

Certainly both benefits would also be true for positive tone chemically amplified resist films prepared by PVD. However, in literature no positive tone chemically amplified resists applicable by PVD have been reported up to today. The reason for this finding might be the need for materials to feature certain properties to assure applicability as chemically amplified positive tone resist materials. Considering the potential benefits, a closer evaluation of these properties seems advisable. First of all, suitable materials have to feature functional groups, which are acid-cleavable. Additionally the resist material must form stable amorphous resist films, which are indispensable for the realization of high resolution features. The glass transition temperature (T_g) of these resist films should be higher than the post exposure bake (PEB) temperature. If T_g is lower than the applied PEB temperature, the increased acid diffusion would affect the maximal realizable resolution of the resist.[139] The applied PEB temperature for a resist system depends on the utilized functional group to allow the efficient acid catalyzed cleavage reaction. Finally, the feasibility of PVD processing requires a high enough thermal stability of the materials to be evaporable without material's decomposition. The evaporation temperature for the PVD processing depends on the molecular weight and the intermolecular interactions of the respective resist material. The decomposition

temperature of a material is given primarily by the decomposition temperature of the weakest functional group in the molecule. For a positive tone photoresist this usually is the utilized protection group.

The solvent coated positive tone molecular glass resist materials investigated in literature (see chapter 1.3) mainly utilize protection groups based on carbonate esters (**Figure 5.1** A) or esters (**Figure 5.1** B). The ester protection group shows an acid-catalyzed reaction under the elimination of an alkene to a carboxylic acid, while the carbonate ester protecting group forms a hydroxyl group under the elimination of an alkene and additionally CO_2. Polymeric materials with such protection groups show thermal decomposition temperatures of around 200 °C depending on the utilized alcoholic compound.[140],[141] This quite high decomposition temperatures make these protection groups potential candidates for the PVD film preparation. Their applicability by PVD is investigated in the following chapter utilizing selected materials out of these classes.
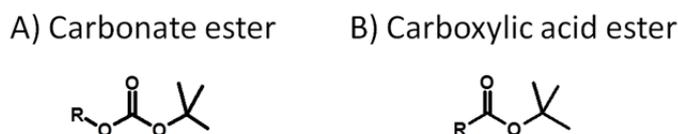
Figure 5.1:   Schematic chemical drawing of acid cleavable protection groups for positive
tone resists: A) Carbonate ester based protection group with a tertiary alcohol
(*tert*-butanol) and an alcoholic function (usually a phenol) of the molecular
glass core (R).
B) Protection group based on an ester of a carboxylic acid function of the
molecular glass core (R) and a tertiary alcohol (*tert*-butanol).

5.2.   Investigation on the processibility by physical vapor deposition of carbonate ester based positive tone chemically amplified resist materials

The most prominent carbonate ester based protection group is the *tert*-Butyloxycarbonyl group (tBoc), utilized recently for the synthesis of several molecular glass resist materials by Ober and coworkers.[66],[142] In this study it turned out, that not fully protected materials show higher T_g, a finding which made them a promising choice for patterning experiments. By utilizing these partly protected materials, even feature sizes below 30nm could be demonstrated by EUV exposure. However, it was also shown, that such partly protected materials showed decreased decomposition temperatures of around 120 °C compared to 160 °C for the fully protected ones. Obviously, this originates from the free acidic phenol

groups in the partly protected materials, which are acidic enough to catalyze the deprotection at enhanced temperatures. Thus fully protected materials have more potential to be evaporable and thus applicable for the film preparation by PVD.

In cooperation with the research group of Prof. Ober (Cornell University) such fully protected materials were investigated for their processability by PVD. In this context Anuja de Silva from the Ober group synthesized several fully protected molecular glass materials, which were investigated by PVD at the University of Bayreuth. The investigated materials are shown in **Figure 5.2** and their thermal properties are summarized in **Table 5.1**.

Bisphenol-AP-tBoc

Phenylene-Bisphenol-tBoc

Trisphenol-tBoc

Trisphenol-2-tBoc
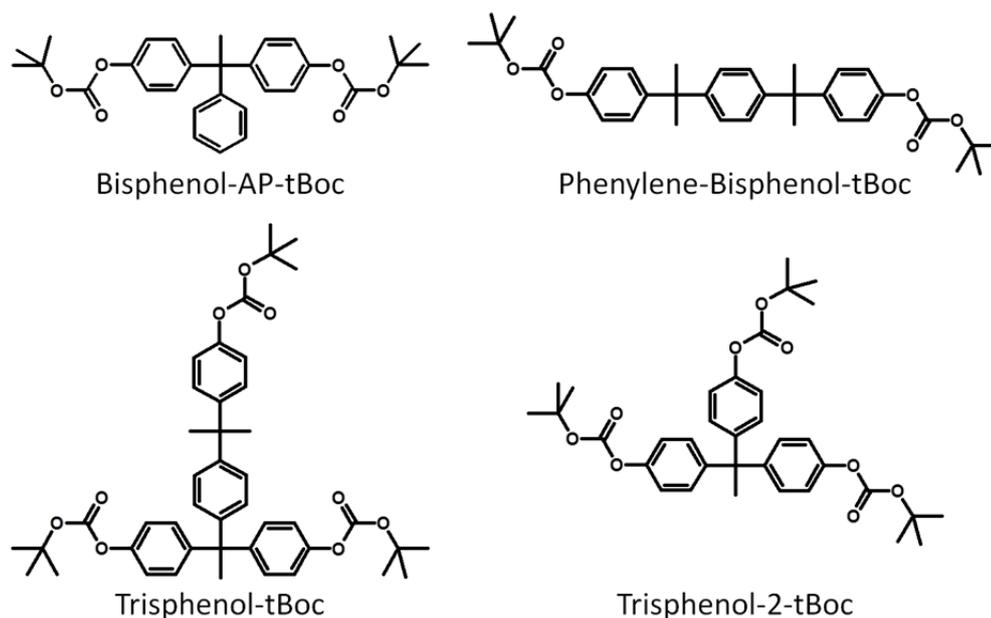
Figure 5.2:   Chemical formula of investigated tBoc protected molecular glasses: The materials were synthesized and characterized by Anuja de Silva (Cornell University). The investigation on PVD processability was performed at the University of Bayreuth.

Table 5.1: Overview of the thermal properties of the investigated tBoc based positive tone molecular glasses.

compound	MW[a] [g/mol]	T_d[b] [°C]	T_g[c] [°C]	PVD processability
Bisphenol-AP-tBoc[142]	490.6	160	33	successful
Phenylene-Bisphenol-tBoc[5]	546.7	160	-[e]	decomposition
Trisphenol-tBoc5	724.9	160	54	decomposition
Trisphenol-2-tBoc5	606.7	160	-[e]	decomposition

[a] Molecular weight. [b] Decomposition temperature measured by Anuja de Silva. [c] Glass transition temperature measured by Anuja de Silva. [e] Not observed.

Unfortunately only the molecular glass with the lowest molecular weight, the Bisphenol-AP-tBoc, allowed the preparation of resist films consisting primarily of the non-decomposed materials. The other investigated materials in contrary required evaporation temperatures which surpassed their decomposition temperatures. Consequently only films consisting of the deprotected material were received. So the Bisphenol-AP-tBoc is the only applicable candidate for a positive tone PVD processible resist with respect to the investigated materials. However, this molecular glass shows a T_g of only 33 °C, which is far lower than the typically applied PEB temperature for tBoc protected molecular glass materials (usually around 90 °C [142]). It is known[139], that materials show a very high acid diffusion at temperatures higher than the T_g, which impacts the realizable resolution in chemically amplified resists. Consequently the Bisphenol-AP-tBoc is not a promising candidate for a high resolution resist material.

In summary, the investigation of tBoc protected molecular glasses showed that only low molecular glass materials with this protection group are evaporable without thermal decomposition. However, such small molecules usually lack stable amorphous phases or show low T_g temperatures, which makes them unsuitable for high performance resist materials.

---

[5] The data for Phenylene-Bisphenol-tBoc, Trisphenol-tBoc Trisphenol-2-tBoc were obtained orally from Anuja de Silva

5.3. **Synthesis and characterization of resist materials based on carboxylic acid esters for positive tone chemically amplified resist processible by physical vapor deposition**

In chapter 5.2 it has been demonstrated that carbonate ester based resist materials show a narrow material window for being processible by PVD. Consequently, further attempts in the synthesis of new molecular glass materials suitable for PVD processing focused on an alternative protection group, which was supposed to open up a bigger window to applicable materials. For this study, the ester protection group was selected. Such esters are a widely applied functional group for resist materials especially utilized in methacrylate based 193nm resist materials.[51] The ester protection group consists usually of a carboxylic acid, which is bound to the polymeric backbone, and a tertiary alcoholic compound.

As a starting point for the synthesic strategy, here reported, the trisphenol core was selected, as it had shown the highest T_g with the tBoc protection group in the previous chapter. Pivalic acid was interlinked to this phenolic core material in order to synthesize the ester compound **1** by esterification. In addition to this core material, the 5,5',6,6'-Tetrahydroxy-3,3,3',3'-tetramethyl-1,1'-spirobisindane (in short: spirobisindane) was esterified with pivalic acid to compound **2** as well as with 1-adamantyl carbonic acid to compound **3**. The obtained low molecular esters are shown in **Figure 5.3** and their thermal properties are summarized in **Table 5.2**.
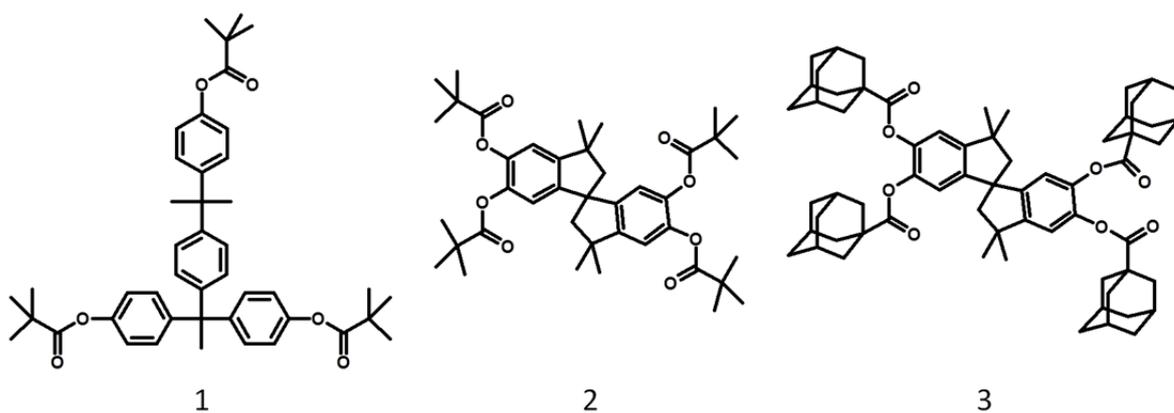
Figure 5.3:   Overview of the synthesized ester materials **1-3**:
       1:   4,4'-[[4-[1-(4-Hydroxyphenyl)-1-methylethyl]phenyl]methylene]bisphenol tri-pivalic acid ester
       2: 5,5',6,6'-Tetrahydroxy-3,3,3',3'-tetramethyl-1,1'-spirobisindane tetra-pivalic acid ester
       3:   5,5',6,6'-Tetrahydroxy-3,3,3',3'-tetramethyl-1,1'-spirobisindane tetra-1-adamantanecarboxylic acid ester

Synthesis of novel positive tone chemically amplified molecular glass resist materials
applicable by physical vapor deposition

Table 5.2:   Thermal properties of the ester molecules **1-3**.

compound	MW[a] [g/mol]	$T_{d;-5wt\%}$[b] [°C]	$CY_{500\,°C}$[c] [%]	T_m[d] [°C]	T_g[e] [°C]	PVD processability
1	676.9	366	2	195	62	successful
2	676.9	290	0	326	-[f]	successful
3	989.4	337	17	~370[g]	-[h]	successful

[a] Molecular weight. [b] Decomposition temperature measured at the weight loss of 5 wt%. [c] Char yield measured at 500 °C. [d] Melting temperature measured in first heating with a heat rate of 10 K/min. [e] Glass transition temperature measured at second heating with a heat rate of 10 K/min. [f] Recrystallization upon cooling at 283 °C (10 K/min). [g] Evaluated by cross-polarized light microscopy. [h] Not evaluated due to decomposition prior to Tm.

The synthesized ester molecules **1-3** showed a very high thermal stability with thermal decomposition temperatures $T_{d,-5wt\%}$ of 290 °C, 337 °C respectively 366 °C. In comparison to industrially utilized polymeric ester based positive tone resist materials, which decompose at around 200 °C, these decomposition temperatures are clearly higher.[141] The minor thermal stability of such materials can be explained by the characteristics of the acid catalyzed deprotection route, leading to an alkene and the carboxylic acid, which can perform without the need of an additional reaction partner. The synthesized materials in contrary have only the saponification reaction for the cleavage of the synthesized ester group, but this type of reaction requires the presence of water. Due to the required additional reactant, the materials show the increased thermal decomposition.

The thermal characterization showed for **1** a melting point at 195 °C at the first heating and a glass transition temperature of 62 °C at the second heating step. The material **2** showed a melting point at 326 °C in the DSC, but upon cooling the material did not form an amorphous phase (even at a cooling rate of 40 K/min), thus no glass transition temperature was detected. The measured melting point surpassed the decomposition temperature of this material. Utilizing cross-polarized light microscopy it was observed that prior to melting, sublimation occurred. Material **3** in contrary showed a melting point of around 370 °C in cross-polarized microscope investigation, but it also changed its color to brown at this temperature, which indicates material decomposition. Thus material **3** was not further investigated by DSC. Out of these three materials, only **1** showed a stable amorphous phase. However, the low T_g of **1**, the crystalline behavior of **2** and **3**, and the difficult deprotection chemistry, which requires the presence of water, make them unfavorable for use as resist materials. But these molecules

had been designed in the first place to estimate the glass transition temperature of structural similar molecular glass resist materials with inverted ester linkages, which undergo the deprotection without the need of water by forming an alkene and the corresponding carboxylic acid. In such materials the core material carries the carboxylic acid function, which is then esterified with a secondary or tertiary alcohol like tert-butanol.

From our cooperation partner - the research group of Prof. Ober (Cornell University) - several phenolic molecular glass materials with high T_g and relatively low molecular weight were known, which were considered suitable as potentials core materials for PVD processible positive tone resists.[142],[66],[137] However, to synthesize this class of materials, which is acid catalyzed cleavable without an additional reactant, it is necessary to start with a carboxylic acid functionality attached on the core, which then is esterified with a suitable secondary or tertiary alcohol to receive a ester based material. For this study, the transformation to a carboxylic material and the protection was realized in one step by the reaction with *tert*-butyl bromoacetate, which introduced both the carboxylic acid function and the targeted ester with *tert*-butanol. In addition to the spirobisindane a twisted biphenol core was used for this synthetic route. Beside this route also a carboxylic acid carrying twisted biphenol core was esterified directly with the secondary alcohol isoborneol. The chemical structures of the synthesized ester materials **4, 5** and **6** are shown in **Figure 5.4** and their thermal properties are summarized in **Table 5.3**.
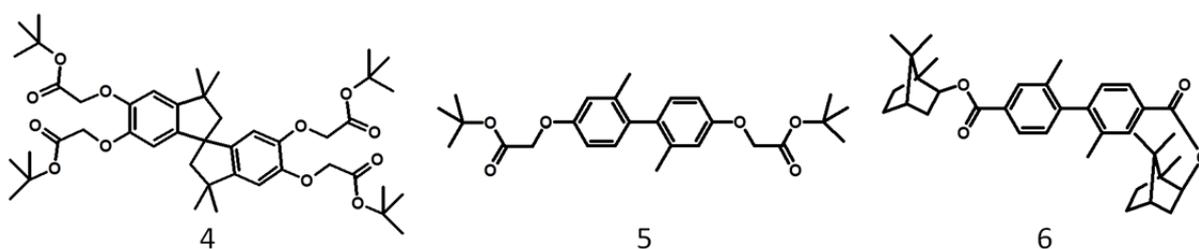
Figure 5.4: Overview of the synthesized ester materials, which are acid cleavable without the need of an additional reactant:
4: 5,5',6,6'-Tetrahydroxy-3,3,3',3'-tetramethyl-1,1'-spirobisindane tetra-*tert*-butyl acetate ether
5: 2,2'-dimethyl-[1,1'-Biphenyl]-4,4'-diol di-*tert*-butyl acetate ether
6: 2,2'-dimethyl-[1,1'-Biphenyl]-4,4'-dicarbonic acid isoborneol ester

Table 5.3: Overview of the thermal properties of the synthesized materials, which are acid cleavable without the addition of an additional reactant.

compound	MW[a] [g/mol]	$T_{d;-5wt\%}$[b] [°C]	$CY_{500\,°C}$[c] [%]	T_m[d] [°C]	T_g[e] [°C]	PVD processability
4	797.0	213	18	165	25	decomposition[g]
5	442.6	209	21	-	-1	not tested[h]
6	542.8	250	2	152	50	successful

[a] Molecular weight. [b] Decomposition temperature measured at the weight loss of 5 wt%. [c] Char yield measured at 500 °C. [d] Melting temperature measured in first heating with a heat rate of 10 K/min. [e] Glass transition temperature measured at second heating with a heat rate of 10 K/min. [g] Investigated by sublimation. [h] Not investigated because material is a liquid at room temperature.

Materials **4** and **5** showed a quite high thermal stability with decomposition temperatures $T_{d;-5wt\%}$ of 209 °C and 213 °C. These decomposition temperatures are lower than the ones measured for the materials (**1-3**) without a water-free acid catalyzed deprotection route. Obviously, the inverted ester protection group reduces the thermal stability. However, in comparison to tBoc protected materials (chapter 5.2), which show decomposition temperatures of around 160 °C, the ester protection group is more stable and thus more promising. The thermal characterization of material **4** showed the melting point at 165 °C and the glass transition temperature T_g at 25 °C. For material **5**, which is a viscous liquid at room temperature, the very low T_g at -1 °C was measured. These very low T_g temperatures most probably resulted from the flexible ether linkage utilized for the bonding of the carboxylic acid function. Consequently, the introduction of the ester based protection group by *tert*-butyl bromoacetate generates low T_g materials. Thus to overcome this T_g issue, a core material with directly bounded acid functions should be used.

To investigate this design concept, 2,2'-dimethyl-[1,1'-Biphenyl]-4,4'-dicarbonic acid was esterified with the isoborneol alcohol. Despite of isoborneol being a secondary alcohol in contrary to the previously used *tert*-butanol, it is known to be acid catalyzed cleavable without an additional reactant upon a intramolecular rearrangement process.[143] However, the acid catalyzed cleavage of the ester group followed by the rearrangement process of the isoborneol group requires high PEB temperatures of around 120 °C. The resultant molecular glass (**6**; **Figure 5.4**) showed a decomposition temperature $T_{d;-5wt\%}$ of 250 °C. This indicated that with the isoborneol, the resultant esters were even more stable than the *tert*-butyl esters **4** and **5**. With this high decomposition temperature the material was capable of being processed

successfully by PVD. The thermal characterization of **6** showed a melting point at 152 °C and a glass transition at 50 °C. Thus unfortunately the material has not a suitably high T_g in the range of the necessary PEB temperature to be applicable as a high performance resist material.

In summary none of the synthesized materials showed a high glass transition temperature within the range of the PEB temperature necessary for resist application. However, it was shown that ester based positive tone materials show high enough thermal decomposition temperatures for being applicable for PVD processing. This was especially the case for material **6** which showed 40 °C higher decomposition temperatures with the attached isoborneol compared to the *tert*-butyl esters. Thus with a suitable core material, a PVD processible molecular glass material with a high enough glass transition temperature should be synthesizable in a future investigation.

6. Novel physical vapor depositable molecular glass photoresist based on ionic interactions

6.1. Introduction

In the International Technology Roadmap for Semiconductors (ITRS) 2011, issues for chemically amplified resists (CARs) are mentioned regarding the realization of resolutions below 20 nm half pitch due to acid diffusion.[61] Proposed measures to deal with these issues comprised both the reduction of acid diffusion length and the change of the sensitizing method. Such diffusion length reduction can be realized by polymer-bound photoacid generators[60] and an increased size of the acid molecule[144] as well as by base additives[145]. However, it is not clear, if the diffusion reduction is sufficient to keep up with the required resolution in the upcoming nodes and if resists based on new sensitizing methods have sufficient performance. That is why the ITRS also mentions non-chemically amplified resists as an alternative concept, which show resolutions below 16 nm and an acceptable line edge roughness (LER). But non-chemically amplified resists typically suffer from low sensitivity.[146] To overcome this issue and to identify non-chemically amplified resists with suitable properties, two routes are pursued in science. In the first one, the processing of a commercial resist is adjusted to achieve a better performance. This concept was investigated e.g. by Shokouhi et al., showing a successful increase in sensitivity for the commercial ZEP-520A electron beam resist by developer change.[147] In the second one, new concepts of creating an alternative development contrast are investigated. These investigation concepts focus mainly on radical crosslinking as an alternative sensitizing method. This was recently investigated for an EUV resist consisting of propargyl-modified Poly(4-hydroxystyrene), a multifunctional thiol compound, and a photoradical generator resulting in a good sensitivity, which was shown for 60 nm l/s features.[148] The sensitizing method of radical crosslinking was also utilized for targeted high sensitive electron beam resists. An eco-friendly water-developable electron beam resist with high sensitivity was realized with an acrylate resist material derived from biomass.[149] However the resolution limit of the resist was not investigated in this study. A very high sensitivity besides a dose switchable dual tone behavior was identified for a resist based on the copolymer poly(2-hydroxyethyl methacrylate-co-2-methacrylamidoethyl methacrylate), but no high resolution features were shown.[150] Thus additional efforts on the optimization of the radical sensitizing concept as

well as the investigation of completely new resist concepts are still needed to realize novel suitable resist materials.

A promising new resist could be the usage of an acid formed during the photoacid generator (PAG) exposure for building a salt in the presence of a corresponding base. The different solubility behavior of the unexposed neutral resist material beside the exposed ionic material should be useable as efficient development contrast. This new resist concept was first investigated as an all dry photoresist system during my diploma thesis.[151] In this work the successful salt formation of the resist, which consisted of a diamine compound and the applied PAG, was proven by infrared (IR) spectroscopy. To be more specific, the resist consisted of Trifluoromethanesulfonic acid 1,3-dihydro-1,3-dioxo-2*H*-benz[*f*]isoindol-2-yl ester (PAG7) and 4,4'-Bis(carbazol-9-yl)biphenyl (Base1) as diamine compound in a molar ratio of 2:1 to have a equimolar ratio of amine sides and PAG molecules. The resultant spectra before and after flood exposure are shown with highlighted characteristic bands in **Figure 6.1**.
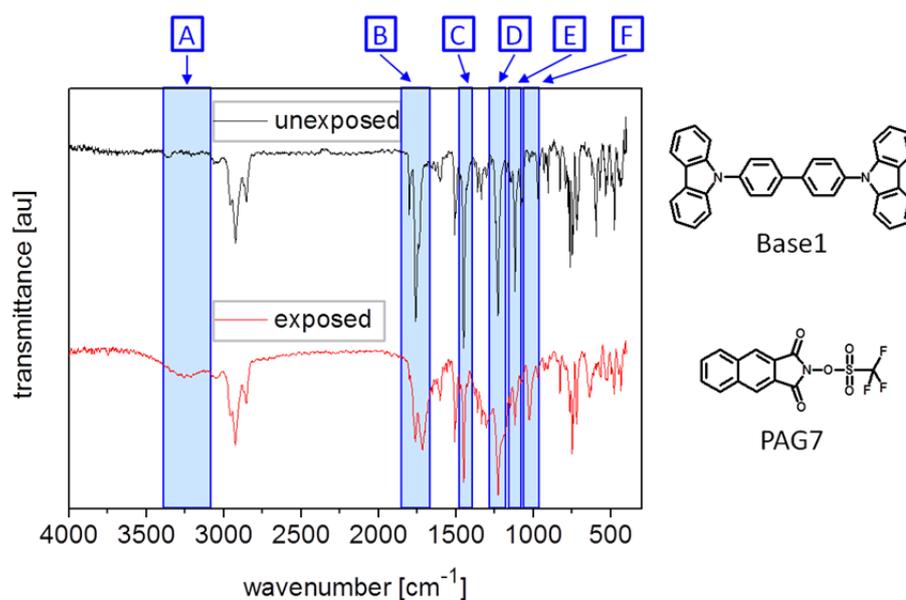
Figure 6.1: IR-spectra[151] of unexposed and exposed resist films with highlighted characteristic bands of the components Base1 and PAG7:
A) signal of R_3NH^+ appearing during exposure at 3250 cm^{-1};
B) band of the carbonyl function in the cyclic imide of PAG7 (unexposed: 1802 cm^{-1} and 1760 cm^{-1}; exposed: 1762 cm^{-1} and 1718 cm^{-1});
C) at 1450 cm^{-1}: overlay of the first band of the bounded sulfonate group in PAG7 and a not assigned band of Base1;
D) at 1228 cm^{-1}: overlay of the band of the C-F bond in PAG7 and a not assigned band of Base1;
E) second band of the bounded sulfonate group in PAG7 at 1120 cm^{-1};
F) band of the formed trifluormethane sulfate at 1027 cm^{-1}.

The IR-spectra before and after exposure differ dramatically and thus demonstrate the successfully formed ionic compounds. The two bands (**B**) of the carbonyl function in the cyclic imide of PAG7 shift from 1802 cm^{-1} and 1760 cm^{-1} to 1762 cm^{-1} and 1718 cm^{-1}, as a result of the acid release due to homolytic cleavage of the N-O-bond and subsequent reactions of the thereby formed radical chromophore. The elimination of the sulfonate group is also obvious due to reduced signal intensity of the bounded sulfonate group (**C**: 1450 cm^{-1} and **E**: 1120 cm^{-1}). As the signal (**E**) results only from the bounded sulfonate group in non exposed PAG7, it allows the approximate estimation of the amount of PAG not activated during the exposure. Besides these signals with decreasing intensity two new bands appear during exposure. The first is found at 1027 cm^{-1} (**F**) at the characteristic position for trifluormethane sulfonate and thus proves the presence of deprotonated acid after exposure.[152],[153] Additionally a broad signal appears at 3250 cm^{-1} (**A**) corresponding to the protonated nitrogen in Base1. Consequently during exposure the salt out of the anion trifluoromethane sulfonate and the cation of protonated Base1 is being formed.

After proving the successful salt formation, the applicability of this resist concept for all-dry processing was investigated in my diploma thesis.[151] Therefore by physical vapor deposition (PVD) prepared films were exposed and thermally developed under vacuum. For a successful realization, the unexposed and exposed resist must differ clearly in their evaporation temperature composing the development contrast. I expected that this evaporation difference originates mainly from higher intermolecular interactions (generated between the resist components due to salt formation) compared to the more neutral unexposed resist materials. In **Figure 6.2** SEM images of the observed features after this thermal vacuum development are shown. They demonstrate that during the applied vacuum development process, the non-exposed material evaporates. However, the resultant linear features are not continuous, which is a consequence of dewetting of the formed salt features during the thermal vacuum development, indicating the melting of the salt material during the thermal treatment under vacuum. However, these results demonstrated for the first time the in principle patternability of a resist system based on a salt formation.
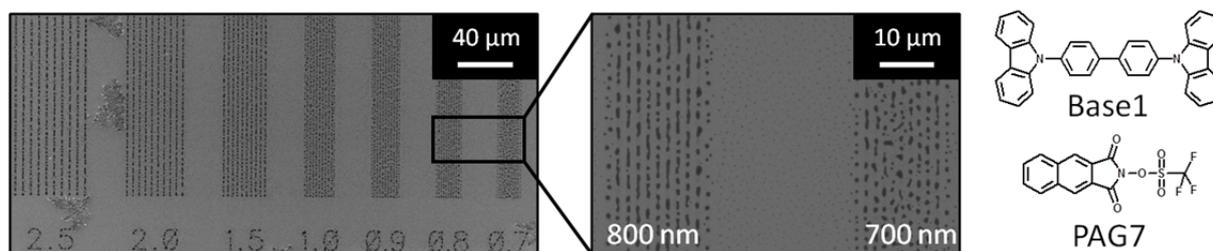
Figure 6.2: SEM images[151] of the realized features with the photoresist out of PAG7 and the base 4,4'-Bis(carbazol-9-yl)biphenyl (Base1): The features were realized using a film composed of 63 mol% PAG7 and 37 mol% Base1, an UV exposure (0.4 mJ/cm², 240 nm - 290 nm) and the thermal vacuum development at 190 °C for 45 min. Even 800 nm wide line-shaped features formed out of droplets due to dewetting are observable. In addition, there is less remaining unexposed crystallized resist material (left side of the left SEM image) shown, which indicates recrystallization of the unexposed resist during thermal vacuum development.

The reason for the dewetting is probably the heating above the glass transition respectively the melting temperature of the formed salt during the thermal vacuum development step. This issue complicates the realization of evaluable features. That is why the evaluation of the patternability of such resist systems based on salt formation for all-dry processing has been investigated in more detail in this thesis.

A possible approach could be the investigation of materials with increased melting respectively glass transition temperatures. However these materials might require even higher development temperatures, thus dewetting might be an issue as well. Too high required development temperatures can also lead to an evaporation of the typically used low molecular weight acid out of the formed salt, resulting in a removal of the exposed negative tone resist material. To overcome this issue an alternative development process might be helpful. An applicable solution was identified by having a closer look on this resist type. During exposure the polarity of the resist changes from unpolar in the unexposed state to highly polar in the exposed state. This polarity switch affects the dissolution behavior of the resist material, which might be useable as dissolution contrast in a solvent-based development process.

As a consequence, the performance of novel resist systems based on salt formation has been investigated in this chapter based on wet development processes in order to eliminate the possibility of patterns being destroyed by the thermal vacuum development. After having investigated the dissolution behavior, the resist processing variables as well as different resist materials themselves were investigated to identify an optimized high performance resist

system. This resist system allowed the evaluation of the potential of the resists class based on salt formation. This novel resist class will be named after the utilized reactive components acid and base as acid-base-resist (ABR) in the following chapters.

6.2. Investigation of dissolution behavior of an acid-base-resist

A crucial characteristic of a resist is a sufficiently high contrast between exposed and unexposed state to realize high quality patterns in the development process. The contrast for solvent based development processes results from the difference in dissolution behavior between exposed and unexposed state. Acid-base-resists exhibit such a contrast due to the polarity change originating from the salt formation. While the unexposed resist consists of less-polar base and PAG molecules, the exposed resist features ionic interactions. Consequently this resist type should form negative tone features upon exposure if the development is performed in unpolar solvents like cyclohexane. This polarity change was investigated utilizing the quartz crystal microbalance technique (QCM) (described in the experimental part; chapter 9.1.3). The very sensitive QCM technique allows the investigation of dissolution and swelling processes and in this study the characterization of the dissolution behavior of exposed and unexposed resist materials.

The acid-base-resist investigated first was selected on the basis of the presented all-dry resist system consisting of PAG7 and the diamine 4,4'-Bis(carbazol-9-yl)biphenyl (Base1). However, this resist showed residual crystals out of unexposed resist material (**Figure 6.2**). By replacing PAG7 by a mixture of the constitutional isomeric PAGs PAG2 and PAG3, the tendency of the unexposed material to crystallize should be suppressed. The investigated resist system ABR1 is shown in **Figure 6.3A**. For the QCM measurement two 140 nm thick films were prepared simultaneously on quartz crystals (QCs) by PVD with a composition of 35 mol% Base1, 32 mol% PAG2 and 33 mol% PAG3. Afterwards the QCs (unexposed respectively exposed: UV exposure: 330 nm - 390 nm, 12 J/cm²) were mounted into the QC holder and their dissolution behavior was investigated in stirred cyclohexane. The resultant dissolution graphs are shown in **Figure 6.3B**.
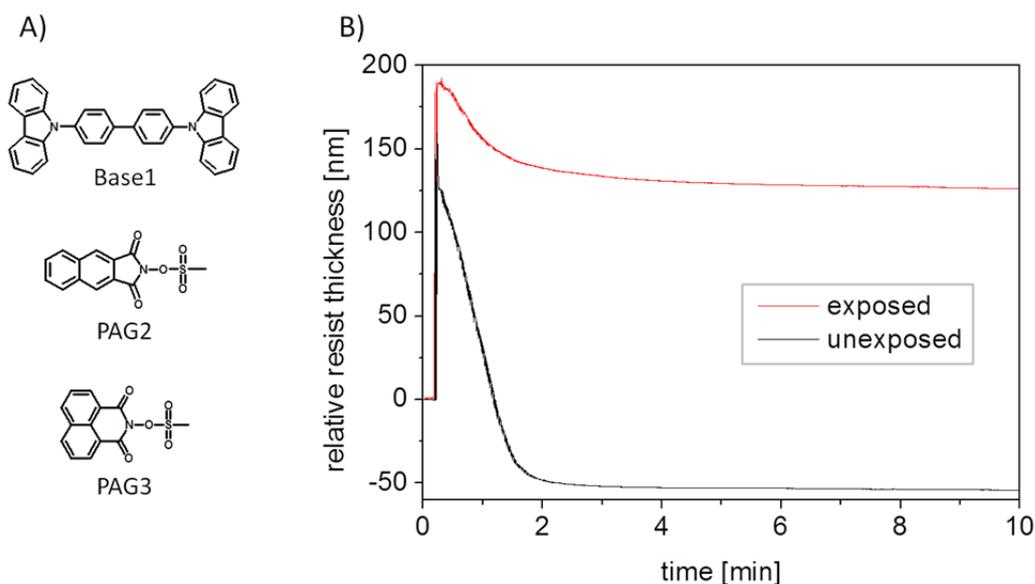
Figure 6.3:   Chemical structures of investigated ABR1 (**A**) and dissolution behavior investigation of exposed and unexposed films prepared by PVD utilizing the QCM technique (**B**): 140 nm thick films with a composition of 35 mol% Base1, 32 mol% PAG2 and 33 mol% PAG3 were prepared; the measurement of the unexposed and exposed films (UV exposure: 330 nm - 390 nm, 12 J/cm²) were performed in stirred cyclohexane. The unexposed film dissolves completely within 2 min. The exposed film on the contrary only shows a moderate loss in film thickness within the first 2 min, which slows down dramatically until the end of the measurement.

Directly after the dipping in stirred cyclohexane the unexposed resist shows a relatively fast complete dissolution at a nearly constant rate within the first 2 min. This observation gives a reference point for the minimal development time of this resist system, as the unexposed resist must be removed completely for successful patterning. The exposed resist on the other hand shows a completely different dissolution behavior. After a moderate film thickness loss at the beginning the dissolution slows down dramatically. This dissolution behavior could be explained by the generation of less-polar aromatic compounds originating from the PAG molecules. During exposure the PAG molecules react to the acid which protonates the base and a free less-polar aromatic part, which might be dissolved out of the surface region of resist film. This dissolution of less-polar material may lead to an enrichment of the ionic resist material at the surface, which explains the slowdown of the dissolution rate due to passivation. Furthermore, the formed salt itself might show some minor dissolution during the development. However, in the very unpolar developer cyclohexane utilized here, the salt is only poorly soluble. A more important influence could be the loss of the salt character due to deprotonation. This can occur, because the utilized base compound Base1 is a very weak base,

which corresponds to a very acidic protonated species. This acid can react with water traces - absorbed on the film surface as well as dissolved in the developer itself. Especially the absorbed water deprotonates the surface area of the film and thus contributes to the moderate dissolution within the first 2 min. In summary, the measured dissolution behavior is explainable by passivation and deprotonation. The remaining exposed resist material is very stable in the developer after the first two minutes and shows an utilizable dissolution contrast to the unexposed material. Consequently, this allows the application of a solvent based development for this acid-base-resist class. However, the resist processing should be adjusted to reduce water traces. The water absorption occurs at normal atmosphere in the transfer times between preparation and exposure respectively exposure and development, thus this transfer should be performed as fast as possible. Additionally the amount of dissolved water in the developer should be reduced by the utilization of anhydrous grade developers.

6.3. Developer screening for the patterning of an acid-base-resist

The already discussed dissolution investigations of the resist ABR1 consisting of the diamine Base1 and a mixture of the PAGs PAG2 and PAG3 have shown an utilizable dissolution contrast in stirred cyclohexane (chapter 6.2). Thus a successful patterning of this resist system with solvent based developing should be possible. A first screening approach was investigated utilizing UV exposure. Besides the developer cyclohexane identified in the dissolution investigations, additional organic solvents with a wide range of different polarities were screened in this work for identifying developer's requirements. Therefore a 130 nm thick resist film was prepared by PVD with a composition of 30 mol% Base1, 45 mol% PAG2 and 25 mol% PAG3 giving around one PAG molecule per amine side. The subsequent exposure by UV light (350 nm - 450 nm) was performed by utilizing a combinatorial mask for the realization of a dose gradient. This mask allows the exposure of multiple features within a square of 1.2 mm edge length. Each feature is exposed with a different dose. For this investigation, the doses 0.2 J/cm², 0.4 J/cm², 0.8 J/cm², 1.2 J/cm², 2.4 J/cm², 4.8 J/cm² and 12 J/cm² were used. After the exposure the film was cut into pieces followed by the development. The development in stirred cyclohexane was performed for 90 s, according to the results of the dissolution investigation. Due to the higher polarity of the developers dichloromethane, dioxane, acetonitrile, THF, ethylacetate, and methanol the development was shortened to 30 s. The evaluation was performed by observing SEM images of obtained

features. However, the development in solvents with moderate polarity (dioxane, dichloromethane and THF) resulted only in residues of the exposed features, as the exposed sectors were hardly observable (images not shown) even for the highest applied exposure dose. Consequently these developers are unsuitable candidates. The SEM images of the more promising investigated developers are shown in **Figure 6.4**.
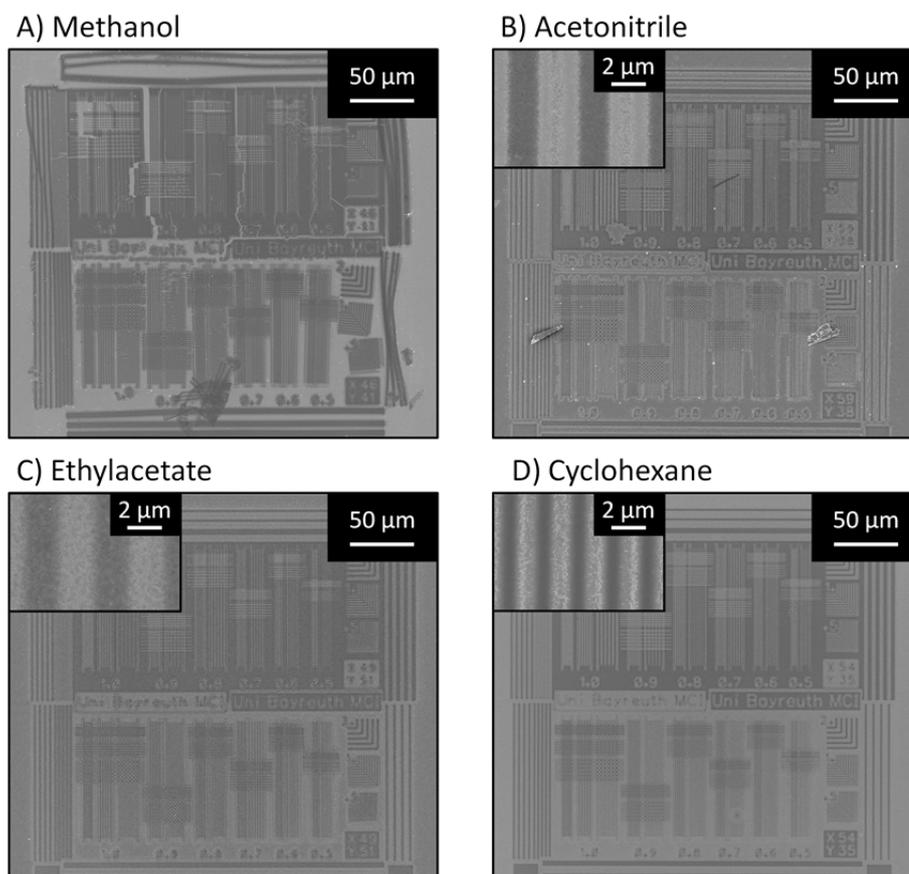
Figure 6.4: SEM images of the realized features out of the developer screening: A 130 nm thick film was prepared by PVD (composition: 30 mol% Base1, 45 mol% PAG2 and 25 mol% PAG3) followed by UV exposure (350 nm - 450 nm) with different exposure doses (0.2 J/cm², 0.4 J/cm², 0.8 J/cm², 1.2 J/cm², 2.4 J/cm², 4.8 J/cm² and 12 J/cm²). Finally the development was performed utilizing different developers (acetonitrile (30 s), ethylacetate (30 s), methanol (30 s) and cyclohexane (90 s)). For methanol (**A**; dose: 1.2 J/cm²), features were received, which were partly stripped. The developer acetonitrile (**B**; dose: 1.2 J/cm²), ethylacetate (**C**; dose: 2.4 J/cm²) and cyclohexane (**D**; dose: 0.4 J/cm²) resulted in stable and likewise similar clear features. However, for all developers some residual material was present between the features.

All four developers show successful pattern formation of negative tone features despite their different polarity. Thus even in the very polar methanol and acetonitrile the formed salt resists the harsh development conditions. The resulting features of **Figure 6.4A** were realized in

methanol for an exposure dose of 1.2 J/cm² and tend to be stripped off the substrate. This very polar solvent can undermine the resist and thus weaken the adhesion of patterns. The other developers in contrary showed no evidence for stripping even at lower exposure doses. They resulted in stable features, which differ between the different developers in the required exposure dose. While the development in acetonitrile required a similar dose as methanol (**B**; 1.2 J/cm²), in ethylacetate a higher dose of 2.4 J/cm² (**C**) and in cyclohexane (**D**) a significantly lower dose of 0.4 J/cm² was necessary. Such higher applied exposure doses increase the fraction of activated PAG in the exposed areas and thus introduce more polarity due to the ionic interactions. In the unpolar cyclohexane the formed salt is barely soluble, thus a small fraction of activated PAG is sufficient for realizing the development contrast. Consequently, cyclohexane is out of the investigated ones the most promising developer solvent for realizing a sensitive resist system. For all the tested developers, the observed features in this screening experiment showed some remaining material in-between, which can be caused by a slight exposure due to scattering of the UV light during exposure or by not completely removed non-exposed material due to a too short development. This issue will be addressed in the optimization of the resist system utilizing electron beam exposure.

Development of the smaller features realized by electron beam exposure is more challenging, so an additional developer screening was performed to select the optimized developer for the acid-base-resist. Therefore the unpolar solvents toluene and n-hexane were investigated along with the three developers (methanol, acetonitrile and cyclohexane) showing a successful pattern formation for an acceptable exposure dose in the previous screening. For this screening 130 nm thick ABR1 resist films were prepared in a first PVD process with a composition of 30 mol% Base1, 45 mol% PAG2 and 25 mol% PAG3 (utilized for methanol, acetonitrile and cyclohexane) and in a second PVD process of 35 mol% Base1, 32 mol% PAG2 and 33 mol% PAG3 (utilized for toluene and n-hexane). Both films show a quite similar PAG amount with 70 mol% compared to 65 mol%, allowing the comparison of the experiments performed on the different films. In the subsequent electron beam exposure the 5th generation writing field design (chapter 3.4) was utilized, which comprises 100 nm line/space features and an internal exposure dose gradient ranging from 100 µC/cm² to 2516 µC/cm². Afterwards the films were developed in acetonitrile (10 s and 30 s), methanol (10 s and 30 s), cyclohexane (30 s, 45 s, 60 s, 100 s), toluene (60 s) and n-hexane (60 s, 120 s). Finally the quality of the resultant features with respect to the different developers was evaluated by observing SEM images (shown in **Figure 6.5**).

A) acetonitrile	B) toluene	C) methanol	D) n-hexane	E) cyclohexane
500 nm	200 nm	200 nm	200 nm	200 nm

development time	10 s	60 s	30 s	120 s	90 s
exposure dose	2516 µC/cm²	2516 µC/cm²	1123 µC/cm²	427 µC/cm²	427 µC/cm²
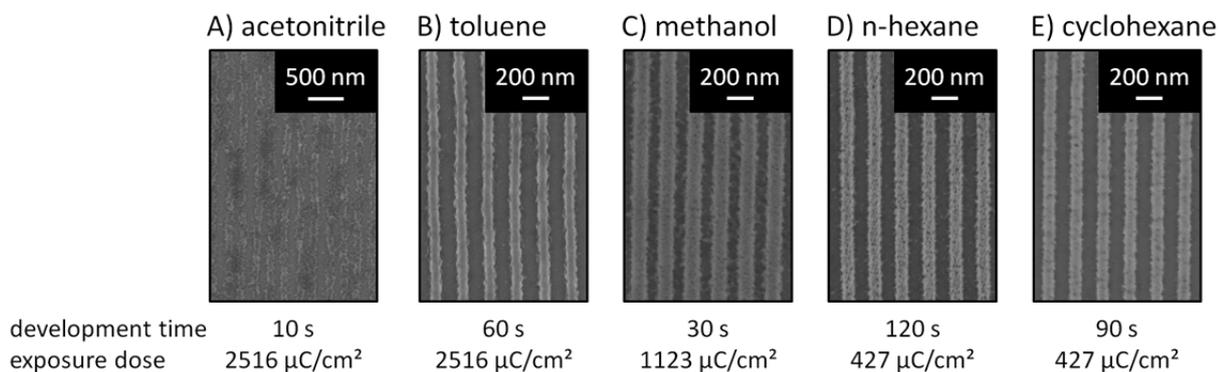
Figure 6.5: SEM images of the realized features utilizing different developers and the respectively applied optimized exposure dose: The 130 nm thick ABR1 films were prepared by PVD (composition: 30 mol% Base1, 45 mol% PAG2 and 25 mol% PAG3 for methanol, acetonitrile and cyclohexane; 35 mol% Base1, 32 mol% PAG2 and 33 mol% PAG3 for toluene and n-hexane) followed by electron beam exposure to the 5th generation writing field design featuring 100 nm features (l/s 1/1) and an internal dose gradient ranging from 100 µC/cm² to 2516 µC/cm². The development was performed in acetonitrile (10 s and 30 s), methanol (10 s and 30 s), cyclohexane (30 s, 45 s, 60 s, 100 s), toluene (60 s) and n-hexane (60 s, 120 s). The development in acetonitrile (**A**) shows only residues of broken lines for the shortest development of 10 s and the highest exposure dose (2516 µC/cm²). Toluene (**B**) in contrary allowed the realization of clear features at a similarly high exposure dose (2516 µC/cm²) and a development time of 60 s. In methanol (**C**; 30 s) a moderate dose of 1123 µC/cm² was necessary to realize features with a decent amount of residues in between. The lowest exposure dose (427 µC/cm²) was required for the very unpolar developers n-hexane (**D**; 120 s) and cyclohexane (**E**; 90 s).

The investigated developer solvents differ drastically in the required exposure dose and the quality of the resultant features. Despite the short development time (10 s) in acetonitrile (**A**) the highest applied exposure dose of 2516 µC/cm² is necessary for the realization of less-quality features. However, these show only residues of the exposed straight lines. Consequently, acetonitrile features a too high solubility of the exposed ionic resist material. A similarly high exposure dose (2516 µC/cm²) is required for toluene (**B**) at a development time of 60 s. The realization of clear features shows the successful patterning utilizing this developer. However, a high activation ratio of PAG and thus a high polarity contrast is necessary to achieve the development contrast. With methanol (**C**; 30 s) only half of the exposure dose (1123 µC/cm²) is necessary to realize stable features but some residual materials in between are present. The stripping, which occurred in the previous experiment with UV exposure, is not observable. This behavior can be explained by differences in the exposure technique. In UV exposure light is absorbed during passing the film. Consequently

areas within the bottom part are less activated compared to the upper part. The resulting lower polarity at the bottom part allows the undermining of the resist and thus stripping. For electron beam exposure in contrary, nearly all electrons penetrate the whole resist film. This results in a continuous exposure within the whole film thickness. The two very unpolar developer solvents n-hexane (**D**; 120 s) and cyclohexane (**E**; 90 s) needed much lower exposure doses (427 µC/cm²) for pattern realization in comparison with the above-mentioned developers. Consequently these two developers are the most promising ones for realizing a relatively sensitive acid-base-resist. The obtained features are quite smooth in both cases, but differ in the amount of residues in between the features. For n-hexane a slightly higher amount of residues is found compared to cyclohexane. Consequently cyclohexane is selected as applied developer for the subsequent investigations on acid-base-resists.

6.4.   Investigation on selected base components for acid-base-resists

The developed novel acid-base-resist (ABR) concept consist of at least one PAG material and one base material. While the PAG material is responsible for releasing the acid, the remaining part of the PAG molecule, typically an aromatic core, does not contribute to the ionic interactions and thus to the stability of the formed salt. Possibly this less-polar aromatic molecule is soluble in the developer and contributes to the enhanced dissolution at the beginning of the development, which was noticed in the QCM investigation (chapter 6.2). The base material with its basicity in contrary directly affects the stability of the ionic interaction. So a higher basicity of the base results in an equilibrium that is shifted more to the protonated species and thus causes more ionic interactions for a similar amount of activated PAG. This might result in a more sensitive resist system. Additionally a higher basicity of the base leads to a lower acidity of the formed salt and thus reduces the sensitivity to absorbed water within the film and water traces in the developer. This would limit the influence of unavoidable water contaminations. The selected base material will probably also differ in solubility in the selected developer cyclohexane, which must be regarded by adjusting the applied development time. This issue is considered by applying a development time gradient in the screening of each investigated base material (shown in **Figure 6.6**). Beside the development time gradient the screening will cover as well an exposure dose gradient to determine the resist sensitivity and the potential patternability. For this screening the resist materials are

applied with a stoichiometric composition ratio featuring one PAG molecule per amino function to receive comparable results for all base materials.
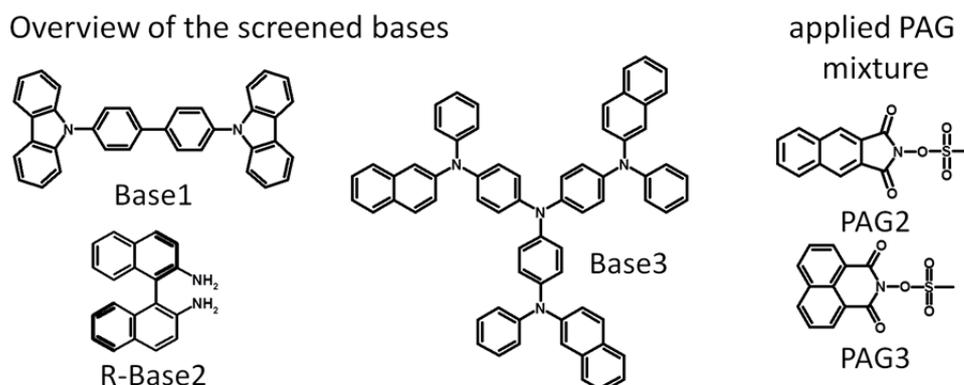
Figure 6.6: Overview of the screened bases and the PAG mixture for the resist based on salt formation: The screened bases feature a different number of amino functions and different basicity. The number of amino groups varies between two for 4,4'-Bis(carbazol-9-yl)biphenyl (Base1) and (R)-1,1'-Binaphthalene-2,2'-diamine ((R)-Base2) and four for 4,4',4"-Tris(N-naphth-2-yl)-N-phenylamino)triphenylamine (Base3). The basicity ranges from very low for the carbazole derivative (Base1) or the triphenylamine derivative (Base3) to moderate for the aniline derivative ((R)-Base2).

6.4.1. Investigation on the base 4,4'-Bis(carbazol-9-yl)biphenyl for the acid-base-resist ABR1

The first screened acid-base-resist ABR1 utilizes the base 4,4'-Bis(carbazol-9-yl)biphenyl (Base1), which was already utilized in the investigation of the dissolution behavior and the developer screening (chapter 6.2 and 6.3). For the screening in this chapter, a 130 nm thick amorphous film (composition: 35 mol% Base1; 32 mol% PAG2; 33 mol% PAG3) was prepared by PVD. This film was exposed to a 20 kV electron beam utilizing the 5th generation writing field design (chapter 3.4) featuring 100 nm thick lines (l/s 1/1) and an internal dose gradient ranging from 100 µC/cm² to 2516 µC/cm². Finally pieces of the film were developed in stirred cyclohexane for 30 s, 60 s, 120 s and 300 s. The received line features for each development time were observed by SEM and selected images are shown in **Figure 6.7**.
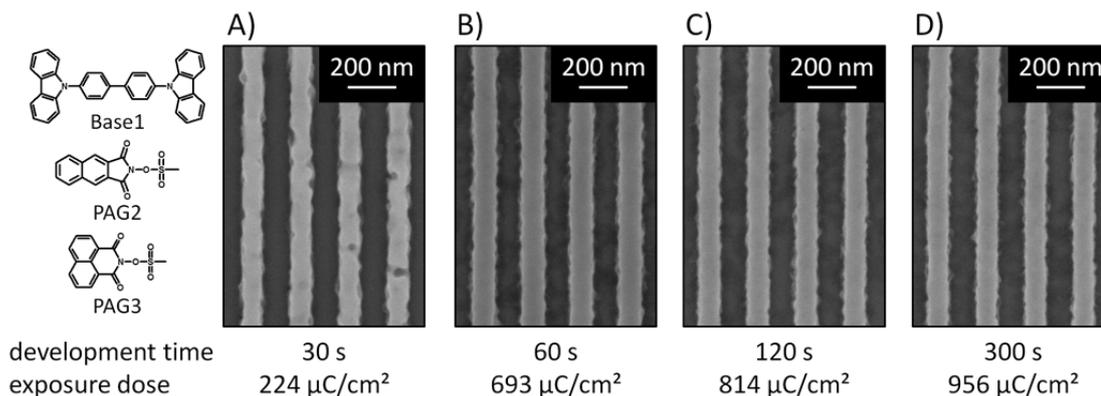
Figure 6.7: SEM images of the unsputtered line features received from patterning of ABR1: A 130 nm thick amorphous film was prepared by PVD (composition: 35 mol% Base1; 32 mol% PAG2; 33 mol% PAG3) followed by electron beam exposure utilizing the 5th generation writing field design featuring 100 nm lines (l/s 1/1) and an internal dose gradient ranging from 100 µC/cm² to 2516 µC/cm². Afterwards the development was performed in stirred cyclohexane for 30 s, 60 s, 120 s, respectively 300 s. The observed line features for the shortest development time required the lowest exposure dose but show defects (**A**). For longer development times (**B-D**) none of such defects were observed, but successively higher exposure doses were needed. However, the features exhibit spikes of exposed resist material at the line edge and some residues in between the lines.

To observe line features at the shortest development time period of 30 s an exposure dose of only 224 µC/cm² (**Figure 6.7A**) was required, while for longer development times higher exposure doses of up to 956 µC/cm² for 300 s (**Figure 6.7D**) were necessary. Consequently a brief exposure to the resist material produces line features which can be developed under gentle conditions, but are very sensitive to irregularities observable by defects (**Figure 6.7A**). These defects lead to holes in the lines which nearly interrupted these lines. For longer development times (**Figure 6.7 B**, **C**, **D**) no such defects have been found. However, for longer development times residues between the lines and spikes at the line edge obvious due to attached material were observable. They show a certain similarity compared to the residues found in the PVD prepared chemically amplified resist system investigated in chapter 4.7, which had been caused by backscattered electrons. For that resist system the application of a bottom layer had been a successful strategy to reduce the amount of backscattered electrons returning to the resist and thus defects could be suppressed. Since the novel acid-base-resists might also be affected by backscattered electrons, their impact should be reduced by applying the bottom layer approach. Because the different bases selected for the current screening might have different ideal bottom layer materials, their investigation was included in the

screening approach for the different base materials. The bottom layer materials have to withstand the development process in cyclohexane and additional feature a surface, where the polar salt formed during the exposure can adhere. Thus the very polar polymers PVA (Polyvinyl alcohol, film thickness: 100 nm) and Amylopectin (non uniform: 70 nm) were selected as bottom layer materials. Additionally a Polyamide (PA) (Poly[imino(1-oxo-1,6-hexanediyl)], 140 nm), a Polycarbonate (PC) (Poly[oxycarbonyloxy-1,4-phenylene(1-methylethylidene)-1,4-phenylene], 90 nm) and P2VP (Poly-(2-vinyl-pyridine), 140 nm) were investigated, which feature moderate polarities. Out of these polymers bottom layers were prepared by spin coating on a silicon substrate. Afterwards the ABR1 film was applied by PVD (34 mol% Base1, 34 mol% PAG2 and 32 mol% PAG3) on each prepared bottom layer and also on a blank silicon wafer in one process. The subsequent resist processing was performed in a combinatorial library consisting of an applied exposure dose gradient ranging from 100 $\mu C/cm^2$ to 2516 $\mu C/cm^2$ (5th generation writing field design featuring 100 nm lines (l/s 1/1)) and development times gradient (60 s and 120 s) in stirred cyclohexane. Finally the received features were investigated by observing SEM images. **Figure 6.8** shows the SEM images of the obtained line features of each sample for 120 s development time period and the matching exposure dose.

To achieve features, exposure doses between 956 $\mu C/cm^2$ and 1123 $\mu C/cm^2$ were needed for all investigated layers, thus the application of a bottom layer had no remarkable impact on the required exposure dose. However, the quality of the observed features differed with respect to applied bottom layer. The reference sample prepared on blank silicon (**A**, 956 $\mu C/cm^2$) showed some residues between the lines and the lines were quite rough. Both phenomena could originate from agglomerates formed due to backscattering. The application of bottom layers out of PA (**B**, 956 $\mu C/cm^2$) and PC (**C**, 1123 $\mu C/cm^2$) resulted in a clearly increased amount of residues in between the lines. The other investigated bottom layers with this resist system showed a similar or slightly better feature quality compared to blank silicon. With Amylopectin (**D**, 1123 $\mu C/cm^2$) and P2VP (**E**, 1123 $\mu C/cm^2$) as bottom layer similar amounts of residues in between the line features were observed. These residues featured a slightly smaller size than the ones observed on the reference sample (blank silicon), thus explaining the also observed smoother line edge. An improvement regarding the amount of residues was found for PVA (**F**, 956 $\mu C/cm^2$), where the features showed a quite smooth line edge with nearly no residues in between. However, with this bottom layer slightly underexposed features collapsed, indicating stability issues of the resist on this bottom layer. This is a huge

drawback for this combination of resist and bottom layer material, as for a potential application in lithography a high steadiness is required. In consequence a slightly higher amount of residues for blank silicon, Amylopectin and P2VP bottom layer is preferable to the loose in steadiness using PVA as bottom layer.
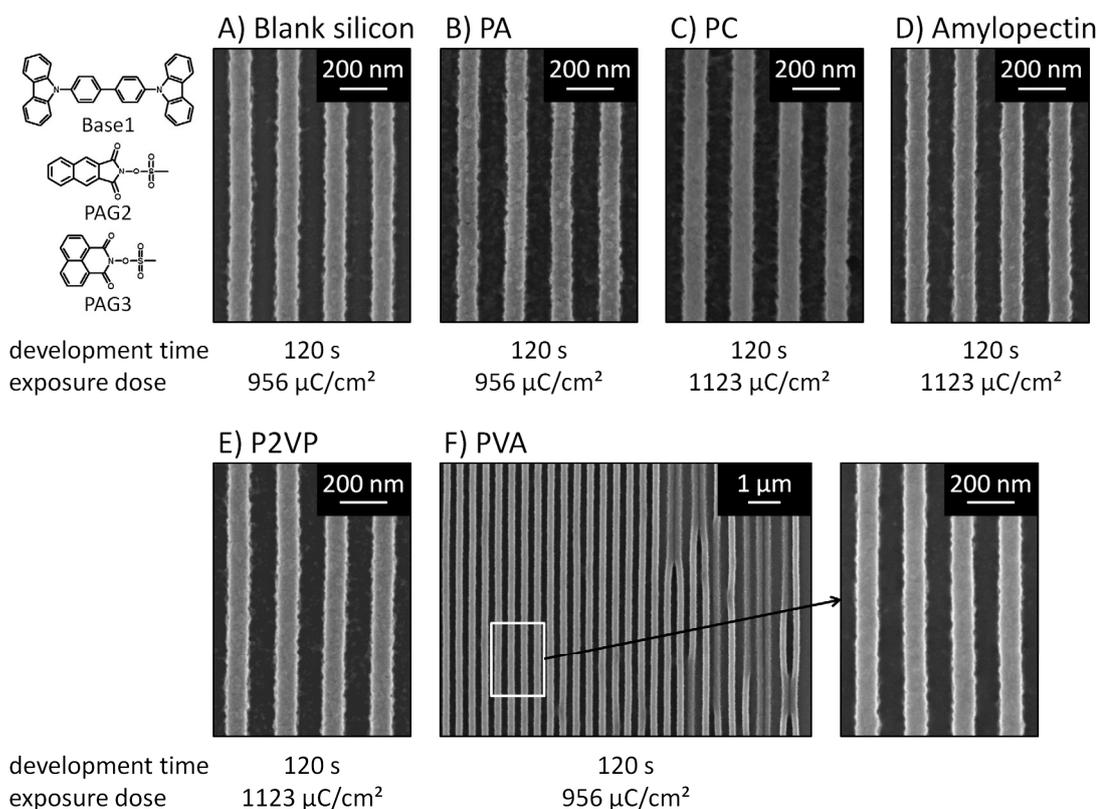
Figure 6.8:   SEM images of optimized line features received from patterning of ABR1 on different bottom layers: The resist films on the different bottom layers were prepared in one PVD process resulting in a 100 nm thick resist film (34 mol% Base1, 34 mol% PAG2 and 32 mol% PAG3). Afterwards each sample was exposed with the 5th generation writing field design featuring 100 nm lines (l/s 1/1) and an internal dose gradient ranging from 100 µC/cm² to 2516 µC/cm². Finally each sample was developed for 60 s (not shown) and 120 s in stirred cyclohexane. With PA (**B**, 956 µC/cm²) and PC (**C**, 1123 µC/cm²) increased amounts of residues compared to blank silicon (**A**, 956 µC/cm²) were observed. Amylopectin (**D**, 1123 µC/cm²) and P2VP (**E**, 1123 µC/cm²) showed better performance and in comparison to blank silicon, similar amounts of residues were present. The lowest amount of residues was observed for PVA (**F**, 956 µC/cm²), but lines were collapsed (right side).

In conclusion there are three bottom layers, blank silicon, Amylopectin and P2VP, which give similarly good results for the investigated resist ABR1. The best performance was thereby realized on blank silicon as the required exposure dose is lower.

6.4.2. Investigation on the base (R)-1,1'-Binaphthalene-2,2'-diamine for the acid-base-resist ABR2

The second screened resist ABR2 utilized the aniline derivative (R)-1,1'-Binaphthalene-2,2'-diamine ((R)-Base2) as a base. This base features also two amine groups but a higher basicity compared to Base1 investigated in the previous chapter. This should increase the stability of the formed salt and positively affect the sensitivity of the resist due to a faster protonation. As patterning of this resist system can also be affected from residues caused by backscattered electrons, the investigation of several bottom layer materials was again included in the screening process. Thus bottom layer films out of a Polyamide (PA) (Poly[imino(1-oxo-1,6-hexanediyl)], 140 nm), a Polycarbonate (PC) (Poly[oxycarbonyloxy-1,4-phenylene(1-methylethylidene)-1,4-phenylene], 90 nm), Amylopectin (non uniform: 70 nm), P2VP (Poly-(2-vinyl-pyridine), 140 nm) and PVA (Polyvinyl alcohol, film thickness: 100 nm) were prepared by spin coating on a silicon substrate. Afterwards the resist film was prepared on top of each of the prepared bottom layer samples plus on a blank silicon reference wafer. For comparability reasons this film preparation was done simultaneously within one PVD process. Thus the realization of the same resist composition of 41 mol% (R)-Base2, 17 mol% PAG2 and 42 mol% PAG3 on all samples was ensured. The subsequent resist processing was performed combinatorially by applying an exposure dose gradient ranging from 100 µC/cm² to 2516 µC/cm² (5th generation writing field design featuring 100 nm lines (l/s 1/1) (chapter 3.4)) and different development time periods of 30 s and 60 s in stirred cyclohexane. Finally the received features of ABR2 were investigated by observing SEM images. **Figure 6.9** shows selected SEM images of optimized features for each bottom layer, 60 s development time period and the matching exposure dose.

The acid-base-resist ABR2 required decreased exposure doses between 427 µC/cm² and 693 µC/cm² compared to ABR1, irrespective of the investigated bottom layer for the realization of patterns. The obtained line features did also not show stripping or pattern collapse independent from the applied bottom layer material. This indicates a strong adhesion to all bottom layer materials and a high stability of the formed salt material. The quality of the line features differed enormously especially with respect to residues in between the lines. The exposed ABR2 applied on the blank reference wafer (**A**, 589 µC/cm²) showed a moderate amount of residues in between the line features. The SEM images (**Figure 6.9**) demonstrated a huge impact of applied bottom layer on the amount of formed residues in between line features. The utilization of PA (**B**, 502 µC/cm²), PC (**C**, 693 µC/cm²) respectively

Amylopectin (**D**, 589 µC/cm²) showed an increased amount of residues compared to the blank silicon reference sample. Consequently the formed salt seems to form a strong adhesion to PA, PC and Amylopectin. Using the bottom layer PVA (**F**, 502 µC/cm²), similar amounts of residues were observed compared to the blank silicon reference wafer.

The best performance for ABR2 showed the P2VP bottom layer (**E**, 427 µC/cm²) with nearly no observable residues and smooth line features. As a result, the introduction of the additional bottom layer P2VP is a clear improvement for ABR2.
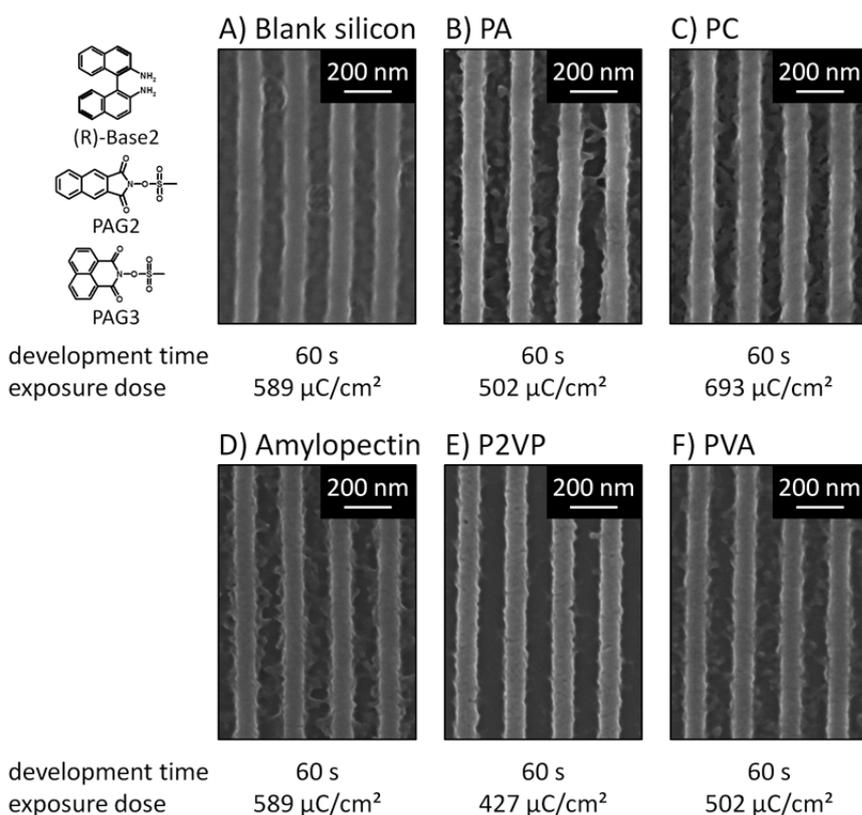
Figure 6.9: SEM images of observed line features received from patterning of ABR2 on different bottom layers: The resist films on the different bottom layers were prepared simultaneously within one PVD process resulting in a 105 nm thick resist film with a composition of 41 mol% (R)-Base2, 17 mol% PAG2 and 42 mol% PAG3. Afterwards each sample was exposed with the 5th generation writing field design featuring 100 nm lines (l/s 1/1) and an internal dose gradient ranging from 100 µC/cm² to 2516 µC/cm². Finally each sample was developed for 30 s and 60 s respectively in stirred cyclohexane (all shown images are developed for 60 s). The realized features on PA (**B**, 502 µC/cm²), PC (**C**, 693 µC/cm²) and Amylopectin (**D**, 589 µC/cm²) showed an enormous amount of residues in between the lines, which partly connected the lines across the space. A moderate amount of residues was observed for PVA (**F**, 502 µC/cm²) and blank silicon (**A**, 589 µC/cm²). The best performance showed the resist on the P2VP bottom layer (**E**, 427 µC/cm²) with less residues.

6.4.3.   Investigation of the base 4,4',4''-Tris(N-naphth-2-yl)-N-phenylamino)triphenyl-amine for the acid-base-resist ABR3

The acid-base-resist ABR3 screened in this chapter utilized the triphenylamine derivative 4,4',4''-Tris(N- naphth-2-yl)-N-phenylamino)triphenylamine (Base3) as a base. This base features a similar basicity as Base1 investigated above (chapter 6.4.1), but differs in the number of amine sides (four instead of two). In the case of protonation of one of these amine sides the polarity switch should be sufficient for an applicable development contrast. Due to the equimolar ratio of PAG to the amino functionalities, a smaller fraction of activated PAG, compared to the investigated bases with two amino functionalities, is supposed to be necessary to switch each base molecule by one protonation in order to form the salt. Consequently an increase in sensitivity of ABR3 because of the tetrafunctional base Base3 compared to the bisfunctional base Base1 in ABR1 is expected.

Similar to the previously investigated resists, this screening experiment included a bottom layer investigation to identify the optimized bottom layer/resist combination. Therefore bottom layer films out of a Polyamide (PA) (Poly[imino(1-oxo-1,6-hexanediyl)], 140 nm), a Polycarbonate (PC) (Poly[oxycarbonyloxy-1,4-phenylene(1-methylethylidene)-1,4-phenylene], 90 nm), Amylopectin (non uniform: 70 nm), P2VP (Poly-(2-vinyl-pyridine), 140 nm) and PVA (Polyvinyl alcohol, 100 nm) were prepared by spin coating on a silicon substrate. Afterwards, the ABR3 film was prepared simultaneously within one PVD process on top of each of the prepared bottom layer samples and on a blank silicon reference wafer, ensuring the realization of the identical resist composition of 21 mol% Base3, 37 mol% PAG2 and 42 mol% PAG3 on all samples. The further resist processing was performed combinatorially with an applied exposure dose gradient ranging from 100 µC/cm² to 2516 µC/cm² (5th generation writing field design featuring 100 nm lines (l/s 1/1) (chapter 3.4)) and subsequent development time periods of 30 s and 60 s in cyclohexane. Finally the obtained line features were investigated by observing SEM images. **Figure 6.10** shows the SEM images of the observed line features on top of each bottom layer after the 60 s development time period and the matching exposure dose.
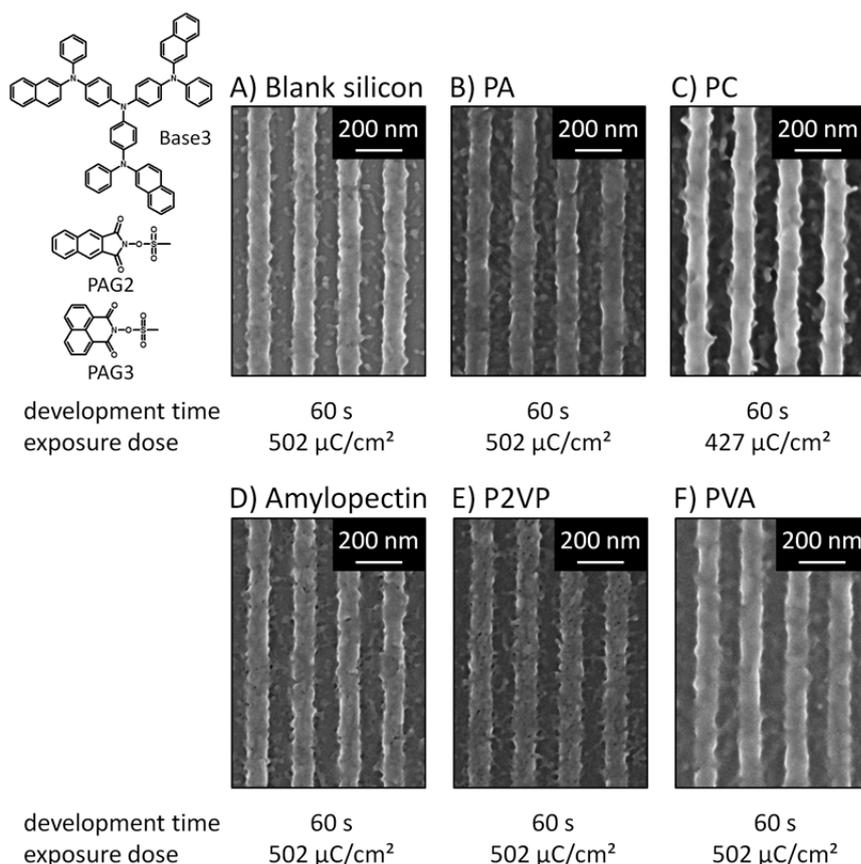
Figure 6.10: SEM images of the realized features utilizing the ABR3 on different bottom layers: The resist films on the different bottom layers were prepared simultaneously within one PVD process achieving a 85 nm thick resist film with the composition of 21 mol% Base3, 37 mol% PAG2 and 42 mol% PAG3. Afterwards each sample was exposed to the 5th generation writing field design featuring 100 nm lines (l/s 1/1) and an internal dose gradient ranging from 100 µC/cm² to 2516 µC/cm². Finally each sample was developed for 30 s (not shown) and 60 s respectively in stirred cyclohexane. The observed line features on PA (**B**, 502 µC/cm²), PC (**C**, 427 µC/cm²) and Amylopectin (**D**, 502 µC/cm²) showed high amounts of residues in between the lines. Slightly fewer residues were observed on the P2VP bottom layer (**E**, 502 µC/cm²) and on PVA (**F**, 502 µC/cm²), but the features on PVA showed no clear line edges. The best features were observed on blank silicon substrate (**A**, 502 µC/cm²) showing the typical amount of residues for this substrate.

On all different bottom layers, the patterning of ABR3 required similar exposure doses between 427 µC/cm² and 502 µC/cm² for the 60 s development time period in stirred cyclohexane. This is a clear increase of sensitivity compared to the Base1 in ABR1 as the applied exposure dose is about halved. The quality of the observed line features differed mainly with respect to the amount of formed residues in between the lines. On blank silicon wafer (**A**, 502 µC/cm²) features were observed which show only a moderate amount of small

residues in between the features similar to the acid-base-resists ABR1 and ABR2 investigated above. However, the application of the bottom layers resulted in a clear increased amount of residues in between the line features for ABR3. This is probably caused by stronger interactions between the formed salt and the more polar bottom layers compared to blank silicon. On P2VP (**E**, 502 µC/cm²) and PVA (**F**, 502 µC/cm²), the resist system ABR3 showed residues in between the lines, which often were connected to the lines. Observing the developed line features on the other investigated bottom layers PA (**B**, 502 µC/cm²), PC (**C**, 427 µC/cm²) and Amylopectin (**D**, 502 µC/cm²), very rough lines and again high amounts of residues in between the lines were visible. In conclusion, the applied bottom layers do not improve but downgrade the performance of the resist ABR3.

6.4.4.   Identification of an optimized resist bottom layer combination

The potential of the novel acid-base-resist concept is demonstrated utilizing the previously investigated three resist compositions which had only differed in the used base component. For a detailed investigation of this potential, the most promising resist/bottom layer combination was identified und investigated in a combinatorial resist optimization. This identification was done on the basis of the feature quality and the corresponding exposure dose as indication of the resist sensitivity. In **Figure 6.11** SEM images of identified line features for the resist systems ABR1, ABR2, and ABR3 are shown with the corresponding base. Additionally the utilized bottom layer or substrate and applied exposure dose are noted.

The screening investigations on bottom layer materials and exposure dose identified different optimized bottom layer materials and in two cases the blank silicon surface as best substrate for the acid-base-resists ABR1, ABR2, and ABR3. As a result, different bottom layers proved to be optimal for different bases, thus the base itself also seemed to have a crucial influence. This influence can originate for example from the base solubility and the different basicity, which influences the stability of the formed salt. For the investigated resists ABR1 on silicon (**A**) and ABR2 on P2VP (**B**), smooth lines with nearly no residues were observed. ABR3 on blank silicon (**C**) in contrary showed very rough lines with a moderate amount of residues in between the lines even on their optimal bottom layers.
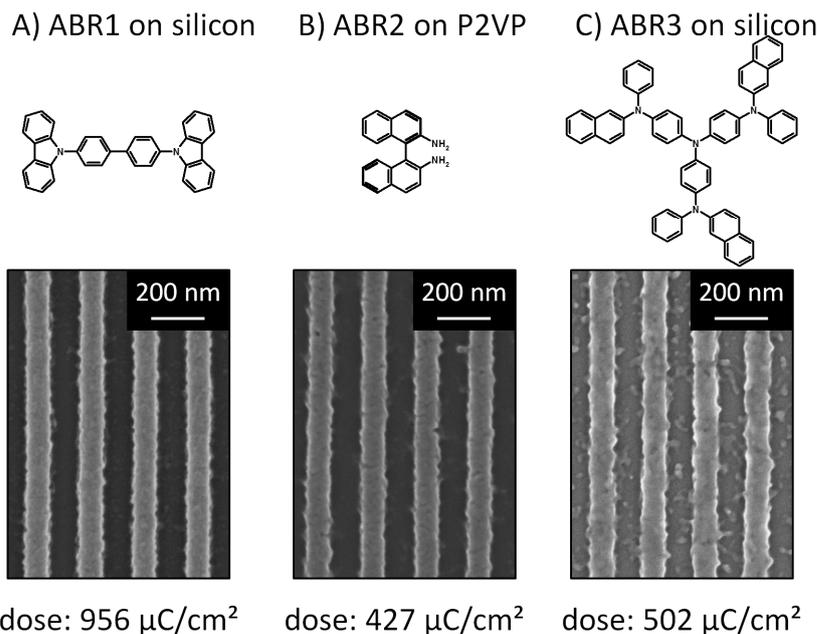
Figure 6.11: SEM images of optimized resist bottom layer combination for ABR1, ABR2, and ABR3. Bottom layer or substrate, base component and the applied exposure dose for the respective resist/bottom layer combination are noted: All resists consisted of a mixture of the PAGs PAG2 and PAG3 and the varying base compound with a molar ratio of one PAG molecule per amino functionality of the base. With ABR1 on blank silicon (**A**) and ABR2 on P2VP (**B**) smooth features with nearly no residues were observed, while for ABR3 on silicon (**C**) very rough line features were received, which also showed a moderate amount of residues in between the lines. The exposure dose for their patterning differed between 427 µC/cm² (**B**) and 956 µC/cm² (**A**).

The optimized applied exposure dose proved to be nearly independent of the application of a bottom layer and thus is characteristic for all of the screened acid-base-resists allowing the estimation of their sensitivity. So a doubling of amine sides (two for Base1 (ABR1)) compared to four for Base3 (ABR3) lead to half the exposure dose of 956 µC/cm² for (**A**) and 502 µC/cm² for (**C**). Also the increase in basicity of the base component coming along with the selection of the triphenylamine derivative (ABR1, **A**) and the primary amine (ABR2, **B**) clearly reduces the required exposure dose from 956 µC/cm² to 427 µC/cm².

In summary, the utilization of base components with a higher number of amino functionalities and a higher basicity increases the overall resist sensitivity. Out of the screened resist compositions, the ABR2 on the P2VP bottom layer shows the highest performance by featuring a relatively high sensitivity due to its high basicity and the observed clear line features with a low amount of residues.

6.5. Estimation of the potential patternability of the acid-base-resist type by investigation of the resist ABR4

Based on the screening results described in the previous chapter, the resist ABR2 consisting of (R)-1,1'-Binaphthalene-2,2'-diamine ((R)-Base2) and the PAGs PAG2 and PAG3 applied on a P2VP bottom layer was identified as the most promising resist system. Based on this result and because of the further suppressed crystallinity of utilizing a racemic mixture, the utilized R-enantiomer in this resist was updated by the corresponding racemic mixture rac-1,1'-Binaphthalene-2,2'-diamine (rac-Base2) for an in-depth investigation to evaluate the potential of this novel resist class. The acid-base-resist ABR4 is shown in **Figure 6.12**.
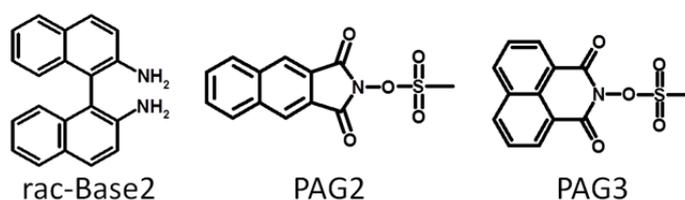
Figure 6.12: Chemical structures of the more detailed investigated resist ABR4.

6.5.1. Optimization of the resist processing for the acid-base-resist ABR4

In the investigated screening (chapter 6.4.2) the resist ABR2 showed the highest performance on P2VP with respect to the relatively high sensitivity and the quality of the observed line features. The still observed low amount of residues was planned to be reduced further by resist processing optimization experiments. Based on the findings a further combinatorial resist investigation to optimize the resist performance was set. Therefore in a first step the influence of bottom layer material thickness of 150 nm and 1 μm on ABR4 was screened to further decrease the number and size of residues according to the concept of an applied bottom layer. Therefore on silicon substrates with 150 nm respectively 1 μm thick P2VP bottom layers, a 70 nm thick ABR4 film was applied by PVD at the composition of 40 mol% rac-Base2, 20 mol% PAG2 and 40 mol% PAG3. The subsequent resist processing was investigated combinatorially by applying an exposure dose gradient ranging from 100 μC/cm² to 2516 μC/cm² (5th generation writing field design featuring 100 nm lines (l/s 1/1) (chapter 3.4)) and two different development time periods of 30 s and 60 s. **Figure 6.13** shows SEM images of the observed features on the different bottom layer thicknesses and the applied development time periods.
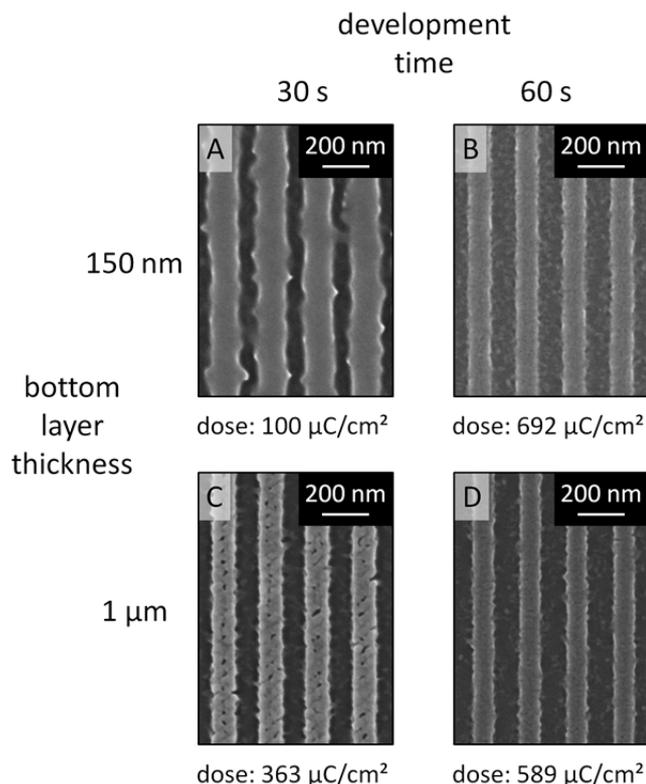
Figure 6.13: SEM images and the corresponding exposure doses of the screening investigation on resist ABR4, consisting of rac-Base2, PAG2 and PAG3 on different P2VP bottom layer thicknesses: The resist films were prepared on two samples with 150 nm respectively 1 µm thick P2VP films simultaneously within one PVD process resulting in a 70 nm thick resist film with a composition of 40 mol% rac-Base2, 20 mol% PAG2 and 40 mol% PAG3. Afterwards each sample was exposed to the 5th generation writing field design featuring 100 nm lines (l/s 1/1) and an internal dose gradient ranging from 100 µC/cm² to 2516 µC/cm². Finally the development was performed for 30 s respectively 60 s in stirred cyclohexane. For 150 nm P2VP bottom layer thickness and 30 s development, the line features (**A**)were not fully developed even for the lowest applied exposure dose of 100 µC/cm². Fully developed line features in contrary were observed after the same 30 s development process utilizing the 1 µm bottom layer sample (**C**) and an exposure of 363 µC/cm². The observed line features (**C**) showed periodic defects and some residues in between the features. With the applied longer development time of 60 s (**B** and **D**), defect-free features were observed. Using an increased bottom layer thickness clearly decreased the number and size of residues in between the lines for ABR4.

The observed line features developed for 30 s differed clearly with respect to both bottom layer thicknesses. While on the 150 nm P2VP bottom layer, the line features were not fully developed even at the lowest applied exposure dose of 100 µC/cm² (**A**), the line features on the 1 µm bottom layer (**C**) showed clearly resolved line features at the exposure dose of

363 µC/cm². This observation could not be explained by bottom layer thickness or exposure dose differences, thus another important processing variable had to show an extreme impact. A reasonable explanation is focused on the development process: Stirring in the developer results in different flow rates within the developer which clearly influence the development process. To overcome this issue of development influences, unstirred developer baths were used in the subsequent investigations. In addition, this investigation demonstrated that the features, received on 1 µm P2VP and exposed to 363 µC/cm², showed periodic defects, which were a consequence of the installed beam blanker (discussion of this phenomena in chapter 3.3.4). In conclusion, following investigations were realized without the electrostatic beam blanker and utilizing unstirred cyclohexane as developer.

However, the observed line features for ABR4 developed for 60 s allowed an interpretation with respect to the effect of the prepared two bottom layer thicknesses. On both investigated bottom layer thicknesses well developed line features were observed when exposed to 692 µC/cm² (150 nm) respectively 589 µC/cm² (1 µm), but both samples differ clearly in the amount of residues in between the space of the lines. The dose behavior between these samples did not meet the expectations, as the simulation performed in chapter 4.7 had demonstrated that the addition of a 600 nm thick bottom layer leads to a 25% reduction of the amount of backscattered electrons and thus to a decrease in the total exposure dose for higher bottom layer thicknesses. This shows on the one side, that the applied thicker bottom layer has no dramatic effect on the required exposure dose for this resist system ABR4. On the other side it indicates that even the higher exposure doses are slightly affected by minor detailed differences during the development process because of stirring. The impact on the amount of formed residues is indeed as expected, as there were more residues on the thinner bottom layer (150 nm) (**B**) in contrast to the 1 µm thick bottom layer (**D**). Thus the applied thicker bottom layer reduces, as intended, the amount of formed residues caused from backscattered electrons. However, as even for the 1 µm thick bottom layer (**D**) a decent amount of residues was still present, further process optimizations were investigated in an ongoing screening of ABR4.

The main origin of residues was assumed to be due to backscattered electrons similar to the residues formed in the case of the chemically amplified resist investigated in chapter 4.7. Wherever these backscattered electrons pass the resist, they locally activate single PAG molecules, which then immediately form the salt structures with an amine. Together with

neighboring salt structures, they agglomerate to the observed residues. Thus by increasing the solubility of these salt structures, the amount of formed residues was supposed to be reduced. This concept was realized in the second screening of ABR4 by the addition of nonionic surfactants. With their polar head, such surfactants feature the possibility to interact with the salt structures while increasing the solubility in the developer cyclohexane with the unpolar tail. Therefore the non-ionic surfactants Sur1 (Polyoxyethylene-(20)-sorbitan-monooleate), Sur2 (Polyoxyethylene-(23)-laurylether) and Sur3 (octadecan-1-ol) were selected for this screening (**Figure 6.14**).
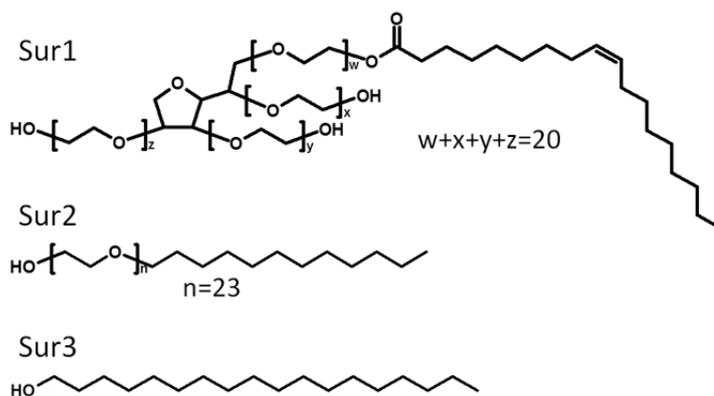
Figure 6.14: Chemical structures of investigated non-ionic surfactants utilized as developer additives for the unpolar developer cyclohexane.

The ABR4 film utilized for the screening was prepared by PVD at a composition of 31 mol% rac-Base2, 39 mol% PAG2 and 30 mol% PAG3 on a silicon substrate coated with a 1 μm thick P2VP bottom layer (prepared by spin coating). The subsequent resist processing was performed combinatorially. First write fields aligned matrix-like (3 columns x 10 rows) were exposed within one process. Each write field featured an internal exposure dose gradient ranging from 100 μC/cm² to 2516 μC/cm² (5th generation writing field design featuring 100 nm lines (l/s 1/1) (chapter 3.4)). Afterwards the substrate was cut along the columns into 10 pieces, each of them featuring three exposed write fields. The subsequent development utilized pure cyclohexane and cyclohexane with additives as developers. As additives, the non-ionic surfactants Sur1, Sur2 and Sur3 were used in the defined concentrations of 0.01 g/l, 0.1 g/l and 1 g/l. Thus overall beside pure cyclohexane, 9 developer solutions with surfactant additives were investigated. Due to the unstirred developer solutions, the development times were expected to be elongated. Consequently the development was run by applying the development time gradient of 210 s, 240 s and 270 s in the respective unstirred developer or developer solutions. Afterwards all samples were immersed into pure cyclohexane for 5 s to

remove residual additives. **Figure 6.15** shows selected SEM images of observed features after this development process.
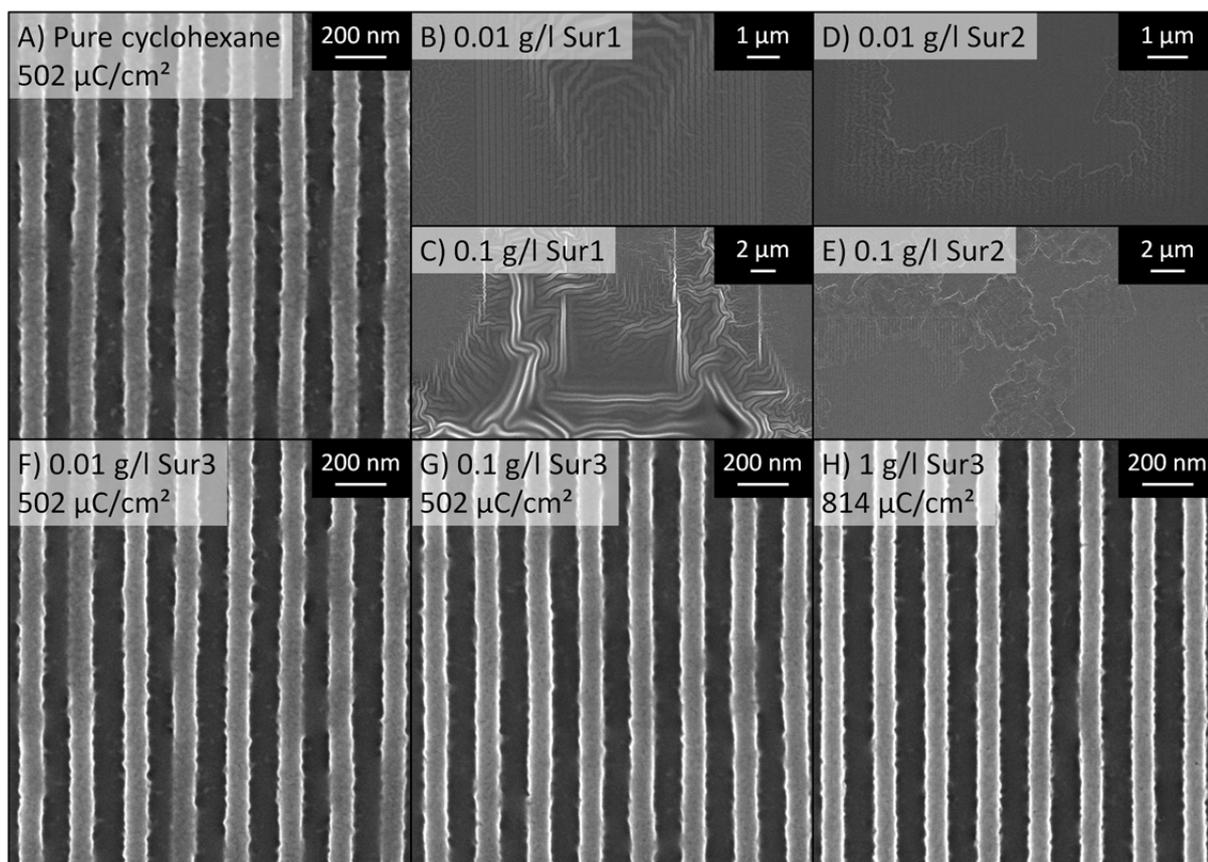
Figure 6.15: Selected SEM images of observed line features out of the second screening of ABR4 utilizing different additivated developer solutions: The ABR4 film was prepared by a PVD process on a silicon wafer coated with 1 µm thick P2VP film (90 nm thick; composition: 31 mol% rac-Base2, 39 mol% PAG2 and 30 mol% PAG3). Afterwards 30 write fields of the 5th generation write field design aligned matrix-like (3 columns x 10 rows) were exposed. Each write field features an internal dose gradient ranging from 100 µC/cm² to 2516 µC/cm². After cutting into ten pieces, the development was run in well-defined unstirred developer solutions for 210 s, 240 s respectively 270 s. Just like in the previous experiments, the features (**A**) observed at an exposure dose of 502 µC/cm² in standard developer cyclohexane (210 s) showed some residues in between the lines. The additivation of the developer at the concentration of 0.01 g/l with the polyoxyethylene based surfactants Sur2 and Sur3 did not result in clear line features (**B** and **D**). For the higher concentration of 0.1 g/l, primarily formed superstructures of the surfactants were identifiable (**C** and **E**). The third investigated additive Sur3 showed no tendency of aggregation and the residue formation in between the features could be reduced successfully by increasing the additive concentration from image **F** to **H**.

The additivation of the developer with the polyoxyethylene based surfactants Sur1 and Sur2 did not show the desired result of residue reduction. Instead both surfactants tended to aggregate on the exposed and thus high-polar features of ABR4. The aggregates formed out of Sur1 integrated the exposed salt line structures at the concentration of 0.01 g/l and formed superstructures, which seemed to have grown out of the line features (**B**). These superstructures were more distinctive for the higher concentrations of 0.1 g/l (**C**) and 1 g/l (not shown) and were observed also on areas apart from the line features. Sur2 (0.01 g/l) also absorbed and aggregated on top of the exposed and formed salt line structures, which resulted in a formed layer or a part of layer on the line features (**D**). The higher concentration of 0.1 g/l (**E**) showed more unstructured and sheet-like superstructures of the surfactant on the developed resist film surface. These superstructures nearly completely covered the substrate surface at the highest concentration of 1 g/l (not shown), making the exposed write-fields identification difficult. The additive Sur3 in contrary showed no tendency of aggregation on top of the patterned features of ABR4 even at the highest concentration of 1 g/l. This is obvious due to the much smaller polar group (hydroxyl-group) and the relatively long unpolar alkyl chain. For the lowest investigated concentration of 0.01 g/l, clear features could be received for an exposure dose of 502 $\mu C/cm^2$ and a development time of 210 s. The observed SEM image (**F**) only showed roughly half the amount of residues in comparison to the sample developed in pure cyclohexane (**A**). These line features were exposed to equal exposure doses and developed for the same development time period. The amount of residues was further reduced at the additive concentration of 0.1 g/l. Here clear features (**G**) were observed at the same patterning conditions with respect to exposure dose (502 $\mu C/cm^2$) and development time (210 s). At the highest investigated additive concentration of 1 g/l, a similar or slightly decreased amount of residues was observed. However, this high additive concentration affected the development strength, so that line features exposed to the same exposure dose of 502 $\mu C/cm^2$ were slightly overdeveloped (not shown). For these tougher development conditions, optimized exposed features were observed at the higher exposure dose of 814 $\mu C/cm^2$ (**H**).

In summary, the additivation of the developer cyclohexane with Sur3 (0.1 g/l) reduces the amount of residues, while the resist sensitivity of ABR4 is not affected. By applying the optimized development additive solution, clear features with nearly no residues can be achieved on a 1 μm thick P2VP bottom layer exposed to the same exposure dose as used for the non additivated cyclohexane developer.

6.5.2. Combinatorial optimization of the acid-base-resist ABR4

Motivated by the encouraging results of the optimization step in the previous chapter, the ABR4 resist consisting of rac-Base2 and the PAGs PAG2 and PAG3 was combinatorially investigated to demonstrate the potential of this novel acid-base-resist class. This task was addressed by the systematic variation of the crucial processing variables, in particular the resist composition, the exposure dose and the development time. Due to the fact that all of these variables influence and interact among each other, this variation was realized in one experiment in a combinatorial library by gradients. This combinatorial library allowed a fast and efficient optimization of the overall performance of this novel resist material. A schematic illustration of the investigated variable gradients arranged in the combinatorial library is shown in **Figure 6.16**.

The developed combinatorial library consisted of a horizontal composition step gradient, a vertical development time gradient and an exposure dose gradient applied in each sector (**A**). The horizontal composition gradient ranged from 28.6 mol% to 49.2 mol% for the base compound rac-Base2 and for the successively decreasing PAG content (mixture out of PAG2 and PAG3) from 71.4 mol% to 50.8 mol%. The preparation of this composition gradient was performed by a sector-wise PVD process on a 1 µm thick P2VP bottom layer. After the film preparation, a set of write fields (**B**) was exposed matrix-like (16 x 5). Each of these sets contained one adapted 5th generation write field design and several write fields for resolution studies. This upgrading was necessary, because the exposure process was performed without the beam blanker in order to overcome the issue of periodic defects (chapter 3.3.4). Without an active beam blanker, the beam is also exposing during the waiting period, when the beam is placed at the waiting position. The waiting position is located in the central position of the write field and thus the center is totally overexposed. Consequently no pattern was exposed at this position in the upgraded designs. Additionally the steepness of the exposure dose gradient was reduced to allow a more precise investigation of the resist potential of ABR4. Thus the adapted 5th generation write field design (**C**) featured 100 nm lines (l/s 1/1) and an internal exposure dose gradient ranging from 100 µC/cm² to 937 µC/cm² (exponential dose increase by 1.125). By the observation of the line features realized with this design, the region of interest was straightforwardly localizable.
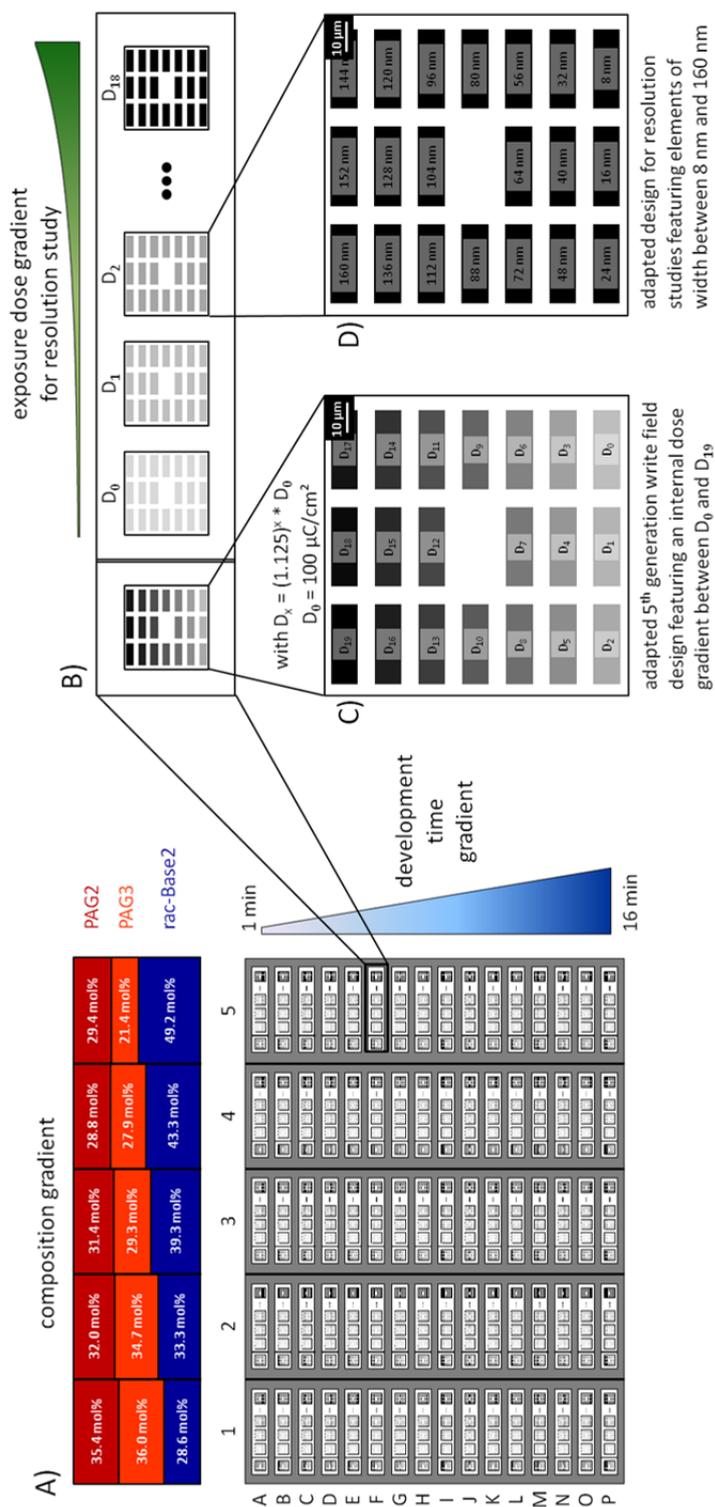
Figure 6.16: Schematic illustration of the prepared combinatorial library for the optimization of resist composition, exposure dose and development time for ABR4: The combinatorial library consisted of a horizontal composition step gradient, a vertical development time gradient and an exposure dose gradient applied in each sector (**A**). The horizontal composition gradient showed (from the left to the right) an increasing base compound (rac-Base2: 28.6 mol% to 49.2 mol%) and a successively decreasing PAG content (mixture out of PAG2 + PAG3: 71.4 % to 50.8 mol%) while the film thickness stayed nearly constant at about 90 nm. The continuous development time gradient between 1 min and 16 min was applied in the vertical direction. A set of write fields (**B**) was exposed matrix-like (16 x 5). Each of these sets contained one adapted 5th generation write field design and several write fields for resolution studies. The utilized adapted 5th generation write field design (**C**) featured 100 nm lines (l/s 1/1) and an internal exposure dose gradient ranging from 100 µC/cm² (D$_0$) to 937 µC/cm² (D$_{19}$). For the resolution studies, 19 write fields (**D**) were exposed, each featuring a width gradient from 6 nm up to 126 nm for lines with l/s 1/2. To each of these 19 write fields an exposure dose between 100 µC/cm² (D$_0$) and 833 µC/cm² (D$_{18}$) was assigned. The developed combinatorial library allowed the investigation of the resolution potential of the investigated novel ABR4 resist.

The upgraded designs for resolution studies (**D**) exposed beside the previous one allowed a more precise investigation of the resolution potential of this novel resist in the localized region of interest. Therefore the design for resolution studies featured a width gradient from 6 nm up to 126 nm (l/s 1/2). By exposing 19 write fields utilizing this upgraded design with different assigned exposure doses, an exposure dose gradient between 100 µC/cm² and 833 µC/cm² (exponential dose increase by 1.125) was realized. After exposure the development was executed by applying a development time gradient arranged in orthogonal direction to the composition gradient. This development time gradient ranging from 1 min and 16 min was realized by continuous immersion of the sample into a developer bath (cyclohexane additivated with 0.1 g/l Sur3) by a step motor drive. Afterwards the development was finished by a 5 s immersion into pure cyclohexane to remove traces of the additive.

The evaluation of this combinatorial investigation focused first on the adapted 5th generation write field design to identify the region of interest. Therefore SEM images of each sector were observed. In each sector the optimal exposure dose was identified with respect to the blur of the observed line features. Consequently the dose was considered optimal, when the desired 100 nm line features with l/s 1/1 were realized with the exact line width. In **Figure 6.17** a selection of the observed SEM images of optimal exposure doses out of different sectors are shown, which allowed the identification of performance trends with respect to the line feature quality in the combinatorial library.

The effect of varying the material composition in the horizontally applied composition gradient was clearly observable in row **I**. The lowest base concentration of 28.6 mol% (**1 I**; 9 min; 462 µC/cm²) resulted in smooth line features showing some residues. With increasing base concentration the overall quality of the line features decreased. A base concentration of 33.3 mol% (**2 I**; 9 min; 462 µC/cm²) resulted in much rougher line features, which showed a similar amount of residues. For the concentration of 39.3 mol% (**3 I**; 9 min; 462 µC/cm²) the roughness increased further and additionally the line feature height decreased. For 43.3 mol% base (**4 I**), an increased exposure dose of 565 µC/cm² was required to observe the selected rough line features. The trend of increasing required exposure dose for higher base content could also be observed in row **P** for the longer development. The decreasing quality is a consequence of the decreasing amount of PAG given by the composition gradient. In the case of electron beam exposure, each PAG molecule has a nearly similar statistical factor of activation from passing electrons, thus the lower PAG amount corresponds to less amount of

acids formed in the exposed regions. The consequently fewer formed salt molecules result in a reduced dissolution contrast between exposed and unexposed regions. This leads to the dissolution of a higher ratio of exposed material during development, responsible for the higher roughness and the feature height loss. By applying a higher exposure dose, the activation ratio of the PAG molecules could be increased, which allowed the realization of more compact line features also for high base concentrations (**4 I**). However, the increased dose came along with an increased line feature width.
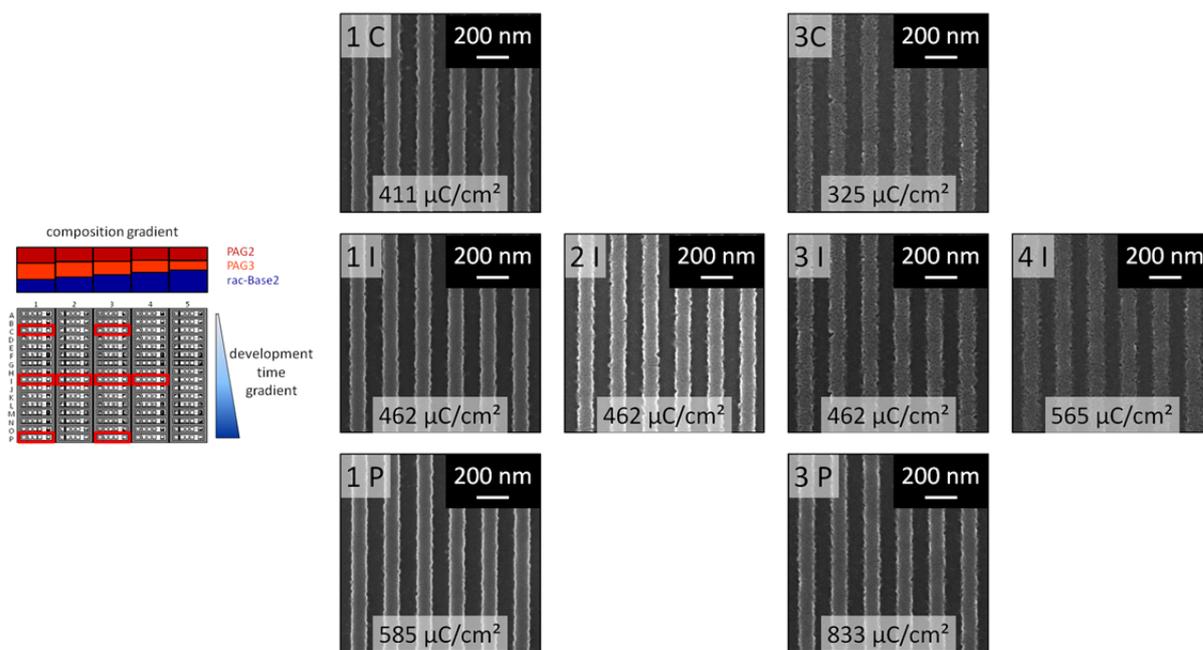
Figure 6.17: Selected SEM images out of the combinatorial library for optimization of the acid-base-resist ABR4: The line features were exposed utilizing the adapted 5th generation write field design. The images from row **I** (9 min development time) allowed the observation of the changing compositions' impact. The lowest base concentration (**1 I**; 28.6 mol%; 462 µC/cm²) resulted in smooth line features. With higher base concentration the lines got rougher (**2 I**; 33.3 mol%; 462 µC/cm²) and lost even film height (**4 I**; 43.3 mol%; 565 µC/cm²). The orthogonally applied development time gradient had an impact on the roughness and the amount of residues. With the short development of 3 min (**1 C**; 411 µC/cm² and **3 C**; 325 µC/cm²) the line features were quite rough and showed relatively much residues. A longer development of 9 min, which came along with a slightly increased exposure dose of 462 µC/cm², resulted in smoother lines with fewer residues in between. This trend continued for longer development times, resulting in the highest line feature quality in row **P**. Consequently, the highest feature quality with smooth lines with nearly no residues could be observed for a development time period of 16 min and an exposure dose of 585 µC/cm² in **1 P**.

Furthermore, the orthogonally applied development time gradient had an impact on the roughness and the amount of residues. For 3 min development (**1 C**; 28.6 mol% base; 411 μC/cm²) the line features were quite rough and showed relatively much residues. When increasing the development time to 9 min (**1 I**; 28.6 mol% base; 462 μC/cm²) the roughness of the line features and the amount of residues in between decreased. This trend continued for even longer development time periods and was confirmed by the behavior in column **3**. Consequently, the highest line feature quality with smooth lines and nearly no residues was observed in sector **1 P** (28.6 mol% base) for the development time of 16 min and the exposure dose of 585 μC/cm². This shows that by applying a harsher development procedure, residues formed by backscattering can be successfully removed. However, this harsher development requires a high activation ratio in the exposed line features to withstand the development procedure. This effect could be observed in sector **1 C** and **1 P** where the required exposure dose increased from 411 μC/cm² for 3 min to 585 μC/cm² for 16 min, respectively. Overall, the resist material showed the optimized line features in column **1** at the lowest base concentration and the longest development time. Consequently, the region of highest feature quality could be identified in column **1** from row **I** to row **P**.

This region was then investigated in detail by observing the resolution study design. The location in direct vicinity to the modified 5th generation write field design ensured an equal processing in the respective sectors and thus comparability within the sector. The sectors were observed by SEM with respect to the line feature size gradient for different exposure doses. In **Figure 6.18** selected SEM images out of the interesting sectors **1 I**, **1 N**, and **1 P** are shown. Similar to the above described combinatorial optimization of this novel resist ABR4, a longer development required an increased exposure dose (585 μC/cm² for 9 min (**1I**); 658 μC/cm² for 14 min (**1N**); 741 μC/cm² for 16 min (**1P**)). The exposure dose itself was thereby higher due to the changed line to space distance (l/s 1/1 for the above described combinatorial optimization, l/s 1/2 here). The broadened line space distance resulted in less backscattered electrons and thus a slightly increased exposure dose. For each sector along the development time gradient only one exposure dose was observed, which allowed the realization of clear 112 nm line features. However, the quality of these line features differed in the LER calculated by SuMMIT (described in the experimental part; chapter 9.1.8). At the longest development time of 16 min (**1P**) a LER of 5.4 was realized, while the more short-term developed ones showed a higher roughness (5.9 for 14 min (**1N**); 6.3 for 9 min (**1I**)). This was consistent to the observation out of the above described combinatorial optimization, which

indicated the highest feature quality at longer development times. The observed LER trend was confirmed by the highest resolution line features realized in each sector (**Figure 6.18**, right column). So the 40 nm line features developed at 16 min (**1P**) showed a LER of 6.1, while the LER for the 48 nm features in the more short-term developed sectors showed increased LERs (7.1 in **1I**; 7.1 in **1N**). The realized very high resolution of 40 nm line features (l/s 1/2) at the 16 min development (**1P**) matched the best realized feature quality which had been optimized within this combinatorial investigation. In conclusion the observed high resolution 40 nm line features with the relatively low LER of 6.4 demonstrated the enormous potential of this novel class of acid-base-resists as the results could be achieved by utilizing a non dedicated 20 kV electron beam lithography tool.
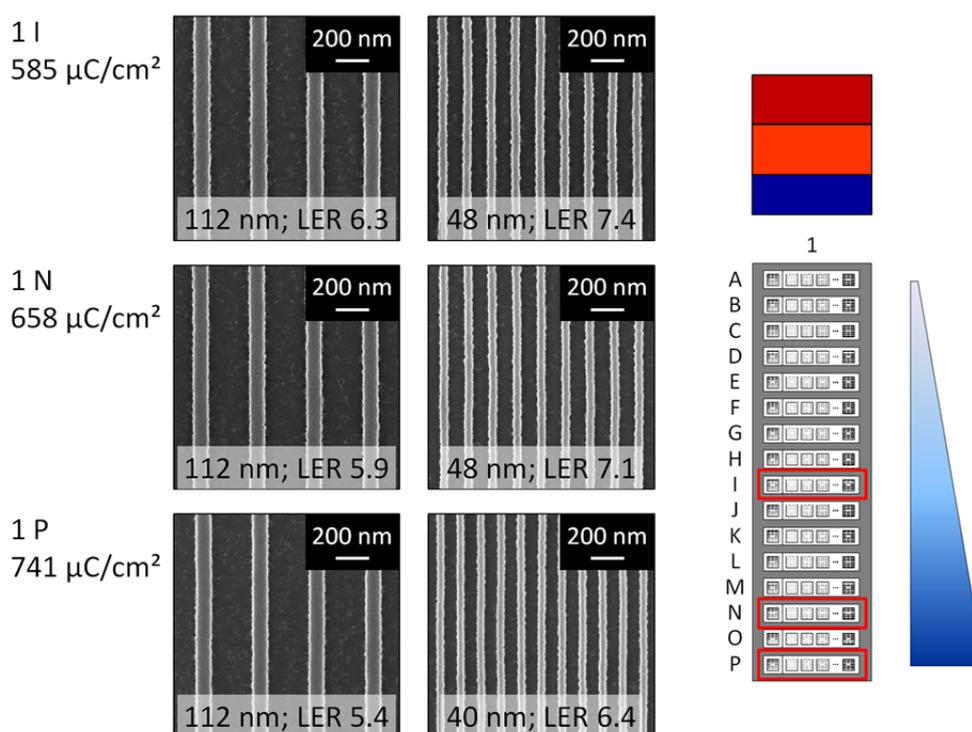
Figure 6.18: Selected SEM images out of interesting sectors **1 I**, **1 N**, and **1 P** were investigated in detail for the acid-base-resist ABR4: The l/s 1/2 line features were prepared utilizing the resolution study design write field. In all three sectors clear 112 nm (**left side**) line features were observed. Increasing the development time period caused a decreasing LER from 6.3 (**1I**) to 5.4 (**1P**). A similar trend for the LER was also observed for the highest realized resolution in the mentioned sectors (SEM images of the right column). While in sector **1I** and **1N** only 48 nm line features were observable, the processing in sector **1P** achieved clear 40 nm line features (l/s 1/2) with the low LER of 6.4.

7. Summary

The progress of our information society in this current era depends mostly on the improvement of the computing speed of microprocessors. Therefore semiconductor industries realize further developments in processor architecture but also in the patterning process which is utilized for the manufacturing of microprocessors. Of great importance is thereby the advancement to smaller feature sizes. However, the state of the art exposing technique 193 nm immersion lithography with applied multi-patterning gradually reaches its limits in the ongoing miniaturization. But for the continuation of miniaturization of integrated circuits in the long term, a further progression in the processing steps as well as the development of further improved materials are essential. Favored exposure methods of the next generation lithography are extreme ultraviolet lithography or multi-beam electron beam lithography, as these techniques provide the opportunity of patterning smaller feature sizes.

In this thesis electron beam lithography, physical vapor deposition as alternative resist preparation technique and the materials development for this film preparation technique are covered. In the first chapter of this thesis the characterization of the utilized electron beam exposure tool but also the establishment of a processing procedure are in the focus. The second chapter covers the investigation of physical vapor deposition (PVD) as an alternative resist film preparation method. Encouraged by the promising result utilizing PVD as film preparation technique, the synthesis of applicable positive tone molecular glass resist materials was addressed in the third chapter. Finally in the fourth chapter a completely new patterning concept based on the salt formation between a base and the acid of an exposed photoacid generator was established, combinatorially optimized and high resolution features were demonstrated.

The *first chapter* of this thesis covers the c*haracterization of the utilized electron beam lithography tool* Zeiss Leo1530 equipped with the lithography control unit Raith Elphy Plus *and the establishment of processing procedures.* The investigation on crucial device parameters and their influence on the pattern quality are the main objects as well as the establishment of an optimized working procedure to prevent irregularities.

Even though the utilized exposure tool is not a dedicated electron beam lithography tool, it allows the realization of *beam diameters* down to 2.1 nm for the acceleration voltage of 20 kV under optimized conditions. This allows the realization of feature elements in the nanometer scale.

The continuous work with this exposure tool during this thesis lead to the *identification of external* and *internal tool* as well as *software parameters* crucial for the achieved patterning quality. The most important identified impact factors are the *beam adjustment,* the *acceleration voltage*, and the *electrostatic beam blanker*.

The *beam adjustment* is a key issue for the achievable feature quality and has to be performed properly. Using a less adjusted beam means the beam diameter is increased and the beam shape might be elliptic. These two deviations both affect the maximal realizable resolution.

The utilized *acceleration voltage* defines the penetration depth of the electrons and thus the number of backscattered electrons and affected area. These backscattered electrons increase the exposure dose of the exposed area and also expose the surrounding of the actual patterns. This effect can be an issue concerning the formation of residues in these surrounding areas. Theoretical simulations of primary electrons' pathways proved the influence of the acceleration voltage on affected area and on the local density of backscattered electrons in dependence of the distance to the beam impact position.

The *electrostatic beam blanker* has its advantages in the avoidance of unintended exposure of the non-blanked beam during movement between different positions on the substrate as well as during the exposure process of the features itself. But during the thesis, also a big disadvantage of the installed electrostatic beam blanker was identified. As soon as it is turned on, the electron beam is affected by a 50 Hz fluctuation, resulting in periodical deflections of the electron beam. These deflections lead to reduced image sharpness in the imaging mode of the scanning electron microscope. They also have an impact on the obtained features written by the lithographic exposure process and result in the formation of periodic defects by utilizing a very sensitive non-chemically amplified resist system. For electron beam exposed chemically amplified resists in contrary, no such defects were identified, which is obviously a consequence of diffusion of the acid utilized in such systems for the chemically amplification reaction.

Additionally, during the research done for this thesis, the *processing procedure* for electron beam lithography with this tool and the thereby utilized *write field designs* were continuously developed further and improved to overcome the identified issues where possible. With the latest generation of these write fields a *toolbox* is now available for the investigation of the resists' sensitivity, for the performing of an exposure dose gradient in a write field with only 100 μm edge length, as well as for the investigation of the resolution capability of novel resists.

The *second chapter* focuses on the *investigation of physical vapor deposition as alternative film preparation technique in lithography*. In the curse of this the influences on resist characteristics of a chemically amplified resist were investigated, which result from two different film application methods, namely the standard spin coating process in comparison to the alternative PVD technique. In the standard spin coating process the whole film is formed at once by solvent evaporation. The PVD technique in contrary is a solvent-free vacuum process, whereby the evaporated material deposits molecule by molecule on the substrate. This results in a continuous increase in film thickness and a statistically controlled distribution of the different materials for multi-component films. The statistical deposition prevents the formation of material aggregates in a multi component system, which can be an issue in the spin coating process due to possible segregation or phase separation. Published simulations show an impact of photo acid generator aggregates in chemically amplified resists. Such aggregates can result in decreased sensitivity, increased line edge roughness and decreased resolution.

For this thesis the resist performance of resist films prepared by the different film application techniques spin coating and PVD was compared for the first time. Therefore a literature known negative tone chemically amplified molecular glass resist was *adapted* for PVD processing.

The resist was investigated *systematically* on the *resist characteristics* dissolution behavior and resist sensitivity as well as on overall *lithographic performance* for both film application techniques. The investigations lead to the conclusion that the solvent-free PVD results in a distinct increase in sensitivity. This increased sensitivity is also demonstrated by higher responsiveness for the formation of residues due to backscattered electrons. This effect can be explained by the individual molecule by molecule deposition step resulting in a more homogeneous distribution, especially of the photoacid generator.

To support this promising result of increased sensitivity of *PVD prepared resist films*, several approaches were pursued in order to reduce the responsiveness for the formation of residues due to backscattering. The investigation of the approaches was performed *highly efficiently* by *ternary combinatorial libraries* of exposure dose, post exposure bake temperature, and development time. As first approach a higher acceleration voltage of 100 kV was applied for exposure instead of the formerly used 20 kV. The higher acceleration voltage successfully decreased the amount of formed residues due to a lowered density of backscattered electrons around the exposed features. However, the effect of the higher acceleration voltage was not

sufficient to completely inhibit residue formation. Thus in a second approach a polymeric bottom layer was applied between the silicon substrate and the resist film. The bottom layer reduces the amount of formed backscattered electrons reaching the resist film and thus decreases the amount of formed residues. The effect of a bottom layer on the number of backscattered electrons was additionally supported by theoretical simulations of primary electrons' pathways. Applying both approaches, clear 100 nm patterns were observed utilizing the high sensitive PVD prepared resist film.

This fundamental investigation demonstrated for the first time that the application of the solvent-free film coating technique PVD is not only an alternative high quality film preparation technique but rather improves the resist performance by homogeneous material blending. This novel interesting scientific finding has been published in Advanced Functional Materials[6].

The *third chapter* covers the *synthesis and characterization of positive tone chemically amplified resist materials utilizable for PVD*. This topic was encouraged by the promising results described in chapter two, where negative tone chemically amplified resist systems had featured higher sensitivity due to film application by PVD. To transfer this result to positive tone chemically amplified resists, PVD suitable materials had to be identified. However, no such materials are literature known. Their properties on the one hand must feature a cleavable group, which has to withstand the thermal stress of the evaporation process without decomposition. On the other hand it must show a stable amorphous phase with a glass transition temperature (T_g) higher than or at least in the range of the post exposure bake temperature. It is especially the required thermal stability that excludes the industrial used polymeric resist materials.

Promising candidates are protected molecular glass materials with suitable acid cleavable groups. The here presented investigation focused on the *functional groups* carbonate esters and carboxylic acid esters, which both are known as cleavable groups from industrial applied polymeric resists.

The *carbonate ester class* was investigated in cooperation with the workgroup of Prof. Ober, where molecular glass materials with tBoc protection groups were synthesized. The thermal

---

[6] T. Kolb, C. Neuber, M. Krysak, C.K. Ober, H.-W. Schmidt, Multicomponent Physical Vapor Deposited Films with Homogeneous Molecular Material Distribution Featuring Improved Resist Sensitivity; Adv. Funct. Mater. **2012**, 18, 3865–3873.

characterization showed a decomposition temperature of around 160 °C of the tBoc protection group regardless of the utilized phenolic core. This low decomposition temperature allowed a successful PVD processing only for a very low molecular weight material. However, such materials missed the required glass transition temperature criteria.

The investigation of *synthesized ester based materials* showed decomposition temperatures of around 210°C for tert-butylester, and even 250 °C for an isobornyl ester. Thus the ester function is thermal more stable and more promising for a PVD processible positive tone chemically amplified resist. The thermal characterization of the synthesized materials showed that an ether linking group dramatically decreases the glass transition temperature and thus disqualifies the synthesized positive tone resist material with this functional group. Most promising turned out to be the direct esterification of a carboxylic acid core with a secondary or tertiary alcohol like isoborneol. But further synthetic efforts are needed to achieve fully operational PVD processible positive tone molecular glass resists.

In summary, for the first time positive tone chemically amplified resist materials were investigated on their PVD processability, which allowed the identification of the ester based material class as the most promising one.

The *fourth chapter* covers the *investigation of a novel physical vapor depositable resist material concept based on exposure induced salt formation*. The background for this topic is the fact that the semiconductor industry is seeking for resist systems, which are capable of realizing sub 20 nm feature sizes. Beside the chemical modification of existing resist types also the investigation of completely new resist material concepts are in the focus to fulfill this demand. With this target in mind a completely new patternable material concept based on salt formation was combinatorially investigated and optimized in this chapter of this thesis. It is based on the formation of ionic interactions between a base molecule and an acid, which is released by the exposure of the photoacid generator. The induced ionic interactions change the polarity of the material, which serves as development contrast.

The *proof of principle* for such acid-base-resist systems was processed with a carbazol derivative as base component and a non-ionic photoacid generator. The formation of the salt was verified by infrared spectroscopy and the produced *development contrast* was investigated by quartz crystal microbalance measurements. A developer screening demonstrated the applicability of developers of a wide polarity range. The optimized resist

performance considering resist sensitivity and feature quality was observed utilizing cyclohexane.

The investigation on *different base materials* demonstrated a strong dependence of the resist sensitivity on the applied base, with beneficial performance for bases with high basicity and many amino functions. The presented *combinatorial investigation* was combined with a polymeric bottom layer investigation to prevent residue formation due to backscattering. The material screening showed that the optimized acid-base-resist consists of 1,1'-Binaphthalene-2,2'-diamine and the mixture of two isomeric photoacid generators applied on a Poly-(2-vinyl-pyridine) bottom layer. Further more detailed screenings on thicker bottom layer and the additivation of the cyclohexane developer with a nonionic surfactant allowed the improvement of feature quality by reducing the amount of residues in between the patterned line features.

Finally the *identified resist* was *combinatorially optimized* to investigate the potential of this new resist material concept. The prepared combinatorial library covered gradients of interacting processing variables as composition, development time and exposure dose, which were applied in a specific layout which allowed both a fast and precise investigation of the resolution potential in the region of interest within the same library. In the optimized sector, *high resolution 40 nm line features* with the *relatively low line edge roughness of 6.4* were observed.

This achievement demonstrates the enormous potential of this novel resist material concept on an acid-base-resist, especially as the high resolution pattern were realized utilizing a non-dedicated 20 kV electron beam lithography tool.

8.   Zusammenfassung

Der Fortschritt unserer Informationsgesellschaft hängt zum Großteil von der Steigerung der Leistungsfähigkeit von Mikroprozessoren und der damit erzielten Verbesserung der Informationsverarbeitung ab. Um dies zu realisieren muss die Halbleiterindustrie sowohl die Architektur der Mikroprozessoren als auch die für deren Herstellung verwendeten Strukturierungsprozesse ständig weiterentwickeln. Eine Schlüsselstellung nimmt dabei die Möglichkeit ein, immer kleinere Strukturen realisieren zu können. Jedoch erreicht die aktuell angewandte Belichtungstechnik, Mehrfachbelichtung mittels 193 nm Immersionslithographie, zunehmend ihre Grenzen für die weitere Miniaturisierung. Langfristig sind für deren Fortsetzung eine Weiterentwicklung der angewandten Verarbeitungsschritte und der Entwicklung von weiter verbesserten Lackmaterialien unabdingbar. Kleinere Strukturgrößen können mit einer Reihe von neuen Belichtungs- und Strukturierungstechniken realisiert werden, wovon die extrem UV-Lithographie (EUV) und Mehrelektronenstrahlenlithographie am Weitesten entwickelt sind und in den nächsten Jahren Marktreife erlangen sollten.

In dieser Arbeit werden die Elektronenstrahllithographie, das "Aufdampfen" (Physical Vapor Deposition; PVD) als alternative Filmherstellungsmethode und die Materialentwicklung für diese Filmherstellungsmethode behandelt. Das erste Kapitel dieser Arbeit beschäftigt sich mit der Charakterisierung des verwendeten Elektronenstrahlbelichters und dem Etablieren von Prozessroutinen, um die Schwachstellen dieses Belichters bestmöglich zu umgehen. Das zweite Kapitel behandelt das Untersuchen des Aufdampfens als alternative Filmherstellungsmethode und das Identifizieren von Einflüssen auf die Lackeigenschaften durch den veränderten Filmherstellungsprozess. Die während der Untersuchung identifizierten verbesserten Lackeigenschaften ermutigten zu der Synthese und Charakterisierung von für diese Filmherstellungsmethode geeigneten positiven Lackmaterialien im dritten Kapitel. Zuletzt wurde im vierten Kapitel ein komplett neues Strukturierungskonzept untersucht, welches die Bildung einer ionischen Verbindung zwischen einer Base und einer Säure ausnutzt. Die Säure wird dafür durch die Belichtung aus dem jeweils eingebrachten photolabilen Säurebildner freigesetzt. Die Untersuchung dieses neuen Strukturierungskonzepts wurde kombinatorisch durchgeführt, und ermöglichte die Realisierung von hoch aufgelösten Strukturen.

Im *ersten Kapitel* wird die *Charakterisierung* und die *Handhabung* des *verwendeten Elektronenstrahlbelichters* Leo1530 von Zeiss in Kombination mit der Lithographieeinheit

Elphy Plus von Raith detailliert thematisiert. Besonderes Augenmerk wurde dabei auf die wichtigen Geräteparameter und deren Einfluss auf die erzeugte Strukturqualität gelegt. Des Weiteren wurde eine optimierte Arbeitsprozedur entwickelt, um mögliche Einflüsse auf die Strukturqualität zu limitieren.

Die Untersuchung ergab, dass der Belichter, obwohl er kein professionaler Elektronenstrahlbelichter ist, *Strahldurchmesser* kleiner als 2.1 nm für eine Beschleunigungsspannung von 20 kV unter idealen Bedingungen erreichen kann. Dies ermöglicht die Realisierung von Strukturen im Nanometerbereich.

Bei der Arbeit mit diesem Belichter wurden verschiedene *externe* und *interne Geräte-* und *Softwareparameter identifiziert*, welche die erhaltene Strukturqualität entscheidend beeinflussen. Den größten Einfluss zeigten die *Fokussierung des Elektronenstrahls*, die verwendete *Beschleunigungsspannung* sowie die *elektrostatische Apparatur zur Strahlauslöschung* (electrostatic beam blanker).

Die *Fokussierung des Elektronenstrahls* nimmt für die Qualität der erhaltenen Strukturen eine Schlüsselstellung ein. So sorgt die Verwendung eines schlecht fokussierten Strahls für einen verbreiterten und möglicherweise auch elliptischen Elektronenstrahl, welcher die erzielbare Auflösung bei der Strukturierung beeinträchtigt.

Die verwendete *Beschleunigungsspannung* beeinflusst die Eindringtiefe der Elektronen in die Probe und damit die Anzahl der zurückgestreuten Elektronen und die Größe des von ihnen beeinflussten Bereichs. Diese rückgestreuten Elektronen erhöhen durch das erneute Durchqueren des Lackfilms die Belichtungsdosis der belichteten aber auch der in Nachbarschaft zu einem belichteten Element befindlichen nicht belichteten Bereiche. Letzteres kann zur Bildung von Rückständen in der Nachbarschaft zu einem belichteten Element führen und somit die erzielte Strukturqualität stark beeinträchtigen. Mittels theoretischer Simulationen der Bahnen von Primärelektronen in der Probe wurde die Abhängigkeit des beeinflussten Bereichs und der lokalen Konzentration der rückgestreuten Elektronen von der Beschleunigungsspannung identifiziert.

Die Verwendung der *elektrostatischen Apparatur zur Strahlauslöschung* führt zur Vermeidung von ungewollter Belichtung während der Bewegung zwischen verschiedenen Positionen auf der Probe sowie auch während der Belichtung der Strukturen selbst. Jedoch zeigte sich während dieser Arbeit auch ein großer Nachteil. Die installierten elektrostatischen Apparatur zur Strahlauslöschung führt im angeschalteten Zustand zu einer periodischen Ablenkung des Elektronenstrahls durch eine 50 Hz-Störung. Diese Ablenkung reduziert die

Bildschärfe bei der Aufnahme rasterelektronischer Bilder. Zusätzlich beeinträchtigt sie auch die erzeugten Strukturen einer lithographischen Belichtung. Dies zeigte sich bei der Strukturierung eines empfindlichen, nicht chemisch verstärkten Lacksystems derart, dass nach entsprechender Belichtung Strukturen mit periodischen Defekten beobachtet wurden. Im Gegensatz dazu zeigten chemisch verstärkte Lacke keine solchen Defekte, was offensichtlich auf eine Kompensation dieses Effektes aufgrund der Säurediffusion hindeutet. Die Säure ist in solchen Systemen für den chemischen Verstärkungsmechanismus verantwortlich.

Zusätzlich wurden während dieser Arbeit die *Prozessroutine* der Elektronenstrahlbelichtung mit diesem Gerät und die dabei verwendeten *Schreibfelddesigns* entwickelt und kontinuierlich verbessert, um identifizierte Probleme soweit möglich zu überwinden. Die letzte Generation der entwickelten Schreibfelder stellt *Werkzeuge* für die Untersuchung der Lackempfindlichkeit, für die Realisierung eines Belichtungsdosisgradienten in einem Schreibfeld mit nur 100 μm Kantenlänge und für die Untersuchung der maximal realisierbaren Auflösung von neuen Lacken zur Verfügung.

Im *zweiten Kapitel* liegt der Fokus auf der *Untersuchung von Änderungen der Lackeigenschaften eines chemisch verstärkten Lacksystems durch die Anwendung der unterschiedlichen Filmpräparationstechniken* Lackschleudern und Aufdampfen. Bei der üblichen Filmpräparation durch Lackschleudern wird die gesamte Filmschicht in einem Prozessschritt durch Lösungsmittelverdampfung erzeugt. Im Gegensatz dazu handelt es sich beim Aufdampfen um einen lösungsmittelfreien Prozess, bei dem sich verdampftes Material Molekül für Molekül auf dem Substrat ablagert. Dadurch wächst die Filmdicke kontinuierlich. Außerdem werden in Mehrkomponentensystemen die einzelnen Materialien statistisch kontrolliert in den Film eingebaut. Durch diesen statistischen Einbau wird die Bildung von Aggregaten verhindert, welche beim Lackschleudern durch Segregation und Phasenseparation auftreten können. Veröffentlichte Simulationen zeigen eine Beeinträchtigung der Lackeigenschaften durch vorhandene Aggregate des photolabilen Säurebildners. Sie äußert sich zum Beispiel in einer reduzierten Empfindlichkeit, größere Kantenrauigkeit und reduzierter erzielbarer Auflösung.

Der Vergleich zwischen den verschiedenen Filmpräparationstechniken Lackschleudern und Aufdampfen bezüglich ihrer Auswirkung auf die Lackleistungsfähigkeit wurde erstmals in dieser Arbeit durchgeführt. Hierzu wurde ein literaturbekannter negativer, chemisch

verstärkter und auf einem organischen Glas basierender Lack für das Verarbeiten mittels Aufdampfen *angepasst*.

Dieser Lack wurde anschließend *systematisch* bezüglich der *Lackeigenschaften* Löslichkeitsverhalten und Empfindlichkeit sowie der allgemeinen *Strukturierbarkeit* für beide Filmherstellungsmethoden untersucht. Diese Untersuchungen zeigten, dass die Filmherstellungsmethode Aufdampfen die Empfindlichkeit des Lacksystems klar erhöht. Diese zeigte sich auch in der deutlich erhöhten Bildung von Rückständen durch rückgestreute Elektronen. Eine mögliche Erklärung ist die Molekül für Molekül erfolgte Ablagerung in der Filmherstellung mittels Aufdampfen, welche zu einer homogeneren Verteilung der einzelnen Lackkomponenten und insbesondere des photolabilen Säurebildners führt.

Um dieses vielversprechende Ergebnis der erhöhten Empfindlichkeit *aufgedampfter Lackfilme* zu untermauern, wurden mehrere Lösungsansätze verfolgt, die die Ausbildung von Rückständen durch rückgestreute Elektronen unterdrücken sollten. Die Untersuchung dieser Lösungsansätze erfolgte dabei *effizient* mittels *ternärer kombinatorischer Sektorenbibliotheken*, in denen die Belichtungsdosis, die Temperatur des Temperierungsprozesses zur Aktivierung der katalytischen Reaktion („post exposure bake"; PEB) und die Entwicklungszeit variiert wurden. Der erste Lösungsansatz umfasste die Steigerung der Beschleunigungsspannung von den ursprünglichen 20 kV auf 100 kV. Diese höhere Beschleunigungsspannung reduzierte die lokale Konzentration von rückgestreuten Elektronen in der Nähe der belichteten Bereiche und damit auch erfolgreich die Menge an gebildeten Rückständen. Jedoch reichte die Veränderung der Beschleunigungsspannung nicht aus, um die Bildung von Rückständen komplett zu unterdrücken. Deshalb wurde in einem zweiten Lösungsansatz ein Polymerfilm als Zwischenschicht zwischen dem Siliziumsubstrat und dem Lack eingebracht. Durch diese Zwischenschicht wurde die Anzahl der rückgestreuten Elektronen und damit auch die Menge der gebildeten Rückständen reduziert. Diese Reduzierung wurde auch mittels theoretischer Simulation des Verhaltens von Primärelektronen in der Probe bestätigt. Zusammen erlaubten diese beiden Herangehensweisen eine rückstandsfreie 100 nm-Strukturierung des hoch empfindlichen, aufgedampften Lackfilms.

Diese erstmals durchgeführte, grundlegende Untersuchung zeigte, dass die Verwendung der lösungsmittelfreien Filmpräparationstechnik Aufdampfen nicht nur eine alternative Filmpräparationstechnik für die Realisierung von qualitativ hochwertigen Filmen ist, sondern zusätzlich auch die Lackeigenschaften durch eine homogenere Materialverteilung verbessert

und dadurch das Lackpotential ideal genutzt werden kann. Diese neue wissenschaftliche Entdeckung wurde erfolgreich in Advanced Functional Materials publiziert[7].

Im *dritten Kapitel* werden die *Synthese und die Charakterisierung von positiv chemisch verstärkten Lackmaterialien bezüglich ihrer Eignung für das Aufdampfen* behandelt. Dieses Thema wurde wegen der vielversprechenden Ergebnisse des zweiten Kapitels gewählt, da der dort untersuchte, negativ chemisch verstärkte Lack eine höhere Empfindlichkeit aufgrund der Filmpräparation mittels Aufdampfen zeigte. Um dieses Ergebnis auf positiv chemisch verstärkte Lacke zu übertragen, mussten geeignete aufdampfbare Lackmaterialien identifiziert werden. Jedoch sind solche Materialien aus der Literatur bislang nicht bekannt. Geeignete Materialien müssen zum Einen eine spaltbare Gruppe besitzen, welche die thermische Beanspruchung während des Aufdampfprozesses ohne Zersetzung überstehen kann. Zum Anderen müssen die Materialien stabile amorphe Filme ausbilden und eine Glasübergangstemperatur (T_g) aufweisen, die entweder über oder zumindest in dem Bereich der Temperatur des Temperierungsprozesses zur Aktivierung der katalytischen Reaktion („post exposure bake"; PEB) liegt. Insbesondere die benötigte thermische Stabilität steht einer Verwendung industriell angewandter, polymerbasierter Lacke im Weg.

Vielversprechende Kandidaten sind stattdessen geschützte organische Gläser, die mit geeigneten spaltbaren Gruppen ausgestattet sind. Die durchgeführte Untersuchung fokussierte sich auf die *spaltbaren Gruppen* Carbonatester und Carbonsäureester, welche beide literaturbekannte spaltbare Gruppen für polymerbasierte Lacksysteme sind.

Die *Carbonatester* wurden in Kooperation mit der Arbeitsgruppe von Professor Ober untersucht, wo auch die Synthese der molekularen Gläser mit der tBoc-Schutzgruppe durchgeführt wurde. In der thermischen Untersuchung zeigte die tBoc-Schutzgruppe Zersetzungstemperaturen um ungefähr 160 °C unabhängig von dem verwendeten Phenolkernmaterial. Wegen dieser niedrigen Zersetzungstemperatur konnte nur ein Material mit sehr geringem Molekulargewicht erfolgreich aufgedampft werden. Jedoch wies dieses Material keine ausreichend hohe Glasübergangstemperatur auf und erfüllte damit dieses Kriterium nicht.

---

[7] T. Kolb, C. Neuber, M. Krysak, C.K. Ober, H.-W. Schmidt, Multicomponent Physical Vapor Deposited Films with Homogeneous Molecular Material Distribution Featuring Improved Resist Sensitivity; Adv. Funct. Mater. **2012**, 18, 3865–3873.

Die Untersuchung der thermischen Eigenschaften der synthetisierten *Carbonsäureester* zeigte Zersetzungstemperaturen um 210 °C für tert-Butylester und sogar um 250 °C für einen Isoborneolester. Folglich ist die Carbonsäureester-Gruppe thermisch stabiler und somit ein aussichtsreicherer Kandidat für die Realisierung eines aufdampfbaren positiv chemisch verstärkten Lackes. Bei der thermischen Charakterisierung der synthetisierten Materialien zeigte sich außerdem, dass eine etherbasierte Verknüpfungsgruppe die Glasübergangstemperatur so stark herabsetzt, dass Materialien mit dieser Verknüpfungsgruppe völlig ungeeignet sind. Es stellte sich heraus, dass die direkte Veresterung eines carbonsäuretragenden Kern mit einem geeigneten sekundären oder tertiären Alkohol, wie z.B. Isoborneol, am vielversprechendsten ist. Jedoch sind weitere synthetische Anstrengungen nötig, um ein einsatzfähiges aufdampfbares positiv chemisch verstärktes molekulares Glasmaterial zu verwirklichen.

Zusammenfassend wurden in diesem Kapitel zum ersten Mal positiv chemisch verstärkte Lackmaterialien bezüglich ihrer Verarbeitbarkeit mittels Aufdampfen untersucht. Die Ergebnisse ermöglichten die Identifizierung der Carbonsäureestergruppe als vielversprechendste Schutzgruppe.

Im *vierten Kapitel* wird die *Untersuchung eines neuartigen aufdampfbaren Lackmaterialkonzepts* behandelt, welches auf der *mittels Belichtung ausgelösten Salzbildung* basiert. Der Hintergrund für dieses Themengebiet ist die Suche der Halbleiterindustrie nach Lacksystemen, die es ermöglichen, Strukturen mit Auflösungen kleiner als 20 nm zu realisieren. Um dieses Ziel zu erreichen, werden neben der Modifizierung von existierenden Lacksystemen auch komplett neue Strukturierungskonzepte untersucht. Das letzte Kapitel dieser Arbeit beschäftigt sich deshalb mit der kombinatorischen Untersuchung und Optimierung eines komplett neuen Strukturierungskonzepts, welches auf der Bildung eines Salzes beruht: Durch die Bildung von ionischen Wechselwirkungen zwischen einer organischen Base und einer Säure, welche durch die Belichtung aus dem eingesetzten photolabilen Säurebildner freigesetzt wird, ändert sich die Polarität des Lackmaterials. Dieser Polaritätsunterschied zwischen belichtetem und unbelichtetem Material wird in diesem Strukturierungskonzept als Kontrast für die Entwicklung verwendet.

Der *Nachweis der Strukturierbarkeit* eines solchen Säure-Base-Lacksystems wurde mit einem Carbazolderivat als Base und einem nicht-ionischen photolabilen Säuregenerator durchgeführt. Mittels Infrarotspektroskopie konnte die erfolgreiche Ausbildung des Salzes

nachgewiesen werden. Zusätzlich wurde durch Schwingquarzmessungen der erzeugte *Entwicklungskontrast* untersucht. In einer Voruntersuchung konnte außerdem gezeigt werden, dass Entwickler mit verschiedener Polarität geeignet sind. Das beste Ergebnis bezüglich Empfindlichkeit des Lackes und erhaltener Strukturqualität wurde für Cyclohexan erhalten.

Eine Untersuchung *verschiedener Basen* zeigte eine starke Abhängigkeit der Lackempfindlichkeit von der verwendeten Base. Vorteilhaft sind dabei Basen mit einer möglichst hohen Basizität sowie vielen protonierbaren Basenfunktionen. Die *kombinatorische Untersuchung* umfasste dabei zusätzlich auch eine Untersuchung verschiedener Polymerfilme als Zwischenschicht zwischen Lack und Substrat, um die Bildung von Rückständen durch rückgestreute Elektronen zu vermeiden. Es stellte sich heraus, dass der Säure-Base-Lack bestehend aus 1,1'-Binaphthalene-2,2'-diamin und einer Mischung aus zwei isomeren photolabilen Säurebildnern in Kombination mit einer Zwischenschicht aus Poly-(2-vinyl-pyridine) die besten Ergebnisse lieferte. Die Anwendung einer dickeren Zwischenschicht und das Additivieren des Entwicklers Cyclohexan mit einem nicht-ionischen Tensid zeigte in zusätzlichen Voruntersuchungen eine Verbesserung der Strukturqualität aufgrund der Reduktion der von rückgestreuten Elektronen gebildeten Rückstände.

Nach diesen Voruntersuchungen wurde das *vielversprechendste Lacksystem kombinatorisch optimiert*, um das Potential dieses neuen Strukturierungskonzepts zu evaluieren. In der verwendeten kombinatorischen Sektorenbibliothek wurden Gradienten der voneinander abhängigen Prozessparameter Zusammensetzung, Entwicklungszeit und Belichtungsdosis untersucht. Der Belichtungsdosisgradient wurde dabei in einem Layout angewandt, das eine schnelle und gleichzeitig auch präzise Untersuchung des Auflösungsvermögens in der gleichen kombinatorischen Sektorenbibliothek ermöglichte. Im optimierten Sektor wurden *hoch aufgelöste Strukturen* mit *40 nm Linienbreite* und einer relativ niedrigen *Kantenrauigkeit von 6.4* realisiert.

Diese Untersuchungen zeigen das enorme Potential dieses neuen Strukturierungskonzepts basierend auf einem Säure-Base-Lacksystem insbesondere wenn man berücksichtigt, dass die hoch aufgelösten Strukturen mit einem nicht professionellen Elektronenstrahlbelichter und der relativ geringen Beschleunigungsspannung von 20 kV erzielt wurden.

9.   Experimental part

9.1.   Methods

9.1.1. Film application

For the film application by physical vapor deposition (PVD) the substrates (silicon wafer for lithography investigations; quartz crystals for sensitivity investigations) were mounted into the Balzer PLS 500 evaporation chamber. The components were coevaporated by utilizing three effusion cells, where the respective evaporation rate is adjusted by heating and monitored by a quartz crystal microbalance (QCM).[94] The ratio of the evaporation rates of each component was selected on the basis of experience, which was received from prior performed evaporation experiments and the determined real film composition. The overall film deposition rate ($\sim$1 Å s^{-1}) and the film thickness were controlled by two additional QCMs just beside the rotating substrate. To achieve an efficient adsorption of the evaporating molecules and to increase the film quality the substrate was cooled by an installed Peltier element to 10 °C. After the evaporation process the realized film thickness was measured by a stylus profiler (Veeco Dektak 150) and the realized film composition by HPLC (9.1.2).

Solvent-based films were prepared by spin coating followed by a PAB for solvent removal and thermal relaxation of the film material.

9.1.2. Evaluation of the resist composition by high performance liquid chromatography

High performance liquid chromatography (HPLC) measurements utilized for the evaluation of the resist composition were performed with an Agilent 1100 series equipped with an Agilent Zorbax Bonus-RP column. The mobile phase (flow rate 1ml/min) was changed depending on the investigated resist ("starting mobile phase"). In some cases the investigated material was interacted strongly with the stationary phase that it was necessary to apply a gradient of the mobile phase during the measurement (change to "end mobile phase"). The detector wavelength was adjusted to the respective resist and mobile phase. The utilized mobile phases and the detector wavelength for the different investigated resist systems are listed in **Table 9.1**.

The evaluation of the resist composition required the measurement of a calibration curve for each component. Therefore solutions with a defined mass content of the component were

prepared and measured. With the received integral of the component signal and the respective defined mass content of each solution, the calibration curves for each component were received. These calibration curves allow the calculation of the mass content of the different compounds of coevaporated resist films. Therefore from a resist film with unknown composition a small defined stripe (size around 1 cm² for 100 nm film thickness) was cut off. This resist film was afterwards dissolved in 300 µl of the organic solvent utilized in the mobile phase. Afterwards the sample is analyzed by HPLC (injection volume: 25 µl) and the integrals for each component are calculated. The values of the integrals allow by utilizing the calibration curve the calculation of the mass content of each component in the sample. The resultant mass contents are afterwards set into relation to receive the resist film composition of the unknown sample.

Table 9.1:   Mobile phases and utilized wavelengths for the HPLC investigation of resist films.

resist	starting mobile phase	end mobile phase	wavelength
trisphenol, crosslinker, PAG1	acetonitrile / water 50/50	-	200 nm
trisphenol, crosslinker, PAG2	acetonitrile / water 50/50	-	200 nm
trisphenol, crosslinker, PAG3	acetonitrile / water 50/50	-	200 nm
trisphenol, crosslinker, PAG4	acetonitrile / water 50/50	-	200 nm
trisphenol, crosslinker, PAG5	acetonitrile / water 50/50	acetonitrile / water 75/25	200 nm
trisphenol, crosslinker, PAG6	acetonitrile / water 50/50	acetonitrile / water 75/25	200 nm
Base1, PAG2, PAG3 (ABR1)	THF /water 30/70	-	254 nm
Base2, PAG2, PAG3 (ABR2 and ABR4)	THF /water 30/70	-	254 nm
Base3, PAG2, PAG3 (ABR3)	THF /water 30/70	THF /water 40/60	254 nm for PAG2 and PAG3 / 334 nm for Base3

9.1.3. Investigation of dissolution properties by quartz crystal microbalance measurements

The investigation on the dissolution behavior is based on monitoring the resonance frequency of quartz crystals (QCs). This frequency changes during application or removal of film material on QC surface, which is proportional to its mass respectively its film thickness.[154] Thus this technique allows a sensitive monitoring of dissolution or swelling processes. Our setup utilizes 1 inch QCs with gold electrodes and a resonance frequency of 5 MHz which are mounted into a Maxtec CHC-100 QC-holder. The data acquisition was performed by a LabVIEW based software.

For the measurements films out of the resist material are prepared on QC either by spin coating or by PVD. For the film application by PVD the QCs are attached to a silicon wafer by double-sided adhesive tape followed by the normal PVD process. Afterwards the QCs are mounted in the QC holder and immersed into the developer solution. The resonance frequency increases, if photoresist material is dissolved, and decreases, if the film swells or material absorbs on the film surface.

Beside this investigation in one developer, a method was established during this thesis to investigate the dissolution behavior with increasing developer strength of a tetramethylammonium hydroxide developer in one experiment. Therefore the QC holder with a resist film coated QC is immersed into stirred deionized water. By adding defined amounts of 10 wt% tetramethylammonium hydroxide solution (1.104 N) a stepwise increase in developer concentration (0.003 N up to 0.26 N) was realized.

9.1.4. Procedure for electron beam patterning with Zeiss Leo 1530 equipped with Raith Elphy Plus

In the following the necessary steps for performing an electron beam patterning experiment with the Zeiss Leo1530 equipped with Raith Elphy Plus are listed.

a) Modifications necessary prior to electron beam lithography
- Switch *Elphy Quantum* and *Beam blanker* on
- Switch lithography computer on (The *Elphy Quantum* must be switched on, otherwise this hardware will not be booted correctly)

- Change the application switch from *EDX* to *Elphy*
- AT SEM-PC: Start program *"RemCon Raith"*
- Login at lithography computer

b) Fixing and locking in of substrate

- Clean the substrate holder and the wafer piece from small fragments
- Place the wafer on the substrate holder
- Fix it by adjusting the clamps (if necessary)
- Lock in the substrate holder

c) Measurement of beam current

- Connect the *ampere meter* (Keithley 486 Picoammeter) to the grounding port of the SEM and the grounded part of the cathodoluminescence detector
- SEM: Move the substrate holder to the *Faraday cage* by macro *"litho-Faraday"*
- SEM: Set up the desired aperture diameter and the desired acceleration voltage (typically 20 kV)
- SEM: Position the beam above the *Faraday cage* and zoom into with highest magnification
- Blank the beam by beam blanker, and switch the *ampere meter* on
- Press the zero check button
- Note the reported zero value current
- Enable the beam
- Note the current
- Blank the beam and disconnect the *ampere meter* from the grounding port and reconnect the grounding cable
- Correct the measured beam current by the zero value
- Record the measured beam current in the txt-file on the desktop of the lithography computer for record purposes
- By abnormal beam currents check for errors: textbook, short-circuits, dust in beam pathway, …

d) Program input

- Start the *"Elphy Quantum" software* on litho computer
- Check the error log (button at bottom right: red "error"; yellow "message"; green "ok")
- Move to a corner of the substrate and focus on the film

Adjustment of the coordinate system

- Open the tap "*Adjustments*"

- Go in the "*Adjust UV*" window to the tap "*Origin Correction*" and press adjust

- Import the coordinates of this corner <u>also</u> as first point for the angle correction (tap "*angle correction*")

- And <u>also</u> import the coordinates of this point as first point for the three point alignment (tap "*3-Point*")

➔ This position will be the origin for the *UV Cartesian coordinate system* and the first point for the coarse adjustment of the three point alignment.

- SEM: Move to the next corner of the substrate and focus on the film

- Import these coordinates as second point for the angle correction (tap "*angle correction*") and press the adjust button

- And <u>also</u> import the coordinates of this point as second point for the three point alignment (tap "*3-Point*")

- Note the length of the substrate (U-coordinate) for your own experiment documentation

➔ This position will be on the U axis of the *UV-coordinate system* and the second point for the coarse adjustment of the three point alignment.

- SEM: Move to the next corner of the substrate and focus on the film

- Import the coordinates of this point as third point for the three point alignment (tap "*3-Point*") and press the adjust button

- Note the width of the substrate (V-coordinate) for your own experiment documentation

➔ This position will be the third point for the coarse adjustment of the 3-point alignment.

➔ With the window "*stage control*" (tap "*destination*") defined positions in UV coordinates on the substrate can now be reached.

Fine adjustment of the three point alignment

- In a second step the *working distance* (*WD*) adjustment by the three point alignment is refined by focusing on contamination spots in the corners of the films (make them with 7.5 µm or 10 µm aperture diameter in "spot" mode; highest magnification; duration 30 s with continuous on and off switching of *beam blanker* (Strg + "b" @ lithography computer); focusing with the desired exposure aperture diameter) [also

adjust the aperture correction on the contamination spots] and controlled by a fourth spot in the outstanding corner

- In a third step the astigmatism correction will be fine adjusted on a contamination spot in the center of the substrate

Planning the exposure procedure of multiple write fields

- Open the tap "*Microscope Control*" and activate the desired write field alignment (depends on write field size and aperture)
- Open the tap "*Design*"
- Open in the window *GDSII Database* the desired database file with the pattern layout
- Open a new *positionlist*
- Copy the desired pattern profile into the *positionlist* window by marking and moving the profile with pressed left mouse button
- Correct the U and V coordinates of the first desired write field position and adjust the exposure layer (normally 0, depends on the settings during the write field designing)
- By *Matrix Copy* (menu: "Filter" → "Matrix Copy") from one or several entries of the position list a matrix can be generated (optional also a dose gradient can be applied to each entry of the matrix)
- By the menu: "*Filter*" → "*Calculate Exposure Time*" the estimated exposure time of the position list can be calculated (to the shown time 3 s per entry in the position list has to be added for correcting the stage drift)

It is possible to add an entry in the *position list*, to allow the movement to a specific position without an exposure process. This can be used, to split a movement into two. The first one should contain the larger portion. Due to the short second movement the probability for stage drift is reduced. Therefore click with the right mouse button at the desired position in the position list and choose "*new*"→"*Insert before*" respectively "*new*"→"*Insert after*".

Adjusting of exposure parameters

- In the tab "*Exposure*" the global exposure parameters for all sectors can be adjusted
- For this purpose press the button "*Calculator*" to open the window "*exposure parameter calculation*"
- Enter the measured *beam current* on the left side
- For each activated exposure mode (areas/curved elements/lines meaning single pixel lines/dots) the parameters have to be adjusted, so that every tab is not marked red

anymore (you need only to activate the exposure modes for the in the write field design included types)

- Area: Enter the lowest desired dose for areas and decrease the dwell time to zero → Press the "*calculator button*" beside the step size followed by the calculator beside the dwell time → if there is still an error (red marking), increase manually the dwell time to around 0.250μs and recalculate step size followed be recalculation of the dwell time.

- Lines: analogous to areas

- Dots: Enter the dose and adjust the dwell time by the calculator

- Confirm the parameters

Additionally for each entry in the position list a dose factor (column "*DoseFactor*") can be set. By this factor the dwell time and thus the starting exposure dose of a write field design is increased, allowing the exposure of one write field design with different doses in one process. This factor is also used, when a dose gradient is applied during the matrix copy.

e) Starting the exposure

- Move the stage to the *U/V-coordinates* of the first write field

- Adjust the microscope magnification in the window "*Microscope Control*" with "*Set*"

- For the exposure select the desired entries in the position list; click with right mouse button and choose "*Scan*".

- After all entries are exposed apply normal lock out procedure (Vent + substrate lock out)

f) After lock out

- Mark the corner of the origin, to reapply the *UV-coordinate system* similar for evaluation purposes after the resist processing

g) End of the experiment

- Close the program "*REMCon Raith*"

- Shut down the "*Elphy Quantum*" *software* and the lithography computer

- Switch off *Elphy Quantum* and *beam blanker*

- Change application switch from *Raith* to *EDX*

- Adjust SEM parameters to normal values (usually 3 kV acceleration voltage and 30 μm aperture)

h) Pattern evaluation

For the sample evaluation with reapplied UV-coordination system the *Elphy Quantum*, the lithography computer, the *"REMCon Raith"* (SEM-PC) as well as the *"Elphy Quantum" software* (lithography computer) are necessary. Do not switch on the beam blanker, as it affects the quality of the resultant images, due to a 50 Hz fluctuation.

- Switch *Elphy Quantum* and afterwards also the lithography computer on
- AT SEM-PC: Start program *"RemCon Raith"*
- Login at lithography computer and start the *"Elphy Quantum" software*
- Fix the substrate on the holder and lock it in
- Reapply the UV-coordinate system for the localization of the exposed write fields in a similar manner as for the exposure
- Reach with the window "*stage control*" (tap "*destination*") the defined positions of exposure in UV coordinates on the substrate.
- When finished perform End of experiment procedure

9.1.5. Simulation of the electron scattering with the Casino software

Simulations of the electron pathways in solid matter were performed with the Casino software version 2.4.8.1, published by Dominique Drouin et al. from the University of Sherbrooke, Canada. The performed simulations used the following models for the different interaction processes:

Total Cross Section:	Mott by Interpolation
Partial Cross Section:	Mott by Interpolation
Effective Section Ionisation	Casnati
Ionisation Potential	Joy and Luo (1989)
Random Number Generator	Press et al. (1986)
Directing Cosin	Drouin (1996)
dE/dS Calculation	Joy and Luo (1989)

For a simulation first the sample was defined by adjusting each layer in the investigated layered architecture with composition, layer thickness and density. For the performed simulations the following materials were investigated:

Silicon substrate   composition: Si   density: 2.33 g/cm³

PMMA resist   composition: $C_5H_8O_2$ density[155]: 1.188 g/cm³

P2VP bottom layer   composition: C_7H_7N density[155]: 1.153 g/cm³

Afterwards the investigated electron energy (10 keV or 20 keV), the number of simulated electrons (1000) and the beam radius (2 nm) were set. Then the different distributions have to be adjusted, which were set on the basis of the default values:

Distribution of Maximum depth of electrons	1000
Distribution of the energy of backscattered electron (BE)	500
Distribution of the energy of transmitted electron	500
Distribution of the surface radius of BE	500
Distribution of the backscattered electron angle	91
Distribution of the backscattered electron angle VS their energy	91
Distribution of energy by position	yes
X Division	50
Y Division	50
Z Division	50
Generate X-Ray	yes (500)
Max Range Parameters	simulated

Finally the display options were adjusted with 1000 shown trajectories and minimum electron energy of 0.05 keV. The number of backscattered electrons was evaluated on the basis of the "Backscatted Energy" plot, which is automatically prepared after the simulation.

9.1.6. Method for the investigation of the resist sensitivity

For the investigation of the resist sensitivity the standard procedure for measuring a contrast curve was applied.[66] Therefore a write field design (see chapter 3.4) containing three 20 μm x 100 μm rectangles with 20 μm gap in between was utilized. This write field was exposed multiple times with different exposure doses featuring an exposure dose gradient. For this

exposure an acceleration voltage of 20 kV and an aperture diameter of 60 μm were utilized at the Zeiss Leo 1530 equipped with Raith Elphy Plus. After PEB (only applied to CAR systems) and subsequent development the dose dependent feature heights were measured by a stylus profiler (Veeco Dektak 150). The presented feature heights are the average of the measured heights from three rectangles in one write field.

9.1.7. Realization of combinatorial libraries for lithographic patterning

9.1.7.1. Experiment design

A combinatorial library is here realized by the application of processing variable gradients in orthogonal direction on a sample, which allows the varying of one variable while the other stays constant.[12] During this thesis usually ternary combinatorial libraries are realized, which consist of two gradients arranged orthogonally and a third gradient, which is applied matrix-like in very small areas, in which the first and the second parameter are effectively constant. The first and the second gradient are selected among a composition gradient, a temperature gradient or a development time gradient. The third gradient was in every performed library an exposure dose gradient. The preparation method of the different gradient is described in the following

9.1.7.2. Composition gradient

Solution based material composition gradient preparation

A film with a continuous internal composition gradient for chapter 4.2 was realized with the syringe pump approach recently published.[12] Therefore two solutions out of PGMEA were prepared with 2.5 wt% organic materials content. Solution 1 consisted of the solid content of 5.0 wt% PAG1 and 95.0 wt% trisphenol, while solution 2 consisted of 5.0 wt% PAG1 and 95.0 wt% crosslinker. Out of these solutions the composition gradient was realized by co-injection with the syringe pump system (Cetoni) into a custom made active mixing chamber stirred with 80 rpm. During extrusion of the ongoing varying gradient mixture on the silicon wafer with a constant velocity of 10 mm/s, the flow rates of the two solutions were continuously changed by ensuring a constant overall flow rate of 30 μl/s. Afterwards the applied gradient mixture extrudate with the internal composition variation was doctor bladed in orthogonal direction to the application direction followed by PAB for 30 s at 115 °C. The evaluation of the so realized composition gradient was performed by cutting a stripe of the

wafer into defined pieces and analyzing the respective film composition of each piece by HPLC (9.1.2).

PVD based material composition gradient preparation

A film with a material composition gradient prepared by PVD was realized by a sector-wise PVD process. Therefore only one sector on the substrate is not covered by a shadow mask at once, on which the film is prepared by the actual evaporation process. By changing the ratios of the different evaporating components between the different sectors, sectors with different material composition are realized. The characterization of the different material compositions in each sector was performed by cutting a stripe of the wafer. After the separation of this stripe into pieces of each sector the respective film composition of each piece was analyzed by HPLC (9.1.2).

9.1.7.3. Temperature gradient

The temperature gradient for PEB were realized on a stainless steel plate by active cooling with liquid nitrogen or ice / water on the one side and heating up to 300 °C by a hot plate on the other side. By an infrared camera the establishment of the equilibrated temperature gradient is monitored and the achieved temperatures are measured on a reference silicon wafer. The exposed film is placed for 30 s just beside the reference wafer in the desired temperature range to apply the corresponding temperature gradient.

9.1.7.4. Development time gradient

Development time gradients were performed in a stepwise or a continuous fashion. For the stepwise method the sample is immersed stepwise into the developer bath to apply the desired development times in the respective areas. The continuous development time gradient in contrary utilizes a motor drive, which immerse the substrate into the developer bath with a constant velocity. In the case of a mentioned stirred developer, it was stirred with 250 rpm. After finishing the corresponding development time gradient the sample was rinsed with a non-threatening solvent.

9.1.7.5. Exposure dose gradient

For the realization of an exposure dose gradient two methods were utilized both based on special designed write fields. In the first one a write field design is utilized, which comprises in a 100 μm times 100 μm sized write field an internal exposure dose gradient. An example of such a write field can be seen in Figure 3.19.

For the second method a write filed with the selected features is designed, which is exposed multiple times beside each other, each with a different corresponding exposure dose. An example of such a write field can be seen in Figure 3.20.

9.1.8. Method for calculation of line edge roughness

Line edge roughness (LER) calculations were performed with the *SuMMIT* software (Version 8.0) from EUV Technology. Therefore a SEM images is observed from the achieved patterns with a sufficient high contrast to be evaluable by the software. Afterwards the LER is calculated from this image by the SuMMIT software with the standard settings. This software identifies the line edge of a feature on the basis of the bright dark contrast in the SEM image. With this border line it calculates the 3σ deviation from the ideal linear line shape, which is called the LER.

9.1.9. Methods for material characterization

Nuclear Magnetic Resonance characterization

^1H-NMR and ^{13}C-NMR spectra were recorded on a Bruker AC 300 spectrometer (300 MHz for ^{1}H and 75.5 MHz for ^{13}C) using $CDCl_3$ as solvent and its solvent signal (^{1}H: 7.26 ppm; ^{13}C: 77.16 ppm) as internal standard for calibration.

Thermal characterization

The thermal characteristics of synthesized materials were investigated by thermogravimetric analysis (TGA) and differential scanning calorimetry (DSC).

TGA was carried out under N_2 atmosphere at a heating rate of 10 °C/min with a Netsch STA 449 F3 or a Mettler Toledo TGA/SDTA851^e.

DSC was conducted on a PerkinElmer DSC Diamond instrument utilizing between 8 mg and 10 mg material in high-pressure pans at a scanning rate of 10 K/min. Indium standard was used for calibration.

9.2.   Materials and synthesis

9.2.1.   Materials

Used solvents were distilled from technical grades ones prior to their use. Special solvents like propylene glycol monomethyl ether acetate (PGMEA) and anhydrous grade solvents were purchased from Aldrich and Acros. The chemicals for the syntheses were purchased from Aldrich and ABCR and were used as received.

For patterning experiments the materials and substrates were purchased from the following sources and used as received if not otherwise stated:

Substrates:

	purchased from
Silicon wafers (crystal orientation (100); n- and p-doped)	Crystec, Si-Mat; Siegert Consulting e.K..
5 MHz Quartz crystals (QCs)	QT Quarztechnik GmbH; Inficon

Resist materials:

abbreviation	chemical name	purchased from
PMMA	Poly(methy methacrylate) (495 kg/mol, 2 % solution in anisole)	Microchem
trisphenol	1,1,1-Tris(4-hydroxyphenyl)-1-ethyl-4-isopropylbenzene	ABCR
crosslinker	N,N,N,N-Tetra(methoxymethyl)glycoluril	Worlée-Chemie
PAG1	1,2,3-Tris(methanesulfonyloxy)benzene	Midori Kagaku
PAG2	Methanesulfonic acid 1,3-dihydro-1,3-dioxo-2*H*-benz[*f*]isoindol-2-yl ester	Midori Kagaku
PAG3	Methanesulfonic acid 1,3-dioxo-1*H*-benz[*de*]isoquinolin-2(3*H*)-yl ester	Midori Kagaku
PAG4	Trifluoromethanesulfonic acid 1,3-dioxo-1*H*-benz[*de*]isoquinolin-2(3*H*)-yl ester	Midori Kagaku
PAG5	1-(9*H*-Fluoren-2-yl)-2,2,3,3,4,4,5,5,6,6-decafluoro-1-Hexanone *O*-[(1,1,2,2,3,3,4,4,4-nonafluorobutyl)sulfonyl]oxime	Ciba Special Chemicals (ceded)
PAG6	2-[2-(4-Methoxyphenyl)ethenyl]-4,6-bis(trichloromethyl)-1,3,5-Triazine	Aldrich
PAG7	Trifluoromethanesulfonic acid 1,3-dihydro-1,3-dioxo-2*H*-benz[*f*]isoindol-2-yl ester	Midori Kagaku
Base1	4,4'-Bis(carbazol-9-yl)biphenyl	Sensient
(R)-Base2	(R)-1,1'-Binaphthalene-2,2'-diamine	Fluka
rac-Base2	Rac-1,1'-binaphthalene-2,2'-diamine	Aldrich
Base3	4,4',4''-Tris(N-naphth-2-yl)-N-phenylamino)triphenylamine	Sensient

Processing chemicals:

abbreviation	chemical name	purchased from
HMDS	Hexamethyldisilazane	ABCR; Aldrich
TMAH	Aqueous tetramethyl ammonium hydroxide solution	Aldrich
P2VP	Poly-(2-vinyl-pyridine) MW 300,000-400,000 (for spin coated resists) MW 50,000 (for PVD films)	Polyscience
PVA	Polyvinyl alcohol 98% hydrolyzed; MW 13,000 - 23,000	Aldrich
Amylopectin	Amylopectin	Fluka
PA (Polyamide)	Poly[imino(1-oxo-1,6-hexanediyl)] Ultramid B27	BASF
PC (Polycarbonate)	Poly[oxycarbonyloxy-1,4-phenylene(1-methylethylidene)-1,4-phenylene] Makrolon 2458	Bayer Material Science
Sur1	Polyoxyethylene-(20)-sorbitan-monooleate (Tween 80)	Fluka
Sur2	(Polyoxyethylene-(23)-laurylether (Brij 35P)	Fluka
Sur3	Octadecan-1-ol	Aldrich

9.2.2. Synthesis of 4,4'-[[4-[1-(4-Hydroxyphenyl)-1-methylethyl]phenyl]methylene]-bisphenol tri-pivalic acid ester (1)

1.14 g (2.685 mmol) 4,4'-[[4-[1-(4-Hydroxyphenyl)-1-methylethyl]phenyl]methylene]-bisphenol and 12 ml (0.097 mol) tri-pivalic acid chloride were added to a baked out flask. The mixture was heated to reflux for 16 h. The excess of tri-pivalic acid chloride was distilled off. After recrystallization from isopropyl alcohol a white powder was obtained (yield: 86 %).

^{1}H-NMR (CDCl$_3$) δ [ppm]: 7.29-7.21 (2H), 7.14-7.07 (6H), 7.00-6.93 (8H), 2.15 (3H), 1.68 (6H), 1.37-1.35 (27H)

^{13}C-NMR (CDCl$_3$) δ [ppm]: 177.34, 177.28, 149.23, 148.94, 148.23, 147.97, 146.40, 145.87, 129.76, 128.30, 127.87, 126.38, 120.86, 120.80, 51.61, 42.38, 39.19, 39.17, 30.87, 30.74, 27.26

9.2.3. Synthesis of 5,5',6,6'-Tetrahydroxy-3,3,3',3'-tetramethyl-1,1'-spirobisindane tetra-pivalic acid ester (2)

340 mg (1 mmol) 5,5',6,6'-Tetrahydroxy-3,3,3',3'-tetramethyl-1,1'-spirobisindane and 0.62 ml (5 mmol) tri-pivalic acid chloride were added to a baked out flask in argon atmosphere and dissolved in 10 ml THF. The mixture was stirred for 16 h. After addition of 1 ml pyridine the

solution was stirred for additional 64 h. After solvent evaporation the residue was dissolved in ethyl acetate and shaken out against water. After drying with magnesium sulfate and evaporation of the ethyl acetate the crude product was purified through column chromatography using a mixture of cyclohexane and ethyl acetate (12:1) as the eluent. The product was received as white powder (yield: 62 %)

^{1}H-NMR (CDCl$_3$) δ [ppm]:   6.89 (2H), 6.57 (2H), 2.40-2.18 (4H), 1.36 (6H), 1.34 (18H), 1.32 (6H), 1.30 (18H)

^{13}C-NMR (CDCl$_3$) δ [ppm]:   176.31, 176.02, 150.50, 147.79, 142.03, 141.83, 118.95, 116.68, 59.37, 57.46, 43.54, 39.28, 39.15, 31.64, 30.25, 27.44, 27.41

9.2.4. Synthesis of 5,5',6,6'-Tetrahydroxy-3,3,3',3'-tetramethyl-1,1'-spirobisindane tetra-1-adamantanecarboxylic acid ester (3)

25 ml thionyl chloride were added to 2.16 g (12 mmol) 1-adamantyl carbonic acid. The mixture was heated to reflux for 130 min and allowed to reach room temperature. The excess of thionyl chloride was distilled off. The acid chloride is distilled (HV) from the residue into the reaction flask giving 2.19 g (11.04 mmol). Afterwards, 300 mg (0.88 mmol) 5,5',6,6'-Tetrahydroxy-3,3,3',3'-tetramethyl-1,1'-spirobisindane were added in argon atmosphere and the mixture was heated to 140 °C for 16 h. The resultant crude product was purified through column chromatography using a mixture of cyclohexane and ethyl acetate (12:1) as the eluent. Due to not hydrolyzed acid chloride the purification failed and the product was received by washing the column with a mixture of cyclohexane and ethyl acetate (4:1) and finally pure ethyl acetate. In a second purification step by column chromatography using a mixture of cyclohexane and THF (16:1) as the eluent the product could be received as white powder (yield: 25 %).

^{1}H-NMR (CDCl$_3$) δ [ppm]:   6.89 (2H), 6.54 (2H), 2.38-2.18 (4H), 2.11-1.65 (60H), 1.35 (6H), 1.30 (6H)

^{13}C-NMR (CDCl$_3$) δ [ppm]:   175.37, 175.10, 150.32, 147.74, 142.00, 141.78, 118.97, 116.70, 59.36, 57.42, 43.55, 41.24, 41.11, 39.02, 38.98, 36.57, 31.66, 30.23, 27.98

9.2.5. Synthesis of 5,5',6,6'-Tetrahydroxy-3,3,3',3'-tetramethyl-1,1'-spirobisindane tetra-*tert*-butyl acetate ether (4)

1 g (2.94 mmol) 5,5',6,6'-Tetrahydroxy-3,3,3',3'-tetramethyl-1,1'-spirobisindane, 4.06 g (29.4 mmol) potassium carbonate, 155 mg (0.59 mmol) 18-crown-6 and 80 ml dimethyl sulfoxide were added to a baked out flask in argon atmosphere. Afterwards 1.74 ml (11.75 mmol) *tert*-butyl bromoacetate were added dropwise. The mixture was stirred at 85 °C for 20 h. The mixture was allowed to reach room temperature and precipitated in water. To enhance the precipitation process sodium chloride was added. After filtration and washing with water the product is dried in HV for 16 h. It is received as white powder (yield: 85 %).

^{1}H-NMR (CDCl$_3$) δ [ppm]:   6.61 (2H), 6.19 (2H), 4.60 (4H), 4.43 (4H), 2.30-2.07 (4H), 1.49 (18H), 1.37 (18H), 1.30 (6H), 1.25 (6H)

^{13}C-NMR (CDCl$_3$) δ [ppm]:   168.55, 168.08, 147.86, 147.74, 145.36, 143.37, 110.04, 108.65, 82.10, 82.04, 67.43, 66.82, 59.54, 57.47, 43.28, 31.66, 30.47, 28.20, 28.07

9.2.6. Synthesis of 2,2'-dimethyl-[1,1'-Biphenyl]-4,4'-diol di-*tert*-butyl acetate ether (5)

1.6 g (7.47 mmol) 2,2'-dimethyl-[1,1'-Biphenyl]-4,4'-diol, 5.16 g (37.3 mmol) potassium carbonate, 395 mg (1.49 mmol) 18-crown-6 and 100 ml dimethyl sulfoxide were added to a baked out flask in argon atmosphere. Afterwards 2.75 ml (18.67 mmol) *tert*-butyl bromoacetate were added dropwise. The mixture was stirred at 85 °C for 16 h. The mixture was allowed to reach room temperature and precipitated in water. To enhance the precipitation process sodium chloride was added. The crude product was received as orange wax-like residue, which was skim off the water surface. The crude product was dissolved in as few as possible ethyl acetate. The resultant solution was used to prepare a column head. The column chromatography was performed using a mixture of cyclohexane and THF (16:1) as the eluent. The product is received as transparent viscous liquid (yield: 67 %)

^{1}H-NMR (CDCl$_3$) δ [ppm]:   6.98 (2H), 6.79 (2H), 6.72 (2H), 4.53 (4H), 2.00 (6H), 1.50 (18H)

^{13}C-NMR (CDCl$_3$) δ [ppm]:   168.36, 156.96, 137.82, 134.52, 130.77, 116.01, 111.42, 82.40, 65.77, 28.16, 20.28

9.2.7. Synthesis of 2,2'-dimethyl-[1,1'-Biphenyl]-4,4'-dicarbonic acid isoborneol ester (6)

0.75 g (2.78 mmol) 2,2'-dimethyl-[1,1'-Biphenyl]-4,4'-dicarbonic acid were dissolved in 20 ml dichloromethane and 10 ml oxalyl chloride. After the addition of one drop of N,N-dimethylformamide as catalyst the mixture was stirred for 18 h while the gaseous reaction products were formed. The solvent and the excess of oxalyl chloride were distilled off and the residue dissolved in 10 ml THF. This solution is added dropwise to the alkoxide solution prepared in the following manner.

1.28 g (8.34 mmol) isoborneol were dissolved in 10 ml THF in a baked out flask in argon atmosphere. At -5 °C 5.7 ml (9.17 mmol) n-butyl lithium were added dropwise and the resultant suspension was stirred for 30 min. Afterwards the already mentioned acid chloride solution is added dropwise. The mixture was heated to 50 °C and stirred for 18 h. The evaporation mixture is distilled in vacuum to dryness and dissolved in ethyl acetate. The solution was shaken out against water and dried with sodium sulfate. After solvent evaporation a brown viscous crude product is received. This crude product was purified through column chromatography using a mixture of cyclohexane and THF (20:1) as the eluent. In a second purification step by column chromatography using toluene as the eluent the product could be received as white powder (yield: 50 %).

^{1}H-NMR (CDCl$_3$) δ [ppm]:   7.93 (2H), 7.87 (2H), 7.14 (2H), 4.94 (2H), 2.08 (6H), 1.95-1.56 (10H), 1.30-1.10 (4H), 1.15 (6H), 0.96 (6H), 0.90 (6H)

^{13}C-NMR (CDCl$_3$) δ [ppm]:   166.17, 145.48, 136.02, 131.23, 130.25, 129.11, 126.96, 81.72, 49.17, 47.19, 45.22, 39.05, 33.87, 27.22, 20.29, 20.26, 19.95, 11.82

10. Literature references

[1] J. S. Kilby, Nobel Lecture 2000: Turning Potential into Reality: The Invention of the Integrated Circuit in *Nobel Lectures in Physics, 1996-2000*, World Scientific, [River Edge] New Jersey **2002**, 474–485.

[2] G. E. Moore, Cramming more components onto integrated circuits, *Electronics* **1965**, *38*, 114–117.

[3] R. N. Noyce, Semiconductor device-and-lead structure *US2981877* **1959**.

[4] Intel Corporation, *Information about Intels' current processor architectures* can be found under http://www.intel.com/. Accessed: **Juli 2013**.

[5] G. Levitin, D. W. Hess, Surface Reactions in Microelectronics Process Technology, *Annu. Rev. Chem. Biomol. Eng.* **2011**, *2*, 299–324.

[6] C. A. Mack, *Fundamental principles of optical lithography: The science of microfabrication*, John Wiley & Sons Ltd, Chichester, England **2007**.

[7] J. Cameron, J. Thackeray, J. W. Sung, S. M. Coley, V. Jain, O. Ongayi, M. D. Wagner, P. LaBeaume, A. Kwok, D. Valeri, M. Hellion, B. Icard, B. Dal'zotto, C. Sourd, L. Pain, Comparison of EUV and e-beam lithographic technologies for sub-22-nm node patterning, *Proc. SPIE* **2012**, *8322*, 83222F/1–12.

[8] M. C. Lemme, D. C. Bell, J. R. Williams, L. A. Stern, B. W. H. Baugher, P. Jarillo-Herrero, C. M. Marcus, Etching of graphene devices with a helium ion beam, *ACS Nano* **2009**, *3*, 2674–2676.

[9] M. Tanaka, A. Rastogi, H. Kudo, D. Watanabe, T. Nishikubo, C. K. Ober, Environmentally friendly patterning of molecular waterwheel (Noria) in supercritical carbon dioxide, *J. Mater. Chem.* **2009**, *19*, 4622–4626.

[10] G. Karbasian, P. J. Fay, H. Xing, D. Jena, A. O. Orlov, G. L. Snider, High aspect ratio features in poly(methylglutarimide) using electron beam lithography and solvent developers, *J. Vac. Sci. Technol., B: Nanotechnol. Microelectron.: Mater., Process., Meas., Phenom.* **2012**, *30*, 06FI01/1–4.

[11] C. Y. Ouyang, J.-K. Lee, M. E. Krysak, J. Sha, C. K. Ober, Environmentally friendly patterning of thin films in linear methyl siloxanes, *J. Mater. Chem.* **2012**, *22*, 5746–5750.

[12] F. Wieberger, T. Kolb, C. Neuber, C. K. Ober, H.-W. Schmidt, Combinatorial techniques to efficiently investigate and optimize organic thin film processing and properties, *Molecules* **2013**, *18*, 4120–4139.

[13] U. Hilleringmann, *Silizium-Halbleitertechnologie: Grundlagen mikroelektronischer Integrationstechnik*, Vieweg + Teubner, Wiesbaden **2008**.

[14] Fuller G.E., Optical Lithography in *Handbook of semiconductor manufacturing technology* (Eds.: R. Doering, Y. Nishi), CRC Press, Boca Raton **2008**, 18/1-50.

[15] B. Fay, Advanced optical lithography development, from UV to EUV, *Microelectronic Engineering* **2002**, *61-62*, 11–24.

[16] Garza C.M., Conley W., Byers J., Photoresist Materials and Processing in *Handbook of semiconductor manufacturing technology* (Eds.: R. Doering, Y. Nishi), CRC Press, Boca Raton **2008**, 19/1-57.

[17] C. Cork, F. Amoroso, A. Poonawala, S. Jang, K. Lucas, Suppressing ringing effects from very strong off-axis illumination with novel OPC approaches for low k1 lithography, *Proc. SPIE* **2010**, *7640*, 76401C/1–11.

[18] P. Xie, B. W. Smith, Analysis of higher order pitch division for sub-32 nm lithography, *Proc. SPIE* **2009**, *7274*, 72741Y/1–8.

[19] H. Yaegshi, K. Oyama, K. Y. S. Yamauchi, A. Hara, S. Natori, Important challenge for optical lithography extension utilizing double patterning process, *J. Photopolym. Sci. Technol.* **2011**, *24*, 491–495.

[20] J. Mulkens, D. G. Flagello, B. Streefkerk, P. Graeupner, Benefits and limitations of immersion lithography, *J. Microlithogr., Microfabr., Microsyst.* **2004**, *3*, 104–114.

[21] I. Bouchoms, M. Leenders, J. J. Kuit, R. Kazinczi, G. R. de, B. Paarhuis, P. Gunter, S. Weichselbaum, M. Beems, M. Verhoeven, B. R. van, Extending 1.35 NA immersion lithography down to 1x nm production nodes, *Proc. SPIE* **2012**, *8326*, 83260L/1–5.

[22] P. Xie, B. W. Smith, Scanning interference evanescent wave lithography for sub-22-nm generations, *J. Micro/Nanolithogr., MEMS, MOEMS* **2013**, *12*, 013011/1–8.

[23] B. J. Lin, The ending of optical lithography and the prospects of its successors, *Microelectron. Eng.* **2006**, *83*, 604–613.

[24] *Intel drops 157-nm tools from lithography roadmap* can be found under http://www.eetimes.com/document.asp?doc_id=1175202. Accessed: **Juli 2013**.

[25] *International Technology Roadmap for Semiconductors _ 2012 Overview* can be found under http://www.itrs.net. Accessed: **July 2013**.

[26] M. LaPedus, *Optical Lithography, Take Two in Semiconductor Manufacturing and Design* can be found under http://semimd.com/blog/2013/02/21/optical-lithography-take-two/. Accessed: **Juli 2013**.

[27] K.-J. Byeon, H. Lee, Recent progress in direct patterning technologies based on nano-imprint lithography, *Eur. Phys. J.: Appl. Phys.* **2012**, *59*, 10001/1–21.

[28] M. Zelsmann, J. Boussey, Materials and processes in UV-assisted nanoimprint lithography in *Generating Micro- and Nanopatterns on Polymeric Materials* (Eds.: A. del Campo, E. Arzt), Wiley-VCH Verlag GmbH & Co. KGaA **2011**, 3–26.

[29] R. R. Dammel, Cost-effective sub-20 nm lithography: smart chemicals to the rescue, *J. Photopolym. Sci. Technol.* **2011**, *24*, 33–42.

[30] B. H. Kim, J. Y. Kim, S. O. Kim, Directed self-assembly of block copolymers for universal nanopatterning, *Soft Matter* **2013**, *9*, 2780–2786.

[31] A. Nunns, J. Gwyther, I. Manners, Inorganic block copolymer lithography, *Polymer* **2013**, *54*, 1269–1284.

[32] J. Sporre, D. N. Ruzic, Extreme ultraviolet light lithography for producing nanofeatures in next-generation semiconductor processing in *Plasma Processing of Nanomaterials* (Ed.: R. M. Sankaran), CRC Press **2011**, 35–54.

[33] T. Kozawa, S. Tagawa, Image formation in chemically amplified resists upon exposure to extreme ultraviolet radiation, *J. Photopolym. Sci. Technol.* **2009**, *22*, 51–58.

[34]   T. Tomie, Tin laser-produced plasma as the light source for extreme ultraviolet lithography high-volume manufacturing: history, ideal plasma, present status, and prospects, *J. Micro/Nanolithogr., MEMS, MOEMS* **2012**, *11*, 021109/1–9.

[35]   P. Naulleau, C. Anderson, S. George, EUV resists: illuminating the challenges, *J. Photopolym. Sci. Technol.* **2011**, *24*, 637–642.

[36]   O. Wood, J. Arnold, T. Brunner, M. Burkhardt, J. H.-C. Chen, D. Civay, S. S.-C. Fan, E. Gallagher, S. Halle, M. He, C. Higgins, H. Kato, J. Kye, C.-S. Koay, G. Landie, P. Leung, G. McIntyre, S. Nagai, K. Petrillo, S. Raghunathan, R. Schlief, L. Sun, A. Wagner, T. Wallow, Y. Yin, X. Zhu, M. Colburn, D. Corliss, C. Smolinski, Insertion strategy for EUV lithography, *Proc. SPIE* **2012**, *8322*, 832203/1–8.

[37]   Z. Gan, Y. Cao, R. A. Evans, M. Gu, Three-dimensional deep sub-diffraction optical beam lithography with 9 nm feature size, *Nat Commun* **2013**, *4*, 2061.

[38]   D. Pires, J. L. Hedrick, S. A. De, J. Frommer, B. Gotsmann, H. Wolf, M. Despont, U. Duerig, A. W. Knoll, Nanoscale Three-Dimensional Patterning of Molecular Resists by Scanning Probes, *Science (Washington, DC, U. S.)* **2010**, *328*, 732–735.

[39]   M. Kaestner, I. W. Rangelow, Scanning probe nanolithography on calixarene, *Microelectron. Eng.* **2012**, *97*, 96–99.

[40]   F. Watt, A. A. Bettiol, K. J. A. Van, E. J. Teo, M. B. H. Breese, Ion beam lithography and nanofabrication: a review, *Int. J. Nanosci.* **2005**, *4*, 269–286.

[41]   D. C. Bell, M. C. Lemme, L. A. Stern, J. R. Williams, C. M. Marcus, Precision cutting and patterning of graphene with helium ions, *Nanotechnology* **2009**, *20*, 455301/1–5.

[42]   T. Kozawa, S. Tagawa, Basic aspects of acid generation processes in chemically amplified electron beam resist, *J. Photopolym. Sci. Technol.* **2005**, *18*, 471–474.

[43]   H. W. Ro, C. L. Soles, Silsesquioxanes in nanoscale patterning applications, *Mater. Today (Oxford, U. K.)* **2011**, *14*, 20–33.

[44]   G. de Boer, M. P. Dansberg, R. Jager, J. J. M. Peijster, E. Slot, S. W. H. K. Steenbrink, M. J. Wieland, W. M. Tong, D. J. Resnick, MAPPER: progress toward a high-volume manufacturing system, *Proc. SPIE* **2013**, *8680*, 86800O/1-12.

[45]   C. Klein, H. Loeschner, E. Platzgummer, 50-keV electron multibeam mask writer for the 11-nm HP node: first results of the proof-of-concept electron multibeam mask exposure tool, *J. Micro/Nanolithogr., MEMS, MOEMS* **2012**, *11*, 031402/1–7.

[46]   T. Gubiotti, J. F. Sun, R. Freed, F. Kidwingira, J. Yang, C. Bevis, A. Carroll, A. Brodie, W. M. Tong, S.-J. Lin, W.-C. Wang, L. Haspeslagh, B. Vereecke, D. J. Resnick, Reflective electron beam lithography: lithography results using CMOS controlled digital pattern generator chip, *Proc. SPIE* **2013**, *8680*, 86800H/1–11.

[47]   T. Maruyama, Y. Machida, S. Sugatani, H. Takita, H. Hoshino, T. Hino, M. Ito, A. Yamada, T. Iizuka, S. Komatsu, M. Ikeda, K. Asada, CP element based design for 14 nm node EBDW high volume manufacturing, *Proc. SPIE* **2012**, *8323*, 832314/1–11.

[48]   C. G. Willson, R. A. Dammel, A. Reiser, Photoresist materials: a historical perspective, *Proc. SPIE-Int. Soc. Opt. Eng.* **1997**, *3050*, 38–51.

[49]   S. F. Wanat, R. R. Plass, M. D. Rahman, Novolak resins and the microelectronic revolution, *J. Micro/Nanolithogr., MEMS, MOEMS* **2008**, *7*, 033008/1–11.

[50]   H. Ito, G. Breyta, D. Hofer, R. Sooriyakumaran, K. Petrillo, D. Seeger, Environmentally stable chemical amplification positive resist: principle, chemistry, contamination resistance, and lithographic feasibility, *J. Photopolym. Sci. Technol.* **1994**, *7*, 433–447.

[51]   D. P. Sanders, Advances in Patterning Materials for 193 nm Immersion Lithography, *Chem. Rev. (Washington, DC, U. S.)* **2010**, *110*, 321–360.

[52]   H. Ito, Chemical amplification resists for microlithography, *Adv. Polym. Sci.* **2005**, *172*, 37–245.

[53]   H. Ito, C. G. Willson, Chemical amplification in the design of dry developing resist materials, *Polym. Eng. Sci.* **1983**, *23*, 1012–1018.

[54]   H. Ito, C. Willson, J. Frechet, New UV Resists with Negative or Positive Tone in *Symp. VLSI Technol., Dig. Tech. Pap* **1982**, 86–87.

[55]   J. G. Maltabes, S. J. Holmes, J. R. Morrow, R. L. Barr, M. Hakey, G. Reynolds, W. R. Brunsvold, C. G. Willson, N. Clecak, a. et, 1X deep UV lithography with chemical amplification for 1-micron DRAM production, *Proc. SPIE-Int. Soc. Opt. Eng.* **1990**, *1262*, 2–7.

[56]   H. Ito, Rise of chemical amplification resists from laboratory curiosity to paradigm enabling Moore's Law, *Proc. SPIE* **2008**, *6923*, 692302/1–15.

[57]   F. Wieberger, C. Neuber, C. K. Ober, H.-W. Schmidt, Tailored Star Block Copolymer Architecture for High Performance Chemically Amplified Resists, *Adv. Mater.* **2012**, *24*, 5939–5944.

[58]   M. Neisser, K. Cho, K. Petrillo, The physics of EUV photoresist and how it drives strategies for improvement, *J. Photopolym. Sci. Technol.* **2012**, *25*, 87–94.

[59]   J. B. Shin, H. S. Joo, S. D. Cho, H. S. Lim, J. H. Kim, S. J. Lee, D. H. Shin, J. Han, D. C. Seo, Study of acid diffusion of anionic or cationic polymer bound PAG, *Proc. SPIE* **2011**, *7969*, 79692N/1–11.

[60]   J. W. Thackeray, J. F. Cameron, M. Wagner, S. Coley, V. P. Labeaume, O. Ongayi, W. Montgomery, D. Lovell, J. Biafore, V. Chakrapani, A. Ko, Advances in low diffusion EUV resists, *J. Photopolym. Sci. Technol.* **2012**, *25*, 641–646.

[61]   *International Technology Roadmap for Semiconductors _ 2011 Lithography* can be found under http://www.itrs.net. Accessed: **Juli 2013**.

[62]   M. Mayberry, *A Look Forward*, presented at Techcon 2010, Austin TX, USA **2010**.

[63]   Y. Shirota, Organic materials for electronic and optoelectronic devices, *J. Mater. Chem.* **2000**, *10*, 1–25.

[64]   M. Yoshiiwa, H. Kageyama, Y. Shirota, F. Wakaya, K. Gamo, M. Takai, Novel class of low molecular-weight organic resists for nanometer lithography, *Appl. Phys. Lett.* **1996**, *69*, 2605–2607.

[65]   T. Kadota, H. Kageyama, F. Wakaya, K. Gamo, Y. Shirota, Novel electron-beam molecular resists with high resolution and high sensitivity for nanometer lithography, *Chem. Lett.* **2004**, *33*, 706–707.

[66]   A. De Silva, C. K. Ober, Hydroxyphenylbenzene derivatives as glass forming molecules for high resolution photoresists, *J. Mater. Chem.* **2008**, *18*, 1903–1910.

[67] D. Shiono, H. Hada, K. Sato, Y. Fukushima, T. Watanabe, H. Kinoshita, Fundamental decomposition analysis of chemically amplified molecular resist for below 22 nm resolution, *J. Photopolym. Sci. Technol.* **2010**, *23*, 649–655.

[68] H. Kudo, Y. Suyama, H. Oizumi, T. Itani, T. Nishikubo, Novel extreme ultraviolet (EUV)-resist material based on noria (water wheel-like cyclic oligomer), *J. Mater. Chem.* **2010**, *20*, 4445–4450.

[69] K. Young-Gil, J. B. Kim, T. Fujigaya, Y. Shibasaki, M. Ueda, A positive-working alkaline developable photoresist based on partially tert-Boc-protected calix[4]resorcinarene and a photoacid generator, *J. Mater. Chem.* **2002**, *12*, 53–57.

[70] M. Ueda, D. Takahashi, T. Nakayama, O. Haba, Three-component negative-type photoresist based on calix[4]resorcinarene, a cross-linker, and a photoacid generator, *Chem. Mater.* **1998**, *10*, 2230–2234.

[71] T. Kasai, T. Higashihara, M. Ueda, Synthesis of calixresorcinarene derivatives with cross-linking units and evaluation of lithographic performance, *J. Photopolym. Sci. Technol.* **2011**, *24*, 631–635.

[72] M. Echigo, D. Oguro, Development of new phenylcalix[4]resorcinarene: its application to positive-tone molecular resist for EB and EUV lithography, *Proc. SPIE* **2009**, *7273*, 72732Q/1-12.

[73] A. De Silva, L. K. Sundberg, R. Sooriyakumaran, L. Bozano, G. Breyta, W. D. Hinsberg, M. Fujiwara, Hexafluoroalcohol (HFA) containing molecular resist materials for high-resolution lithographic applications, *Proc. SPIE* **2011**, *7972*, 79721Z/1–10.

[74] N. Niina, H. Kudo, K. Maruyama, T. Kai, T. Shimokawa, H. Oizumi, T. Itani, T. Nishikubo, Multicomponent negative-type photoresist based on Noria analog with 12 ethoxy groups, *Polym. J. (Tokyo, Jpn.)* **2011**, *43*, 407–413.

[75] H. Kudo, M. Jinguji, T. Nishikubo, H. Oizumi, T. Itani, Extreme ultraviolet (EUV)-resist materials of noria (water wheel-like cyclic oligomer) derivatives containing acetal moieties, *J. Photopolym. Sci. Technol.* **2010**, *23*, 657–664.

[76] R. A. Lawson, L. M. Tolbert, C. L. Henderson, Single-component molecular resists containing bound photoacid generator functionality, *J. Micro/Nanolithogr., MEMS, MOEMS* **2010**, *9*, 013015/1–7.

[77] T. Kasai, T. Higashihara, M. Ueda, A novel photo-acid generator bound molecular glass resist with a single protecting group, *J. Polym. Sci., Part A: Polym. Chem.* **2013**, *51*, 1956–1962.

[78] A. De Silva, N. M. Felix, C. K. Ober, Molecular glass resists as high-resolution patterning materials, *Adv. Mater.* **2008**, *20*, 3355–3361.

[79] T. Nishikubo, H. Kudo, Recent development in molecular resists for extreme ultraviolet lithography, *J. Photopolym. Sci. Technol.* **2011**, *24*, 9–18.

[80] B. Geffroy, P. Le Roy, C. Prat, Organic light-emitting diode (OLED) technology: materials, devices and display technologies, *Polym. Int* **2006**, *55*, 572–582.

[81] B. C. Popere, A. M. Della Pelle, A. Poe, S. Thayumanavan, Macromolecular architectures for organic photovoltaics, *Phys. Chem. Chem. Phys.* **2012**, *14*, 4043–4057.

[82]   E. C. P. Smits, S. G. J. Mathijssen, P. A. van Hal, S. Setayesh, T. C. T. Geuns, K. A. H. A. Mutsaers, E. Cantatore, H. J. Wondergem, O. Werzer, R. Resel, M. Kemerink, S. Kirchmeyer, A. M. Muzafarov, S. A. Ponomarenko, B. de Boer, P. W. M. Blom, D. M. de Leeuw, Bottom-up organic integrated circuits, *Nature* **2008**, *455*, 956–959.

[83]   Y. Ma, Y. Wen, Y. Song, Ultrahigh density data storage based on organic materials with SPM techniques, *J. Mater. Chem.* **2011**, *21*, 3522–3533.

[84]   F. C. Krebs, Fabrication and processing of polymer solar cells: A review of printing and coating techniques, *Sol. Energy Mater. Sol. Cells* **2009**, *93*, 394–412.

[85]   K. Norrman, A. Ghanbari-Siahkali, N. B. Larsen, Studies of spin-coated polymer films, *Annu. Rep. Prog. Chem., Sect. C: Phys. Chem.* **2005**, *101*, 174–201.

[86]   J.-Y. Jung, Y.-T. Kang, J. Koo, Development of a new simulation model of spin coating process and its application to optimize the 450mm wafer coating process, *Int. J. Heat Mass Transfer* **2010**, *53*, 1712–1717.

[87]   D. W. Schubert, T. Dunkel, Spin coating from a molecular point of view: its concentration regimes, influence of molar mass and distribution, *Mater. Res. Innovations* **2003**, *7*, 314–321.

[88]   N.-H. Kim, P.-J. Ko, W.-S. Lee, Improvement of the surface roughness and sensing properties of cerium dioxide thin film by chemical mechanical polishing, *J. Vac. Sci. Technol. A* **2008**, *26*, 794–797.

[89]   T. Leveder, S. Landis, N. Chaix, L. Davoust, Thin polymer films viscosity measurements from nanopatterning method, *J. Vac. Sci. Technol. B* **2010**, *28*, 1251–1258.

[90]   S. Tang, M. Liu, P. Lu, H. Xia, M. Li, Z. Xie, F. Shen, C. Gu, H. Wang, B. Yang, Y. Ma, A molecular glass for deep-blue organic light-emitting diodes comprising a 9,9'-spirobifluorene core and peripheral carbazole groups, *Adv. Funct. Mater.* **2007**, *17*, 2869–2877.

[91]   K. L. Choy, Chemical vapor deposition of coatings, *Prog. Mater. Sci.* **2003**, *48*, 57–170.

[92]   S. M. Rossnagel, Thin film deposition with physical vapor deposition and related technologies, *J. Vac. Sci. Technol. A* **2003**, *21*, S74-S87.

[93]   F. Pfeiffer, N. M. Felix, C. Neuber, C. K. Ober, H.-W. Schmidt, Physical vapor deposition of molecular glass photoresists: a new route to chemically amplified patterning, *Adv. Funct. Mater.* **2007**, *17*, 2336–2342.

[94]   C. Neuber, M. Bate, M. Thelakkat, H.-W. Schmidt, H. Hansel, H. Zettl, G. Krausch, Combinatorial preparation and characterization of thin-film multilayer electro-optical devices, *Rev. Sci. Instrum.* **2007**, *78*, 072216/1-11.

[95]   M. C. Petty, Organic thin film deposition techniques in *Encyclopedia of Nanoscience and Nanotechnology*, Vol. 8 (Ed.: H. S. Nalwa), American Scientific Publishers **2004**, 295–304.

[96]   S. F. Swallen, K. L. Kearns, M. K. Mapes, Y. S. Kim, R. J. McMahon, M. D. Ediger, T. Wu, L. Yu, S. Satija, Organic Glasses with Exceptional Thermodynamic and Kinetic Stability, *Science (Washington, DC, U. S.)* **2007**, *315*, 353–356.

[97] K. L. Kearns, T. Still, G. Fytas, M. D. Ediger, High-Modulus Organic Glasses Prepared by Physical Vapor Deposition, *Adv. Mater.* **2010**, *22*, 39–42.

[98] S. J. Keough, T. L. Hanley, A. B. Wedding, J. S. Quinton, Grazing incidence X-ray studies of ultra-thin Lumogen films, *Surf. Sci.* **2007**, *601*, 5744–5749.

[99] M. Krbal, T. Wagner, T. Kohoutek, P. Nemec, J. Orava, M. Frumar, The comparison of Ag-As33S67 films prepared by thermal evaporation (TE), spin-coating (SC) and a pulsed laser deposition (PLD), *J. Phys. Chem. Solids* **2007**, *68*, 953–957.

[100] Y. J. Guo, X. T. Zu, X. D. Jiang, X. D. Yuan, S. Z. Xu, B. Y. Wang, D. B. Tian, Experimental research of laser-induced damage of the monolayer ZrO2 PVD and sol-gel films, *Opt. Laser Technol.* **2008**, *40*, 677–681.

[101] X. Wang, S. Ochiai, K. Kojima, A. Ohashi, T. Mizutani, Organic field-effect transistors based on vapor-deposited pentacene and soluble pentacene precursor, *J. Vac. Soc. Jpn.* **2008**, *51*, 169–171.

[102] E. L. Jablonski, V. M. Prabhu, S. Sambasivan, D. A. Fischer, E. K. Lin, D. L. Goldfarb, M. Angelopoulos, H. Ito, Surface and bulk chemistry of chemically amplified photoresists: segregation in thin films and environmental stability issues, *Proc. SPIE* **2004**, *5376*, 302–311.

[103] J. W. Lee, Y. S. Choi, W. H. Jo, Diketopyrrolopyrrole-based small molecules with simple structure for high VOC organic photovoltaics, *Org. Electron.* **2012**, *13*, 3060–3066.

[104] M. A. Baldo, S. Lamansky, P. E. Burrows, M. E. Thompson, S. R. Forrest, Very high-efficiency green organic light-emitting devices based on electro-phosphorescence, *Appl. Phys. Lett.* **1999**, *75*, 4–6.

[105] K. Kreger, M. Baete, C. Neuber, H.-W. Schmidt, P. Strohriegl, Combinatorial development of blue OLEDs based on star shaped molecules, *Adv. Funct. Mater.* **2007**, *17*, 3456–3461.

[106] V. P. Korchkov, T. N. Martynova, V. S. Danilovich, All-dry vacuum submicron lithography, *Thin Solid Films* **1983**, *101*, 369–372.

[107] S. V. Babin, A. I. Holopkin, M. N. Lyakhov, K. A. Valiev, L. V. Velikov, E. N. Zhikharev, Investigation of new dry high sensitive resist using 100 kV electron lithography, *Microelectron. Eng.* **1994**, *23*, 303–305.

[108] U. Masahito, T. Morio, Ion-beam lithographic pattern-forming method *JP60131961A* **1985**.

[109] Y. K. Mikhailovskii, V. A. Azarko, V. E. Agabekov, Photochemical transformations of sulfophthaleine dyes in thin film state, *J. Photochem. Photobiol., A* **1994**, *81*, 211–218.

[110] M. Sato, M. Iijima, Y. Takahashi, Fabrication of polyurea resists by vapor deposition polymerization for all dry process, *J. Photopolym. Sci. Technol.* **1995**, *8*, 137–140.

[111] V. E. Agabekov, V. I. Potkin, R. V. Kaberdin, Y. I. Gudimenko, V. A. Azarko, Y. A. Oldekop, N. I. Mitskevich, Light-sensitive compounds in vacuum photolithographic processes *SU1351426A1* **1996**.

[112] V. A. Azarko, T. V. Konysheva, G. V. Pshenichnyi, V. E. Agabekov, Derivatives of 9-H-carbazole as light-sensitive thermal-development material, *Vestsi Nats. Akad. Navuk Belarusi, Ser. Khim. Navuk* **1999**, 63–66.

[113] E. A. Dikusar, N. G. Kozlov, V. I. Potkin, V. A. Azarko, A. P. Yuvchenko, Synthesis, film-forming properties, and photosensitivity of 4-alkoxy(acyloxy)-3-alkoxyphenylmethylene-(biphenyl-4-yl)amines, *Russ. J. Gen. Chem.* **2007**, *77*, 1766–1768.

[114] E. A. Dikusar, N. G. Kozlov, V. I. Potkin, V. A. Azarko, A. P. Yuvchenko, Synthesis, film-forming properties, and thermal and light sensitivity of N,N'-bis[4-hydroxy(alkoxy, acyloxy)-3-alkoxyphenylmethylidene]benzene-1,4-diamines, *Russ. J. Gen. Chem.* **2008**, *78*, 281–285.

[115] E. A. Dikusar, N. G. Kozlov, V. I. Potkin, V. A. Azarko, A. P. Yuvchenko, Synthesis and study of film-forming properties and light sensitivity of 4-acyloxy-3-methoxy(ethoxy)phenylmethylidene-(chrysen-2-yl)amines, *Russ. J. Gen. Chem.* **2007**, *77*, 278–281.

[116] M. P. Bei, V. A. Azarko, A. P. Yuvchenko, Synthesis, film-forming, and light-sensitivity properties of allyl and propargyl maleopimarates and cytraconopimarates, *Russ. J. Gen. Chem.* **2010**, *80*, 940–943.

[117] F. Pfeiffer, C. Neuber, H.-W. Schmidt, All-dry photoresist systems: physical vapor deposition of molecular glasses, *Proc. SPIE* **2008**, *6923*, 69231F/1-8.

[118] F. Pfeiffer, N. M. Felix, C. Neuber, C. K. Ober, H.-W. Schmidt, Towards environmentally friendly, dry deposited, water developable molecular glass photoresists, *Phys. Chem. Chem. Phys.* **2008**, *10*, 1257–1262.

[119] A. Morinaka, S. Oikawa, Heat-mode lithography with dye deposited films, *J. Electrochem. Soc.* **1988**, *135*, 1275–1278.

[120] V. E. Agabekov, V. A. Azarko, O. P. Nevdakh, Dry resist material on base of perylene tetracarboxylic acid derivatives for laser lithography, *Proc. SPIE-Int. Soc. Opt. Eng.* **1995**, *2438*, 828–835.

[121] V. A. Azarko, E. V. Scharendo, V. E. Agabekov, V. E. Obuchov, E. I. Tochitsky, Lithographic properties of perylenetetracarboxylic acid derivatives films, *Proc. SPIE-Int. Soc. Opt. Eng.* **1997**, *3179*, 99–102.

[122] M. A. McCord, M. J. Rooks, Electron Beam Lithography in *Handbook of microlithography, micromachining, & microfabrication: Microlithography*, SPIE Optical Engineering Press [etc.], Bellingham, Washington **1997**, 139–249.

[123] H. C. Pfeiffer, Direct write electron beam lithography: a historical overview, *Proc. SPIE* **2010**, *7823*, 782316/1–6.

[124] Carl Zeiss AG, *Image* can be found under http://www.zeiss.com. Accessed: **July 2012**.

[125] Raith, *Service documentation beam blanker*.

[126] Cornell NanoScale Science and Technology Facility, *Description of JEOL JBX-9300FS Electron Beam Lithography System* can be found under http://www.cnf.cornell.edu/. Accessed: **December 2013**.

[127] W.-A. C. Bauer, *Kombinatorische Optimierung eines niedermolekularen Negativresistsystems für die Elektronenstrahllithographie*, Diploma thesis University of Bayreuth **2008**.

[128] C. A. Mack, D. A. Legband, S. Jug, Data analysis for photolithography, *Microelectron. Eng.* **1999**, *46*, 65–68.

[129] H. Zhong, J. Smith, S. Rossbauer, A. J. P. White, T. D. Anthopoulos, M. Heeney, Air-Stable and High-Mobility n-Channel Organic Transistors Based on Small-Molecule/Polymer Semiconducting Blends, *Adv. Mater.* **2012**, *24*, 3205–3211.

[130] T. Hirayama, D. Shiono, S. Matsumaru, T. Ogata, H. Hada, J. Onodera, T. Arai, T. Sakamizu, A. Yamaguchi, H. Shiraishi, H. Fukuda, M. Ueda, Development of electron beam resists based on amorphous polyphenols with low molecular weight and narrow dispersion, *Proc. SPIE* **2005**, *5753*, 738–745.

[131] S. J. Limb, B. E. Scruggs, K. K. Gleason, Distribution and motion of trifluoromethanesulfonate anions in poly(p-hydroxystyrene) and polystyrene films studied by multiple-quantum NMR, *Macromolecules* **1993**, *26*, 3750–3757.

[132] D. L. VanderHart, V. M. Prabhu, E. K. Lin, Proton NMR Determination of Miscibility in a Bulk Model Photoresist System: Poly(4-hydroxystyrene) and the Photoacid Generator, Di(tert-butylphenyl)Iodonium Perfluorooctanesulfonate, *Chem. Mater.* **2004**, *16*, 3074–3084.

[133] R. A. Lawson, C. L. Henderson, Mesoscale kinetic Monte Carlo simulations of molecular resists: the effect of PAG homogeneity on resolution, LER, and sensitivity, *Proc. SPIE* **2009**, *7273*, 727341/1–10.

[134] T. Kozawa, H. Yamamoto, S. Tagawa, Effect of inhomogeneous acid distribution on line edge roughness- relationship to line edge roughness originating from chemical gradient, *J. Photopolym. Sci. Technol.* **2010**, *23*, 625–630.

[135] W.-A. C. Bauer, C. Neuber, C. K. Ober, H.-W. Schmidt, Combinatorial Optimization of a Molecular Glass Photoresist System for Electron Beam Lithography, *Adv. Mater.* **2011**, *23*, 5404–5408.

[136] Y. Maekawa, K. Yuasa, K. Enomoto, H. Matsushita, J. Kato, T. Yamashita, K. Itoh, M. Yoshida, Electron-Beam-Induced Color Imaging of Acid-Chromic Polymer Films, *Chem. Mater.* **2008**, *20*, 5320–5324.

[137] A. De Silva, L. K. Sundberg, H. Ito, R. Sooriyakumaran, R. D. Allen, C. K. Ober, A fundamental study on dissolution behavior of high-resolution molecular glass photoresists, *Chem. Mater.* **2008**, *20*, 7292–7300.

[138] L. D. Jackel, R. E. Howard, P. M. Mankiewich, H. G. Craighead, R. W. Epworth, Beam energy effects in electron beam lithography: The range and intensity of backscattered exposure, *Appl. Phys. Lett* **1984**, *45*, 698–700.

[139] D. S. Fryer, S. Bollepali, P. J. J. de, P. F. Nearley, Study of acid diffusion in resist near the glass transition temperature, *J. Vac. Sci. Technol., B* **1999**, *17*, 3351–3355.

[140] H. Ito, Solid-state thermolysis of poly(p-tert-butoxycarbonyloxystyrene) catalyzed by polymeric phenol: effect of phase separation, *J. Polym. Sci., Part A: Polym. Chem.* **1986**, *24*, 2971–2980.

[141] H. Ito, M. Ueda, Thermolysis and photochemical acidolysis of selected polymethacrylates, *Macromolecules* **1988**, *21*, 1475–1482.

[142] A. De Silva, J.-K. Lee, X. Andre, N. M. Felix, H. B. Cao, H. Deng, C. K. Ober, Study of the Structure-Properties Relationship of Phenolic Molecular Glass Resists for Next Generation Photolithography, *Chem. Mater.* **2008**, *20*, 1606–1613.

[143] R. D. Allen, G. M. Wallraff, R. A. Dipietro, D. C. Hofer, R. R. Kunz, Single layer resists with enhanced etch resistance for 193 nm lithography, *J. Photopolym. Sci. Technol.* **1994**, *7*, 507–516.

[144] H. Tsubaki, T. Tsuchihashi, T. Tsuchimura, Resolution and LWR improvements by acid diffusion control in EUV lithography, *Proc. SPIE* **2009**, *7273*, 72731K/1–8.

[145] A. R. Pawloski, Christian, P. F. Nealey, The Multifunctional Role of Base Quenchers in Chemically Amplified Photoresists, *Chem. Mater.* **2002**, *14*, 4192–4201.

[146] X. Thrun, K.-H. Choi, M. Freitag, A. Grenville, M. Gutsch, C. Hohle, J. K. Stowers, J. W. Bartha, Evaluation of direct patternable inorganic spin-on hard mask materials using electron beam lithography, *Microelectron. Eng.* **2012**, *98*, 226–229.

[147] B. Shokouhi, M. Zhang, B. Cui, Very high sensitivity ZEP resist using MEK:MIBK developer, *Micro Nano Lett.* **2011**, *6*, 992–994.

[148] M. Shirai, K. Maki, H. Okamura, K. Kaneyama, T. Itani, EUV negative-resist based on thiol-yne system, *Proc. SPIE* **2011**, *7972*, 79721E/1–8.

[149] S. Takei, A. Oshima, T. Wakabayashi, T. Kozawa, S. Tagawa, Eco-friendly electron beam lithography using water-developable resist material derived from biomass, *Appl. Phys. Lett.* **2012**, *101*, 033106/1–4.

[150] V. Canalejas-Tejero, S. Carrasco, F. Navarro-Villoslada, F. J. L. Garcia, M. d. C. Capel-Sanchez, M. C. Moreno-Bondi, C. A. Barrios, Ultrasensitive non-chemically amplified low-contrast negative electron beam lithography resist with dual-tone behavior, *J. Mater. Chem. C* **2013**, *1*, 1392–1398.

[151] T. Kolb, *Neue niedermolekulare Materialien für eine lösungsmittelfreie Photolithographie*, Diploma thesis University of Bayreuth **2008**.

[152] P. A. Bergstroem, J. Lindgren, An infrared spectroscopic study of the hydration of the triflate ion (CF3SO3-) in aqueous solution, *J. Mol. Struct.* **1990**, *239*, 103–111.

[153] A. R. Katritzky, A. Zia, Reactions of five-membered heteroaromatic oxonium cations with amines, *J. Chem. Soc., Perkin Trans. 1* **1982**, 131–136.

[154] W. Hinsberg, F. A. Houle, S.-W. Lee, H. Ito, K. Kanazawa, Characterization of Reactive Dissolution and Swelling of Polymer Films Using a Quartz Crystal Microbalance and Visible and Infrared Reflectance Spectroscopy, *Macromolecules* **2005**, *38*, 1882–1898.

[155] V. P. de, I. Abril, R. Garcia-Molina, Inelastic scattering of electron and light ion beams in organic polymers, *J. Appl. Phys.* **2011**, *109*, 094901/1-8.

(Eidesstattliche) Versicherungen und Erklärungen

(§ 5 Nr. 4 PromO)

Hiermit erkläre ich, dass keine Tatsachen vorliegen, die mich nach den gesetzlichen Bestimmungen über die Führung akademischer Grade zur Führung eines Doktorgrades unwürdig erscheinen lassen.

(§ 8 S. 2 Nr. 5 PromO)

Hiermit erkläre ich mich damit einverstanden, dass die elektronische Fassung meiner Dissertation unter Wahrung meiner Urheberrechte und des Datenschutzes einer gesonderten Überprüfung hinsichtlich der eigenständigen Anfertigung der Dissertation unterzogen werden kann.

(§ 8 S. 2 Nr. 7 PromO)

Hiermit erkläre ich eidesstattlich, dass ich die Dissertation selbständig verfasst und keine anderen als die von mir angegebenen Quellen und Hilfsmittel benutzt habe.
Ich habe die Dissertation nicht bereits zur Erlangung eines akademischen Grades anderweitig eingereicht und habe auch nicht bereits diese oder eine gleichartige Doktorprüfung endgültig nicht bestanden.

(§ 8 S. 2 Nr. 9 PromO)

Hiermit erkläre ich, dass ich keine Hilfe von gewerbliche Promotionsberatern bzw. -vermittlern in Anspruch genommen habe und auch künftig nicht nehmen werde.

…………………………………………………………………………………………….

Ort, Datum, Unterschrift